SILANES IN SUSTAINABLE PROCESSES: APPLICATIONS IN POLYMER GRAFTING, CARBON DIOXIDE CAPTURE, AND GOLD NANOPARTICLE SYNTHESIS

A Thesis
Presented to
The Academic Faculty

By

Emily C. Nixon

In Partial Fulfillment
Of the Requirements for the Degree
Doctor of Philosophy in Chemistry

Georgia Institute of Technology

December, 2012

SILANES IN SUSTAINABLE PROCESSES: APPLICATIONS IN POLYMER GRAFTING, CARBON DIOXIDE CAPTURE, AND GOLD NANOPARTICLE SYNTHESIS

Dr. Charles Liotta, co-advisor
School of Chemistry and Biochemistry
Georgia Institute of Technology

Dr. Charles Eckert, co-advisor
School of Chemical & Biomolecular Engineering
Georgia Institute of Technology

Dr. Stefan France
School of Chemistry and Biochemistry
Georgia Institute of Technology

Dr. Leslie Gelbaum
School of Chemistry and Biochemistry
Georgia Institute of Technology

Dr. Carson Meredith
School of Chemical & Biomolecular Engineering
Georgia Institute of Technology

Date Approved: August 27, 2012

DEDICATION

for Don Parkhurst
who taught me to love chemistry

ACKNOWLEDGEMENTS

First and foremost, many thanks to my advisors, Dr. Charles Liotta and Dr. Charles Eckert, for giving me a chance. I would also like to thank the many professors I encountered during my time at Georgia Tech—some of the best classes I have ever taken have been here. I also greatly appreciate the input and feedback I've received from my committee members over the past few years; thank you to Dr. Stefan France, Dr. Les Gelbaum, and Dr. Carson Meredith. We all work together in this research group, and so I have many group members—former and present—to be grateful for. These include but are not limited to: Pam Pollet, Beth Cope, Elizabeth Biddinger, Steve Saunders, Amy Rohan, Wilmarie Medina-Ramos, Hillary Huttenhower, and Swetha Sivaswamy. You have smoothed my path considerably.

Thank you as well to my mother and sister for being there for me. The past couple of years have been trying, but we seem to have made it through relatively intact. Bill Reuter, my grandfather, was always willing to talk shop. Fritz taught me to never give up. All my other family members, who smiled and nodded politely when I described what I was doing: thank you for being so patient.

To my friends that I made while in grad school—I'm so very glad to have crossed your paths. Thanks to: Kyle Flack, Kristen Kitagawa Fisher, Oguz Karvan, Pasha Fedorenko, Mike Bayless, and Evan Davey. J.R. Johnson, thank you for all the food and libations. Natalie-Claire Woods, thank you for many hilarious meals (mostly at Ru San's).

Finally, to Ryan Hart: I couldn't have done this without you.

TABLE OF CONTENTS

LIST OF TABLES

LIST OF FIGURES

LIST OF ABBREVIATIONS

αDMTEtSA	2-methyl-4-(triethylsilyl)-butyl-2-amine
αMTEtSA	4-(triethylsilyl)-butyl-2-amine
βMTEtSA	2-methyl-3-(triethylsilyl)propylamine
γ	surface tension
ΔH_{regen}	enthalpy of regeneration
λ_{max}	wavelength of maximum absorption
ρ	density
$(COCl)_2$	oxalyl chloride
ACN	acetonitrile
Al_2O_3	alumina
$AlCl_3$	aluminum chloride
AMBEHB	aminomethyl-calix[4]arene *bis*(4-(2-ethylhexyl)benzocrown-6)
AOT	dioctyl sulfosuccinate sodium salt
APT	attached proton test
ATR	attenuated total reflectance
AuNP	gold nanoparticles
BHT	butylated hydroxytoluene
BOBCalixC6	calyx[4]arene-bis(*tert*-octylbenzo-crown-6)
CI	chemical ionization
CMC	critical micelle concentration
CO_2	carbon dioxide
$CoCl_2$	cobalt (II) choride

Cs-7SBT	1-(2,2,3,3-tetrafluoropropoxy)-3-(4-*sec*-butylphenoxy)-2-propanol
CSSX	caustic-side solvent extraction
CTAB	cetyltrimethylammonium bromide
DBU	1,8-diazobicyclo[5.4.0]undec-7-ene
DCE	1,2-dichloroethane
DEPT	distortion enhancement by polarization transfer
DFT	density functional theory
DLS	dynamic light scattering
DMF	*N*,*N*-dimethylformamide
DOE	Department of Energy
DSC	differential scanning calorimetry
DTBP	di-*tert*-butyl peroxide
EI	electrospray ionization
EOR	enhanced oil recovery
Et_2O	diethyl ether
ETMS	ethyltrimethoxysilane
ETOAc	ethyl acetate
EtOH	ethanol
ETPS	ethyltriphenylsilane
FAB	fast atom bombardment
FSA	((3-aminopropyl)diisopropyl(1H,1H,2H,2H-perfluoropentyl)silane
FTIR	Fourier transform infrared spectrometry
GC-TCD	gas chromatograph-thermal conductivity detector
h	height of capillary rise

$HAuCl_4$	gold (III) chloride trihydrate, or tetrachloroauric acid
HAW	high activity waste
HCl	hydrochloric acid
HF	hydrofluoric acid
HPLC	high pressure liquid chromatography
HSQC	heteronuclear single quantum correlation
iBTMS	isobutyltrimethyoxysilane
iBTPS	isobutyltriphenylsilane
IL	ionic liquid
$IrCl_3$	iridium (III) chloride
m/z	mass-to-charge ratio
MALDI	matrix-assisted laser desorption-ionization
MEA	monoethanolamine
MEHB	25,27-*bis*(3-aminopropoxy)-calix[4]arene-4-(2-ethylhexyl)benzocrown-6
MeLi	methyllithium
$MgSO_4$	magnesium sulfate
ML	molecular liquid
MS	mass spectrometry
N_2H_4	hydrazine
Na_2CO_3	sodium carbonate
$NaBH_4$	sodium borohydride
NaOH	sodium hydroxide
$n Bu_2O$	dibutyl ether
*n*BuLi	*n*-butyllithium

n$BuNH_2$	*n*-butylamine
NH_3	ammonia
NH_4Cl	ammonium chloride
NH_4OH	ammonium hydroxide
$NiCl_2$	nickel (II) chloride
NMR	nuclear magnetic resonance spectrometry
NO_x	nitrogen oxides
NP	nanoparticles
PCC	post-combustion carbon capture
PE	polyethylene
PhLi	phenyllithium
PhMe	toluene
PTC	phase transfer catalyst
Pt-DVDS	platinum(0)-1,3-divinyl-1,1,3,3-tetramethyldisiloxane
PUREX	plutonium recovery by extraction process
r	inner radius of capillary
RevIL	reversible ionic liquid
r_h	hydrodynamic radius
RI	refractive index
SAXS	small angle X-ray scattering
$scCO_2$	supercritical carbon dioxide
SiO_2	silica
SO_x	sulfur oxides
SPR	surface plasmon resonance band

SREX	strontium extraction process
TBP	tri-*n*-butyl-phosphate
TEM	transmission electron microscope/microscopy
TESA	(3-aminopropyl)triethoxysilane
TEtSA	(3-aminopropyl)triethylsilane
T_{evap}	evaporation temperature
THF	tetrahydrofuran
THSA	(3-aminopropyl)trihexylsilane
TiO_2	titania
TMBG	2-butyl-1,1,3,3-tetramethylguanidine
TMOS	tetramethylorthosilicate
TMS	tetramethylsilane
TMSA	(3-aminopropyl)trimethoxysilane
TOA	trioctylamine
TOAB	tetraoctylammonium bromide
TOCSY	total correlation spectroscopy
TPSA	(3-aminopropyl)tripropysilane
T_{rev}	reversal temperature
TSIL	task-specific ionic liquid
UV-Vis	ultraviolet-visible (spectroscopy)
VTMS	vinyltrimethoxysilane
VTPS	vinyltriphenylsilane
XLPE	crosslinked polyethylene

SUMMARY

Vinyltrialkoxysilanes are grafted onto polyolefins via a peroxide-initiated free radical mechanism; in a subsequent step, the pendant alkoxysilanes undergo hydrolysis and condensation upon exposure to water, resulting in crosslinking of the polymer.[1] This crosslinking gives the resulting polymer a higher melting point and better insulating properties when used in cable and wire coating. The straight chain hydrocarbons dodecane and heptane were used as model compounds to investigate the regioselectivity of vinyltrimethoxysilane (VTMS) grafting. To render the water-sensitive grafted products bench-stable, nucleophilic substitution of the alkoxy groups with phenyllithium (PhLi) was used. It was found that this reaction must be carried out for a minimum of three days to ensure full substitution of the grafted products. Up to 6 grafts were observed per heptane backbone via MALDI mass spectrometry, and up to 8 grafts were observed per dodecane backbone. The grafted products were then separated on a weight basis using semi-preparative HPLC. Analysis of the di-grafted fraction using the advanced NMR techniques edited HSQC and HSQC-TOCSY showed that radical propagation occurs via 1,4- and 1,5-intramolecular hydrogen shifts along the hydrocarbon backbone, resulting in multiple grafts per backbone.[2]

Post-combustion carbon capture (PCC) targets carbon dioxide (CO_2) emissions from large point sources, such as coal-fired power plants, for capture and sequestration.[3] A new class of potential carbon capture agents known as reversible ionic liquids (RevILs)[4] has been synthesized and evaluated in terms of potential performance parameters, such as CO_2 capacity, viscosity, and enthalpy of regeneration. These RevILs take the form of silylated amines, which react with CO_2 to form a salt comprising an ammonium cation and a

carbamate anion that is liquid at or near room temperature.[5] Structural modifications of the basic silylamine skeleton result in drastic differences in the performance of the resulting RevIL. Systematic variation of the silylated amines allowed determination of a structure-property relationship, and continued iterations will allow development of an ideal candidate for scale-up.

The properties and potential applications of gold nanoparticles (AuNP) are highly dependent on their size and shape, which are commonly controlled during liquid-phase synthesis through the use of capping agents.[6] These capping agents must be removed following synthesis in order to prevent deactivation of the surface of the AuNP.[7] Reverse micelles can also be used to control the morphology of AuNP during their synthesis.[8] When RevILs are used in the formation of these reverse micelles, either as the disperse phase or as the surfactant, the built-in switch can be used to release the nanoparticles following their synthesis. This release on command could decrease the post-synthetic steps required to clean and purify AuNP prior to use.[9] We have successfully synthesized AuNP using a number of different RevILs.

References

1. Ghosh-Dastidar, A.; Sengupta, S. S.; Flory, A.; Cogen, J. M. In *Effect of silane grafting level and crosslink structure on properties of moisture crosslinkable systems*, International Wire & Cable Symposium and Conference, Providence, Rhode Island, Providence, Rhode Island, 2008; pp 138-145.

2. Pollet, P.; Liotta, C. L.; Eckert, C. A.; Verma, M.; Nixon, E. C.; Sivaswamy, S.; Jha, R.; Gelbaum, L.; Chaudhary, B. I.; Cogen, J. M. Radical mediated graft modification of polyolefin models with vinyltrimethoxysilane: A fundamental study. *Ind. Eng. Chem. Res.* **2011**, 12246-12253.

3. United States Department of State. U.S. Climate Action Report 2010. Global Publishing Services: Washington, D.C., June 2010.

4. (a) Jessop, P. G.; Heldebrant, D. J.; Li, X. W.; Eckert, C. A.; Liotta, C. L. Green chemistry - Reversible nonpolar-to-polar solvent. *Nature* **2005,** *436* (7054), 1102-1102; (b) Phan, L.; Chiu, D.; Heldebrant, D. J.; Huttenhower, H.; John, E.; Li, X. W.; Pollet, P.; Wang, R. Y.; Eckert, C. A.; Liotta, C. L.; Jessop, P. G. Switchable solvents consisting of amidine/alcohol or guanidine/alcohol mixtures. *Ind. Eng. Chem. Res.* **2008,** *47* (3), 539-545.

5. (a) Hart, R.; Pollet, P.; Hahne, D. J.; John, E.; Llopis-Mestre, V.; Blasucci, V.; Huttenhower, H.; Leitner, W.; Eckert, C. A.; Liotta, C. L. Benign coupling of reactions and separations with reversible ionic liquids. *Tetrahedron* **2010,** *66* (5), 1082-1090; (b) Blasucci, V.; Dilek, C.; Huttenhower, H.; John, E.; Llopis-Mestre, V.; Pollet, P.; Eckert, C. A.; Liotta, C. L. One-component, switchable ionic liquids derived from siloxylated amines. *Chem. Commun.* **2009,** (1), 116-118; (c) Blasucci, V.; Hart, R.; Mestre, V. L.; Hahne, D. J.; Burlager, M.; Huttenhower, H.; Thio, B. J. R.; Pollet, P.; Liotta, C. L.; Eckert, C. A. Single component, reversible ionic liquids for energy applications. *Fuel* **2010,** *89* (6), 1315-1319.

6. Cushing, B. L.; Kolesnichenko, V. L.; O'Connor, C. J. Recent advances in the liquid-phase syntheses of inorganic nanoparticles. *Chem. Rev.* **2004,** *104* (9), 3893-3946.

7. Campelo, J. M.; Luna, D.; Luque, R.; Marinas, J. M.; Romero, A. A. Sustainable preparation of supported metal nanoparticles and their applications in catalysis. *Chemsuschem* **2009,** *2* (1), 18-45.

8. (a) Pileni, M. P. Reverse micelles used as templates: a new understanding in nanocrystal growth. *J. Exp. Nanosci.* **2006,** *1* (1), 13-27; (b) Uskoković, V.; Drofenik, M. Synthesis of materials within reverse micelles. *Surf. Rev. Lett.* **2005,** *12* (2), 239-277.

9. Dahl, J. A.; Maddux, B. L. S.; Hutchison, J. E. Toward greener nanosynthesis. *Chem. Rev.* **2007,** *107* (6), 2228-2269.

CHAPTER 1. INTRODUCTION

The concept of green chemistry is not new—the concept was first proposed by Paul Anastas in 1991[1]—but in recent years, interest in the field has increased, in part due to increased consumer demand for products that are green or sustainable. Whereas the environmental movements of the 1970s and 1980s focused on the role of the individual in sustainability, the current movement focuses more on the role of industry in sustainability. To this end, Anastas developed the 12 principles of green chemistry, listed in Figure 1.1.

1. It is better to prevent waste than to treat or clean up waste after it is formed.
2. Synthetic methods should be designed to maximize the incorporation of all materials used in the process into the final product.
3. Wherever practicable, synthetic methodologies should be designed to use and generate substances that possess little or no toxicity to human health and the environment.
4. Chemical products should be designed to preserve efficacy of function while reducing toxicity.
5. The use of auxiliary substances (e.g. solvents, separation agents, etc.) should be made unnecessary wherever possible, and innocuous when used.
6. Energy requirements should be recognized for their environmental and economic impacts and should be minimized. Synthetic methods should be conducted at ambient temperature and pressure.
7. A raw material of feedstock should be renewable rather than depleting wherever technically and economically practicable.
8. Unnecessary derivatization (blocking group, protection/deprotection, temporary modification of physical/chemical processes) should be avoided whenever possible.
9. Catalytic reagents (as selective as possible) are superior to stoichiometric reagents.
10. Chemical products should be designed so that at the end of their function they do not persist in the environment and break down into innocuous degradation products.
11. Analytical methodologies need to be further developed to allow for real-time, in-process monitoring and control prior to the formation of hazardous substances.
12. Substances and the form of a substance used in a chemical process should be chosen so as to minimize the potential for chemical accidents, including releases, explosions, and fires.

Figure 1.1. The twelve principles of green chemistry.[1]

The primary focus of the green chemistry movement is the avoidance of waste—to prevent the formation of waste, rather than cleaning it up afterwards. This movement has spread beyond the traditional purview of the chemical industry itself: non-chemical industries are advertising their green credentials and discussing the details of their production methods. Recently, a new method for dying fabric has been introduced that uses supercritical CO_2 ($scCO_2$) to dissolve the solid textile dye in place of water, saving 25 liters of water per shirt. The clothing manufacturer Adidas is using this fabric for their garments and is touting this DryDye technology in their advertisements.[2] Additionally, green chemistry is being introduced at an earlier stage in the education of chemistry students. The University of Oregon has integrated experiments demonstrating the principles of green chemistry into its undergraduate laboratory curriculum.[3] Worldwide, the combined earnings of the top 50 chemical concerns in 2011 was close to $1 trillion[4]—clearly, the chemical industry has the power to make a huge impact by widely adopting the principles of green chemistry.

One of the classic examples of an industrial-scale process in the chemical industry that has been greatly improved by the application of the principles of green chemistry is the production of ibuprofen. In the traditional synthesis of ibuprofen, the first step entails a Friedel-Crafts acylation of isobutylbenzene to form 4-isobutylacetophenone, shown in Figure 1.2.[5]

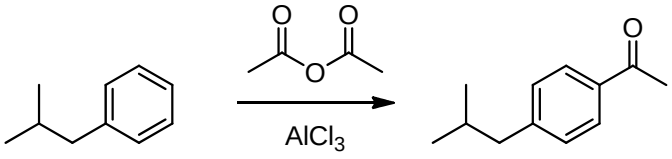

Figure 1.2. Friedel-Crafts acylation of isobutylbenzene to 4-isobutylacetophenone, using acetic anhydride and $AlCl_3$.[5]

This electrophilic aromatic substitution is catalyzed by a strong Lewis acid such as aluminum chloride ($AlCl_3$). As this acid complexes with the desired product, the complex must be broken up to isolate the product. In the industrial synthesis of 4-isobutylacetophenone, this is done with water. To produce one million kilograms of 4-isobutylacetophenone, 0.76 million kilograms of $AlCl_3$ are required—none of the $AlCl_3$ is recycled.[6] Overall, production of nearly 14 million kilograms of ibuprofen using this six-step synthesis results in 20 million kilograms of waste.[7]

In 1991, Boots Hoechst Celanese developed an alternative industrial process which uses hydrofluoric acid (HF) as the acid catalyst, shown in Figure 1.3.[8]

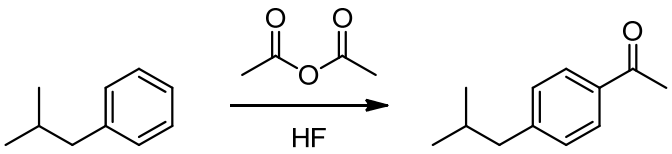

Figure 1.3. Friedel-Crafts acylation of isobutylbenzene to 4-isobutylacetophenone, using acetic anhydride and HF.[5]

The benefit here is that the HF can be recycled; however, this may at first appear to be a pyrrhic victory of sorts. Everyone who has been trained in laboratory safety is aware that HF is highly corrosive and extremely hazardous. Clark notes that the capital outlay required to build a plant that can safely handle HF is quite considerable; however, unlike $AlCl_3$, HF can be recycled and reused.[6] Additionally, the acetic acid produced as a byproduct in the HF process is recovered and used in other syntheses.[7] In the end, this should result in savings to the company; not only are fewer reagents needed, but less waste ultimately will have to be disposed of. Above all, any improvements must be financially beneficial to the business in question, or they will not be put into practice.

I would like to frame my introduction of my thesis projects in terms of the principles of green chemistry and the specific goals these projects aim to accomplish. I chose to come to Georgia Tech and join the Eckert-Liotta research group for two reasons: the interdisciplinary nature of the group, and the focus on green chemistry and engineering. I hope to show in the following pages that my work over the past few years combines aspects of both. In my opinion, there is no one right solution when it comes to green chemistry—there are only *better* solutions. Referring back to the improved industrial synthesis of 4-isobutylacetophenone, the catalyst was changed from $AlCl_3$ to HF. The use of HF does not obey principle 3 in Figure 1.1: "Wherever practicable, synthetic methodologies should be designed to use and generate substances that possess little or no toxicity to human health and the environment." However, the use of a recyclable acid rather than a once-through acid greatly decreases the amount of waste produced. One must keep in mind that there are a number of factors to be balanced. The three topics I will present are: the grafting of silanes onto polyolefin model compounds; the synthesis and characterization of novel silylated amines for CO_2 capture; and the use of reversible ionic liquids (RevILs) in the synthesis of gold nanoparticles (AuNP).

In Chapter Two I will present my investigations into the grafting reaction of silanes onto polyolefin analogs. Modification of polymers such as polypropylene (PP) or polyethylene (PE) is commonly used to create specialty polymers from inexpensive ones.[9] An example of such a specialty polymer is cross-linked polyethylene (XLPE), which can be formed from the peroxide-initiated grafting reaction of vinyltrimethoxysilane (VTMS) onto PE.[10] In a subsequent step, the grafted PE is exposed to moisture, which causes hydrolysis of the alkoxy groups and crosslinking.[11] The yield of this grafting reaction is low with respect to VTMS.[12] In current industrial processes, the excess VTMS is simply driven off with heat

and not recovered for later use, thereby generating additional waste. Furthermore, it has been demonstrated that the graft distribution along the polymer backbone is highly uneven—the grafts are clustered together, leaving stretches of the backbone unmodified.[13] Therefore, the ability to precisely control the graft distribution per segment of backbone would allow for a more efficient use of resources. Our goal in this project is to understand the mechanistic and regiochemical fundamentals of the grafting process, using hydrocarbon model compounds as PE analogs to simplify analysis.[14]

In Chapter Three I examine the development of three iterations of silylated amines for use in CO_2 capture. Our research group has previously demonstrated that compounds of the form (3-aminopropyl)trialkylsilane, when reacted with CO_2, form reversible ionic liquids (RevILs) comprising an ammonium-carbamate ion pair.[15] The RevIL can then continue to physisorb CO_2 as shown in Figure 1.4, increasing the CO_2 capacity via a dual capture mechanism (chemi- and physisorption).[16]

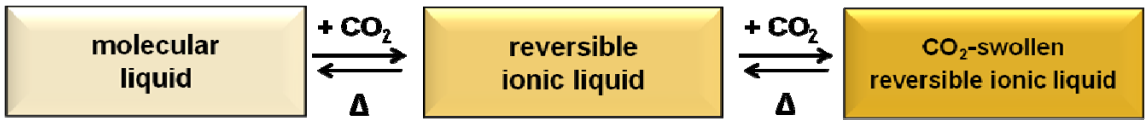

Figure 1.4. Reaction of CO_2 with molecular liquid, *left*, to form reversible ionic liquid, *middle*. This further absorbs CO_2 to form a CO_2-swollen reversible ionic liquid, *right*.

When heated or sparged with inert gas, these RevILs release CO_2 and revert back to their molecular liquid (ML) form. We have proposed the use of these novel materials as carbon capture agents from the flue gas of coal fired power plants. I will discuss how I improved the conditions of the hydrosilylation reaction used to synthesize these silylated amines and developed a new class of silylated amines with an unsaturation in the backbone linking the

silicon and the 1° amine. I will also present how my familiarity with these unsaturated amines allowed me to synthesize novel branched amines, in which the amine moiety, though still primary, is sterically hindered. This leads to improved physical and thermodynamic properties when these amines are considered for use in CO_2 capture.

Currently, the most mature technology for post-combustion carbon capture (PCC) is monoethanolamine (MEA), which has been used as a liquid sorbent to remove CO_2 from natural gas deposits and slip streams of flue gas from power plants.[17] It is not only chemoselective for CO_2, but also recyclable and inexpensive. MEA, while possessing properties that clearly make it advantageous to use as a carbon capture agent, has several disadvantages. From a green chemistry standpoint, two important problems are its volatility[18] and its corrosivity.[19] To inhibit these drawbacks, and also to decrease the viscosity of the liquid salt formed upon reaction with CO_2, MEA is commonly run as an aqueous solution (20-30 wt% MEA depending on usage). To strip this solution of CO_2 and recycle it for further use, it must be heated to 110-120°C;[20] the high heat capacity of water means that a great deal of energy is required to heat the solution to this temperature, decreasing the efficiency of the power plant to which such a scrubber would be attached.[21] In addition, the degradation of MEA over time (2.2 kg MEA per metric ton of CO_2 captured) increases the amount of waste resulting from this process.[22] We seek a solvent that can act as a replacement for MEA and improve on its performance. Such a solvent must not only be selective for CO_2 and have a high CO_2 capture capacity, it must also exhibit a low viscosity, low volatility, and a low energy of regeneration. I will present how our novel silylated amines perform in these areas.

Chapter Four deals with the use of these same RevILs as capping agents for gold nanoparticles. The synthesis of gold nanoparticles was selected as a proof-of-concept

reaction, as AuNP synthesized via other liquid-phase methods have been extensively characterized. From a green chemistry standpoint, catalytic reactions are preferable to reactions in which stoichiometric amounts of reagents are used, as this decreases the amount of waste produced (Principle 9 in Figure 1.1). Our original goal for this project was to create a sustainable synthesis for a sustainable catalyst—AuNP have been shown to be an efficient oxidation catalyst of carbon monoxide and propene at low temperatures.[23] Anastas cautions that it is not enough to create sustainable alternatives—we must also produce these sustainable alternatives in a sustainable manner.[24] Hydrazine was chosen not only because it is a quick reducing agent, but also because it cleanly decomposes into nitrogen and hydrogen.

Originally, we sought to use two-component RevILs, made up of a guanidinium cation and a methylcarbonate anion,[25] as the core of reverse micelles (reaction A in Figure 1.5).

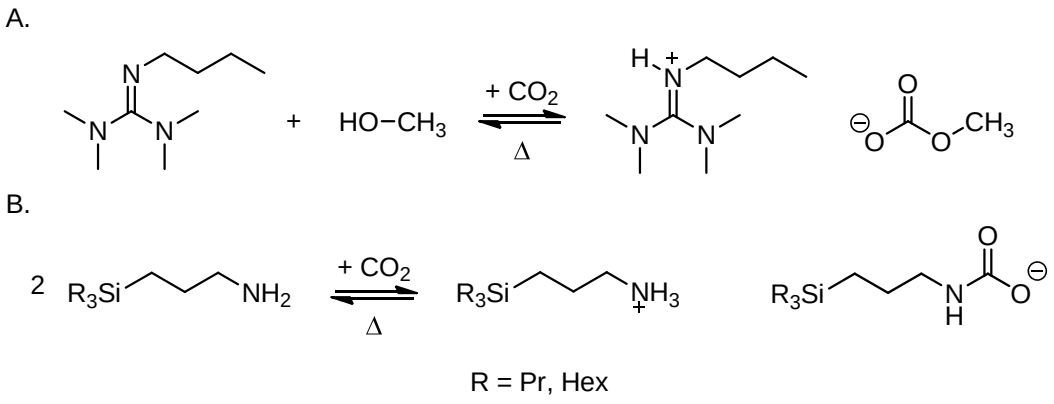

Figure 1.5. Reaction *A*, formation of 2-component RevIL from TMBG and methanol; *B*, formation of 1-component RevIL from silylated amines.

Hydrogen bonding between the protonated guanidinium and the polar head of a novel sulfonamide surfactant stabilized the micellar structure.[26] The salt tetrachloroauric acid ($HAuCl_4$) was dissolved in the RevIL core of the reverse micelles. By controlling the size of the reverse micelles, we can theoretically control the size of the nanoparticles we form therein.[27] Upon heating the system, CO_2 was removed and hydrogen bonding capabilities were lost, causing destruction of the reverse micellar structure. This released the nanoparticles essentially on command. Our original goal upon inception of this project was that we would have a fully recyclable system—after isolating the nanoparticles, we would prime the system for recycle by adding more gold salt and methanol, then sparging the system with more CO_2 to re-form the reverse micelles. Although we realized that the buildup of HCl (formed as a byproduct of reduction) precluded us from having a wholly recyclable system, we were able to apply this experience to subsequent work in which we used one-component RevILs. However, these were used not as the core of the reverse micelles, but as "switchable surfactants:" the long alkyl chains on the silicon group act as the hydrophobic tails of the surfactant, while the ammonium and carbamate moieties act as the polar heads (reaction B in Figure 1.5). Using these one-component RevILs, we have been able to successfully and reproducibly synthesize spherical nanoparticles.

Finally, in Chapter Five, I will summarize the conclusions of my research and present my recommendations for future work. Two appendices are included in this document. The first one (Appendix A) chronicles our preliminary work with switchable crown ethers; the second appendix (B) details the experimental procedures for the synthesis of bimetallic and layered supported metal catalysts for the controlled decomposition of hydrazine into ammonia.

1.1 References

1. Anastas, P. T.; Warner, J. C., *Green Chemistry: Theory and Practice*. Oxford University Press: Oxford, England, 1998.

2. The Yeh Group, DryDye™ fabrics--exclusively from the Yeh Group [press release]. Retrieved from http://www.knittingindustry.com/uploads/1090/drydye-tech-paper-wol.pdf, August 6, 2012.

3. Reed, S. M.; Hutchison, J. E., Green Chemistry in the Organic Teaching Laboratory: An Environmentally Benign Synthesis of Adipic Acid. *J. Chem. Educ.* **2000,** *77* (12), 1627.

4. Tullo, A. H., C&EN's global top 50 chemical firms. *Chem. Eng. News* July 30, 2012, 2012, pp 15-18.

5. Nicholson, J. S.; Adams, S. S. Phenyl propionic acids. 3,385,886, 1968.

6. Clark, J. H., Green chemistry: challenges and opportunities. *Green Chem.* **1999,** *1* (1), 1-8.

7. Cann, M. C.; Connelly, M. E., *Real World Cases in Green Chemistry*. American Chemical Society: Washington, D.C., 2000.

8. Lindley, D. D.; Curtis, T. A.; Ryan, T. R.; de la Garza, E. M.; Hilton, C. B.; Kenesson, T. M. Process for the production of 4'-isobutylacetophenone. 5,068,448, 1991.

9. Isac, S.; George, K. E., Silane grafting of polyethylenes. *Int. J. Polymer. Mater.* **2005,** *54* (5), 397-413.

10. Morshedian, J.; Hoseinpour, P. M., Polyethylene cross-linking by two-step silane method: a review. *Iranian Polymer Journal* **2009,** *18* (2), 103-128.

11. (a) Allermann, G. A. Silane crosslinkable polyethylene. US20040024138 A1, 2004; (b) Scott, H. G. Cross-linking of a polyolefin with a silane. 3646155, 1972; (c) Ultsch, S.; Fritz, H. G., Crosslinking of LLDPE and VLDPE via graft-polymerized vinyltrimethoxysilane. *Plastics and Rubber Processing and Applications* **1990,** *13* (2), 81-91.

12. Ghosh-Dastidar, A.; Sengupta, S. S.; Flory, A.; Cogen, J. M. In *Effect of silane grafting level and crosslink structure on properties of moisture crosslinkable systems*, International Wire & Cable Symposium and Conference, Providence, Rhode Island, Providence, Rhode Island, 2008; pp 138-145.

13. Sirisinha, K.; Meksawat, D., Preparation and properties of metallocene ethylene copolymer crosslinked by vinyltrimethoxysilane. *Polym. Int.* **2005,** *54* (7), 1014-1020.

14. (a) Parent, J. S.; Parodi, R.; Wu, W., Radical mediated graft modification of polyolefins: Vinyltriethoxysilane addition dynamics and yields. *Polym. Eng. Sci.* **2006,**

46 (12), 1754-1761; (b) Forsyth, J. C.; Baker, W. E.; Russell, K. E.; Whitney, R. A., Peroxide-initiated vinylsilane grafting: Structural studies on a hydrocarbon substrate. *J. Polym. Sci., Part A: Polym. Chem.* **1997,** *35* (16), 3517-3525; (c) Spencer, M.; Parent, J. S.; Whitney, R. A., Composition distribution in poly(ethylene-graft-vinyltrimethoxysilane). *Polymer* **2003,** *44* (7), 2015-2023.

15. (a) Blasucci, V.; Dilek, C.; Huttenhower, H.; John, E.; Llopis-Mestre, V.; Pollet, P.; Eckert, C. A.; Liotta, C. L., One-component, switchable ionic liquids derived from siloxylated amines. *Chem. Commun.* **2009,** (1), 116-118; (b) Blasucci, V.; Hart, R.; Mestre, V. L.; Hahne, D. J.; Burlager, M.; Huttenhower, H.; Thio, B. J. R.; Pollet, P.; Liotta, C. L.; Eckert, C. A., Single component, reversible ionic liquids for energy applications. *Fuel* **2010,** *89* (6), 1315-1319.

16. Hart, R.; Pollet, P.; Hahne, D. J.; John, E.; Llopis-Mestre, V.; Blasucci, V.; Huttenhower, H.; Leitner, W.; Eckert, C. A.; Liotta, C. L., Benign coupling of reactions and separations with reversible ionic liquids. *Tetrahedron* **2010,** *66* (5), 1082-1090.

17. Rubin, E. S.; Mantripragada, H.; Marks, A.; Versteeg, P.; Kitchin, J., The outlook for improved carbon capture technology. *Prog. Energy Combust. Sci.* **2012**, in press.

18. Veawab, A.; Aroonwilas, A.; Chakma, A.; Tontiwachwuthikul, P., Solvent formulation for CO_2 separation from flue gas streams. In *First National Conference on Carbon Sequestration*, Washington, D.C., 2001.

19. Strazisar, B. R.; Anderson, R. R.; White, C. M., Degradation pathways for monoethanolamine in a CO_2 capture facility. *Energy Fuels* **2003,** *17* (4), 1034-1039.

20. Rochelle, G. T., Amine scrubbing for CO_2 capture. *Science* **2009,** *325* (5948), 1652-1654.

21. D'Alessandro, D. M.; Smit, B.; Long, J. R., Carbon Dioxide Capture: Prospects for New Materials. *Angew. Chem. Int. Ed.* **2010,** *49* (35), 6058-6082.

22. Aaron, D.; Tsouris, C., Separation of CO_2 from flue gas: A review. *Sep. Sci. Technol.* **2005,** *40* (1-3), 321-348.

23. Min, B. K.; Friend, C. M., Heterogeneous gold-based catalysis for green chemistry: Low-temperature CO oxidation and propene oxidation. *Chem. Rev.* **2007,** *107* (6), 2709-2724.

24. Anastas, P. T., The Transformative Innovations Needed by Green Chemistry for Sustainability. *Chemsuschem* **2009,** *2* (5), 391-392.

25. Phan, L.; Chiu, D.; Heldebrant, D. J.; Huttenhower, H.; John, E.; Li, X. W.; Pollet, P.; Wang, R. Y.; Eckert, C. A.; Liotta, C. L.; Jessop, P. G., Switchable solvents consisting of amidine/alcohol or guanidine/alcohol mixtures. *Ind. Eng. Chem. Res.* **2008,** *47* (3), 539-545.

26. Liu, J. H.; Cheng, S. Q.; Zhang, J. L.; Feng, X. Y.; Fu, X. G.; Han, B. X., Reverse micelles in carbon dioxide with ionic-liquid domains. *Angew. Chem. Int. Ed.* **2007,** *46* (18), 3313-3315.

27. Pileni, M. P., Reverse micelles used as templates: a new understanding in nanocrystal growth. *J. Exp. Nanosci.* **2006,** *1* (1), 13-27.

CHAPTER 2. A FUNDAMENTAL STUDY OF SILANE GRAFTING ONTO POLYETHYLENE ANALOGS

2.1 Introduction

Post-reactor modification of polyolefins is a commercially important method of introducing functionalities to polymers, thereby creating specialty polymers from commodity ones and tailoring them to particular uses. As polyolefins themselves contain no functional groups capable of crosslinking, these bonds must be introduced via other means. There are three main methods by which this is achieved: irradiation, addition of peroxides, and grafting of functional groups to the polyolefin backbone.[1] The third option, modification of the polyolefin backbone via grafting, has grown in popularity in the past few decades, in part due to the ease of the process—it does not require significant capital outlay (as for irradiation crosslinking),[2] and it provides a more reliable and safer means of crosslinking than peroxides.[3] Irradiation-induced crosslinking is also limited by the depth to which the ionizing radiation penetrates into the molded polymer.[3]

Crosslinked polyethylene (XLPE) is used in a variety of applications, including cable insulation, hot water pipes, and temperature-resistant gaskets.[4] These applications are made possible only by the presence of the crosslinks, as uncrosslinked polyethylene (PE) is thermoplastic and has a relatively low melting temperature of 100°C, limiting its range of applications.[3, 5] In comparison, XLPE has a melting point above 150°C.[3] As the temperature of a conducting cable is proportional to the current carried by said cable, XLPE-sheathed cables can carry more current than PE-sheathed cables.[6] Additionally, XLPE-sheathed cables have been found to be better insulators than comparable PE- or ethylene propylene rubber (EPR)-sheathed cables, decreasing dielectric losses even at elevated operating temperatures.[7]

There are two primary methods by which moisture-crosslinkable moieties, such as alkoxysilanes, are grafted onto PE backbones. The MONOSIL method of producing moisture-crosslinkable PE is a one-step method in which the PE, graftable crosslinker, and peroxide initiator are blended together and extruded into the desired shape; moisture is introduced later.[8] In contrast, the SIOPLAS process of introducing moisture-curable silanes to PE is a two-step method; this method was introduced in 1972 by Dow.[8-9] Vinyltrialkoxysilanes are grafted onto the PE backbone in the presence of an initiator in an extruder; the grafted polymer thus formed can then be stored until cross-linking is desired. When exposed to moisture in a second step, the grafted alkoxysilanes hydrolyze and condense, forming siloxane bonds and crosslinking the polymer chains, as shown in Figure 2.1.[10] A commonly used silane is vinyltrimethoxysilane, or VTMS.

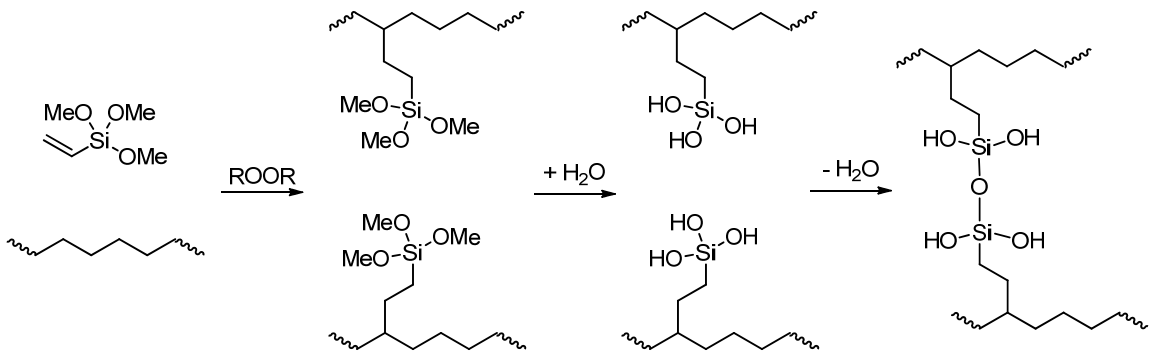

Figure 2.1. Peroxide-initiated grafting of vinyltrimethoxysilane (VTMS), followed by hydrolysis of methoxy groups and subsequent crosslinking via condensation.[10]

This crosslinking step can occur in the presence of water alone;[11] however, in industry, the reaction is generally sped up via the addition of tin catalysts at the compounding stage.[12] Degradation temperature of XLPE increases as the extent of grafting increases;[13] therefore,

fine control over the grafting conditions is essential to control the properties of the final crosslinked polymer.[14] Sirisinha *et al.* point out that, while the crosslinked areas of the polymer exhibit different mechanical properties than the unmodified regions, the distribution is uneven, and the uncrosslinked regions behave similarly to the unmodified PE.[15] Additionally, current processing techniques use an excess of VTMS—the unreacted silane is driven off with heat and not recovered. The grafting yield with respect to silane can be as low as 50%.[10] The extent of grafting cannot be controlled simply by adding more peroxide, as there is typically an optimal concentration of peroxide above which chain termination reactions begin to dominate.[5b] The ability to precisely control the graft distribution per segment of PE backbone would allow for a more efficient use of resources.

However, thorough exploration of the mechanistic and regiochemical aspects of post-reactor grafting is complicated by the huge range of possible products when polyolefins are used as substrates—therefore, model compounds such as long-chain saturated hydrocarbons (e.g. tetradecane) are commonly employed as polymer analogs, or model compounds.[16] The goal of this project was to understand the fundamentals of how the grafting process works, using model compounds to simplify the analysis of the products.[16a] Although the kinetics of vinylsilane grafting to polyolefins has been reported from grafting studies using PE and reactor torque measurements,[11] systematic investigations of the mechanism, in terms of the regio- and stereoselectivity of the reaction, remain scarce. By separating and characterizing the products of the model compound grafting reactions, we will be able to gain an insight into the mechanism of the reaction and its radical intermediates.

2.2 Background

Three chain propagation pathways in peroxide-initiated grafting of silanes onto PE are reported in the literature. Initiation occurs via temperature-induced homolytic cleavage of the oxygen-oxygen bond in the peroxide (e.g di-*tert*-butyl peroxide, or DTBP, as shown below in Figure 2.2) to yield an alkoxy radical. This alkoxy radical then abstracts a hydrogen atom from the PE backbone, which adds to the double bond of the vinylsilane, forming a pendant α-silyl radical. This α-silyl radical can propagate in one of three ways: intermolecular hydrogen abstraction to yield a singly-grafted substrate; intramolecular hydrogen abstraction to yield another reactive site on the same PE backbone; or addition to another vinylsilane to yield pendant oligomeric grafts.[16a] These three pathways are depicted in Figure 2.2, bottom.

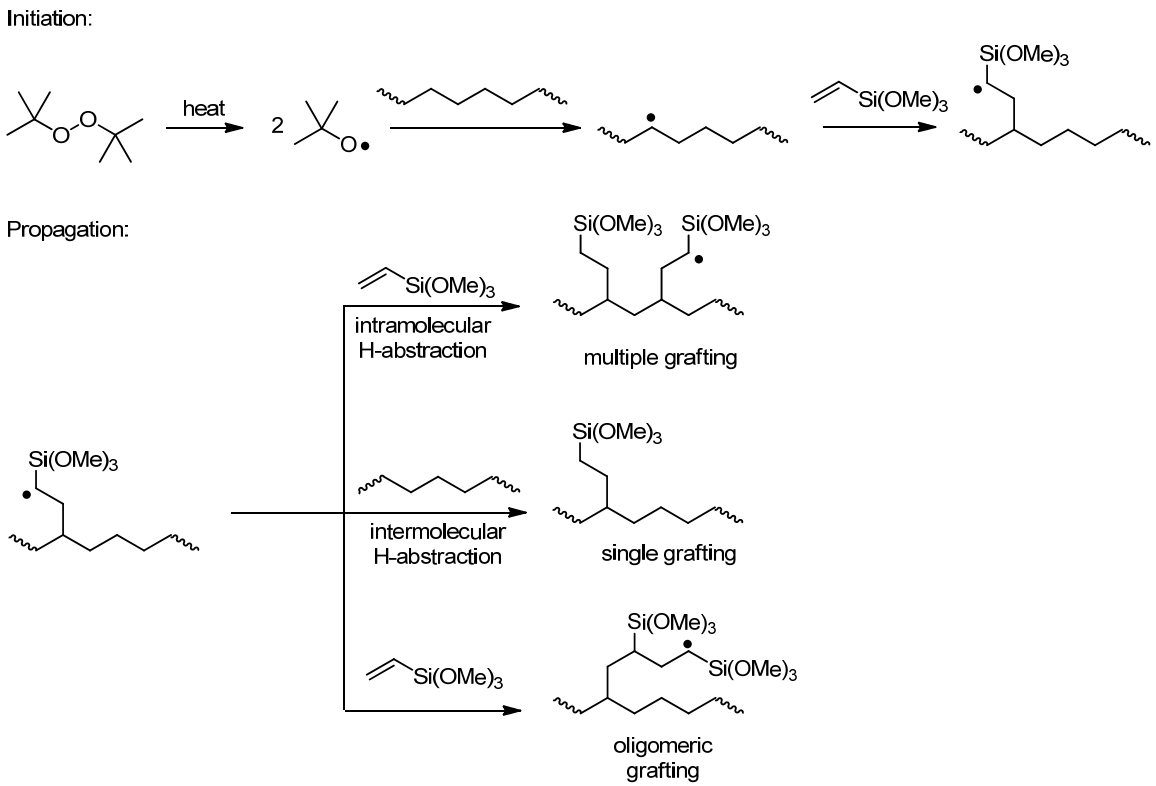

Figure 2.2. Initiation and possible propagation pathways for DTBP-initiated grafting of vinyltrimethoxysilane.

Oligomeric grafting, or homopolymerization, is disfavored for VTMS in the presence of peroxides or γ-radiation.[16b, 17] Several groups have examined the preference for inter- or intramolecular hydrogen abstraction.

Forsyth *et al.* investigated the grafting of VTMS onto the polyethylene model compound dodecane, using the peroxide Lupersol L-101 [2,5-dimethyl-2,5-di-(*tert*-butylperoxy)hexane] as an initiator. Crude separation was achieved via Kugelrohr, and the resulting product fractions were analyzed using a variety of techniques, including ^{1}H NMR, ^{13}C NMR, Fourier transform infrared spectroscopy (FTIR) and mass spectrometry (MS) with chemical ionization (CI). By comparing the integration of the grafted methoxy protons to that of the hydrocarbon protons in the ^{1}H NMR spectrum, they determined that the average number of grafts per dodecane molecule was 2.37. The maximum number of grafts observed per backbone molecule via mass spectral analysis was 5, although a small peak thought to correspond to the mass-to-charge ratio (*m/z*) of hexa-grafted material was present as well. The presence of multiple grafts per substrate molecule was attributed to the thermodynamic favorability of intramolecular hydrogen transfer as the mode of radical chain propagation.[16c]

Building on this work, Spencer *et al.* investigated tetradecane as a model compound, in conjunction with VTMS and dicumyl peroxide.[16a] After grafting, but prior to analysis, the water-sensitive methoxy groups were replaced with phenyl rings via reaction with phenyllithium (PhLi). The product mixture was then separated using semi-preparative high performance liquid chromatography (HPLC), which allowed for isolation of the various grafted fractions by mass. Spencer found multiple grafts per substrate molecule (average: 4.2) via ^{1}H NMR, with a maximum of 5; it was concluded that the primary mode of radical propagation was the intramolecular hydrogen shift, rather than the formation of pendant

VTMS oligomers.[16a] However, both groups readily acknowledged the inherent difficulty of the analyses due to the large variety of grafted products.

2.3 Experimental Section

2.3.1 Materials

All chemicals were purchased from Sigma-Aldrich and used as received unless otherwise noted. Chemicals used were: dodecane (anhydrous, ≥99%); heptane (anhydrous, 99%); vinyltrimethoxysilane (VTMS; 98%); di-*tert*-butyl peroxide (DTBP; 98%); ethyltrimethoxysilane (ETMS; 97+%); isobutyltrimethoxysilane (*i*BTMS; ≥98%); tetramethylorthosilicate (TMOS; ≥99%); cyclohexane (anhydrous, 99.5%); 2-bromopyridine (99%); phenyllithium (PhLi; 1.8 *M* in di-*n*-butyl ether, nBu$_2$O); *n*-butyllithium (*n*BuLi; 2.4 *M* in hexanes); methyllithium (MeLi; 1.6 *M* in diethyl ether); and 2-thienyllithium (1.0 *M* in THF/hexanes). Experiments carried out in the carousel reactor used PhLi acquired from TCI America (1.6 *M* in 70:30 cyclohexane:diethyl ether). Hexane (CHROMASOLV Plus, for HPLC, ≥95%) and ethyl acetate (CHROMASOLV, for HPLC, ≥99.7%) were used as mobile phases for semi-preparative HPLC.

2.3.2 Experimental

2.3.2.1 Glassware Reactions

A typical grafting/capping reaction for dodecane in glassware was carried out as follows. 50 mL dodecane (0.22 mol) and 5 wt% VTMS (12 mmol) were placed in a round bottomed flask fitted with a magnetic stirbar and a dry ice condenser under inert atmosphere. The initiator DTBP (750 ppm) was introduced to the system, and the reaction mixture was heated at 200°C for 7 hours. After the reaction mixture had cooled to room temperature, 33.8 mL of 1.6 *M* PhLi in 70:30 cyclohexane:diethyl ether (4:1 PhLi:VTMS) was

added. After stirring for the allotted time, a solution of saturated ammonium chloride (NH_4Cl) was added to quench the excess PhLi; the organic layer was separated, dried with magnesium sulfate ($MgSO_4$), and rotovapped to remove solvents; and the unreacted dodecane was separated from the product mixture via Kugelrohr. Fractions removed via Kugelrohr were analyzed by ^1H NMR to rule out the presence of grafted products.

Reactions carried out in the carousel were performed using proportions of reagents identical to those reactions carried out in normal glassware; however, the reactions were scaled down to fit in the smaller vessels. A typical grafting/capping reaction in the carousel was carried out as follows. 5 mL dodecane (44 mmol) and 0.2 mL VTMS (2.4 mmol) were placed in a 25-mL carousel tube under inert atmosphere. The initiator DTBP (750 ppm) was introduced to the system, and the reaction mixture was heated at reflux at 200°C for 7 hours. After the reaction mixture had cooled to room temperature, 3.4 mL of 1.6 *M* PhLi in 70:30 cyclohexane:diethyl ether (4:1 PhLi:VTMS) was added. After stirring for the allotted time, a solution of NH_4Cl was added to quench the excess PhLi. The organic layer was separated, dried with $MgSO_4$, and rotovapped to remove solvents. The unreacted dodecane was not separated from the product mixture for carousel reactions.

2.3.2.2 Parr Autoclave Reactions

A typical grafting reaction for heptane was performed in a Parr autoclave via the following method. Prior to reaction, the Parr was placed under vacuum for 5 minutes to remove any atmosphere from the reactor. 50 mL anhydrous heptane (0.341 mol), 1.8 mL VTMS (11.15 mmol; 5 wt% wrt heptane), and 1.1 mL of a solution of DTBP in anhydrous heptane (750 ppm) was added to the reactor, which was then placed under inert atmosphere. The reaction vessel was heated to 200°C for 7 hours with vigorous stirring. After the reaction mixture had cooled to room temperature, 28 mL of 1.6 *M* PhLi in di-*n*-butylether

(4:1 PhLi:VTMS) was added and the reaction mixture was stirred for 3 days. 20 mL of a solution of saturated NH_4Cl was added to quench the excess PhLi; the organic layer was dried with $MgSO_4$ and rotovapped to remove nBu$_2$O and the unreacted heptane.

Reactions investigating the effects of pressure on grafting were carried out using dodecane as the substrate, following the reaction conditions in the Parr detailed above. After introduction of the reagents to the reactor, the reactor was pressurized using a Teledyne Isco syringe pump. Prior to addition of PhLi, the Parr was placed under vacuum to remove the CO_2 and then refilled with an inert gas to prevent formation of phenylcarboxylate salts.

2.3.2.3 Capping Agents

Variants of the PhLi capping agent (methyllithium, 2-pyridyllithium, and 2-thienyllithium) were used in the same molar ratio of capping agent to VTMS. 2-pyridyllithium was not commercially available and had to be prepared prior to use. In oven-dried glassware under inert atmosphere, 24.24 mL *n*-butyllithium (*n*BuLi; 58.2 mmol; 0.306 *M*) was slowly added to 4.74 mL 2-bromopyridine (49.7 mmol; 0.262 *M*) in 190 mL diethyl ether (1.81 mol) at -78°C. After stirring, this mixture was injected into the Parr containing the grafted product mixture at room temperature. The reaction was allowed to stir for three days and worked up according to the usual procedures.

2.3.2.4 Graft Analog Synthesis

Graft analogs were synthesized as follows. To a solution of 3 mL silane (18.77 mmol ETMS; 15.64 mmol iBTMS) in 30 mL anhydrous cyclohexane (0.278 mol) was added a 1.8 *M* solution of PhLi in nBu$_2$O (42 mL or 75.60 mmol for ETMS reaction; 35 mL or 63.00 mmol for iBTMS reaction) under inert atmosphere at -10°C. Following addition, the reaction flask was allowed to warm to room temperature and stir overnight. 30 mL saturated NH_4Cl solution was then added to the reaction flask and allowed to stir for 1 hour. The

organic layer was separated and dried with $MgSO_4$; the solvent was removed via rotavap. The product ethyltriphenylsilane (ETPS) was recrystallized from isopropanol; the product isobutyltriphenylsilane (iBTPS) was recrystallized from methanol, using water as an antisolvent. Both products presented as white fluffy crystals. The structures were verified via ^{1}H and ^{13}C NMR.

For ETPS: ^{1}H NMR (400.13 MHz, $CDCl_3$) 7.54 (m, 6H), 7.37 (m, 9H), 1.39 (q, J = 7.8 Hz, 2H), 1.12 (t, J = 7.8 Hz, 3H)

^{13}C NMR (100.57 MHz, $CDCl_3$) 135.87, 135.40, 129.55, 128.04, 7.99, 5.27

For iBTPS: ^{1}H NMR (400.13 MHz, $CDCl_3$) 7.54 (m, 6H), 7.36 (m, 9H), 1.95 (heptet, J = 6.6 Hz, 1H), 1.41 (d, J = 6.8 Hz, 2H), 0.90 (d, J = 6.6 Hz, 6H)

^{13}C NMR (100.57 MHz, $CDCl_3$) 136.00, 135.93, 129.47, 127.99, 26.77, 24.96, 23.68

2.3.2.5 Diluent Experiments

Diluent reactions were carried out under the same heptane grafting conditions previously established. 5 wt% of the diluent was used in addition to the 5 wt% of VTMS. Additional phenyllithium was required to replace the methoxy groups present on the diluents molecules. A typical diluent reaction was carried out as follows. Prior to reaction, the Parr was placed under vacuum for 5 minutes to remove any atmosphere from the reactor. 50 mL anhydrous heptane (0.341 mol); 1.8 mL VTMS (11.15 mmol; 5 wt% wrt heptane); a 1.1 mL of a solution of DTBP in anhydrous heptane (750 ppm;); and 5 wt% of diluent (1.8 mL ETMS; 1.7 mL TMOS) was added to the reactor, which was then placed under inert atmosphere. The reaction vessel was heated to 200°C for 7 hours with vigorous stirring. After the reaction mixture had cooled to room temperature, 1.6 *M* PhLi in di-*n*-butylether (4:3 PhLi:–OMe; 51 mL for ETMS reactions; 57 mL for TMOS reactions) was added and the reaction mixture was stirred for 3 days. 20 mL of a solution of saturated ammonium

chloride was added to quench the excess PhLi; the organic layer was dried with $MgSO_4$ and rotovapped to remove $n$$Bu_2O$ and the unreacted heptane.

2.3.3 Instrumentation

Mass spectrometry analysis was performed on an Applied Biosystems Voyager DE STR instrument. The matrix was dithranol, and silver trifluoroacetate was used as an ionization agent. As such, the m/z of silver (109) is included in the peaks present in the MALDI spectra.

Chromatotron separations were carried out using a Chromatotron 7924T from Harrison Research. The layer thickness was 2 mm, prepared using approximately 60 g of silica (60 PF_{254} from EMI) in 120 mL DI H_2O. The eluent reservoir was stationed 55 cm above the surface of the laboratory bench. Bands were visualized using a UV lamp at 254 nm.

Graft separation was carried out using a Waters 2690 Separations Module. The stationary phase used was a Supelcosil PLC-Si column; the mobile phase was 99:1 hexanes:EtOAc; and the method of detection was UV-Vis. Two columns were used in series to increase throughput. In a typical separation run, 400 μL of the crude product mixture was injected and each peak was collected in a separate flask. The identity of each peak was verified via HPLC, ^{1}H NMR, and MALDI. These collections were combined, concentrated, and repeated numerous times until enough material was present for 2D NMR (approximately 10-15 mg per sample).

Product fractions thus collected were analyzed via edited heteronuclear single quantum correlation (edited HSQC) and HSQC-total correlation spectroscopy (HSQC-TOCSY) using a Bruker DRX-500 with an indirect detection probe. To minimize the prep HPLC collection time for the samples, solvent-matched Shigemi tubes were used, which

require very small amounts of NMR lock solvent. All experiments were run using standard Bruker pulse sequences for edited HSQC (hsqcedetgp)[18] and HSQC-TOCSY (hsqcetgpml).[19] ^{1}H and ^{13}C NMR spectra were collected on a Varian Mercury Vx 400, using $CDCl_3$ as the lock solvent.

Dynamic light scattering (DLS) experiments were performed at 20°C by a single-mode optical fiber coupled to an avalanche photodiode detector using a Dynapro DLS. Due to the similarity of the refractive indices of hexane (RI = 1.387 *n*20/D) and VTMS (RI = 1.392 *n*20/D), DLS experiments were conducted with dodecane (RI = 1.421 *n*20/D) for higher contrast. Solutions of varying concentrations of VTMS (5, 8, 10, 20, 30, 40, 50 wt%) in dodecane were prepared and analyzed via DLS.

2.4 Results and Discussion

2.4.1 Dodecane as Model Compound

Our initial experiments investigated dodecane as a model compound.[16a, 16c] To accurately analyze the reaction products and minimize inaccuracy due to crosslinking from inherent trace amounts of moisture, we decided to "cap" the methoxy groups via a substitution reaction with phenyllithium (PhLi) prior to analysis, as seen in Figure 2.1.[16a]

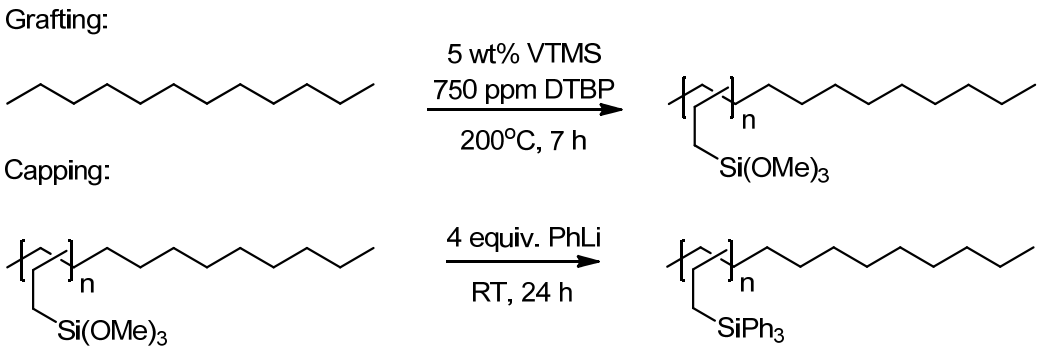

Figure 2.3. Di-*tert*-butyl peroxide initiated grafting reaction (*top*) of VTMS onto dodecane. Capping reaction (*bottom*) replacing labile methoxy groups with moisture-stable phenyl groups for analysis.

50 mL dodecane, 5 wt% VTMS, and 750 ppm DTBP were heated at 200°C for 7 hours. After cooling to room temperature, excess PhLi in dibutylether (nBu$_2$O) was added and allowed to stir for 24 hours. The excess PhLi was quenched with saturated ammonium chloride (NH_4Cl), and the organic layer removed and concentrated. Unreacted dodecane was removed via Kugelrohr. Analysis of the product mixture (referred to as dodecane-*g*-VTPS) by ^{1}H NMR (Figure 2.4) showed an average of 2.2 grafts per dodecane molecule, with a maximum of 6 grafts seen via MALDI analysis (Figure 2.5).

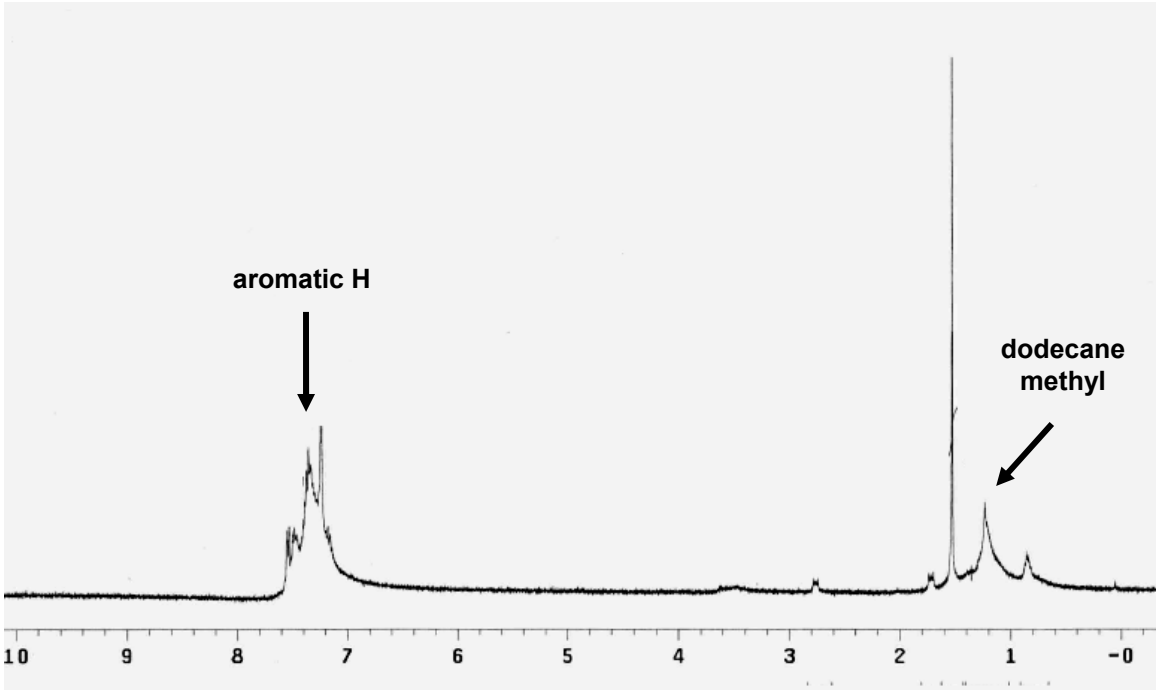

Figure 2.4. ^{1}H NMR spectrum of dodecane-*g*-VTPS with one day PhLi capping reaction. Integrations are not pictured.

Determination of the average number of grafts per dodecane molecule was calculated from the ^{1}H NMR of the product mixture, shown in Figure 2.4. The integration of the signal resulting from the terminal methyl groups in the dodecane backbone (at δ1.2) was compared to the integration of the phenyl signal (from δ6.8-7.6). The molecular weights of the various grafted fractions can be seen in Table 2.1, in addition to the molecular weights with the addition of silver (m/z 109). Silver complexes preferentially with the phenyl rings of the capped, grafted products, and aids ionization.[20]

Table 2.1. Molecular weights of various fractions of dodecane-*g*-VTPS, including *m/z* of Ag^+ (109).

Number of grafts	[MW]	$[MW + Ag]^+$
1	456	565
2	743	852
3	1029	1138
4	1316	1425
5	1602	1711
6	1889	1998
7	2175	2284
8	2461	2570

The MALDI spectrum of a representative dodecane-*g*-VTPS product mixture can be seen in Figure 2.5. The *m/z* visible in the MALDI spectrum corresponds to the molecular weight of the particular grafted fraction in addition to silver. We were unable to separate discrete grafted fractions via Kugelrohr.

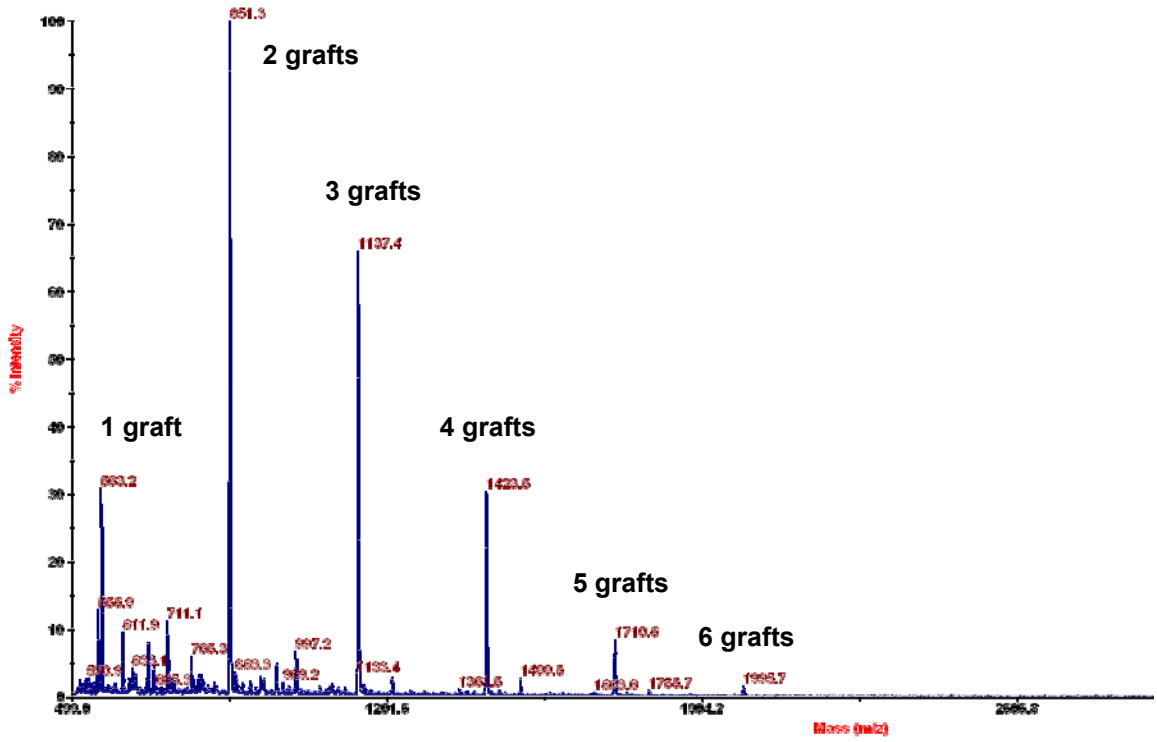

Figure 2.5. Ag-assisted MALDI spectrum of dodecane-*g*-VTPS. *m/z* includes that of Ag^+ (109).

It is important to note that MALDI is a semi-quantitative method of analysis and that the relative intensities observed do not necessarily correlate to the actual distribution of grafted products.

2.4.2 Capping Reaction with Phenyllithium

It soon became apparent that a one day reaction with PhLi was not sufficient to fully replace all of the methoxy groups. Upon standing, a white solid precipitated from the crude product mixture. ^{1}H NMR analysis of this precipitate revealed the presence of unsubstituted methoxy groups in the δ3.5 region of the spectrum, as shown in Figure 2.6.

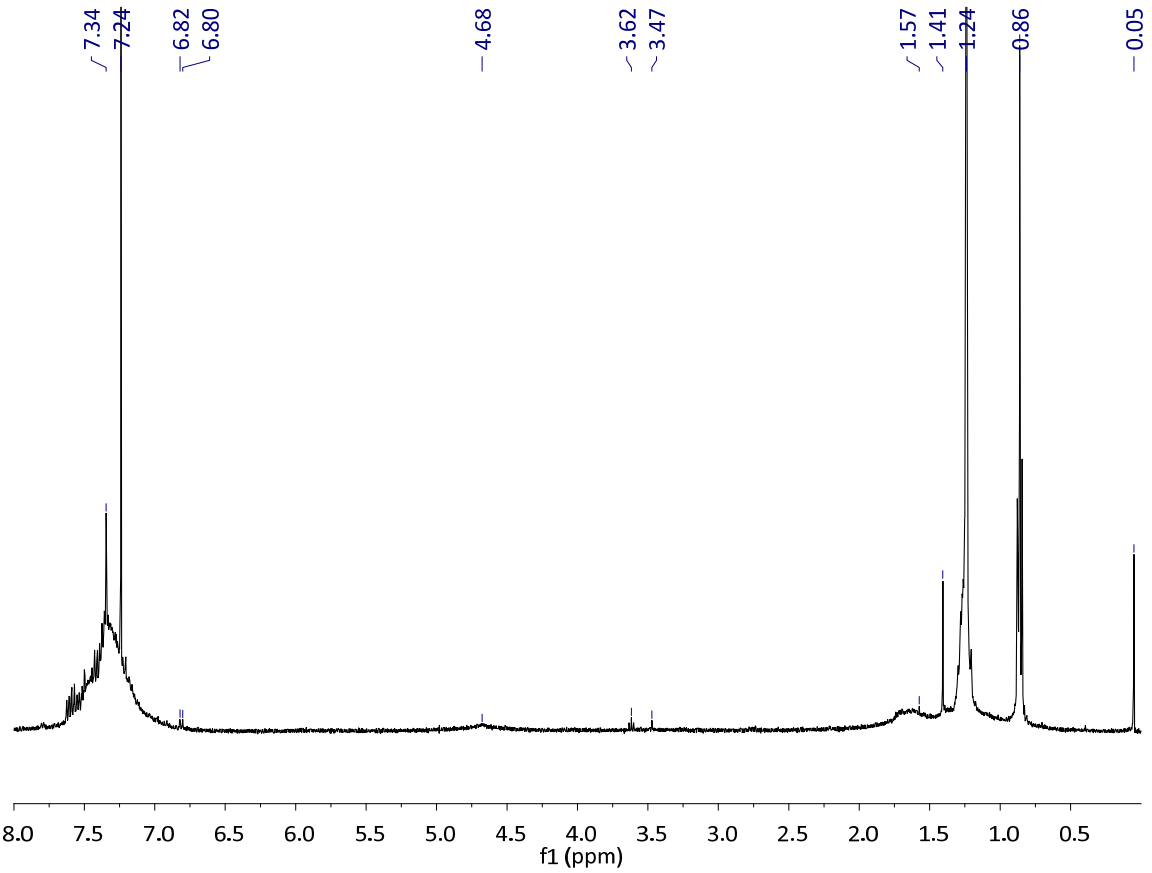

Figure 2.6. ^{1}H NMR spectrum of precipitate resulting from 24 hour PhLi capping reaction.

The sheer steric bulk of the phenyl rings may preclude the total substitution of the methoxy groups, particularly on the higher grafted products. As a consequence, we continued using PhLi as the capping agent, but decided to increase the time required for the capping reaction.

In order to determine the optimum amount of time that would be required to substitute all of the methoxy groups in the grafted material, the reactions were carried out in a Radleys Carousel 12 reaction station. This allowed us to start and run six reactions under identical conditions, capping and working up one reaction per day over the course of six days. The samples were worked up as previously described: aqueous NH_4Cl was added to quench the excess PhLi; the organic phase was separated and dried with $MgSO_4$; and

solvents were removed via rotavap. Due to the small sample size (5 mL) of dodecane, excess unreacted dodecane was not removed via Kugelrohr as previously, and we therefore could not determine the average number of grafts per backbone.

The crude product mixtures were then analyzed via ^{1}H NMR, and the heights of the methoxy peaks (δ3.5-3.7) compared, as seen in Figure 2.7. The overlain spectra are labeled according to the length of time the capping reaction was carried out.

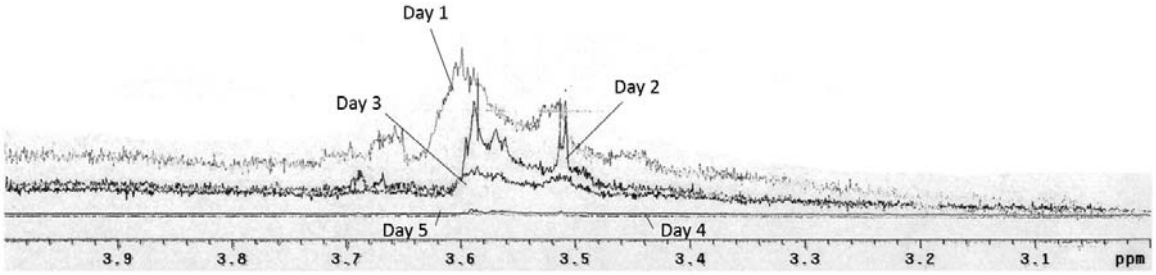

Figure 2.7. Overlaid NMR spectra from carousel reactions, showing relative heights of methoxy peaks.

Formation of a precipitate during the workup of samples from days 1-3 prevented us from obtaining representative NMR samples of the final product mixture, so the quantitative extent of substitution could not be determined. However, after the third day of reaction with PhLi, the methoxy peak was determined to be insignificant. Additionally, after this reaction time, no precipitate was seen upon prolonged standing of the reaction mixture. Virtually no methoxy peak was observable in samples from days 4-6. Three days was then used as the standard reaction time for subsequent capping reactions with PhLi. This is significantly longer than the one hour reaction time reported in literature.[16a]

Analysis of the product mixture resulting from the 3-day capping reactions showed an average of 2.2 grafts per molecule, comparable to the results from the 1-day capping reactions. However, the maximum number of grafts seen via MALDI increased to 8 (*m/z*: 2567; Table 2.1), as seen in Figure 2.8. No methoxy peaks were seen via ^{1}H NMR.

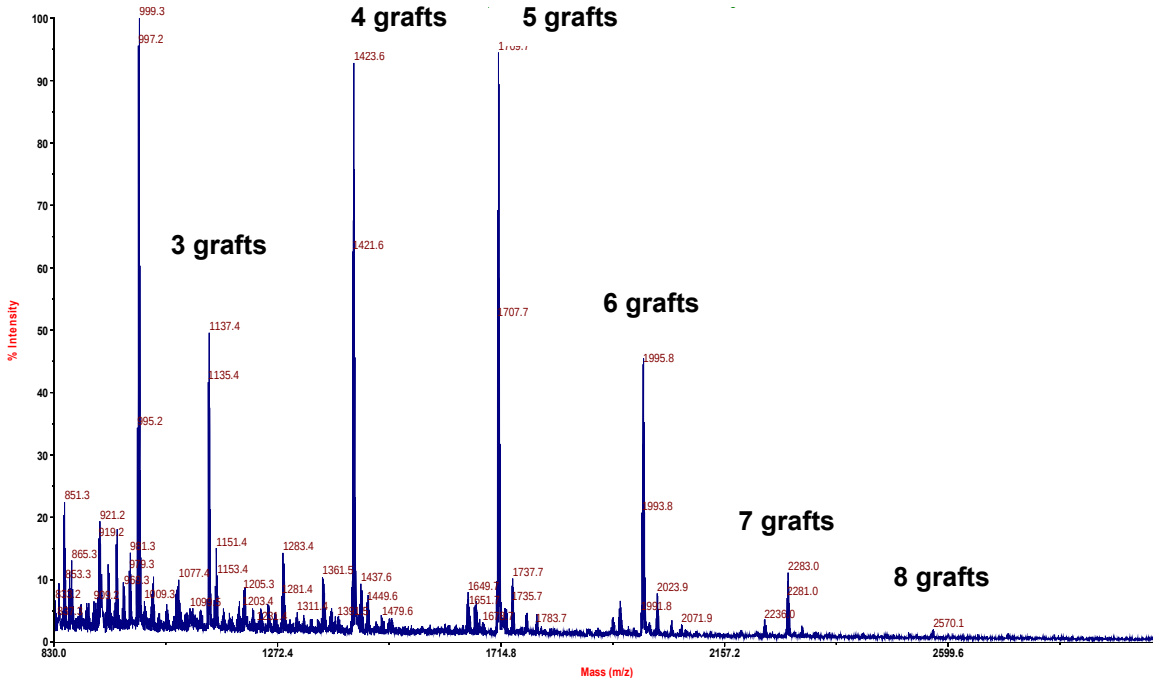

Figure 2.8. Ag-assisted MALDI spectrum of dodecane-*g*-VTPS with extended PhLi capping time. *m/z* includes that of Ag^{+} (109). Grafts 3-8 are visible; lower grafted fractions are present but not visible in this particular spectrum.

The presence of the 8-grafted product fraction challenged two commonly held tenets in the literature. First, that a one day capping reaction is sufficient to fully replace the methoxy groups on the grafted products; and second, that intramolecular hydrogen abstraction proceeds only via a 1,5-shift—this would result in a maximum of six grafts per dodecane molecule, with every other carbon of the backbone substituted. Indeed, several research groups have reported a maximum of six grafts per dodecane molecule using similar reaction

conditions with a one-day PhLi capping reaction.[16a, 16c] The presence of 8-grafted dodecane molecules in the product mixture suggests that the accepted 1,5-hydrogen shift can be only one of the modes of reaction. The mechanisms of 1,3-, 1,4-, and 1,5-intramolecular hydrogen shifts, including the transition states of these reactions, can be seen in Figure 2.9.

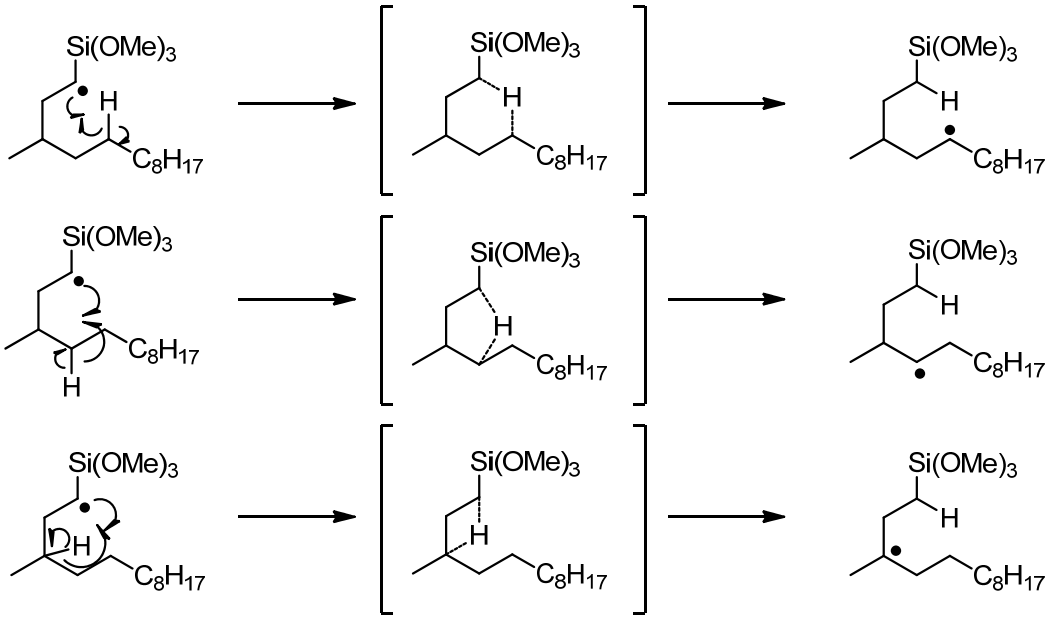

Figure 2.9. Radical intermediates formed from 1,5-, 1,4-, or 1,3-hydrogen shifts (*top to bottom*). Only the 1,5-shift is assumed in literature.

The 1,3-intramolecular hydrogen shift proceeds via a 4-membered transition state and would result in two grafts per carbon of the dodecane backbone. The 1,4-intramolecular hydrogen shift occurs via a 5-membered transition state, which would result in a graft on every carbon of the dodecane backbone. Finally, a 1,5-intramolecular hydrogen shift, occurring via a 6-membered transition state, would yield a silane graft on every other carbon of the dodecane backbone.

We took into consideration the possibility that the perceived increase in grafts per molecule could be a result of oligomeric grafting (see Figure 2.2). Although oligomeric grafting and even homopolymerization is common with other post-reactor additives, such as maleic anhydride,[21] vinylsilanes typically react via inter- or intramolecular H-abstraction.[16b, 17a] In order to test the possibility of oligomeric grafting, we doubled the amount of VTMS in the system to 10 wt%. If oligomeric grafting were contributing to the product formation, an increase in available VTMS should result in an increase in the amount of grafts per molecule. The MALDI spectrum for a typical reaction with 10 wt% VTMS can be seen in Figure 2.10.

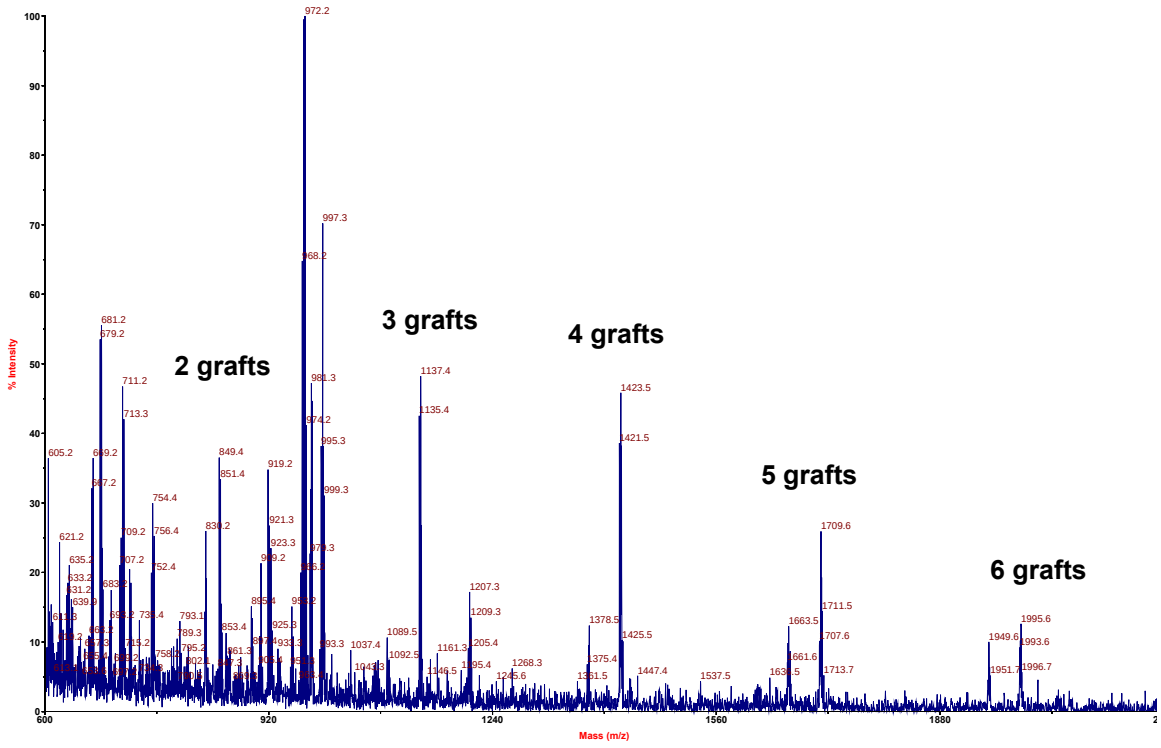

Figure 2.10. Ag-assisted MALDI spectrum of dodecane-*g*-VTPS with 10 wt% VTMS. *m/z* includes that of Ag^+ (109).

Up to 6 grafts per dodecane molecule can be seen at this higher loading of VTMS; higher grafted fractions (i.e. more than 6 grafts per dodecane backbone) were not observed. The absence of these higher molecular weight fractions indicates that oligomeric grafting was not responsible for the increase in observed grafts per molecule, and suggested that the 1,3- or 1,4-intramolecular hydrogen shifts could instead be the cause. This discovery was quite exciting and formed the basis for our next steps.

2.4.3 Heptane as Model Compound

We decided to begin using heptane as our model substrate, rather than dodecane, due to ease of product analysis. The shorter hydrocarbon chain has fewer grafting sites, resulting in a smaller range of possible products, which can be more easily separated.

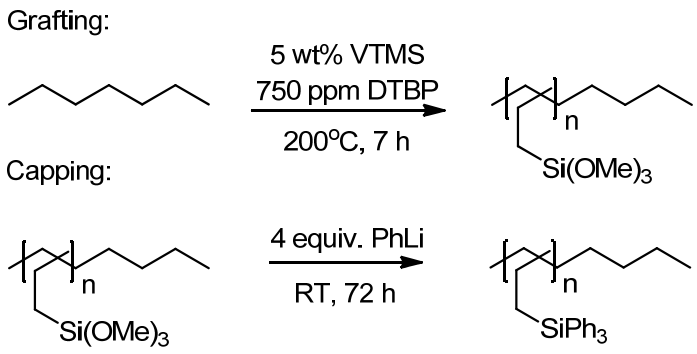

Figure 2.11. Di-*tert*-butyl peroxide initiated grafting reaction (*top*) of VTMS onto heptane. Capping reaction (*bottom*) replacing labile methoxy groups with moisture-stable phenyl groups for analysis; note extended time of capping reaction.

The lower boiling point of heptane, however, necessitated carrying out the reaction in a Parr autoclave in order to reach the temperatures required for the reaction; all other reaction conditions were kept identical. Isolation of the grafted product mixture was achieved by removal of the unreacted heptane via rotavap, rather than distillation as with dodecane.

Analysis of the product mixture (heptane-*g*-VTPS) via MALDI showed a range of 1-6 grafts, shown in Figure 2.12. As with dodecane, we were unable to separate discrete grafted fractions via distillation or Kugelrohr. The molecular weights of the various grafted fractions can be seen in Table 2.2, in addition to the molecular weights with silver.

Table 2.2. Molecular weights of various fractions of heptane-*g*-VTPS, including *m/z* of Ag^+ (109).

Number of grafts	[MW]	$[MW + Ag]^+$
1	386	495
2	672	781
3	958	1067
4	1244	1353
5	1530	1639
6	1816	1925

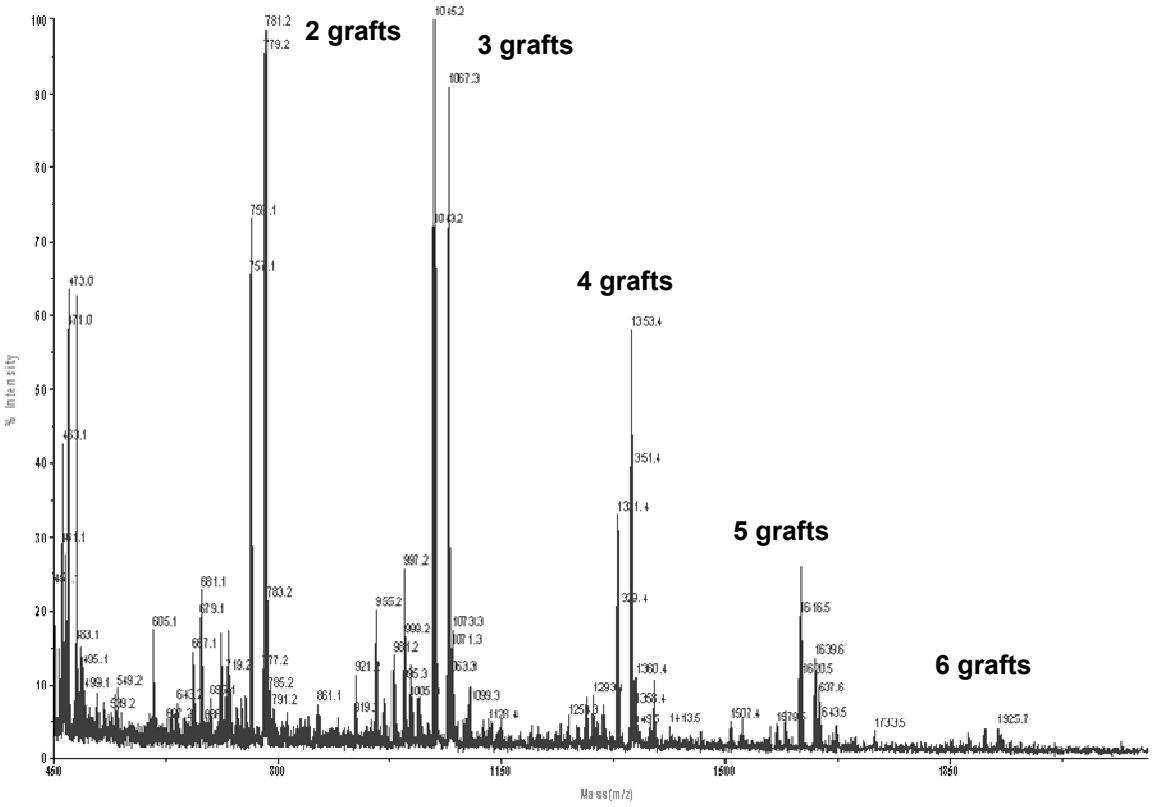

Figure 2.12. Ag-assisted MALDI spectrum of heptane-*g*-VTPS. *m/z* includes that of Ag^+ (109).

Initial reactions using heptane as a model compound encountered problems with reproducibility—the range of grafted products varied from reaction to reaction. We speculated that the issue might lie in the analysis, rather than the initial reaction. We considered that the silver ion used as an additive to increase ionization in the MALDI analysis might be complexing preferentially with the higher grafted products, rather than the lower grafted fractions.[20] Silver ions are good ionizing agents for polymers containing double bonds and aromatic moieties (e.g. polystyrene, polybutadiene), and poor ionizing agents for polymers that do not contain multiple bonds.[22] If this were the case, we would expect to see more of the multiply grafted products than was truly representative of our product distribution—the lower grafted fractions would be less likely to complex and ionize, and, as

such, would be underrepresented in the MALDI spectrum. To eliminate the need for additional ionization agents such as silver in MALDI, we considered a number of alternative capping agents, described below.

2.4.4 Alternative Capping Agents

The first alternative we considered was methyllithium (MeLi), which, when used as a capping agent, would result in a lower molecular weight of the grafted product; this would enable us to use alternative ionization techniques such as fast atom bombardment (FAB). The useful molecular weight limit for FAB-MS analysis is 6 kDa, while MALDI is typically used for compounds larger than this (up to several hundred thousand kDa).[23] Although both techniques use a matrix to assist in desorption, FAB does not require additional ionization agents.

The MeLi capping agent was originally used with the dodecane model compound. We also anticipated that the smaller capping agent would cut down on reaction time, as the steric hindrance to full substitution of the methoxy groups would be minimized. Complete substitution of the methoxy groups was indeed observed via ^{1}H NMR. However, product analysis was complicated by the overlap of the methyl group signal in the ^{1}H NMR with the other alkyl groups adjacent to silicon. Additionally, extensive fragmentation of the molecular ion was seen when the crude product mixture was analyzed using FAB-MS, and the molar masses of the capped grafted products were too low to be accurately identified via MALDI due to overlap between the m/z of the sample and that of the matrix (dithranol, MW = 226.23 g·mol^{-1}). We next investigated replacing the PhLi capping agent commonly found in literature with a pyridyllithium capping agent, synthesized via a metal-halogen exchange reaction.[24]

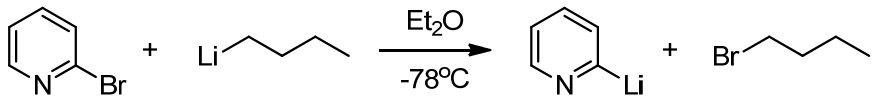

Figure 2.13. Synthesis of pyridyllithium capping agent.

However, upon introduction of the capping agent to the cooled Parr autoclave, a significant pressure buildup occurred, forcing us to discontinue addition of the capping agent. MALDI analysis of the product mixture showed that the methoxy groups had not been fully substituted. Complicating the analysis was the mix of substitution products, with both butyl and pyridyl substitution at the silicon. To avoid this product mixture, arising as a result of incomplete transmetallation, we used a commercially available solution of 2-thienyllithium in THF and hexanes as our capping agent. However, upon workup of the reaction, it was discovered that the reaction mixture had formed a brown, sticky mass, most likely due to polymerization of the excess thienyllithium. This was confirmed via MS, and the use of this capping agent was also abandoned. Ultimately, we decided to continue the use of PhLi as a capping agent, and treat our MALDI data as semi-quantitative; that is, we could use the MALDI analyses to garner an idea of the range of grafted products, but could not assume that the size of the peaks correlated directly to the graft distribution. We decided, rather, to focus on separating the various PhLi-capped grafted fractions by number of grafts in order to analyze each fraction independently.

2.4.5 Graft Analog Synthesis

In order to obtain a first approximation of the chemical shifts for the protons and carbons nearest to the triphenylsilyl grafts, two graft analogs were synthesized. The starting materials used were the commercially available silanes ethyltrimethoxysilane (ETMS) and

isobutyltrimethoxysilane (iBTMS), as shown in Figure 2.14. These alkyltrimethoxysilanes were substituted with PhLi in the same manner as our actual heptane-*g*-VTMS.

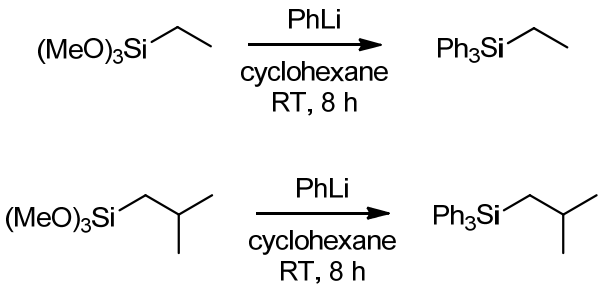

Figure 2.14. Synthesis of graft analogs. *Top*, ethyltrimethoxysilane (ETMS) is reacted with PhLi to yield ethyltriphenylsilane (ETPS). *Bottom*, isobutyltrimethoxysilane (iBTMS) is reacted with PhLi to yield isobutyltriphenylsilane (iBTPS).

The excess PhLi was quenched with aqueous NH_4Cl; the organic layer was then separated and dried using $MgSO_4$. Removal of the solvent and recrystallization yielded the product alkyltriphenylsilanes, both of which were white crystalline solids. Ethyltriphenylsilane, or ETPS, contains a methylene group *a* to the silicon and a methyl group *β* to the silicon; isobutyltriphenylsilane, or iBTMS, also contains a methylene group *a* to the silicon, in addition to a methine group *β* to the silicon and two methyl groups *γ* to the silicon. Although the synthesized molecules are not wholly identical to fragments of the heptane-*g*-VTPS products, the similarity between the two allowed Dr. Pamela Pollet and Dr. Les Gelbaum to determine the regions of interest for the methine groups in the advanced 2D NMR experiments. For details regarding the ^{1}H and ^{13}C NMR spectra of these compounds, refer to the Experimental Details section (page 19).

2.4.6 Theoretical Considerations

Experimental results have shown that multiple grafts per heptane backbone are not uncommon. At first, this is surprising, given the large excess of heptane used—one would expect the majority of the product mixture to be singly-grafted. Furthermore, steric considerations would seem to prohibit the formation of highly-grafted molecules. Figure 2.15 shows a ball-and-stick model of a heptane molecule with grafts at the 2 and 6 positions, prior to the capping reaction (i.e., where the methoxy groups have not yet been replaced by phenyl groups). Even with only two grafts present on the backbone, the molecule is already quite bulky.

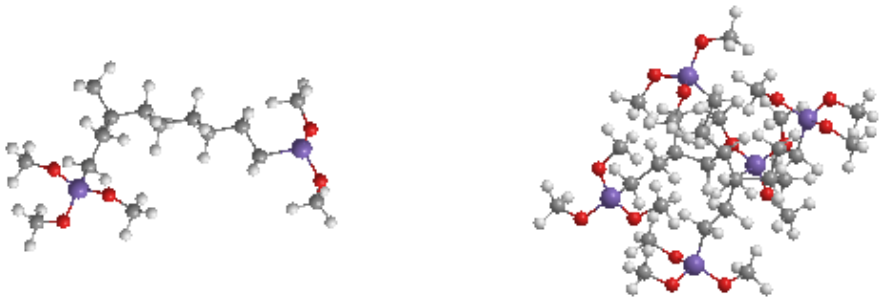

Figure 2.15. Ball-and-stick model of heptane with: *left*, 2 methoxy-substituted grafts at the 2 and 6 positions; *right*, 5 methoxy-substituted grafts at positions 2-6.

The penta-grafted model on the right Figure 2.15, is so sterically hindered that it is no longer clear where the heptane backbone is.

It is commonly held that the initial silyl addition intermediate undergoes an intramolecular hydrogen atom transfer, resulting in a new radical center on the hydrocarbon backbone.[16a] This is followed by the addition of another vinyltrimethoxysilane to the newly formed radical site on the backbone, assumed to occur primarily via a 1,5-intramolecular

hydrogen shift. However, evidence that would confirm this 1,5-shift is lacking. To investigate the possibility of other concurrent modes of radical propagation, we initially looked at the energies of formation of the backbone radicals resulting from the 1,3-, 1,4-, and 1,5-intramolecular hydrogen shifts. The theoretical calculations described in this section were carried out by Dr. Charles Liotta using density functional theory (DFT) with the basis set B3LYP-6.31G*. It was assumed that the initial grafting event occurred at the second carbon of the heptane backbone.

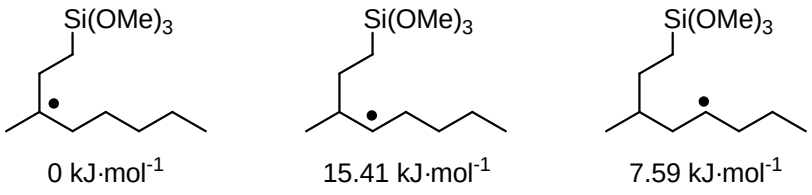

Figure 2.16. Relative energies of backbone radicals formed from intramolecular H-atom transfers.

As anticipated, the tertiary radical formed from the 1,3-intramolecular hydrogen shift is the most stable—one might expect the lower energy of this radical to be the cause of multiple grafts per hydrocarbon backbone. However, the energies of formations of the transition states leading to these radicals must also be considered. Dr. Liotta calculated these energies for the 1,3-, 1,4-, and 1,5-intramolecular hydrogen transfers; as above in Figure 2.16, he assumed that the initial grafting event occurred at the second carbon of the heptane backbone. The stereochemistries of the hydrogen transfer transition states were also considered. All energies reported are relative to the energy of formation of a 1,5-intramolecular hydrogen transfer with all equatorial substitutents in the 6-membered transition state, shown below in Figure 2.17.

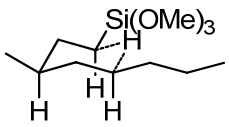

0 kJ·mol^{-1}

Figure 2.17. Transition state energy for 1,5-intramolecular transfer where all substitutents (methyl, trimethoxysilyl, and propyl) are equatorial in the 6-membered transition state.

This stereoisomer was found to have the lowest energy of formation, as expected—all three of the substituents are equatorial, minimizing unfavorable transannular interactions.

For the 1,3-intramolecular hydrogen transfer, only one stereoisomer was considered—that where the bulkiest substitutents, the trimethoxysilyl group and the pentyl group, are *trans* to one another on the 4-membered transition state.

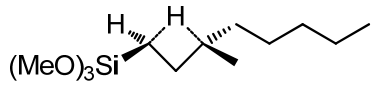

83.57 kJ·mol^{-1}

Figure 2.18. Relative transition state energy for 1,3-intramolecular hydrogen transfer.

Again, the energy is reported in reference to that of the transition state shown in Figure 2.17. The relative activation energy was found to be 83.57 kJ·mol^{-1}; this was the highest activation energy calculated for any of the intramolecular hydrogen shifts. Although the resulting tertiary radical is the most stable due to hyperconjugation, the energy required to form this radical is quite high.

For the 1,4-intramolecular hydrogen transfer, two stereoisomers of the 5-membered transition state were considered, shown in Figure 2.19.

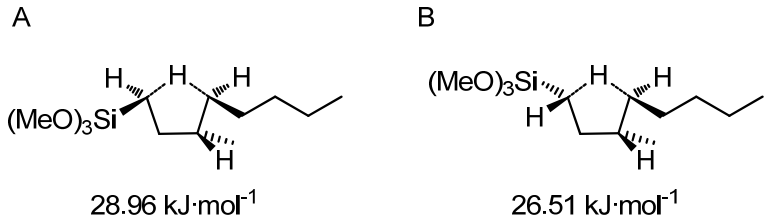

Figure 2.19. Relative transition state energies for 1,4-intramolecular hydrogen transfer.

In structure A, the bulkiest groups (the trimethoxysilyl group and the butyl group) are *cis* to one another; in structure B, they are *trans* to one another. In both the *cis* and the *trans* cases, the transition state energies (28.96 and 26.51 kJ·mol^{-1}, respectively) are lower than that of the 1,3-intramolecular hydrogen transfer intermediate.

For the 1,5-intramolecular hydrogen transfer, there are many more stereochemical possibilities for the arrangement of the 6-membered transition state. Five stereoisomers were considered, shown in Figure 2.20. The equatorial or axial positions of the three substitutents, methyl, trimethoxysilyl, and propyl, are summarized in Table 2.3, along with their relative energies.

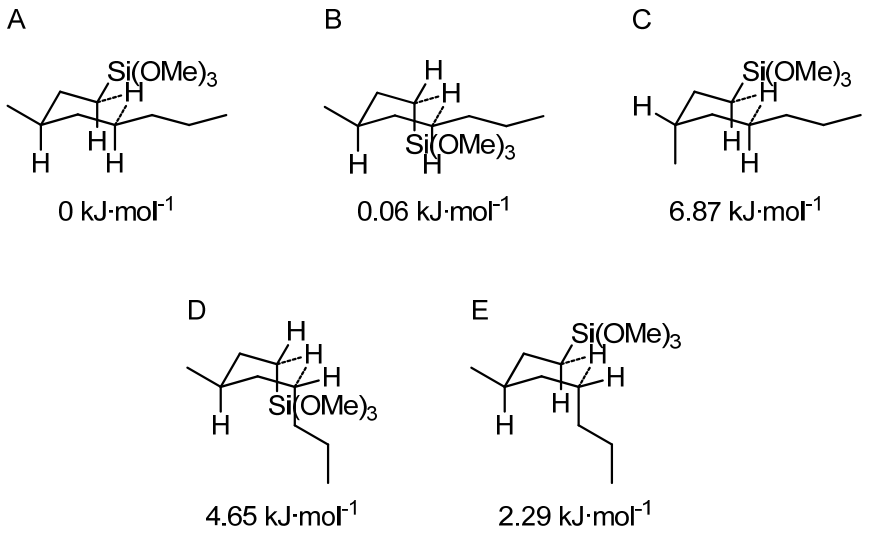

Figure 2.20. Relative transition state energies for 1,5-intramolecular hydrogen transfer.

Table 2.3. Positions of methyl, trimethoxysilyl, and propyl substituents in 1,5-hydrogen transfer transition states A-E, with energies of said transition states.

Structure	–Me	–Si(OMe)$_3$	–Pr	Energy (kJ·mol^{-1})
A	eq	eq	eq	0
B	eq	ax	eq	0.06
C	ax	eq	eq	6.87
D	eq	ax	ax	4.65
E	eq	eq	ax	2.29

Structure A is the aforementioned reference point—all the substitutents are equatorial and the energy is given as 0 kJ·mol^{-1}. Comparison of structure A, where the trimethoxysilyl group is equatorial, and structure B, where it is axial, shows little difference between the transition state energies. A carbon-carbon single bond is 1.53 Å long, while a carbon (sp^3)-silicon bond is 1.88 Å long,[25] meaning that the trimethoxysilyl group could be positioned further away from the ring when in the axial position. This would minimize any unfavorable interactions between the substituents. The highest energy transition state is represented by structure C where the inflexible methyl group is in an axial position. In total, the difference between the

transition states for the 1,4-intramolecular hydrogen transfer and the 1,5-event differ only by approximately 15 $kJ \cdot mol^{-1}$.

Having computational support that the 1,4- and 1,5-intramolecular hydrogen shifts do not differ greatly in energy, we sought out evidence of these concurrent shifts in our product mixture. It must be recognized that as the extent of grafting increases, the number of possible products increases exponentially. There are not only regioisomers formed but also stereoisomers, making the NMR spectra both complex and difficult to interpret. As a consequence, we chose to isolate specifically the digrafted and the pentagrafted products of the heptane model compund to study via 2D NMR techniques, namely, edited heteronuclear single quantum correlation (edited HSQC) and HSQC-total correlation spectroscopy (HSQC-TOCSY).

2.4.7 Separation and Analysis of Grafted Product Mixture

2.4.7.1 DEPT 135 Analysis

To quantify the number of grafts per heptane molecule, distortionless enhancement by polarization transfer (DEPT) NMR experiments were used, permitting us to distinguish between 1°, 2°, 3°, and 4° carbons, as shown in Figure 2.21.

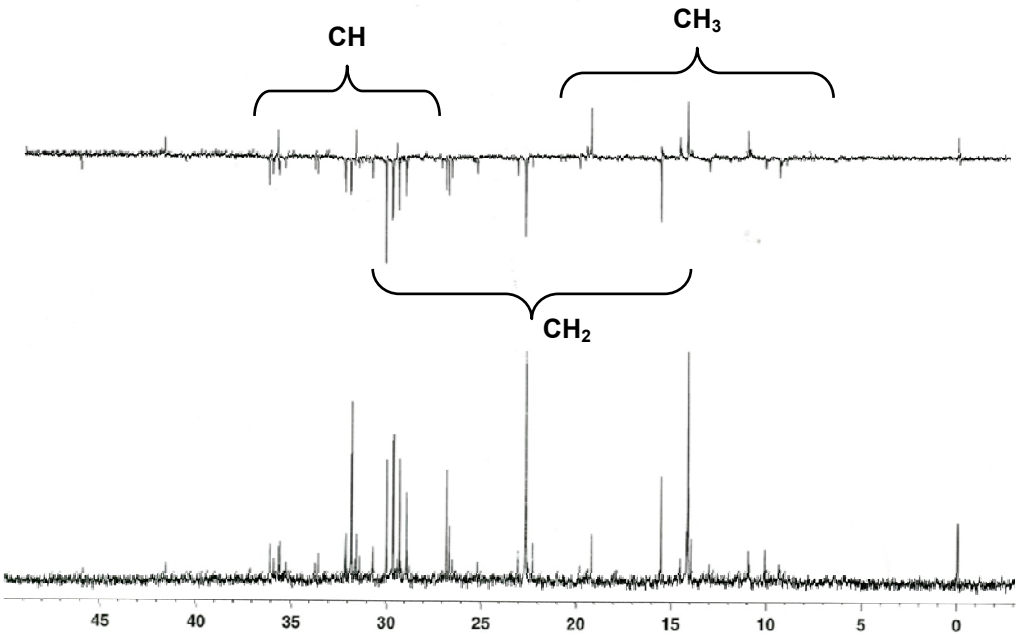

Figure 2.21. Normal ^{13}C NMR spectrum of heptane-*g*-VTPS mixture, *bottom*, and DEPT 135 mixture of same mixture, *top*.

In a DEPT 135 spectra, the chemical shifts are the same as in a ^{13}C NMR spectrum; however, CH and CH_3 groups are phased up, while CH_2 groups are phased down. Quaternary carbons do not appear in a DEPT 135 spectrum. Assuming that the terminal methyl groups are unreactive due to the formation of relatively unstable primary radicals, each graft-bearing backbone site is a tertiary carbon, whereas unreacted backbone sites are secondary carbons. Examples of these carbons can be seen in Figure 2.22, which depicts a hypothetical tri-grafted product.

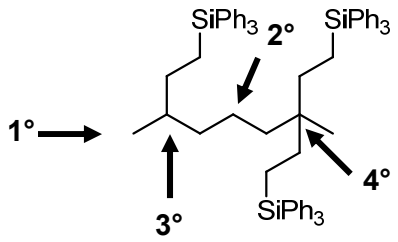

Figure 2.22. Examples of methyl (1°), methylene (2°), methine, (3°), and quaternary (4°) carbons on a hypothetical tri-grafted product.

Any methine groups in a DEPT spectrum would allow us to determine the number of chemically non-equivalent grafting sites. Methyl carbons appear upfield from methine carbons (δ10-30 and δ25-60, respectively),[23] permitting us to distinguish between the two classes of carbons even though they have the same phasing in a DEPT 135 spectrum. DEPT 135 spectra of the unseparated product mixture were dominated by the peaks from the unreacted heptane, but small peaks corresponding to new methine carbons were seen, as shown in the top spectrum in Figure 2.21.

2.4.7.2 Chromatotron Separations

In order to obtain a more concentrated sample containing these methine carbons, the product mixture was then separated via chromatotron—a form of normal-phase radial chromatography—using hexane as the eluent. Although full separation of the product mixture was not achieved, we were able to separate the products based on weight, i.e., number of grafts per heptane molecule. These fractions were analyzed via ^{1}H NMR, ^{13}C NMR, DEPT, and MS using electrospray ionization (EI), CI, and MALDI. In addition to the grafted fractions, the following side products were identified: vinyltriphenylsilane (VTPS, formed from the substitution of unreacted VTMS with PhLi); phenethyl-triphenylsilane (formed from attack of the phenyl anion at the double bond of VTMS or VTPS); and a di-

heptane monograft. The structures of these side products can be seen in Figure 2.23. We have been able to successfully reproduce this separation a number of times.

Table 2.4. Identities of eluent bands from a typical normal phase chromatotron separation. Structures assigned via ^{1}H NMR, ^{13}C NMR, and MALDI.

Chromatotron band	Proposed structures
1	Di-heptane monograft
2	Mono-graft Di-heptane monograft VTPS
3	Phenethyl-triphenylsilane
4 and 5	Di-graft
6	Tri-graft
7	Tetra- and penta-graft

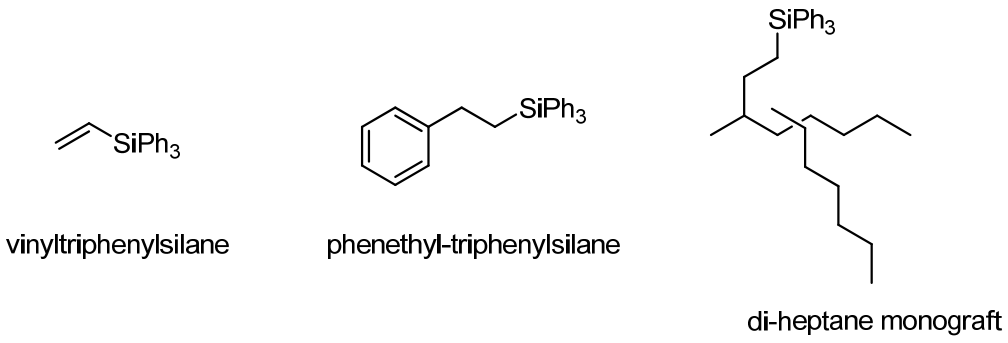

Figure 2.23. Side products of grafting reaction with heptane. Structures assigned via ^{1}H NMR, ^{13}C NMR, and MALDI.

Grignard reagents such as phenylmagnesium bromide are known in the literature to add to the double bond of vinylsilanes when present in excess, so the presence of phenethyl-triphenylsilane was not unexpected.[26] Likewise, peroxides are known to cause the formation of carbon-carbon crosslinks in PE chains;[3, 16c] we posit that such a reaction yielded the di-heptane monograft seen in Figure 2.23, although a grafted carbon-carbon cross-linked model

compound has not been identified in the literature before. The side products, therefore, do not indicate that any unexpected side reactions are occurring.

2.4.7.3 Prep HPLC Separations

The product mixture from the heptane reaction was also separated via semi-preparative HPLC, following a method adapted from Spencer *et al.*[16a] The stationary phase used was a Supelcosil PLC-Si column; two columns were used in series to increase throughput. The optimal mobile phase that resulted in the greatest amount of separation was determined to be 99:1 hexanes:EtOAc, and the flow rate was 5 $mL \cdot min^{-1}$. The presence of the phenyl rings on the grafts renders the products ultraviolet light (UV) active, allowing us to use a UV-Vis detector. The resulting chromatogram of the separation can be seen in Figure 2.24; the HPLC was more efficient than the chromatotron, allowing for separation of the product mixture by number of grafts on a semi-preparative scale.

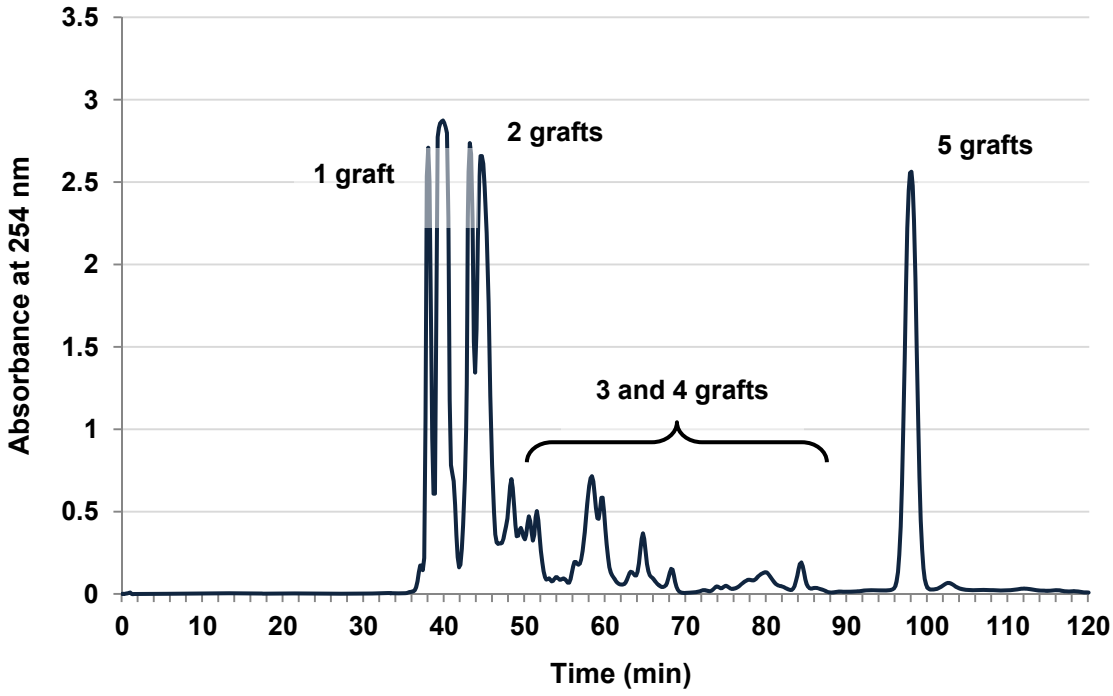

Figure 2.24. Semi-preparative HPLC chromatogram of typical heptane-*g*-VTPS product mixture. Peaks were collected, isolated, and identified via HPLC, ^{1}H NMR, and MALDI.

Elution of the product mixture begins after approximately 35 minutes. In order to initially identify the peaks, each peak was timed and collected. The individual peaks were then analyzed via ^{1}H NMR, to obtain the ratio of aromatic to aliphatic protons, and MALDI, to determine the molecular weights of the compounds present in the collected fraction. It was found that the di-grafted material eluted at approximately 40 minutes, while the penta-grafted material eluted after approximately 90 minutes, as seen above in Figure 2.24. We focused on the di- and penta-grafted material to gain the most structural information. It is important to note that the intensity of the peak does not necessarily correspond to the amount of grafted material present in the product mixture. The other grafted fractions, while collected and identified via MALDI, were not studied via 2D NMR. Several peaks are

observed for the tri- and tetra-grafted fractions; this is most likely due to the various possible regioisomers of these grafted fractions.

2.4.7.4 2D NMR Experiments: Di-Grafted Product Fraction

As described above, the di-grafted product fraction peak was identified in the prep HPLC chromatogram via repeated collection, concentration, and analysis via MALDI, and isolated over a series of elution runs with the goal of analyzing it via 2D NMR. 400 µL of the crude product mixture was injected for each run, which was then collected in "sections," in order to decrease the amount of time required for each run. Sections 1, 2, and 3 can be seen in Figure 2.25.

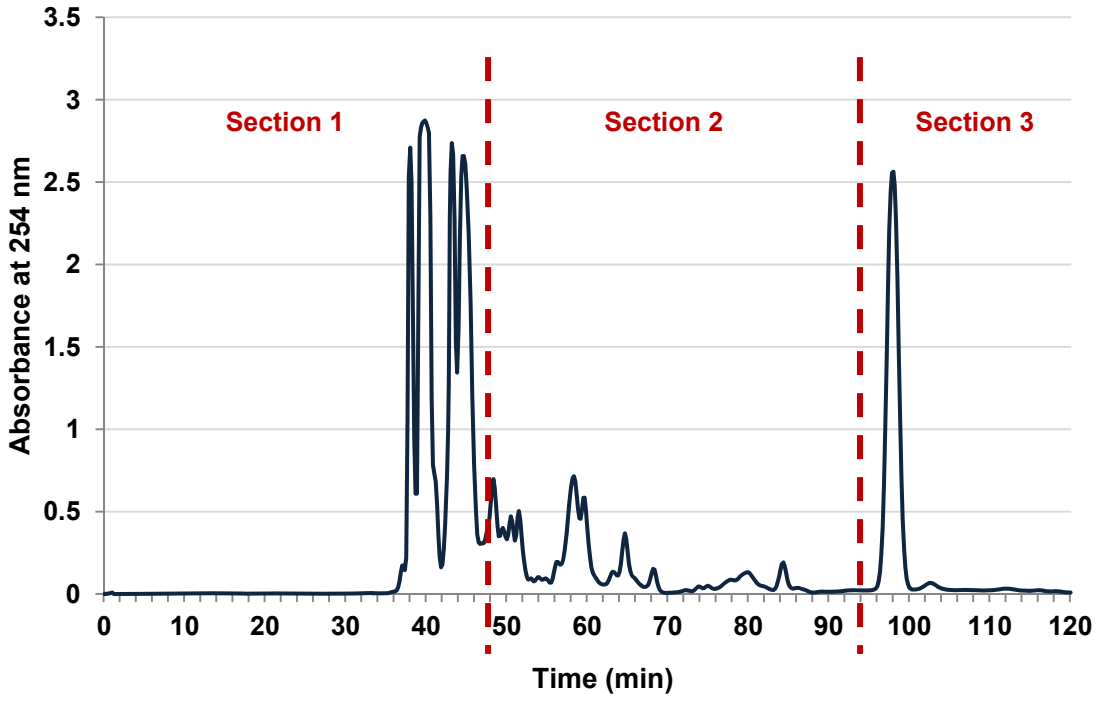

Figure 2.25. Semi-preparative HPLC chromatogram of typical collection run for heptane-g-VTPS, showing "sections."

Approximately 20 runs worth of each section was collected and concentrated. The purity of the section was then verified via semi-preparative HPLC. For Section 1, comprising the lower weight grafted fractions, it was important to verify that none of the higher weight grafted fractions had been collected, as these would remain on the column and contaminate subsequent runs. As can be seen in Figure 2.26, relatively little of Section 2 was collected in conjunction with Section 1, and this enabled us to shorten each run time for specific peak collection to 60 minutes.

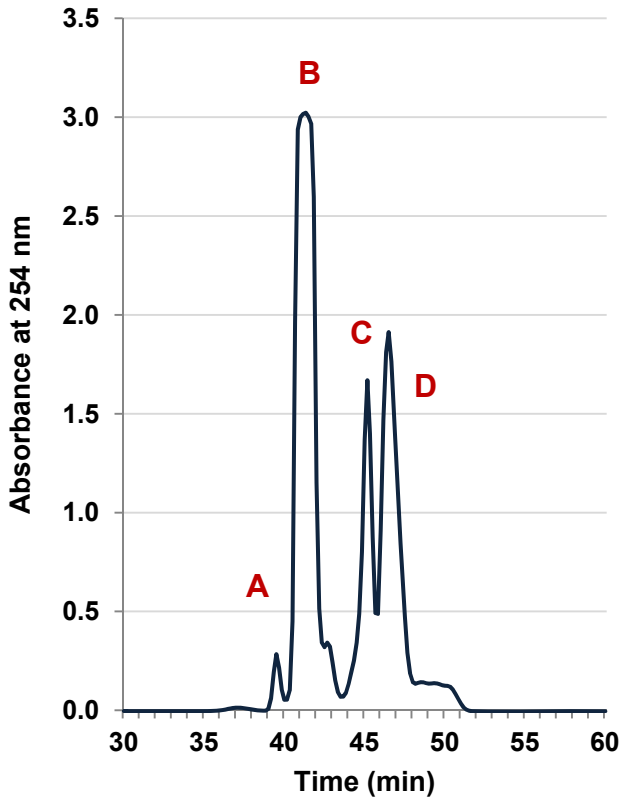

Figure 2.26. Semi-preparative HPLC chromatogram of Section 1, showing peaks A, B, C, and D from Figure 2.25.

Each peak was then collected individually; the purity was verified via semi-preparative HPLC and MALDI. Peak D was found to be the di-grafted product fraction; the chromatogram of this peak can be seen in Figure 2.27.

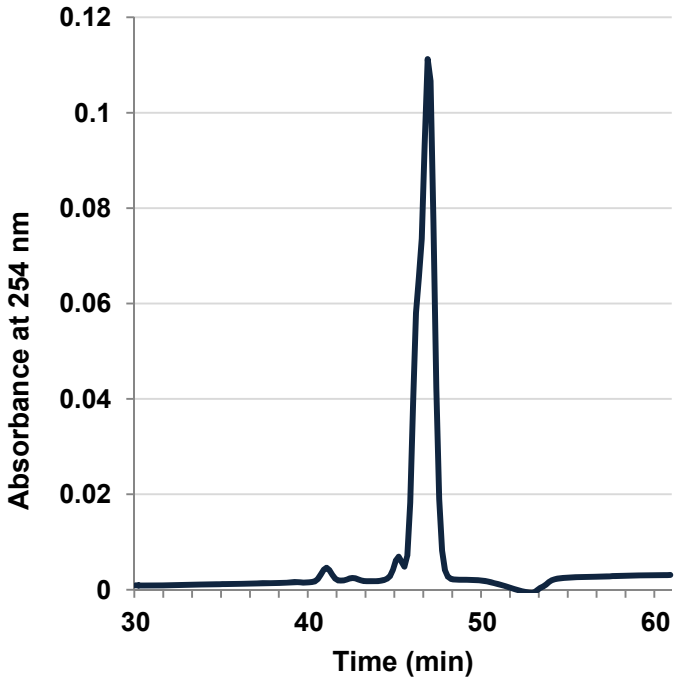

Figure 2.27. Semi-preparative HPLC chromatogram of di-grafted fraction (Peak D in Figure 2.26).

The small peaks preceding the elution of peak D in Figure 2.27 were contaminants and were removed by further purification using semi-preparative HPLC. The MALDI analysis (Figure 2.28) of this doubly-purified peak showed that there were no contaminants and that we had isolated the pure di-grafted fraction by mass ($m/z + Ag^+ = 781$).

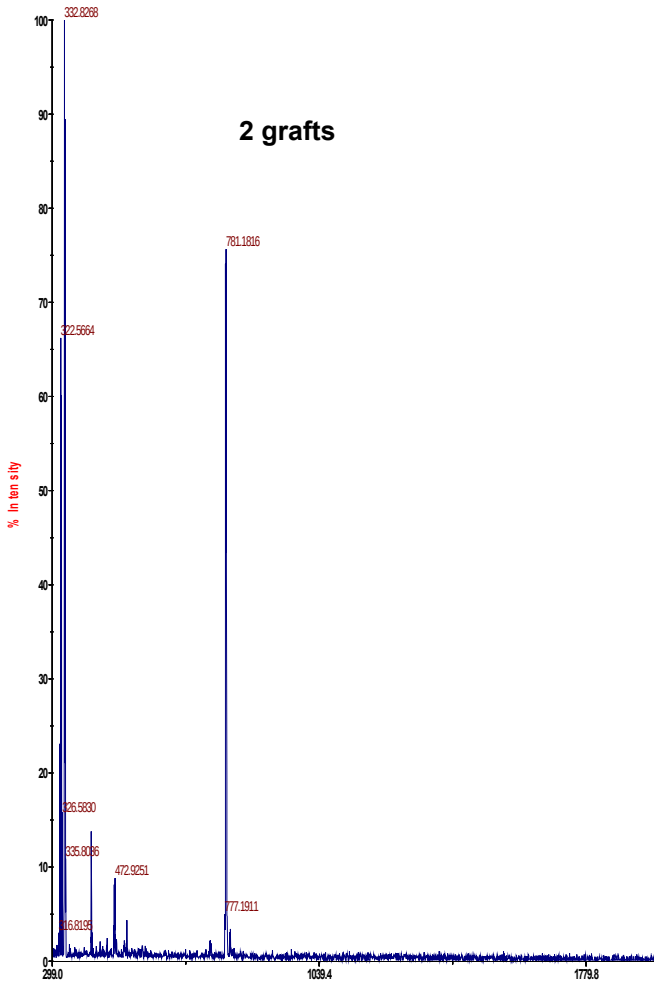

Figure 2.28. Ag-assisted MALDI spectrum of isolated di-grafted product fraction (m/z + Ag^+ = 781).

Approximately 10 mg of the di-grafted fraction was ultimately collected and purified over the course of several months. As this amount was too dilute for standard NMR techniques, a solvent-matched Shigemi tube ($CDCl_3$) was used for sample analysis. Shigemi tubes are NMR tubes that have a reduced sample volume; the glass of the tube is treated to match the magnetic susceptibility of the solvent in question. The tube is sealed with a glass plunger, also susceptibility matched, so that the total volume of deuterated solvent required for a

sample is quite small (approximately 0.25 mL).[27] The ^{1}H NMR spectrum of the isolated di-grafted fraction analyzed in this manner is seen in Figure 2.29, below.

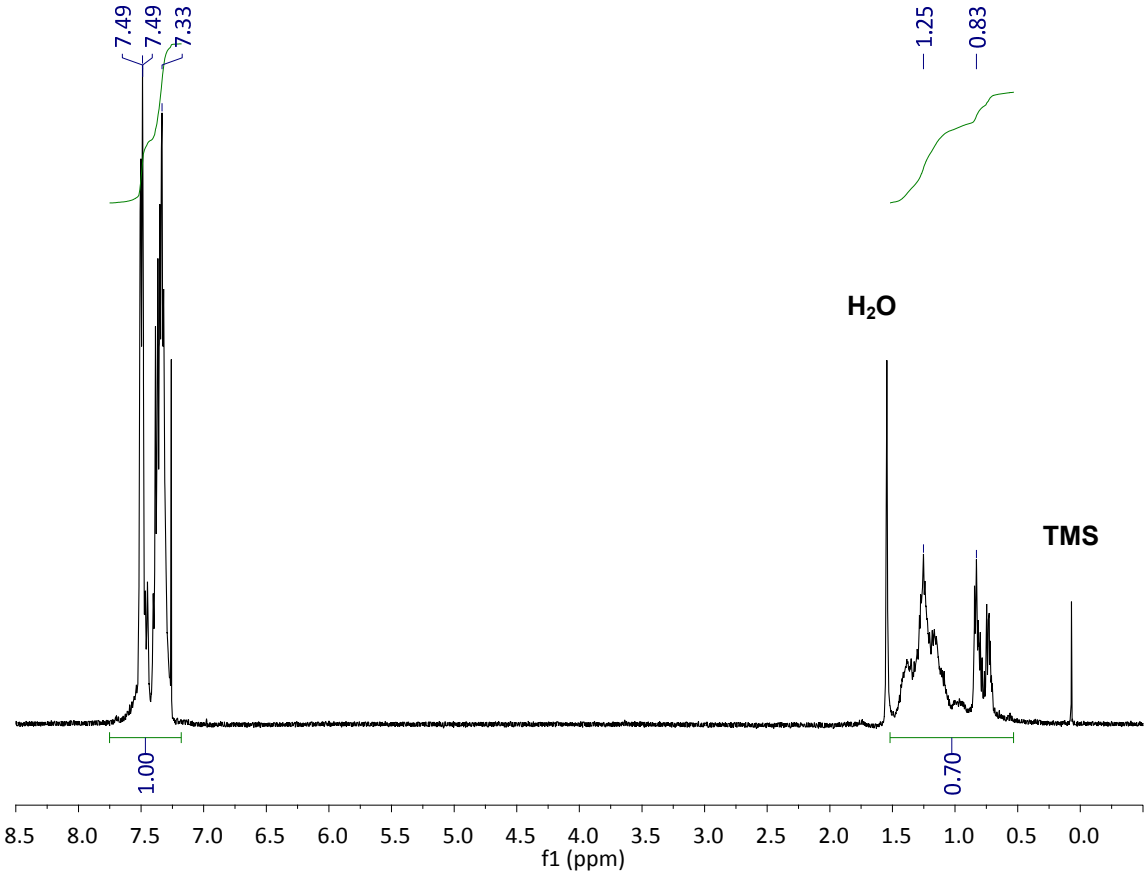

Figure 2.29. ^{1}H NMR (in $CDCl_3$-matched Shigemi tube) of di-grafted product fraction. Singlet at δ1.56 is due to water.

The aromatic peaks corresponding to the phenyl-protected grafts can be seen from δ7.75-7.25, while the aliphatic peaks from δ1.5-0.5 arise from not only the heptane backbone, but also the alkyl chains attaching the silicon to the backbone. The large singlet at δ1.56 is due to the presence of water, while the singlet at δ0 is due to tetramethylsilane (TMS).

In a di-grafted molecule, regardless of regio- or stereochemistry, there will be 30 aromatic protons and 22 aliphatic protons. The theoretical ratio of aliphatic protons to aromatic protons should then be 0.73 for all di-grafted isomers; as shown in Figure 2.29, the experimental ratio was found to be 0.70. However, while we were able to determine the number of grafts on the heptane backbone for this fraction, no information pertaining to regiochemistry could be obtained from these particular analyses. Confident that we had isolated a sample comprising solely di-grafted product material, we obtained the ^{13}C NMR spectrum of the sample, as well as DEPT 135. A comparison of the two spectra showed that no quaternary carbon was present—a structural feature that would only be present if two grafts were on the same backbone carbon.

From the absence of any quaternary carbons in the di-grafted product fraction, we can rule out the possibility of 1,3-intramolecular hydrogen shifts (as seen in Figure 2.9) contributing in a major way to the product distribution—if the grafted fractions resulting from these 1,3-shifts are present, they are below the detection limit of the NMR. In addition, the calculated transition state energy of the 1,3-transition state (Figure 2.18) suggests that this high-energy pathway is disfavored. All possible remaining regioisomers arising from 2 grafts on the heptane backbone are shown in Figure 2.30. As some of these are structural duplicates, we can reduce the range of possible di-grafted products down to 4 unique regioisomers, shown in Figure 2.31.

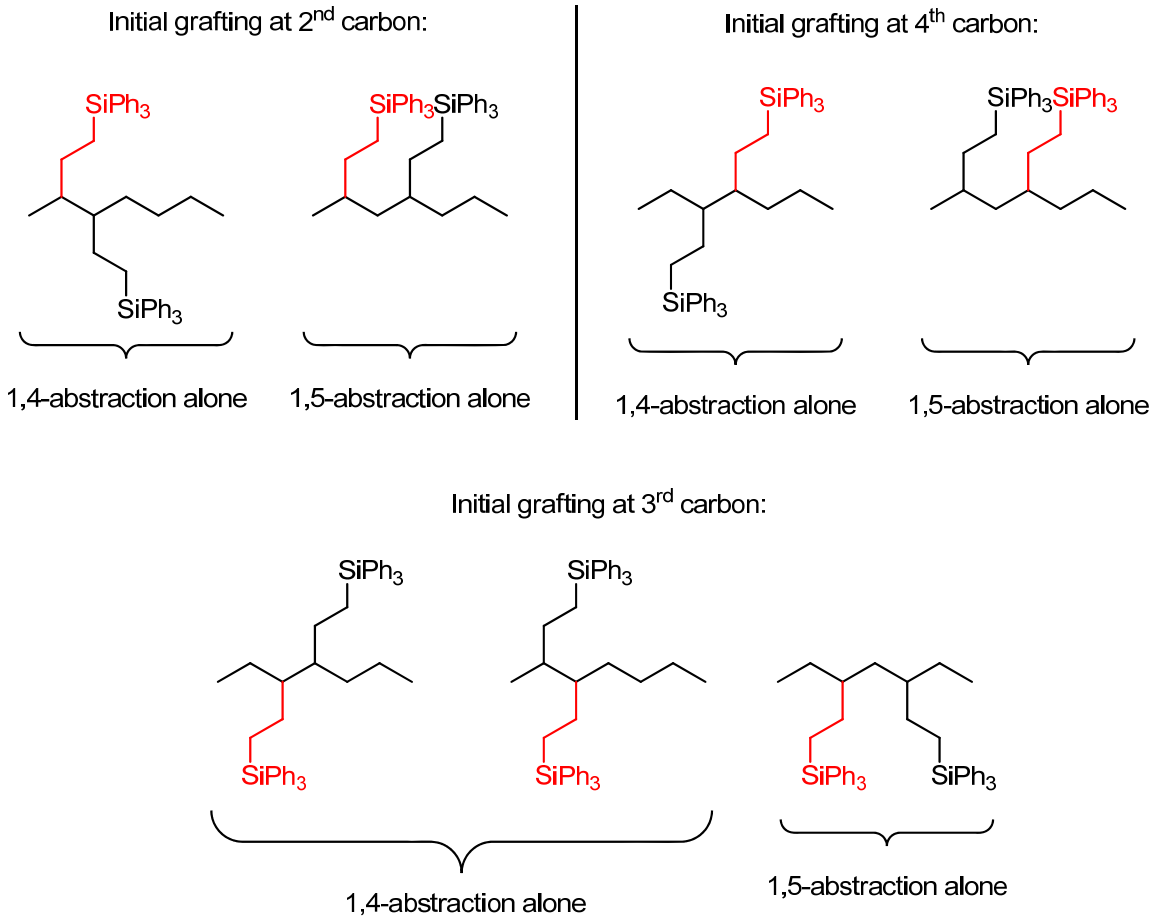

Figure 2.30. Possible regioisomers in di-grafted fraction, separated according to site of initial graft. Stereoisiomers not included in this consideration.

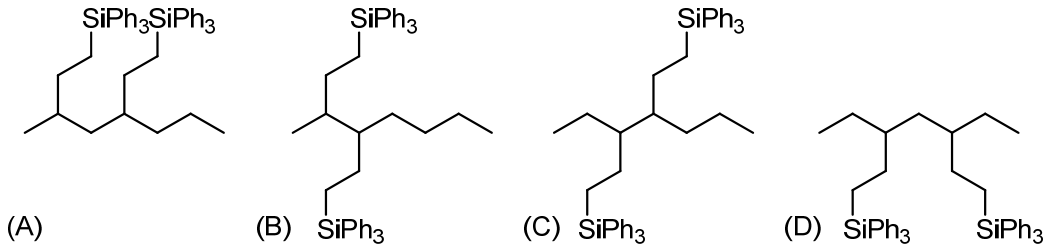

Figure 2.31. Unique regioisomers of di-grafted product fraction.

Structures A and B in Figure 2.31 both contain a methine group adjacent to a methyl group; however, this methine group in structure B is adjacent to another methine group, whereas

this methine group in structure A is next to a methylene group. As seen in Figure 2.30, these two structures represent the products obtained when initial grafting at the second carbon of the heptane backbone is followed by a 1,5- and a 1,4-hydrogen shift, respectively. Structures C and D do not contain a methine group adjacent to a methyl group.

Edited HSQC spectroscopy provides information not only about the protons and carbons in a molecule, but also how many protons a particular carbon bears—similar to a DEPT 135 spectrum. The edited HSQC spectrum of the isolated di-grafted fraction can be seen in Figure 2.32.

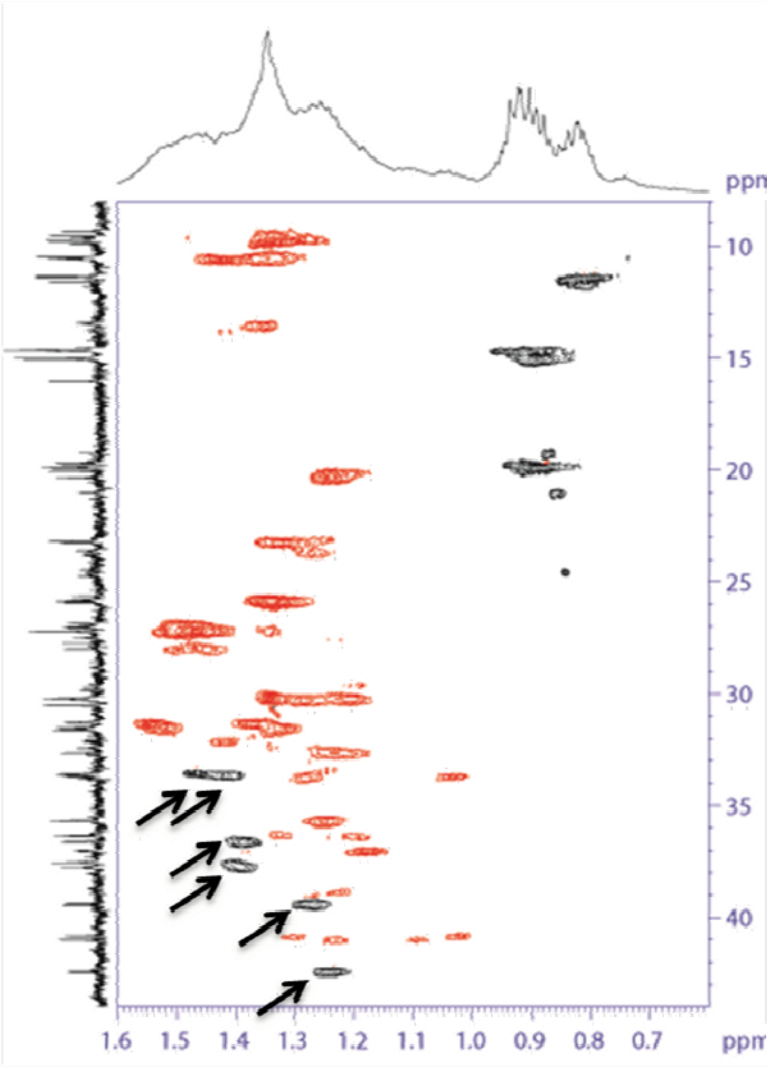

Figure 2.32. Edited HSQC spectrum of di-grafted product fraction. Red signals indicate methylene groups, while black signals indicate methine groups and methyl groups. Arrows indicate methine groups.

The ^{1}H spectrum of the di-grafted product fraction is the *x*-axis of this 2D NMR, while the ^{13}C spectrum is the *y*-axis. For the sake of clarity, the spectrum has been cropped to focus on the aliphatic region. The red signals indicate the methylene groups present, while the black signals indicate the methine and methyl groups. The methyl groups are more shielded than the methine groups, and therefore have a lower chemical shift. Six methine groups are indicated by the black arrows in the ^{1}H range of δ1.2-1.5 and the ^{13}C range of δ33-44. For

further information regarding connectivity of these methine groups, an HSQC-TOCSY experiment was performed, the results of which can be seen in Figure 2.33.

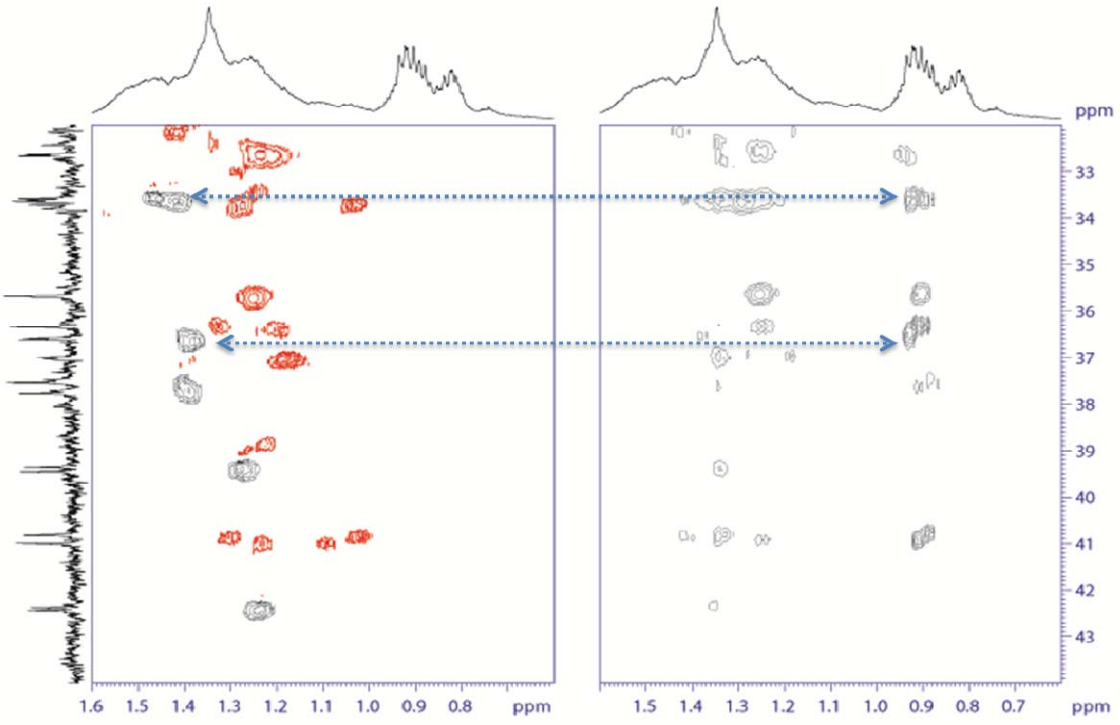

Figure 2.33. *Left*, edited HSQC spectrum from Figure 2.32; *right*, HSQC-TOCSY spectrum of di-grafted product fraction. Arrows show connectivity between carbons.

Two methine groups in the HSQC spectrum on the left are adjacent to two methyl groups in the TOCSY spectrum on the right; this supports the presence of not only regioisomer A from Figure 2.31, which results from a 1,5-intramolecular hydrogen shift, but also regioisomer B, which results from a 1,4-shift. These two regioisomers account for four of the six methine groups seen via edited HSQC, leaving two methine groups unaccounted for. These methine groups correspond to regioisomer C or D in Figure 2.31, but there is insufficient data available to determine which other regioisomer is present. However, we do

have evidence supporting the presence of products arising from not only a 1,5-intromolecular shift, but also a 1,4-intramolecular hydrogen shift.

2.4.7.5 Advanced NMR Experiments: Penta-Grafted Product Fraction

The penta-grafted product fraction (Section 3 in Figure 2.25) was also collected, concentrated, and purified in the same manner outlined above. This fraction elutes after the other products, and was relatively easy to isolate. Approximately 20 runs' worth of this eluent was collected. The semi-preparative HPLC chromatogram of the isolated fraction can be seen in Figure 2.34, below.

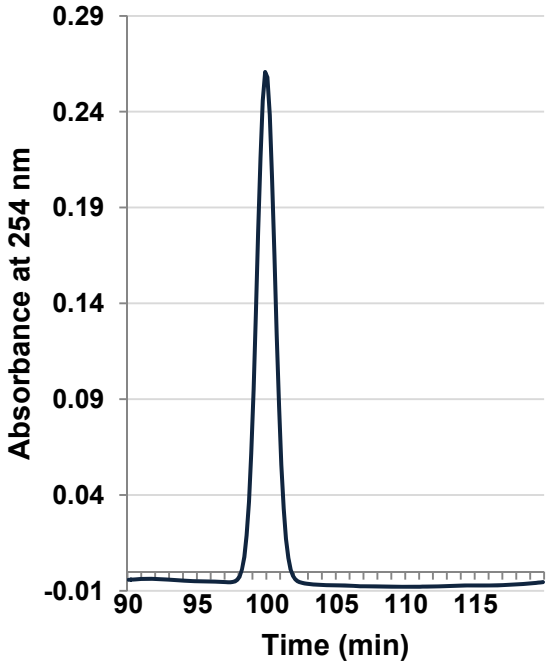

Figure 2.34. Semi-preparative HPLC chromatogram of penta-grafted fraction (Section 3 in Figure 2.25).

No further purification was required for this particular section. MALDI analysis (Figure 2.35) showed that the pure penta-grafted fraction was obtained ($m/z + Ag^+ = 1639$).

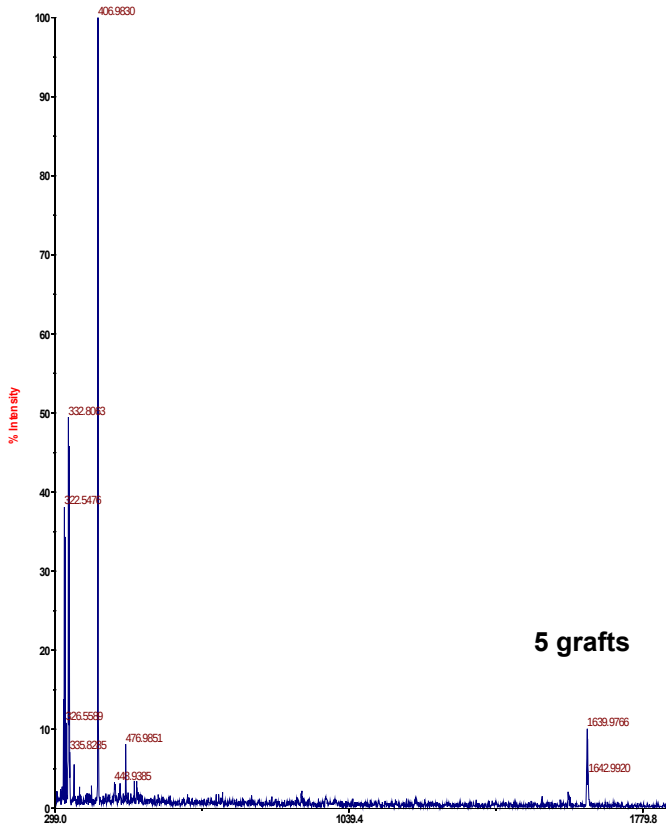

Figure 2.35. Ag-assisted MALDI spectrum of isolated penta-grafted product fraction (*m/z* + Ag^+ = 1639).

^{13}C NMR analysis of the penta-grafted product fraction was carried out. In addition, attached proton test (APT) and DEPT 135 experiments were performed. The results of these three NMR experiments are compared in Figure 2.36. In a regular ^{13}C NMR spectrum, all carbons are phased up, regardless of the number of attached protons. In a DEPT 135 spectrum, methine and methyl carbons are phased up, and methylene groups are phased down. Quaternary carbons do not appear. In contrast, in an APT spectrum, methine and methyl carbons are phased up; both quaternary and methylene carbons are phased down. Comparison of the APT and DEPT 135 spectra should therefore reveal the presence of any

quaternary carbons—any downward-phased peaks that are present in the APT spectrum but absent in the DEPT 135 spectrum arise from quaternary carbons.

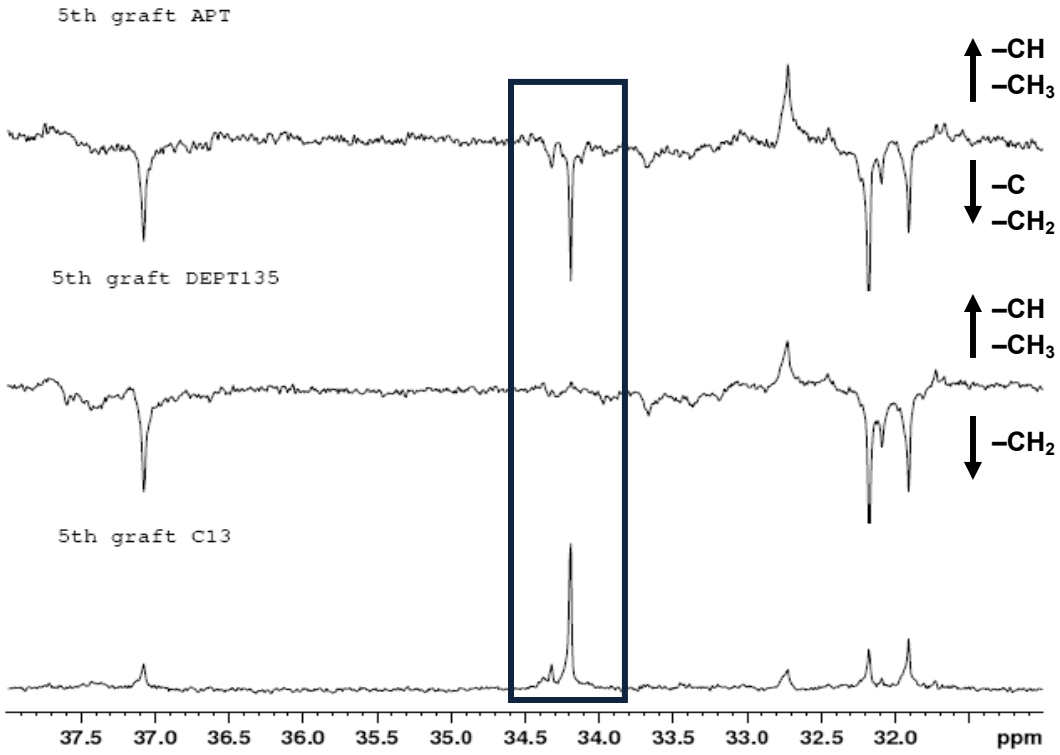

Figure 2.36. From top to bottom, aliphatic region of APT, DEPT 135, and ^{13}C NMR spectra of penta-grafted product fraction isolated via semi-preparative HPLC.

One such quaternary carbon can be seen in Figure 2.36, at δ34.2. A quaternary carbon in the aliphatic region of the ^{13}C NMR spectrum can only exist if two grafts were present on the same carbon; the presence of this quaternary carbon in the mixture of penta-grafted regioisomers indicates that a relatively large part of the penta-grafted product fraction contains a doubly-grafted carbon.

2.4.8 Diluent Experiments

2.4.8.1 Dynamic Light Scattering

Although we have determined that multiple grafts do occur per heptane molecule, it is not clear why this phenomenon is strongly favored. Other groups have noticed this same phenomenon—Rätzsch *et al.* refer to the grouping of grafts along the polymer backbone as "nests" of grafts.[28] There is a very small amount of the grafting material in the reaction mixture in what is, essentially, a "sea" of heptane molecules. One possible explanation for the formation of higher grafted fractions could be the presence of aggregates in the solution. Solutions of VTMS in heptane are visually homogeneous up to at least 50 wt% (the highest wt% attempted), however, microemulsions, which are forms of aggregates, are also visually homogeneous. Dynamic light scattering (DLS) was therefore used to investigate the presence of any aggregates present in solutions of VTMS in dodecane.

DLS is a common method of determining the size of particles in solution, whether they are small suspended solids or aggregates. A laser beam is shone at the solution in question, and the deflected photons are counted by a detector. The intensity of the scattered light is correlated to the Brownian motion of the particles or aggregates in solution, and from these correlation functions, the hydrodynamic radius (r_h) of the particle or aggregate can be determined. Solutions of VTMS in dodecane were prepared with the VTMS concentration ranging from 5 to 50 wt%; measured via DLS at ambient conditions; and the correlation functions thereof gathered. 20 measurements were taken and the resulting r_h averaged. Dodecane was used as the model compound, as it has a higher refractive index than heptane (n20/D = 1.421 versus n20/D = 1.387), which would present a greater contrast with VTMS (n20/D = 1.392) and thus better sensitivity.

The samples were analyzed using a Dynapro DLS instrument. As a control experiment, pure dodecane was used; no correlation function was observed, which was expected for a pure compound. For solutions with 10, 20, 30, 40, and 50 wt% VTMS in dodecane, in experiments run by one researcher, correlation functions did show a smooth exponential decay indicative of the presence of aggregates; it was also reported that no aggregation was seen for solutions containing 5 or 8 wt%.[29] However, I do not hold these results to be indicative of our system. Other researchers were not able to reproduce these results under identical conditions, despite attempting on numerous occasions. In fact, no aggregation was detected at any concentration of VTMS in dodecane up to 50 wt%. Moreover, further investigation into the raw data from the original DLS experiments showed that, although 20 measurements were indeed made for each sample, not all of the measurements were retained by the instrument—many measurements were discarded, as they fell outside the tolerance limits of the instrument. In the most extreme case, the r_h of one sample (50 wt%) was actually represented as being derived from an average of 20 measurements, when in fact it resulted from one single measurement. Further attempts to investigate the behavior of VTMS in dodecane by other researchers in our group have not shown any evidence that aggregates are present via DLS. It could be that our system does have aggregates, but that they are simply too small to be detected by the instrument we have used.

2.4.8.2 Non-Grafting Silanes

We also used synthetic techniques to determine if aggregates were present—namely, introducing non-grafting silanes to the grafting reaction. These were compounds that would theoretically behave like VTMS in terms of aggregation, but lacked one key structural element—the vinyl group required to graft onto the hydrocarbon backbone. However, they

would contain methoxy groups attached to silicon, which would make the molecule polar. The two non-grafting silanes, or diluents, chosen were ethyltrimethoxysilane (ETMS) and tetramethylorthosilicate (TMOS), seen below in Figure 2.37.

Figure 2.37. Diluents ethyltrimethoxysilane (*left*, ETMS) and tetramethylorthosilicate (*right*, TMOS).

We reasoned that these non-grafting silanes could be able to participate in any aggregation occurring in solution, and therefore essentially decrease the local concentration of VTMS. They could not, however, graft to the heptane backbone due to the lack of a vinyl group. This could result in a decrease in the observed number of grafts per heptane molecule. The heptane grafting reactions were carried out in the Parr autoclave as described previously; however, in addition to 5 wt% VTMS, 5 wt% of either of the two diluents was also added. The amount of DTBP used (750 ppm) remained unchanged. The product mixtures were capped with PhLi. The excess PhLi was quenched with NH_4Cl; the organic phase was separated and dried with $MgSO_4$; and the solvent was removed via rotavap. The resulting crude product mixtures were analyzed via MALDI (Figure 2.38 and Figure 2.39) and semi-preparative HPLC. These experiments were repeated in triplicate; representative MALDI spectra are shown.

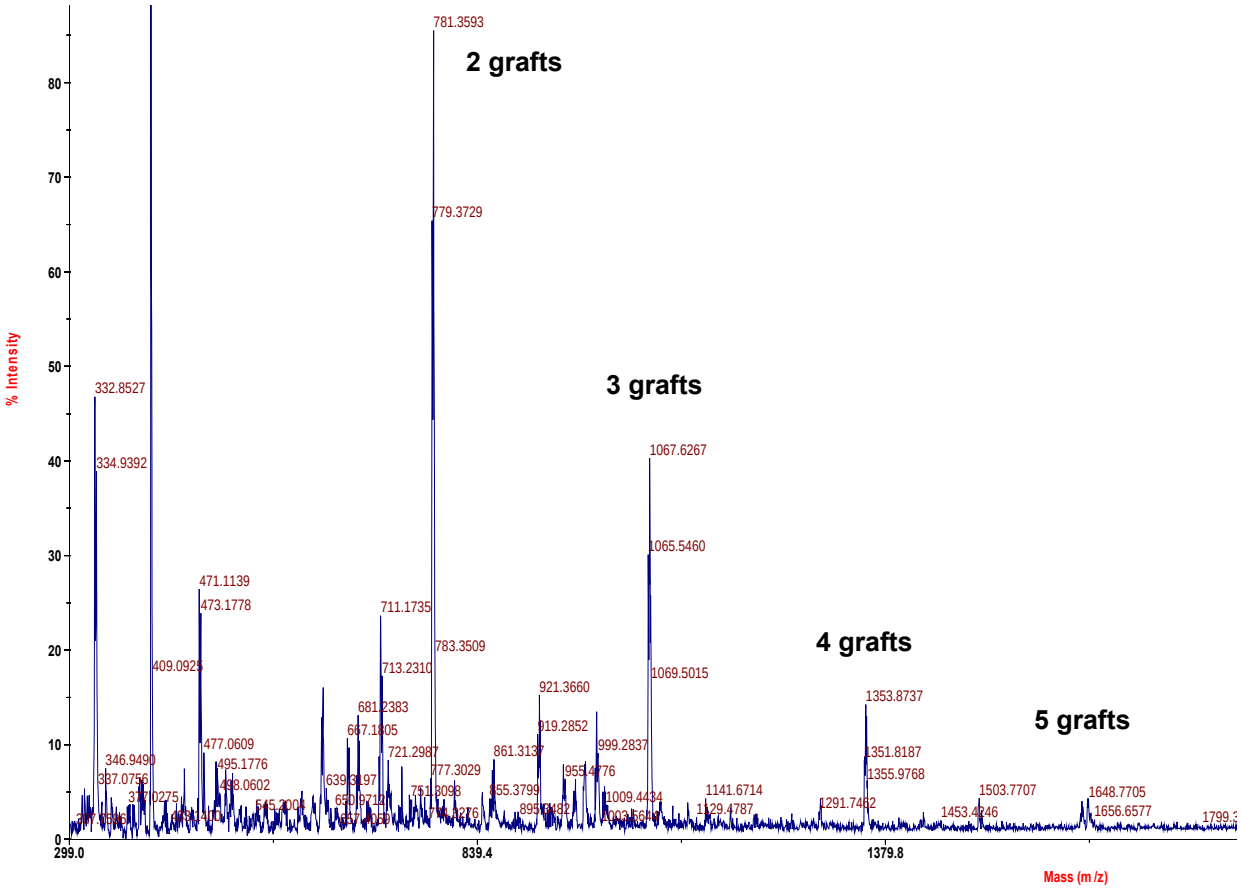

Figure 2.38. Ag-assisted MALDI spectrum of crude heptane-*g*-VTPS product mixture; reaction run with 5 wt% VTMS and 5 wt% ETMS. *m/z* includes that of Ag^+ (109).

In Figure 2.38, up to 5 grafts per heptane molecule can be seen in the product mixture when VTMS is grafted to heptane in the presence of ETMS.

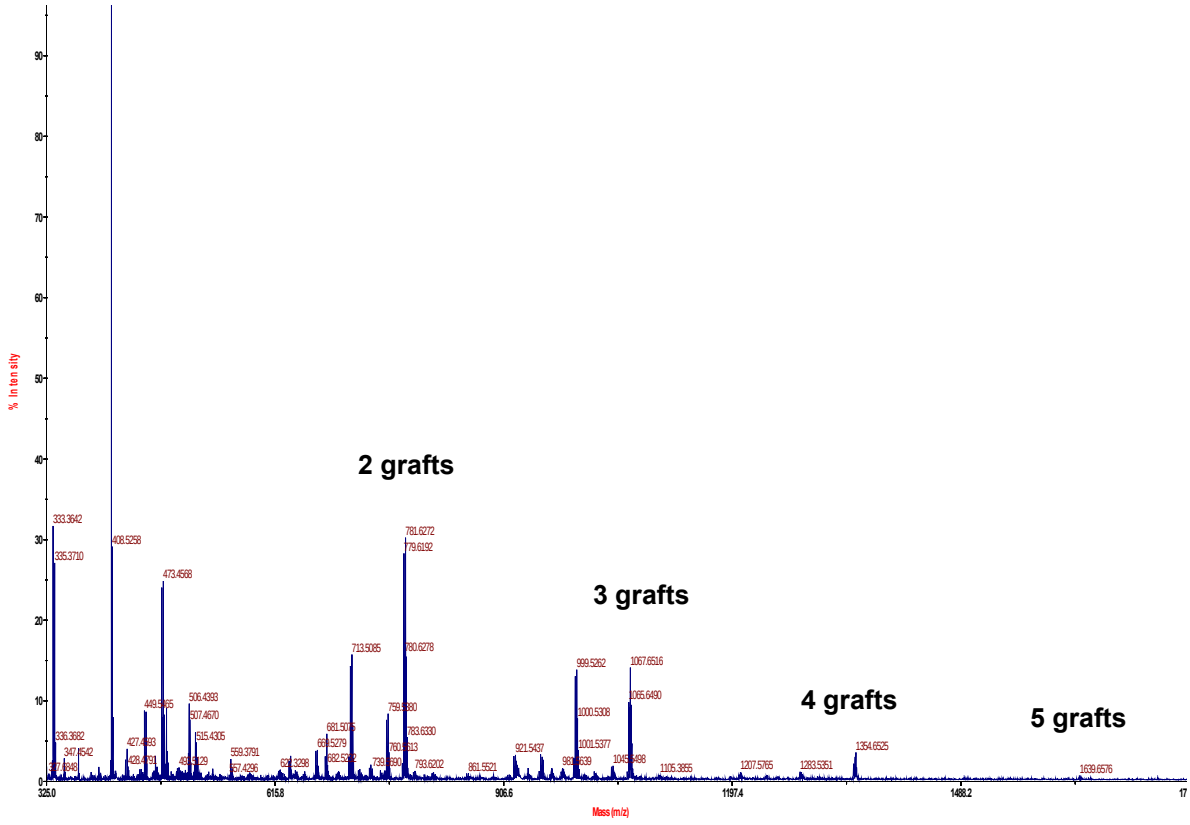

Figure 2.39. Ag-assisted MALDI spectrum of crude heptane-*g*-VTPS product mixture; reaction run with 5 wt% VTMS and 5 wt% TMOS. *m/z* includes that of Ag^+ (109).

In Figure 2.39, again, up to 5 grafts per heptane molecule can be seen in the product mixture when VTMS is grafted to heptane in the presence of TMOS. All three heptane systems investigated—whether with VTMS, VTMS and ETMS, or VTMS and TMOS—show the same range of grafted products, i.e., ranging from 1 to 5 grafts per heptane backbone. Again, as MALDI is only a semi-quantitative form of analysis, we cannot draw any conclusions based on the relative peak heights of the molecular ions.

The crude product mixtures were also analyzed using semi-preparative HPLC, although the individual grafted fractions were not separated. The chromatograms from these separations can be seen below in Figure 2.40 and Figure 2.41.

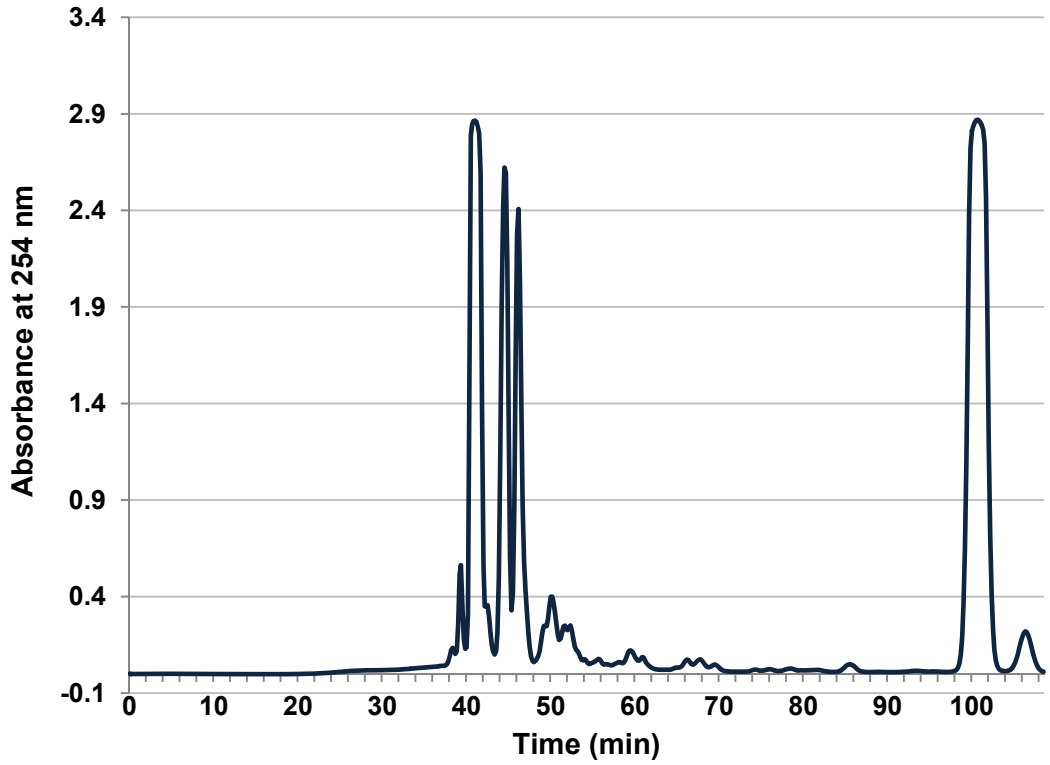

Figure 2.40. Semi-preparative HPLC chromatogram of crude product mixture of heptane-*g*-VTPS, formed in presence of ETMS.

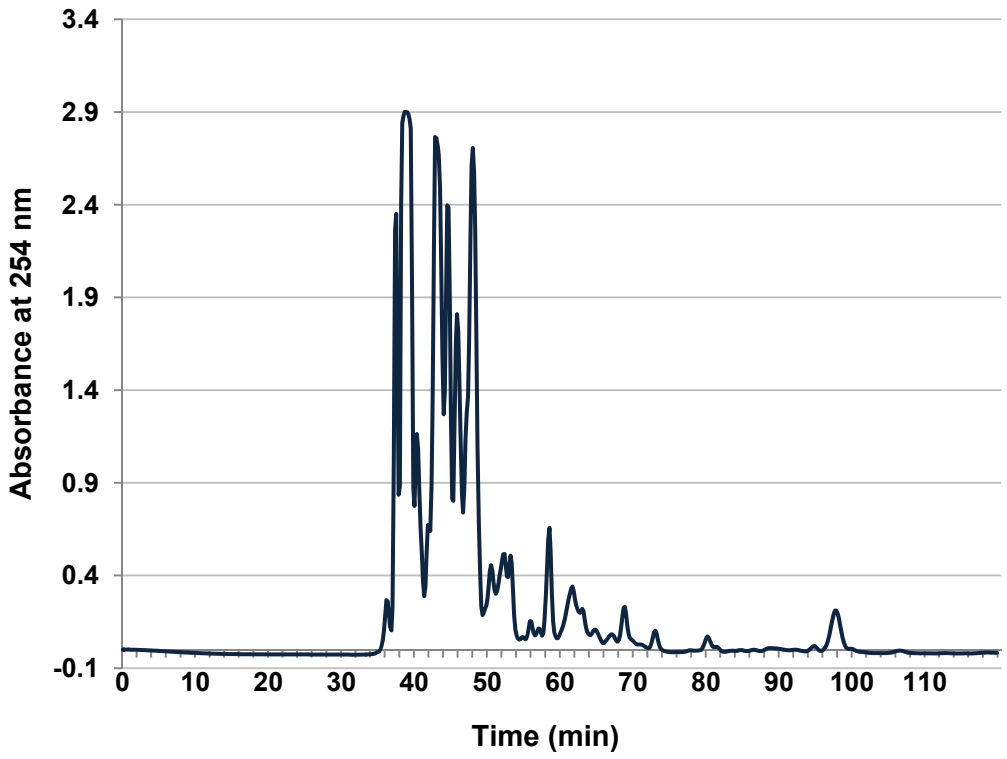

Figure 2.41. Semi-preparative HPLC chromatogram of crude product mixture of heptane-*g*-VTPS, formed in presence of TMOS.

The chromatograms of the crude product mixtures from reactions using non-grafting silanes do not differ greatly from those of the typical reactions performed with VTMS (Figure 2.24). The most significant difference, seen in Figure 2.41, is the peak height for the compound that elutes at 98 minutes—the peak is much smaller for the VTMS-TMOS reaction than for the VTMS reaction. Whether the presence of the non-grafting silane TMOS affects the relative amount of penta-grafted material produced in the grafting reaction, however, is not known, as we do not have a quantitative means of determining the graft distribution. Separation and identification of the products of these diluents reactions were not undertaken.

2.4.8.3 Carbon Dioxide

As mentioned before, one of the main goals of this research was not just to gain a clearer picture of the grafting distribution, but also to control said distribution. It was hypothesized that, by tuning reaction conditions with different pressures of CO_2, we could affect the extent of grafting. CO_2 has been shown to swell polymers,[30] which could increase mixing of VTMS into the hydrocarbon model compound. Experiments investigating the effect of CO_2 pressure were carried out using dodecane as the model compound in the Parr autoclave. The reagents were introduced to the Parr as in the heptane experiments; however, prior to heating, CO_2 was added to the Parr using an ISCO syringe pump. After grafting but prior to capping, the Parr was placed under vacuum to remove any CO_2 and prevent its reaction with PhLi; the reaction was then worked up according to the usual protocol. Analysis was carried out using MALDI mass spectrometry. The three CO_2 pressures investigated were 70, 100, and 150 bar. As a control, these reactions were also carried out under nitrogen at the same pressures, to determine if any changes in graft distribution were an effect of CO_2 or merely due to increased hydrostatic pressure. The ranges of grafted products are shown in Table 2.5.

Table 2.5. Grafting distributions observed under range of nitrogen and carbon dioxide pressures.

	# of grafts	
Pressure (bar)	**N_2**	**CO_2**
1	1-6	--
70	1-6	1-4
100	1-5	1-4
150	1-5	1-5

As seen in Table 2.5, the maximum number of grafts detected via MALDI decreases from 6 in the control experiment to 4 at 70 and 100 bar, but increases to 5 at 150 bar. At the highest pressures of both gases, none of the 6-grafted substrate is detected. However, this is seen with both N_2 and CO_2 at high pressures. It may be that pressure, rather than type of gas, is the dominating effect. However, due to the semi-quantitative view of the heptane-*g*-VTPS product mixture that MALDI offers, no firm conclusions as to the effect of CO_2 pressure on extent of grafting can be made at this time.

2.5 Conclusions

Grafting reactions of VTMS onto model compounds dodecane and heptane were carried out, and the resulting grafted products were protected via capping with phenyllithium. We found that a reaction time of 24 hours with phenyllithium—standard in the literature—was not sufficient to obtain an accurate analysis of the product distribution. Once a longer capping reaction time of three days was instituted, it was found that a maximum of 6 grafts per heptane backbone were present—a number that could not be accounted for with only a 1,5-intramolecular hydrogen shift. The presence of multiple grafts along one hydrocarbon backbone could be a result of enhanced local concentrations of VTMS within the bulk hydrocarbon, although we have not found conclusive evidence of these clusters. Subsequent isolation of the di-grafted and penta-grafted fractions and analysis via advanced NMR techniques showed conclusively the presence of products resulting from not only a 1,5-intramolecular hydrogen shift, but also via a concurrent 1,4-shift. Several side products, including one resulting from carbon-carbon bond formation, were also identified.

2.6 References

1. Bhattacharya, A.; Ray, P. Basic features and techniques. In *Polymer Grafting and Crosslinking*, Bhattacharya, A.; Rawlins, J. W.; Ray, P., Eds. John Wiley & Sons, Inc.: Hoboken, N.J., 2009.

2. Lazár, M.; Rado, R.; Rychlý, J. Crosslinking of polyolefins. In *Polymer Physics*, Springer Berlin / Heidelberg: 1990; Vol. 95, pp 149-197.

3. Morshedian, J.; Hoseinpour, P. M. Polyethylene cross-linking by two-step silane method: a review. *Iran. Polym. J.* **2009,** *18* (2), 103-128.

4. Narkis, M.; Tzur, A.; Vaxman, A.; Fritz, H. G. Some properties of silane-grafted moisture-crosslinked polyethylene. *Polym. Eng. Sci.* **1985,** *25* (13), 857-862.

5. (a) Basfar, A. A.; Mosnáček, J.; Shukri, T. M.; Bahattab, M. A.; Noireaux, P.; Courdreuse, A. Mechanical and thermal properties of blends of low-density polyethylene and ethylene vinyl acetate crosslinked by both dicumyl peroxide and ionizing radiation for wire and cable applications. *J. Appl. Polym. Sci.* **2008,** *107* (1), 642-649; (b) Isac, S.; George, K. E. Silane grafting of polyethylenes. *Int. J. Polymer. Mater.* **2005,** *54* (5), 397-413.

6. Barzin, J.; Azizi, H.; Morshedian, J. Preparation of silane-grafted and moisture crosslinked low density polyethylene. Part II: Electrical, thermal and mechanical properties. *Polym. Plast. Technol. Eng.* **2007,** *46* (3), 305-310.

7. Ramachandran, S.; Hartlein, R.; Chandak, P. A comparative economic analysis for underground distribution cables insulated with TR-XLPE and EPR. In *Transmission and Distribution Conference*, New Orleans, LA, 1999; Vol. 1, pp 112-119.

8. Allermann, G. A. Silane crosslinkable polyethylene. US20040024138 A1, 2004.

9. Scott, H. G. Cross-linking of a polyolefin with a silane. 3646155, 1972.

10. Ghosh-Dastidar, A.; Sengupta, S. S.; Flory, A.; Cogen, J. M. In *Effect of silane grafting level and crosslink structure on properties of moisture crosslinkable systems*, International Wire & Cable Symposium and Conference, Providence, Rhode Island, Providence, Rhode Island, 2008; pp 138-145.

11. Ultsch, S.; Fritz, H. G. Crosslinking of LLDPE and VLDPE via graft-polymerized vinyltrimethoxysilane. *Plast. Rubber Compos. Process. Appl.* **1990,** *13* (2), 81-91.

12. Sen, A. K.; Mukherjee, B.; Bhattacharyya, A. S.; De, P. P.; Bhowmick, A. K. Kinetics of silane grafting and moisture crosslinking of polyethylene and ethylene propylene rubber. *J. Appl. Polym. Sci.* **1992,** *44* (7), 1153-1164.

13. Barzin, J.; Azizi, H.; Morshedian, J. Preparation of silane-grafted and moisture cross-linked low density polyethylene: Part I: Factors affecting performance of grafting and cross-linking. *Polymer-Plastics Technology and Engineering* **2006,** *45* (8), 979-983.

14. Shieh, Y. T.; Tsai, T. H. Silane grafting reactions of low-density polyethylene. *J. Appl. Polym. Sci.* **1998,** *69* (2), 255-261.

15. Sirisinha, K.; Meksawat, D. Preparation and properties of metallocene ethylene copolymer crosslinked by vinyltrimethoxysilane. *Polym. Int.* **2005,** *54* (7), 1014-1020.

16. (a) Spencer, M.; Parent, J. S.; Whitney, R. A. Composition distribution in poly(ethylene-graft-vinyltrimethoxysilane). *Polymer* **2003,** *44* (7), 2015-2023; (b) Parent, J. S.; Parodi, R.; Wu, W. Radical mediated graft modification of polyolefins: Vinyltriethoxysilane addition dynamics and yields. *Polym. Eng. Sci.* **2006,** *46* (12), 1754-1761; (c) Forsyth, J. C.; Baker, W. E.; Russell, K. E.; Whitney, R. A. Peroxide-initiated vinylsilane grafting: Structural studies on a hydrocarbon substrate. *J. Polym. Sci., Part A: Polym. Chem.* **1997,** *35* (16), 3517-3525.

17. (a) Mixer, R. Y.; Bailey, D. L. The mode of peroxide-catalyzed polymerization of vinyltriethoxysilane. *Journal of Polymer Science* **1955,** *18* (90), 573-582; (b) Seyferth, D.; Son, D. Y.; Tasi, M. The ^{60}Co g-radiation-induced polymerization of vinylalkoxysilanes. *Organometallics* **1995,** *14* (5), 2225-2231.

18. Willker, W.; Leibfritz, D.; Kerssebaum, R.; Bermel, W. Gradient selection in inverse heteronuclear correlation spectroscopy. *Magn. Reson. Chem.* **1993,** *31* (3), 287-292.

19. Williamson, R. T.; Marquez, B. L.; Gerwick, W. H. Use of ^{1}H-^{15}N PEP-HSQC-TOCSY at natural abundance to facilitate the structure elucidation of naturally occurring peptides. *Tetrahedron* **1999,** *55* (10), 2881-2888.

20. Zenobi, R. Ionization processes and detection in MALDI-MS of polymers. In *MALDI Mass Spectrometry for Synthetic Polymer Analysis*, Li, L., Ed. John Wiley and Sons, Inc.: Hoboken, New Jersey, 2010; pp 9-26.

21. Ranganathan, S.; Baker, W. E.; Russell, K. E.; Whitney, R. A. Peroxide-initiated crafting of maleic anhydride onto linear and branched hydrocarbons. *J. Polym. Sci., Part A: Polym. Chem.* **1999,** *37* (20), 3817-3825.

22. (a) Belu, A. M.; DeSimone, J. M.; Linton, R. W.; Lange, G. W.; Friedman, R. M. Evaluation of matrix-assisted laser desorption ionization mass spectrometry for polymer characterization. *J. Am. Soc. Mass. Spectrom.* **1996,** *7* (1), 11-24; (b) Deery, M. J.; Jennings, K. R.; Jasieczek, C. B.; Haddleton, D. M.; Jackson, A. T.; Yates, H. T.; Scrivens, J. H. A study of cation attachment to polystyrene by means of matrix-assisted laser desorption/ionization and electrospray ionization-mass spectrometry. *Rapid Commun. Mass Spectrom.* **1997,** *11* (1), 57-62.

23. Silverstein, R. M.; Webster, F. X.; Kiemle, D. J. *Spectrometric Identification of Organic Compounds*. 7th ed.; John Wiley & Sons, Inc.: Hoboken, New Jersey, 2005.

24. Bowen, R. J.; Garner, A. C.; Berners-Price, S. J.; Jenkins, I. D.; Sue, R. E. Convenient synthetic routes to bidentate and monodentate 2-, 3- and 4-pyridyl phosphines: potentially useful ligands for water-soluble complex catalysts. *J. Organomet. Chem.* **1998,** *554* (2), 181-184.

25. Allen, F. H.; Kennard, O.; Watson, D. G.; Brammer, L.; Orpen, A. G.; Taylor, R. Tables of bond lengths determined by X-ray and neutron diffraction. 1. Bond lengths in organic compounds. *J. Chem. Soc., Perkin Trans. 2* **1987,** (12), S1-S19.

26. (a) Buell, G. R.; Corriu, R.; Guerin, C.; Spialter, L. Addition of Grignard reagents to vinylsilanes. *J. Am. Chem. Soc.* **1970,** *92* (25), 7424-&; (b) Cason, L. F.; Brooks, H. G. An interesting side-reaction in the preparation of triphenylvinylsilane. *J. Am. Chem. Soc.* **1952,** *74* (18), 4582-4583.

27. (a) Wieruszeski, J.-M.; Fritzinger, B.; Hanoulle, X.; Martins, J. C.; Lippens, G. Sandwich-ELISE NMR: Reducing the sample volume of NMR samples. *J. Magn. Reson.* **2008,** *193* (1), 37-40; (b) Shigemi, Inc. http://www.shigeminmr.com/#! (accessed July 16, 2012).

28. Rätzsch, M.; Bucka, H.; Ivanchev, S. S.; Mesh, A. M.; Khaikine. Some peculiar features of radiation grafting of monomers of various structures and reactivities onto polyolefins. *J. Appl. Polym. Sci.* **2000,** *77* (4), 711-718.

29. Pollet, P.; Liotta, C. L.; Eckert, C. A.; Verma, M.; Nixon, E. C.; Sivaswamy, S.; Jha, R.; Gelbaum, L.; Chaudhary, B. I.; Cogen, J. M. Radical mediated graft modification of polyolefin models with vinyltrimethoxysilane: A fundamental study. *Ind. Eng. Chem. Res.* **2011**, 12246-12253.

30. Li, D.; Liu, Z. M.; Han, B. X.; Song, L. P.; Yang, G. Y.; Jiang, T. Preparation of nanometer dispersed polypropylene/polystyrene interpenetrating network using supercritical CO_2 as a swelling agent. *Polymer* **2002,** *43* (19), 5363-5367.

CHAPTER 3. SYNTHESIS OF SILYLATED AMINES FOR POST-COMBUSTION CO_2 CAPTURE

3.1 Introduction

Carbon dioxide (CO_2) emissions from the combustion of fossil fuels are thought to be a major contributor to the phenomenon of global warming. CO_2 is one of the primary targets for capture and sequestration, in large part due to its prevalence.[1] Coal fired power plants represent large point sources of CO_2 emissions—for example, a 1000 MW coal-fired power plant emits between 6 and 8 Mt of CO_2 per year.[2] In total, the flue gas emitted by coal fired power plants represents nearly one-third of all CO_2 emissions in the United States. The flue gas emitted by these plants is a technically challenging medium. The bulk of flue gas is made up of chemically inert nitrogen; at the other end of the spectrum, it also contains ppm levels of highly reactive SO_X and NO_X compounds. Carbon dioxide makes up approximately 16 vol% of flue gas, as shown in Figure 3.1.[3] Additionally, the typical temperature of flue gas as it exits the smokestack is 40°C.[4]

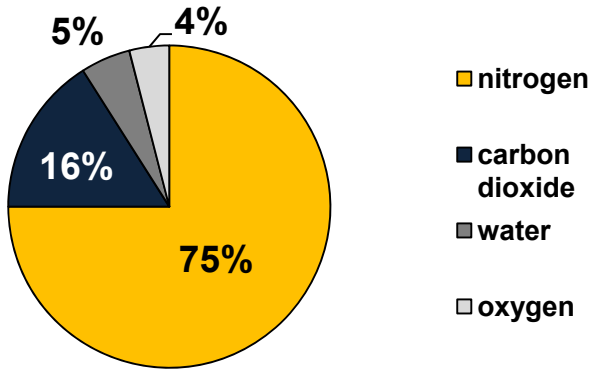

Figure 3.1. Major components of flue gas by volume. Also present are ppm levels of SO_x and NO_x.

Therefore, any post-combustion system to capture CO_2 will have to meet three main criteria. 1.) It will have to be selective for CO_2, which comprises only a small portion of the flue gas stream. 2.) The system will also have to be recyclable, due to the sheer volume of CO_2 emitted.[3] While the reactive sulfur oxides (SO_x) and nitrogen oxides (NO_x) present in small quantities in flue gas can be neutralized via a single-use sorbent, the amount of CO_2 released just by one coal-fired power plant in one year of operation is far too high for a single-use sorbent.[3] 3.) Finally, the system must be cost-effective. The United States Department of Energy (DOE) has outlined standards for developing carbon capture programs dictating a CO_2 capture efficiency of 90% with a concomitant rise in resulting energy costs of less than 35%.[5]

CO_2 capture technology was, ironically, originally developed in order to capture and use large amounts of CO_2 for gas injection in enhanced oil recovery (EOR) from depleted oil and natural gas reservoirs.[6] There are three main classifications of CO_2 scrubbers: membranes, solid adsorbents, and liquid absorbents.[7] Liquid absorbents are by far the most developed technology of the three, and have the added benefit of operating in scrubbing units that are relatively simple to retrofit to existing power plants.[3] The most promising current technology used to capture CO_2 is an aqueous solution (20-30 wt%) of monoethanolamine, or MEA. It is currently used to sweeten natural gas, or scrub CO_2 from CO_2-contaminated natural gas reserves.[8] MEA reacts with CO_2 in a 2:1 molar ratio to form an ammonium-carbamate ion pair, as seen in Figure 3.2, via a zwitterionic intermediate.[9] The hydroxyl group decreases the vapor pressure of the compound, while the amine group provides the compound's reactivity.[10]

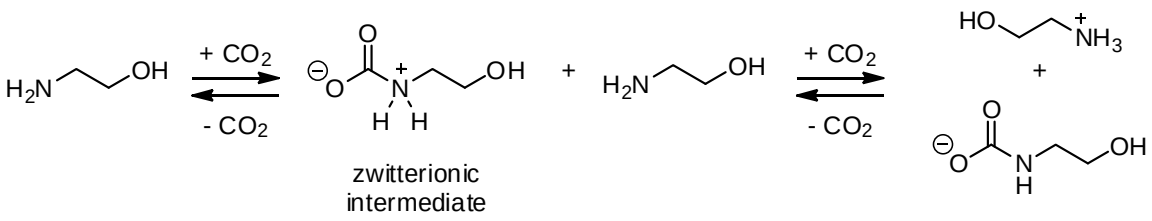

Figure 3.2. Reaction of MEA with CO_2 to form zwitterionic intermediate, *middle*, and further reaction with another molecule of MEA to form ammonium-carbamate ion pair, *right*.

MEA is a promising liquid sorbent, as it is not only chemoselective for CO_2, it is also recyclable and inexpensive; the 2004 cost of MEA was $1.25 per kilogram.[11] A schematic of the absorption and desorption of CO_2 by MEA in an actual process is shown in Figure 3.3.

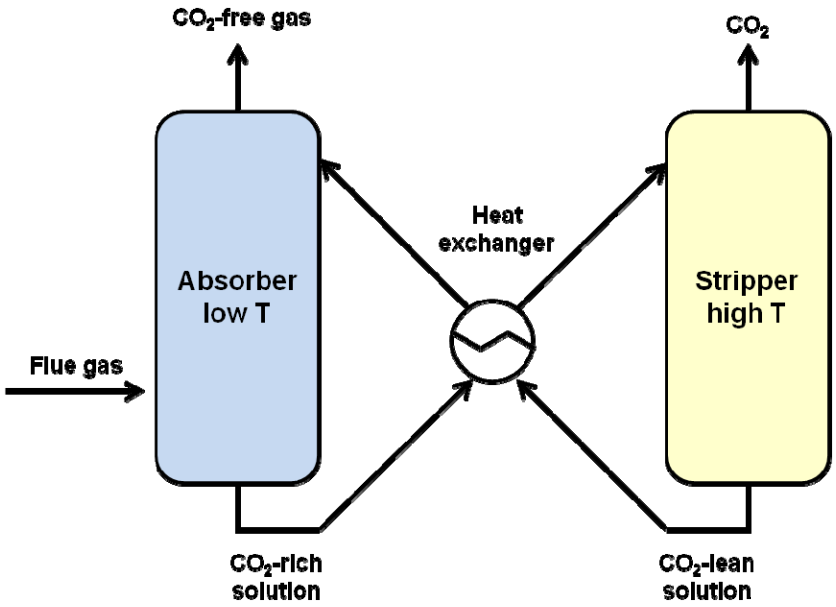

Figure 3.3. Schematic of CO_2 capture and release by a recyclable solution of MEA. Diagram adapted from Puxty *et al.*[12]

Flue gas enters the absorber column, where it reacts with the MEA-containing sorbent solution. Steam heating the aqueous solution of MEA releases the CO_2, which can be

removed for sequestration (often in geologic formations); the solvent can then be reused to remove more CO_2 from the flue gas stream.[12] However, due to the high heat capacity of water, this regeneration step can account for 70-80% of the energy required to run a typical power plant.[7] The water is required not only to decrease the viscosity of the highly viscous salt formed upon reaction of MEA with CO_2, but also to decrease the corrosivity of MEA, which has been found to be the most corrosive of the various alkanolamines being explored as CO_2 capture agents.[13] Additionally, the presence of the hydroxyl group on MEA does contribute to degradation pathways,[10] and a significant amount of the sorbent must be replaced due to this breakdown—approximately 2.2 kilograms per metric ton of CO_2 captured.[13a] To remove byproducts, a reclaimer is used on a slip stream of up to 10% of the MEA solution; this further increases operating costs.[14]

Although MEA has several advantages as a carbon capture agent, the drawbacks associated with its use drive research towards other possible liquid sorbent replacements. Traditional ionic liquids (ILs) have been proposed as alternatives to MEA. ILs are salts that are liquid at or near room temperature. Whereas MEA captures CO_2 via chemisorption, ILs capture CO_2 via physisorption (and, as such, are better suited to processes where there is a higher partial pressure of CO_2).[4]

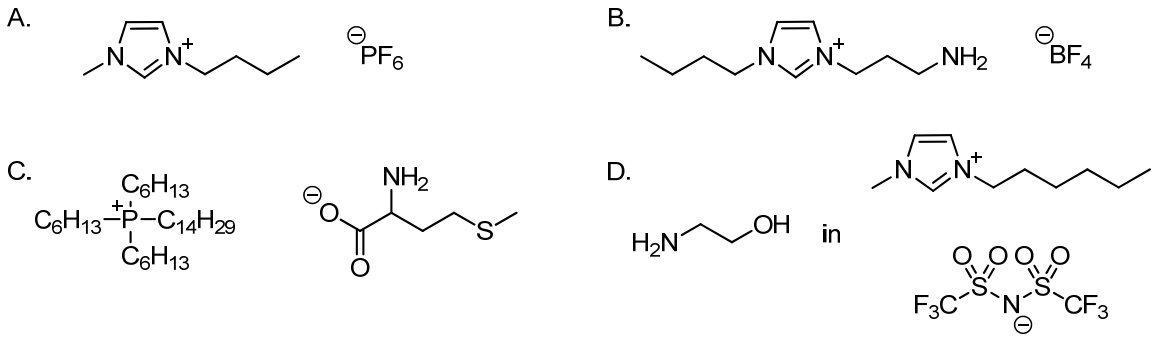

Figure 3.4. Examples of ionic liquid based CO_2 capture technologies.

Imidazolium-based ionic liquids (such as compound A in Figure 3.4) show a preference for physisorption of CO_2 over N_2 and O_2.[15] Some task-specific ionic liquids (TSILs) have been modified with amine moieties to capture CO_2 via chemi- and physisorption. Bates *et al.* tethered a primary amine to the imidazolium cation of a traditional ionic liquid and showed a CO_2 capacity near the theoretical chemisorption limit of 0.5 moles of CO_2 per mole of IL (compound B, Figure 3.4).[16] Brennecke *et al.* have shown even higher capacities when the amine functionality is tethered to the anion of a traditional IL (compound C, Figure 3.4).[17] However, ILs typically have extremely high viscosities, which limits their industrial viability as CO_2 capture agents. The upper limit for viscosity in industrial processes is typically 100 cP, whereas ILs exhibit viscosities several orders of magnitude greater. TSILs modified with amine groups exhibit the same high viscosity, which becomes even higher upon reaction with CO_2.[15, 18] One group has even proposed dissolving MEA in ILs to make use of both chemisorptive and physisorptive capabilities (compounds D, Figure 3.4), but the MEA-carbamate salt formed upon reaction with CO_2 precipitates out of the ILs investigated, making this solvent mixture an unlikely industrial solution.[19]

The goal for this project is to develop a liquid sorbent that can serve as a replacement for MEA, exhibiting high capacity and selectivity for CO_2 while enabling high

efficiency in terms of cost and energy required for regeneration. Our group has pioneered and developed a class of solvents known as reversible ionic liquids (RevILs).[20] These solvents are molecular liquids (MLs) that, upon reaction with CO_2, form a salt that is liquid at or near room temperature. Heating of the RevIL releases the CO_2 and reforms the molecular liquid; this cycle can be repeated multiple times, with no change in activity of the molecular or ionic liquid seen from cycle to cycle. This reversibility is very useful when considering the use of RevILs as CO_2 capture materials; if a RevIL is used to capture CO_2 from flue stack gas, the CO_2 can later be stripped and stored for sequestration, and the molecular liquid can be reused. Moreover, the structure of the RevILs could be tuned to optimize carbon capture performance.

3.2 Background

Aminosilicones have previously been explored by Perry *et al.* as CO_2 capture agents; however, the particular compounds used were found to form solids or "very viscous liquids" when reacted with CO_2, causing chemisorption to be incomplete and mass-transfer limited.[21] Cosolvents were used to mitigate the viscosity; although these cosolvents contributed to the system's capacity via physisorption of CO_2, such physisorption is ultimately limited by the partial pressures of CO_2 in the capture stream.[22] Additionally, such a solvent—even a non-aqueous one—would still impose an energy penalty on the system during regeneration. Our group has previously used the commercially available trialkoxysilanes (3-aminopropyl)trimethoxysilane (TMSA) and (3-aminopropyl)triethoxysilane (TESA), seen in Figure 3.5, to extract hydrocarbons from tar sands; they are known to form liquids upon reaction with CO_2 (Figure 3.6), rather than solids.[20d] It was proposed that we investigate the utility of these compounds as carbon capture materials.

(3-aminopropyl)trimethoxysilane
TMSA

(3-aminopropyl)triethoxysilane
TESA

Figure 3.5. Commercially available trialkoxysilanes TMSA and TESA.

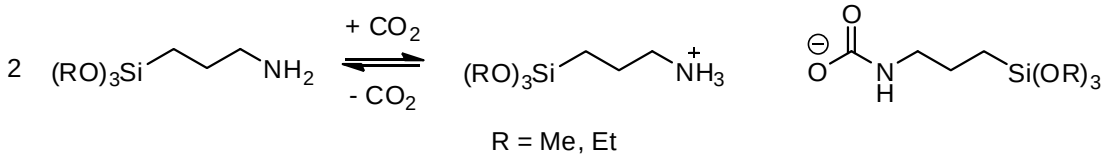

Figure 3.6. Reaction of trialkoxysilylpropylamines with CO_2 to form ammonium-carbamate ion pairs.

CO_2 reacts with the silylated amine in a 2:1 molar ratio of amine to CO_2, forming an ammonium-carbamate ion pair (Figure 3.6) that acts as a reversible ionic liquid; this RevIL can then continue to physisorb CO_2, leading to a CO_2-swollen RevIL, as shown in Figure 1.4. RevILs therefore enable a dual capture mechanism by combining chemisorption and physisorption.

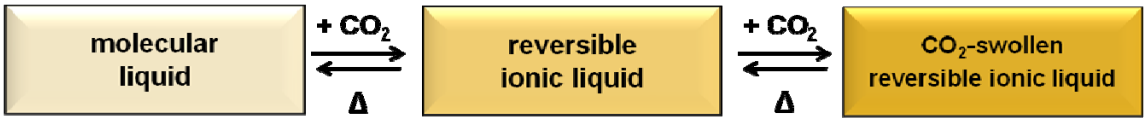

Figure 3.7. Reaction of CO_2 with molecular liquid, *left*, to form reversible ionic liquid, *middle*. This further absorbs CO_2 to form a CO_2-swollen reversible ionic liquid, *right*.

The use of RevILs also confers several other advantages on a CO_2 capture system. The volume of solvent required to capture one mole of CO_2 is much smaller than for aqueous solutions of MEA;[23] the reaction is chemoselective for CO_2 over N_2, which comprises the

bulk of the flue gas; and the (3-aminopropyl)trialkoxysilanes exhibit higher capacities than traditional sorbents.[20e] However, alkoxysilanes are susceptible to hydrolysis, so a more robust molecular precursor was developed simply by replacing the alkoxy groups with moisture-stable alkyl groups. I will refer to these RevILs, with modification occurring via alkyl groups on the silicon, as "first-generation RevILs." Silanes with various alkyl subsitutents are widely available, and via hydrosilylation reactions with Karstedt's catalyst, we synthesized a series of trialkylsilylpropylamines in which the length of the alkyl chains were systematically varied.[20c, d] The general form of this reaction can be seen in Figure 3.8.

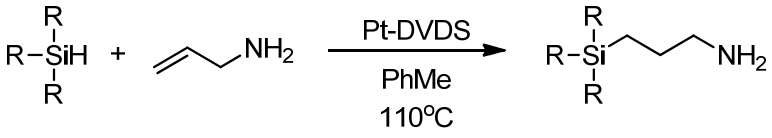

Figure 3.8. General form of hydrosilylation reaction of allylamine with silanes using Karstedt's catalyst (structure shown below in Figure 3.9).

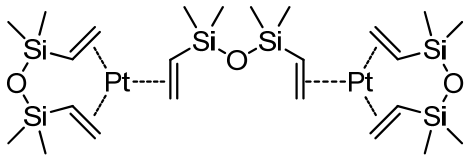

Figure 3.9. Structure of Karstedt's catalyst.

The zero-valent platinum in Karstedt's catalyst has been found to be widely tolerant of various functional groups, including the amino group, which is commonly thought of as a poison of platinum catalysts.[24] Using this method, we have synthesized and characterized a number of 1-component RevILs bearing different alkyl substituents on the silicon. In this

work, I will discuss the four first-generation RevILs that have been studied the most extensively; the structures and names of these are shown in Figure 3.10.

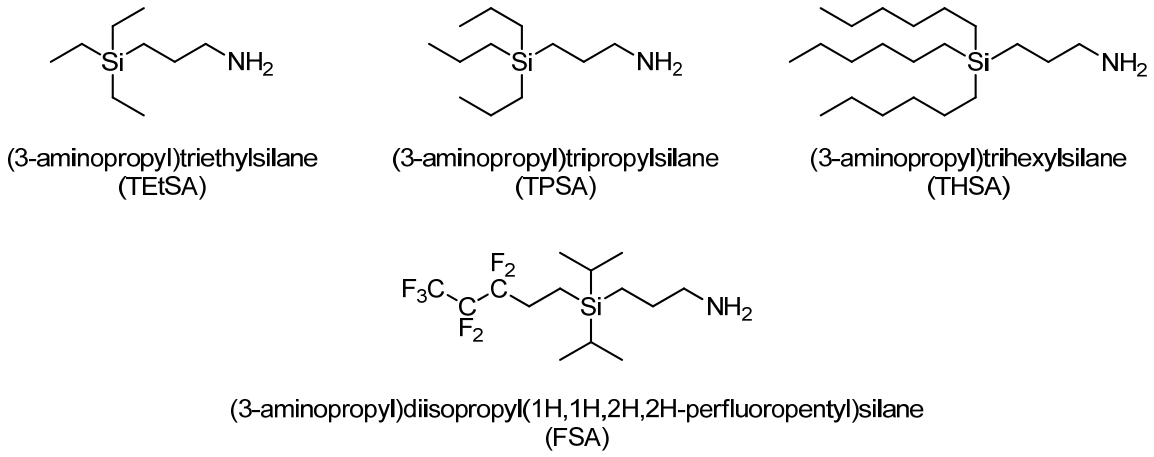

Figure 3.10. Structures and names of selected first generation RevILs (molecular forms).

I will present their synthesis and characterization, and discuss how the properties exhibited by these first-generation RevILs—CO_2 capacity, viscosity, reversal temperature, and enthalpy of regeneration—dictated the continuing course of my research. I will then present the conceptualization and synthesis of "second-generation" RevILs, in which the propyl linker between the silicon and the amino group contains an unsaturation; and "third-generation" RevILs, which contain branching near the amino group.

3.3 Experimental Section

3.3.1 Materials

All chemicals were purchased from Sigma-Aldrich and used as received unless otherwise noted. All chemicals were stored under inert dry atmosphere. Chemicals used were: triethylsilane (99%); tripropylsilane (99%); trihexylsilane (98%); allylamine (99+%);

platinum(0)-1,3-divinyl-1,1,3,3-tetramethyldisiloxane complex solution in xylene (Karstedt's catalyst; 2 wt% Pt); toluene (PhMe; anhydrous, 99.8%); 0.5 *M* 2,8,9-triisobutyl-2,5,8,9-tetraaza-1-phosphabicyclo[3.3.3]undecane in diethyl ether (Et_2O); tetrahydrofuran (THF; anhydrous, inhibitor-free, ≥99.9%); 2-methyl-2-propen-1-ol (98%); crotyl alcohol (mixture of *cis* and *trans*, 96%); prenyl alcohol (99%); diethyl ether (anhydrous, ≥99.0%, containing 1% BHT as inhibitor); sodium hydride (60% dispersion in mineral oil); trichloroacetonitrile (98%); 3-chloro-1-butene (96%); potassium phthalimide (98%); hydrazine (anhydrous, 98%); 2-methyl-3-butyn-2-amine (95%); Pd on activated charcoal (5 wt% Pd basis); Celite 545; heptane (anhydrous, 99%); hexanes (anhydrous, mixture of isomers, ≥99%); *p*-xylene (99%); and methanol (anhydrous, 99.8%).

Diisopropyl-(1H,1H,2H,2H-perfluoropentyl)silane was purchased from Fluorous Technologies and used as received. Propargylamine (95%) was acquired from TCI America, used as received, and stored in the dark under inert atmosphere at 5°C. 2-methylallylamine (97%) was purchased from Acros Organics and used as received. Carbon dioxide used was SFE grade from Airgas (99.999%).

3.3.2 Experimental

3.3.2.1 (3-Aminopropyl)triethylsilane (TEtSA)

A typical synthesis was carried out as follows. To a 3-neck 250 mL round bottomed flask fitted with a condenser and magnetic stirbar under inert atmosphere was added 80 mL anhydrous toluene (0.751 mol), 25.5 mL triethylsilane (0.160 mol), and 1.2 mL 2 wt% Pt-DVDS in xylenes (3.243×10^{-4} mol Pt; 0.20% catalyst loading wrt silane). This was allowed to stir at room temperature for approximately five minutes, at which point 24 mL allylamine (0.320 mol) was added and the reaction was heated to 110°C overnight. Reaction progress was monitored via ^{1}H NMR for the disappearance of the silane proton (~3.7 ppm). When

this peak was no longer present, the reaction mixture was allowed to cool to room temperature; the solvent and excess allylamine was then removed via rotavap. The product (3-aminopropyl)triethylsilane was distilled from the catalyst under reduced pressure (bp: 80°C at 2 mmHg) to yield 24.7916 g (0.143 mol; 89.4% isolated yield).

^{1}H NMR (400.13 MHz, $CDCl_3$, 25°C) δ = 2.55 (t, *J* = 7.0 Hz, 2H), 1.32 (m, 6H), 0.99 (s, 2H), 0.82 (t, *J* = 7.9 Hz, 9H), 0.38 (q, *J* = 7.9 Hz, 8H)

^{13}C NMR (100.57 MHz, $CDCl_3$, 25°C) 45.47, 27.88, 18.63, 7.90, 6.95, 2.87

Calculated % for $C_9H_{23}NSi$ (MW: 173.37 g·mol^{-1}): C 62.35, H 13.37, N 8.08, Si 16.20; found: C 62.41, H 13.42, N 7.94

3.3.2.2 (3-Aminopropyl)tripropylsilane (TPSA)

A typical synthesis was carried out as follows. To a 3-neck 500 mL round bottomed flask fitted with a condenser and magnetic stirbar under inert atmosphere was added 160 mL anhydrous toluene (1.502 mol), 61.0 mL tripropylsilane (0.292 mol), and 7 mL 2 wt% Pt-DVDS in xylenes (6.136 x 10^{-4} mol Pt; 0.21% catalyst loading wrt silane). This was allowed to stir at room temperature for approximately five minutes, at which point 44 mL allylamine (0.586 mol) was added and the reaction was heated at 110°C overnight. Reaction progress was monitored via ^{1}H NMR for the disappearance of the silane proton (~3.7 ppm). When this peak was no longer present, the reaction mixture was allowed to cool to room temperature; the solvent and excess allylamine was removed via rotavap. The product (3-aminopropyl)tripropylsilane was distilled from the catalyst under reduced pressure (bp: 75°C at 0.8 mmHg) to yield 62.5763 g (0.290 mol; 99.5% isolated yield). The synthesis of TPSA is typically carried out on this larger scale due to the widespread use of TPSA within the group.

^{1}H NMR (400.13 MHz, $CDCl_3$, 25°C) 2.60 (t, *J* = 7.0 Hz, 2H), 1.37 (p, *J* = 8.1 Hz, 2H), 1.30 (sextet, *J* = 7.8 Hz, 6H), 1.05 (s, 2H), 0.93 (t, *J* = 7.2 Hz, 9H), 0.48 (m, 8H)

^{13}C NMR (100.57 MHz, $CDCl_3$, 25°C) 45.85, 28.30, 18.63, 17.45, 15.27, 9.55

Calculated % for $C_{12}H_{29}NSi$ (MW: 215.45 g·mol^{-1}): C 66.90, H 13.57, N 6.50, Si 13.04; found: C 66.74, H 13.64, N 6.35

3.3.2.3 (3-Aminopropyl)trihexylsilane (THSA)

A typical synthesis was carried out as follows. To a 3-neck 250 mL round bottomed flask fitted with a condenser and magnetic stirbar under inert atmosphere was added 80 mL anhydrous toluene (0.751 mol), 30.9 mL trihexylsilane (8.675 x 10^{-2} mol), and 2 mL 2 wt% Pt-DVDS in xylenes (1.753 x 10^{-4} mol Pt; 0.20% catalyst loading wrt silane). This was allowed to stir at room temperature for approximately five minutes, at which point 13.75 mL allylamine (0.183 mol) was added and the reaction was heated at 110°C overnight. Reaction progress was monitored via ^{1}H NMR for the disappearance of the silane proton (~3.7 ppm). When this peak was no longer present, the reaction mixture was allowed to cool to room temperature; the solvent and excess allylamine was removed via rotavap. The product (3-aminopropyl)trihexylsilane was distilled from the catalyst under reduced pressure (bp: 160°C at 1 mmHg) to yield 17.9009 g (5.239 x 10^{-2} mol; 60.4% isolated yield). The relatively low isolated yield for THSA is most likely due to the high boiling point of the compound and the related difficulties in distillation.

^{1}H NMR (400.13 MHz, $CDCl_3$, 25°C) 2.61 (t, J = 7.0 Hz, 2H), 1.37 (m, 2H), 1.23 (s, 24H), 1.11 (s, 2H), 0.85 (t, J = 6.9 Hz, 9H), 0.44 (m, 8H)

^{13}C NMR (100.57 MHz, $CDCl_3$, 25°C) 45.87, 33.58, 31.53, 28.34, 23.84, 22.61, 14.11, 12.40, 9.45

Calculated % for $C_{21}H_{47}NSi$ (MW: 341.69 g·mol^{-1}): C 73.82, H 13.86, N 4.10, Si 8.22; found: C 72.87, H 13.59, N 4.07

3.3.2.4 (3-Aminopropyl)diisopropyl(1H,1H,2H,2H-perfluoropentyl)silane (FSA)

A typical synthesis was carried out as follows. To a 2-neck 250 mL round bottomed flask fitted with a condenser and magnetic stirbar under inert atmosphere was added 40 mL anhydrous toluene (0.375 mol), 17.0 mL diisopropyl-(1H,1H,2H,2H-perfluoropentyl)silane (62.81 mmol), and 1.2 mL 2 wt% Pt-DVDS in xylenes (1.052×10^{-4} mol Pt; 0.17% catalyst loading wrt silane). This was allowed to stir at room temperature for approximately five minutes, at which point 8.0 mL allylamine (0.107 mol) was added and the reaction was heated at 110°C overnight. Reaction progress was monitored via ^{1}H NMR for the disappearance of the silane proton (~3.7 ppm). When this peak was no longer present, the reaction mixture was allowed to cool to room temperature; the solvent and excess allylamine was removed via rotavap. The product (3-aminopropyl)diisopropyl(1H,1H,2H,2H-perfluoropentyl)silane was distilled from the catalyst under reduced pressure (bp: 100°C at 1 mmHg) to yield 18.9746 g (5.136×10^{-2} mol; 81.8% isolated yield).

^{1}H NMR (400.13 MHz, $CDCl_3$, 25°C) 2.68 (t, J = 7.0 Hz, 2H), 2.03 (m, 2H), 1.45 (m, 2H), 1.02 (s, 16H), 0.79 (m, 2H), 0.58 (m, 2H)

^{13}C NMR (100.57 MHz, $CDCl_3$, 25°C) 46.10, 28.50, 26.25, 26.01, 25.78, 18.35, 18.34, 11.22, 6.74, -0.79

Calculated % for $C_{14}H_{26}F_7NSi$ (MW: 369.44 g·mol^{-1}): C 45.52, H 7.09, F 36.00, N 3.79, Si 7.60; found: C 45.29, H 7.12, N 3.84

3.3.2.5 (*trans*)-3-(Triethylsilyl)prop-2-en-1-amine (*trans*-TEtSA)

A typical reaction was carried out as follows. In a 3-neck 250 mL round bottomed flask fitted with a condenser under inert atmosphere, 17.8 mL 2% Pt-DVDS in xylenes (1.560×10^{-3} mol Pt; 1.00% loading wrt silane) was combined with 3.1 mL 0.5 *M* 2,8,9-triisobutyl-2,5,8,9-tetraaza-1-phosphabicyclo[3.3.3]undecane solution (1.625×10^{-3} mol) in

diethyl ether. The reaction mixture was heated at 60°C for 10 minutes and then allowed to cool to room temperature. 100 mL anhydrous inhibitor-free THF (1.233 mol) was added to the flask, which was then cooled to approximately -10°C in an ice-and-brine bath. 27.5 mL triethylsilane (0.172 mol) was then added dropwise to the flask and allowed to stir for approximately 5 minutes. 10 mL of propargylamine (0.156 mol) was then added dropwise to the reaction mixture, which was kept in the ice bath until the large exotherm had ceased. The reaction was then allowed to stir at room temperature overnight; reaction progress was monitored by the disappearance of the terminal alkyne carbon in the ^{13}C NMR (approximately δ91). The solvent and excess triethylsilane were then removed via rotavap, and the product was distilled under reduced pressure (bp: 75°C at 6 mmHg) to yield 12.1926 g of the *trans*-isomer only (0.0711 mol; 45.57% yield).

^{1}H NMR (400.13 MHz, $CDCl_3$, 25°C) 6.13 (dt, J = 18.8, 4.8 Hz, 1H), 5.67 (dt, J = 18.9, 1.8 Hz, 1H), 3.33 (dd, J = 4.8, 1.8 Hz, 2H), 1.12 (s, 2H) 0.98 (t, J = 7.9 Hz, 9H) 0.57 (q, J = 7.9 Hz, 6H)

^{13}C NMR (100.57 MHz, $CDCl_3$, 25°C) 149.10, 124.22, 47.19, 7.55, 3.70

3.3.2.6 2-Methyl-3-(triethylsilyl)propylamine (βMTEtSA)

Several methods were attempted to synthesize βMTEtSA before a successful one was found. The initial synthesis attempts used the Overman rearrangement, but ultimately a simple hydrosilylation was successful.

3.3.2.6.1 Overman Rearrangement

A typical synthesis was carried out as follows. A solution consisting of 8.5 mL 2-methyl-2-propen-1-ol (0.101 mol) in 15 mL anhydrous diethyl ether (0.1429 mol)was added to a 3-neck 250 mL round bottomed flask containing sodium hydride (60% dispersion in mineral oil; 0.494 g prior to washing with anhydrous heptane; 1.24 x 10^{-2} mol) in 60 mL

anhydrous Et_2O at -10°C. The reaction mixture was stirred at that temperature until evolution of hydrogen gas ceased. 10 mL trichloroacetonitrile (0.100 mol) was then added dropwise over the course of 20 minutes. The reaction mixture became first yellow, then brown. It was allowed to warm to room temperature and the solvent was removed via rotavap. Upon addition of 100 mL of 99:1 hexanes:methanol to the resulting brown oil, a brown precipitate formed. This was removed via gravity filtration and 18.8450 of the crude product trichloroacetimidate was recovered. The trichloroacetimidate was not purified further and carried on "as-is" to the next step. The crude trichloroacetimidate was dissolved in 180 mL *p*-xylene and heated at reflux overnight. 19.8477 g of the crude trichloroacetamide was recovered.

3.3.2.6.2 Hydrosilylation

Synthesis of βMTEtSA was carried out as follows. A 3-neck 250 mL round-bottomed flask was fitted with a condenser and stirbar and placed under argon. 40 mL anhydrous toluene (0.376 mol) was added to the flask, followed by 16.5 mL triethylsilane (103 mmol; 2.58 *M*) and 2.70 mL 2 wt% Pt-DVDS in xylenes (2.395×10^{-4} mol Pt; 0.23% loading wrt silane). The reaction mixture was allowed to stir at room temperature for several minutes; 5 g 2-methylallylamine (70.3 mmol; 1.75 *M*) was then added and the reaction mixture was heated at 110°C for 24 hours. Reaction progress was checked via ^{1}H NMR for disappearance of the vinyl peaks of the 2-methylallylamine. The solvent was removed via rotavap and the product distilled under reduced pressure to yield 10.0744 g product (53.7 mmol; 76.4% isolated yield).

^{1}H NMR (400.13 MHz, $CDCl_3$, 25°C) δ = 2.52 (dd, *J* = 12.5, 5.5 Hz, 1H), 2.42 (dd, *J* = 12.5, 5.5 Hz, 1H), 1.54 (m, 1H), 1.09 (s, 2H), 0.90 (m, 12H), 0.62 (dd, *J* = 14.7, 4.5 Hz, 1H), 0.50 (q, *J* = 7.9 Hz, 6H), 0.31 (dd, *J* = 14.7, 5.4 Hz, 1H)

^{13}C NMR (100.57 MHz, $CDCl_3$, 25°C) 51.75, 32.79, 20.39, 16.69, 7.46, 4.01

Calculated % for $C_{10}H_{25}NSi$ (MW: 187.40 g·mol^{-1}): C 64.09, H 13.45, N 7.47, Si 14.99; found: C 63.31 H 13.54, N 7.33

3.3.2.7 4-(Triethylsilyl)-butyl-2-amine (αMTEtSA)

The Overman rearrangement was initially used in the synthesis of αMTEtSA. Although the protected branched amine was successfully used as a hydrosilylation substrate, removal of the protecting group in high yields was not attainable. An alternative method, wherein a Gabriel synthesis was used to form the protected branched amine, was used instead. This substrate was then successfully hydrosilylated and deprotected using the Ing-Manske protocol.

3.3.2.7.1 Overman Rearrangement

An example of a typical synthesis follows. A solution consisting of 8.5 mL crotonyl alcohol (99.96 mmol) in 15 mL anhydrous diethyl ether (0.1429 mol) was added to a 3-neck 250 mL round bottomed flask containing sodium hydride (60% dispersion in mineral oil; 0.492 g prior to washing with anhydrous heptane; 12.3 mmol) in 50 mL anhydrous Et_2O (0.476 mol) at -10°C. The reaction mixture was stirred at that temperature until evolution of hydrogen gas ceased. 10.1 mL trichloroacetonitrile (101 mmol) was then added dropwise over the course of 20 minutes. The reaction mixture became first yellow, then brown. It was allowed to warm to room temperature and the solvent was removed via rotavap. Upon addition of 100 mL of 99:1 hexanes:methanol to the resulting brown oil, a brown precipitate formed. This was removed via gravity filtration and 20.518 g of the crude product trichloroacetimidate was recovered. The trichloroacetimidate was not purified further and carried on "as-is" to the next step. The crude trichloroacetimidate was dissolved in 200 mL *p*-xylene and heated at reflux overnight. 20.518 g of the crude trichloroacetamide was

recovered. Column chromatography gave the pure trichloroacetamide in approximately 17% yield (mp: 30-32°C).

^{1}H NMR (400.13 MHz, $CDCl_3$, 25°C) 6.55 (s, 1H), 5.86 (ddd, *J* = 17.2, 10.5, 5.2 Hz, 1H), 5.25 (d, *J* = 17.2 Hz, 1H) 5.19 (d, *J* = 10.7 Hz, 1H), 4.53 (sextet, *J* = 6.8 Hz, 1H), 1.35 (d, *J* = 6.8 Hz, 3H)

^{13}C NMR (100.57 MHz, $CDCl_3$, 25°C) 160.98, 137.59, 115.56, 92.69, 49.04, 19.71

3.3.2.7.2 Hydrosilylation

In a round-bottomed flask fitted with a condenser, 2.8 g of the isolated α-methyl trichloroacetamide (13 mmol; 2.6 *M*) was combined with 2.5 mL triethylsilane (15.6 mmol; 3.12 *M*) and 7.5 x 10^{-2} mL 2 wt% Pt-DVDS in xylenes (6.57 x 10^{-6} mol Pt, 0.04% loading wrt silane) in 5 mL anhydrous toluene (46.9 mmol). The reaction mixture was then heated at 110°C for 48 hours; progress was monitored via ^{1}H NMR for the disappearance of the silane proton (~3.7 ppm). The reaction mixture was then allowed to cool to room temperature, and the solvent and excess silane was removed via rotavap to obtain 1.531 g of the desired silylated product (40% yield) as a yellow oil.

3.3.2.7.3 Gabriel Synthesis

A typical synthesis of αMTEtSA was achieved via the series of reactions detailed below. In a round-bottomed flask fitted with a condenser, 9.05 g 3-chloro-1-butene (100 mmol), 24.17 g potassium phthalimide (130 mmol), and 4.14 g potassium carbonate (0.030 mol) were added to 90 mL DMF (0.969 mol) and heated at reflux overnight. The reaction mixture was then poured over ice, forming a brown precipitate, which was isolated via vacuum filtration. The solid was washed with 200 mL 1 *M* NaOH, 100 mL distilled water, 100 mL 1 N HCl, and 100 mL distilled water; it was then vacuum dried, resulting in a 67% yield of the desired 3-phthalimido-1-butene (mp: 76-79°C).

^{1}H NMR (400.13 MHz, $CDCl_3$, 25°C) δ = 7.82 (m, 2H), 7.70 (m, 2H), 6.19 (ddd, *J* = 17.2, 11.2, 6.6 Hz, 1H), 5.19 (dt, *J* = 17.2, 1.2 Hz, 2H), 4.93 (dt, *J* = 10.2, 1.1 Hz, 1H), 1.58 (pt, *J* = 6.9, 1.2 Hz, 3H)

^{13}C NMR (100.57 MHz, $CDCl_3$, 25°C) 167.92, 136.80, 133.84, 133.02, 123.11, 116.33, 48.93, 18.21

3.3.2.7.4 Hydrosilylation

In a round-bottomed flask fitted with a condenser, 20.1 g of the isolated 3-phthalimido-1-butene (100 mmol) and 1.54 mL 2 wt% Pt-DVDS in xylenes (1.35 x 10^{-4} mol Pt, 0.104% loading wrt silane) was added to 60 mL of anhydrous toluene (0.563 mol). The reaction mixture was then heated to 50°C, at which point the protected amine became soluble. 20.7 mL triethylsilane (130 mmol) was then added to the reaction mixture, which was then heated to 110°C and kept at that temperature overnight. The reaction was allowed to cool; the solvent was removed via rotavap and the crude 3-(phthalimidobutyl)triethylsilane was distilled under reduced pressure with a 75% yield of the desired product 3-(phthalimidobutyl)triethylsilane (bp: 120°C at 0.7 mmHg).

^{1}H NMR (400.13 MHz, $CDCl_3$, 25°C) δ = 7.82 (m, 2H), 7.70 (m, 2H), 4.23 (s, 1H), 2.01 (m, 1H), 1.72 (m, 1H), 1.46 (d, *J* = 7.0 Hz, 3H), 0.88 (t, *J* = 7.8 Hz, 9H), 0.48 (q, *J* = 7.8 Hz, 8H)

^{13}C NMR (100.57 MHz, $CDCl_3$, 25°C) 168.61, 133.73, 132.01, 123.01, 50.58, 28.14, 18.30, 8.42, 7.37, 3.10

3.3.2.7.5 Ing-Manske Deprotection

16.9 g 3-(phthalimidobutyl)triethylsilane (53 mmol) was dissolved in 250 mL anhydrous methanol (6.172 mol). 5 mL of anhydrous hydrazine (187 mmol) was slowly added and the reaction mixture was heated at 60°C for 4 hours. A cloudy white network formed, which was precipitated via addition of 2 *M* HCl. The resulting solid was removed

from the desired liquid product mixture via vacuum filtration and washed with 100 mL distilled water. The solvent was removed via rotavap and NaOH was added to the crude product until the pH was greater than 9. Extraction with ether, drying with magnesium sulfate, and distillation under reduced pressure yielded the pure product, 4-(triethylsilyl)-butan-2-amine in 62% yield (bp: 73°C at 2.7 mmHg).

^{1}H NMR (400.13 MHz, $CDCl_3$, 25°C) δ = 2.67 (sextet, *J* = 6.3 Hz, 1H), 1.17 (m, 2H), 1.04 (s, 2H), 0.94 (d, *J* = 6.3 Hz, 3H), 0.83 (t, *J* = 8.0 Hz, 9H), 0.40 (m, 8H)

^{13}C NMR (100.57 MHz, $CDCl_3$, 25°C) 49.71, 34.18, 23.25, 7.48, 7.37, 3.14

Calculated % for $C_{10}H_{25}NSi$ (MW: 187.40 g·mol^{-1}): C 64.09, H 13.45, N 7.47, Si 14.99; found: C 63.03, H 13.47, N 7.39

3.3.2.8 2-Methyl-4-(triethylsilyl)-butyl-2-amine (αDMTEtSA)

Several methods were attempted to synthesize αDMTEtSA before a successful one was found. I was able to successfully use the Overman rearrangement to synthesize the trichloroacetamide-protected branched amine, but hydrosilylation using the protected branched amine was unsuccessful. An alternative method was used to synthesize multi-gram amounts of the desired αDMTEtSA: hydrosilylation using a branched alkyne substrate, followed by hydrogenation of the resulting internal double bond.

3.3.2.8.1 Overman Rearrangement

A solution consisting of 15.5 mL prenyl alcohol (0.1526 mol) in 25 mL anhydrous diethyl ether was added to a 3-neck 250 mL round bottomed flask containing sodium hydride (60% dispersion in mineral oil; 0.6998 g prior to washing with anhydrous heptane; 0.0175 mol) in 80 mL anhydrous Et_2O at -10°C. The reaction mixture was stirred until evolution of hydrogen gas ceased. 14.8 mL trichloroacetonitrile (0.1476 mol) was then added dropwise over the course of 20 minutes. The reaction mixture became first yellow, then

brown. It was allowed to warm to room temperature and the solvent was removed via rotavap. Upon addition of 100 mL of 99:1 hexanes:methanol to the resulting brown oil, a brown precipitate formed. This was removed via gravity filtration and 31.833 of the crude product trichloroacetimidate was recovered. The trichloroacetimidate was not purified further and carried on "as-is" to the next step.

In a 1000 mL round bottomed flask, 31.833 g of the crude trichloroacetimidate was dissolved in 300 mL *p*-xylene (2.433 mol). The flask was then fitted with a condenser, purged with argon, and heated at 140°C overnight. The reaction was then allowed to cool to room temperature and the solvent was removed via rotavap to yield a yellow oil, which, upon standing and cooling, formed greasy yellow crystals (32.7269 g; 96.2 % crude yield). These were allowed to dry under vacuum for 2 days; the yield of the resulting dry trichloroacetamide was found to be 27.5893 g (0.120 mol; 81.08% yield). Although no impurities were detected via ^{1}H NMR, this product is described in literature as forming white needle-like crystals. Decolorization with activated charcoal (in ethanol) and filtration through Celite yielded pale yellow needle-like crystals.

^{1}H NMR (400.13 MHz, $CDCl_3$, 25°C) 6.60 (s, 1H), 6.00 (dd, J = 17.4, 10.7 Hz, 1H), 5.20 (d, J = 17.4 Hz, 1H), 5.15 (d, J = 9.0 Hz, 1H), 1.52 (s, 6H)

^{13}C NMR (100.57 MHz, $CDCl_3$, 25°C) 160.20, 141.86, 113.15, 93.14, 55.82, 26.34

3.3.2.8.2 Hydrosilylation

Hydrosilylation reactions using the α-dimethyl trichloroacetamide as the substrate with triethylsilane and 0.2 mol% Pt-DVDS were unsuccessful. No product was detected via ^{1}H NMR after a reaction time of 1 week in refluxing PhMe.

3.3.2.8.3 Hydrosilylation and Hydrogenation

A 3-neck 250 mL round bottomed flask was fitted with a condenser and stirbar and placed under argon. To this was added 13.75 mL 2 wt% Pt-DVDS in xylenes (1.205×10^{-3} mol Pt; 1.268% catalyst loading wrt silane) and 2.4 mL 0.5 *M* 2,8,9-triisobutyl-2,5,8,9-tetraaza-1-phosphabicyclo[3.3.3]undecane solution (1.200×10^{-3} mol) in diethyl ether. The reaction mixture was heated at 60°C for 10 minutes. After cooling to room temperature, 80 mL of anhydrous inhibitor-free THF (0.9865 mol) was added to the flask, which was then cooled to approximately -10°C in an ice-and-brine bath. 21.25 mL triethylsilane (0.133 mol) was then added dropwise to the flask and allowed to stir for approximately 5 minutes. 10 mL of 2-methyl-3-butyn-2-amine (9.503×10^{-2} mol) was then added dropwise to the reaction mixture, which was kept in the ice bath until the large exotherm had ceased. The reaction was then allowed to stir at room temperature overnight; reaction progress was monitored by the disappearance of the terminal alkyne carbon in the ^{13}C NMR (approximately δ91). The solvent and unreacted silane were removed via rotavap. Distillation under reduced pressure yielded 4.7772 g of the alkene product 2-methyl-4-(triethylsilyl)but-3-en-2-amine as a clear oil (bp 60°C at 5 mmHg; 79.8% yield).

^{1}H NMR (400.13 MHz, $CDCl_3$, 25°C) δ = 6.10 (dd, *J* = 19.0, 2.0 Hz, 1H), 5.55 (dd, *J* = 19.0, 2.0 Hz, 1H), 1.17 (s, 2H), 1.14 (s, 6H), 0.88 (t, *J* = 7.9 Hz, 9H), 0.52 (q, *J* = 7.9 Hz, 6H)

^{13}C NMR (100.57 MHz, $CDCl_3$, 25°C) 157.73, 118.81, 52.47, 30.43, 7.51, 3.70

Hydrogenation of the alkene was carried out in a Parr reactor. The reactor was first loaded with 0.1367 g 5 wt% Pd/C (6.42×10^{-5} mol Pd; 0.11% catalyst loading wrt alkene) and then purged several times with dry nitrogen. 30 mL anhydrous ethanol (0.513 mol) and 11.9032 mL of 2-methyl-4-(triethylsilyl)but-3-en-2-amine (59.69 mmol) were added to the reactor, which was then pressurized with hydrogen (80 psi) and heated at 50°C for 12 hours.

Upon cooling the next morning, the excess H_2 was vented, and the catalyst was removed from the reaction mixture via filtration with Celite. ^{1}H NMR of the product mixture revealed the total absence of any alkene peaks, indicating that the reaction had gone to completion. Removal of the solvent via rotavap yielded 9.1850 g of the desired saturated crude product, which was then distilled at reduced pressure (bp 65°C at 1.5 mmHg; 76.4% isolated yield).

^{1}H NMR (400.13 MHz, $CDCl_3$, 25°C) δ = 1.24 (m, 2H), 1.09 (s, 2H), 0.99 (s, 6H), 0.86 (t, J = 8.0 Hz, 9H), 0.45 (m, 8H)

^{13}C NMR (100.57 MHz, $CDCl_3$, 25°C) 50.20, 38.76, 29.52, 7.42, 5.08, 3.15

Calculated % for $C_{11}H_{27}NSi$ (MW: 201.42 g·mol^{-1}): C 65.59, H 13.51, N 6.95, Si 13.94; found: C 64.03, H 13.51, N 6.67

3.3.2.9 RevIL Synthesis

For all RevILs discussed in this chapter, synthesis was carried out as follows unless otherwise noted. A 2 dram vial was fitted with a rubber septum and purged with inert gas for 5 minutes. The capped vial was then weighed; approximately one gram of the molecular liquid in question was added and the capped vial was weighed again. Dry carbon dioxide was sparged through the molecular liquid for 75 minutes at a flow rate of 200 mL·min^{-1} at 25°C and 1 atm, using a diffuser tube (glass tube with frit on the end). The resulting ionic liquid in the capped vial was then weighed in order to determine that complete conversion had been achieved.

3.3.3 Instrumentation

Attenuated total reflectance Fourier transform infrared spectroscopy (ATR FTIR) data was collected using a Shimadzu IRPrestige21 with a DLaTGS detector with 32 scans and a resolution of 1 cm^{-1}, used in combination with a Specac, Ltd. heated "Golden Gate" ATR accessory with a diamond crystal and zinc selenide lenses.[20e, 25]

^{1}H and ^{13}C NMR spectra were collected on a Varian Mercury Vx 400, using $CDCl_3$ as the lock solvent. Molecular liquids were diluted directly with $CDCl_3$; due to the high viscosities of the ionic forms, the RevILs were synthesized in the NMR tube under solvent-free conditions, and a capillary tube containing $CDCl_3$ was placed inside the sample. Elemental analysis (C, N, and H) of molecular liquids was performed by Atlantic Microlab in Norcross, GA. Samples were stored under inert gas and either delivered in person or sent via FedEx. The elemental analyses of the RevIL forms were obtained but ultimately not used to determine conversion, as there was no way to ascertain the proper low-temperature, CO_2 atmosphere storage of the samples after they were delivered.

Viscosities of all RevILs were obtained using a Rheosys Merlin II viscometer with a 2° cone and plate system; RevILs were pre-formed, allowed to thermally equilibrate on the instrument, and measured in triplicate. Densities of all MLs and RevILs (used in gravimetric calculation of CO_2 uptake) were obtained in triplicate using an Anton Paar DMA 38 Laboratory Density Meter.

For refractive index (RI) measurements, a Reichert Arias 500 Abbe-style refractometer was used, with a circulated cooling bath (heat transfer fluid: glycol). RI were determined in triplicate. Differential scanning calorimetry (DSC) measurements were used to determine the reversal temperatures (T_{rev}) of the RevILs and the evaporation temperatures (T_{evap}) of the MLs. The instrument used was a Q20 TA Instruments DSC; hermetically sealed aluminum pans were used, into which approximately 2 mg of the compound under consideration was measured. The temperature was ramped from -40°C to 400°C with a ramp rate of $5°C \cdot min^{-1}$, and the temperatures of the reversal or boiling events were determined by the intersect of the baseline of the event and the line tangent to the peak of the event.

3.4 Results and Discussion

3.4.1 First-Generation RevILs

Synthesis of the silylated amines had been performed before by our group, but optimization of the catalyst loading showed that 0.2% Pt with respect to the silane limiting reagent afforded quantitative yield via ^{1}H NMR after only a few hours of reaction. Previous work in our group using a lower catalyst loading had required reaction times times as long as one week for some of the bulkier silanes. A former colleage, Dr. Julia Hahne, found that allowing the catalyst and silane to stir together for approximately 10 minutes prior to addition of the allylamine greatly increased the hydrosilylation yields.

Following synthesis of the molecular liquids, each ML was purified and reacted with CO_2. Proof of reaction was obtained via a number of methods, including ^{1}H and ^{13}C NMR, as well as FTIR. Sample NMR spectra of a representative ML and RevIL, TPSA, can be seen in Figure 3.11, Figure 3.12, and Figure 3.13. The ^{1}H spectrum of the TPSA RevIL form is not included; the high viscosity of the NMR sample leads to extensive peak broadening, and very little can be determined regarding the chemical shifts of the various protons.

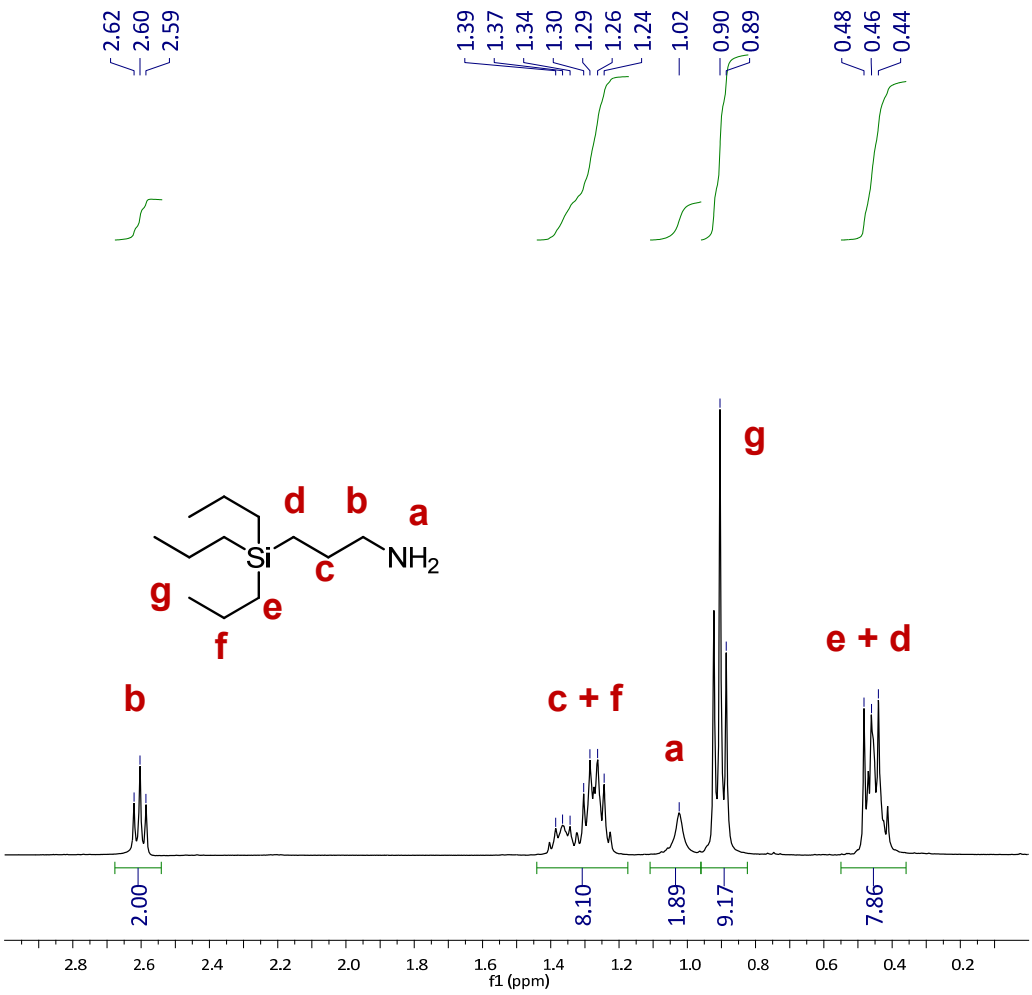

Figure 3.11. ^{1}H NMR of TPSA molecular liquid.

During synthesis, conversion is determined via ^{1}H NMR. The integration of the silane proton in the starting material (typically around 3.7) is compared to that of the triplet that arises around 2.6, which is only seen in the product (peak *b* in Figure 3.11).

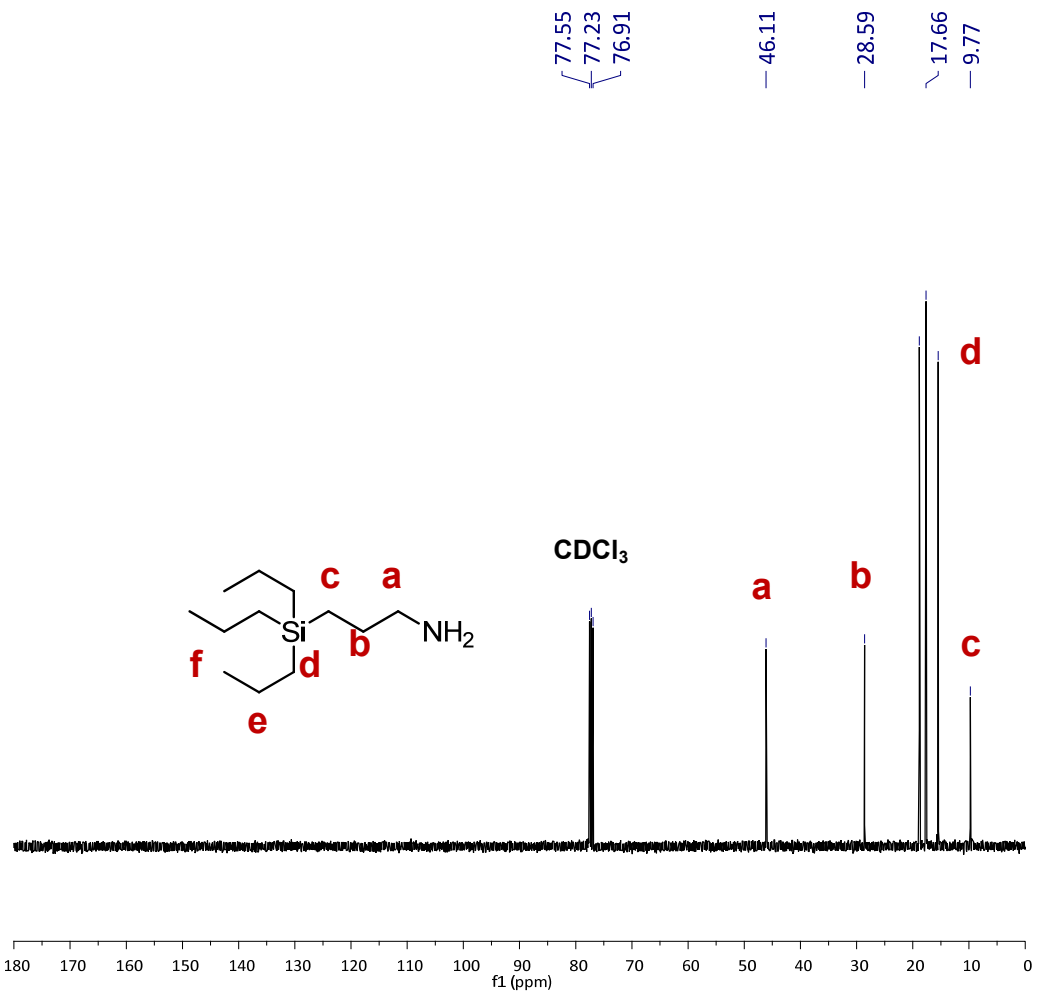

Figure 3.12. ^{13}C NMR of TPSA molecular liquid.

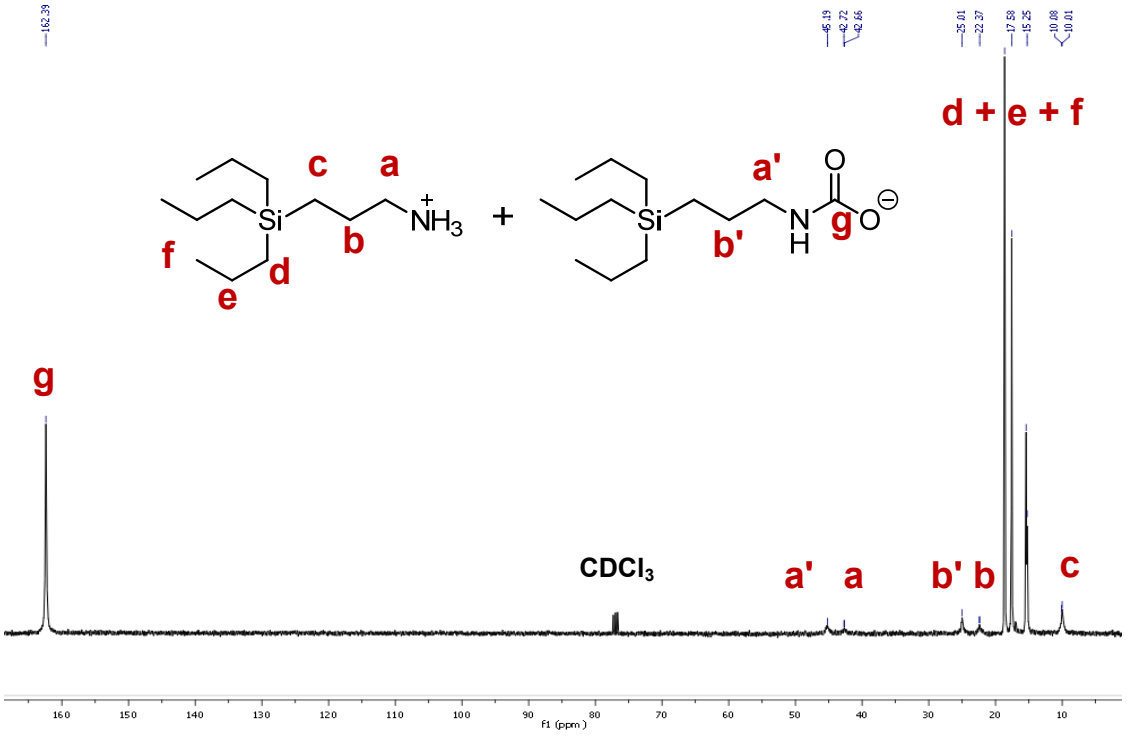

Figure 3.13. ^{13}C NMR spectrum of TPSA RevIL.

The greatest change can be seen when comparing the ^{13}C spectra before and after reaction with CO_2 (Figure 3.12 and Figure 3.13)—a carbamate peak appears at δ162.39 (peak *g* in Figure 3.13) upon reaction with CO_2. The conversion of ML to RevIL can also be observed when focusing on peaks *a* and *b* in the ^{13}C spectra. Peak *a* corresponds to the carbon α to the amine; in Figure 3.13, we can see that this peak has split into two (the downfield *a*' and the upfield *a*) due to the formation of the carbamate anion and ammonium cation, respectively. Peak *b*, corresponding to the carbon *β* to the amine, undergoes a similar split. The remaining carbons appear to be too distant from the amine to undergo a change in the ^{13}C NMR spectrum upon reaction with CO_2.

3.4.1.1 First Generation RevILs: CO_2 Capacity

The silylated amines we have synthesized react with CO_2 in a 2:1 stoichiometric ratio—that is, 0.5 moles of CO_2 per mole of ML. The theoretical chemisorptive capacity of

each amine can therefore be calculated and expressed in a commonly used industrial unit, moles of CO_2 per kilogram of ML. These theoretical capacities were then compared with the experimental capacities found using the gravimetric method detailed above (page 95). The results for the first-generation RevILs are shown below in Figure 3.14.

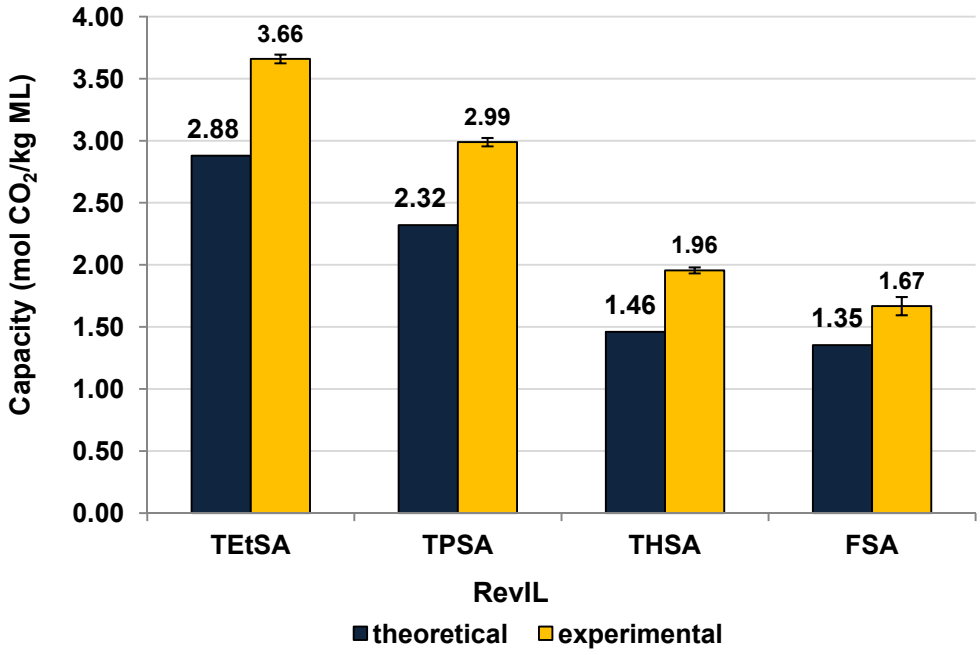

Figure 3.14. Comparison of theoretical and experimental CO_2 capacities for first-generation RevILs.

The experimental capacity of all 4 first-generation RevILs was greater than the theoretical capacity, i.e. CO_2 capture via chemisorption only. As the length of the residual group on the silicon increases, the capacity decreases—this is due to the increase in molecular weight of the ML. Increasing the molecular weight of the sorbent, while retaining the same 2:1 stoichiometric ratio of moles of ML to moles of CO_2, results in a decrease in capacity.

Converting these measurements to another unit of capacity, moles of CO_2 per mole of ML, allows us to compare compare CO_2 capacities on a mole-to-mole basis (Figure 3.15).

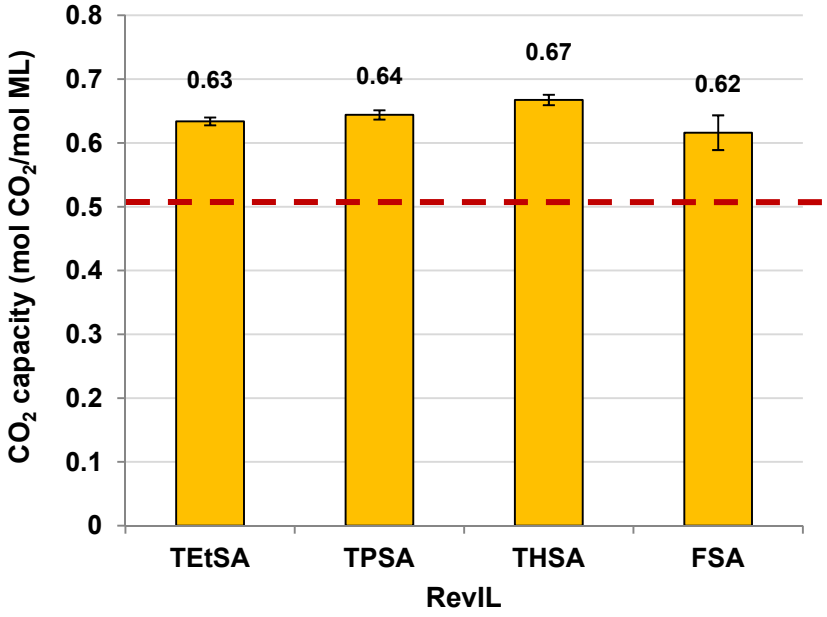

Figure 3.15. Experimental CO_2 capacities expressed in moles of CO_2 per mole of ML for first-generation RevILs. Red line indicates theoretical chemisorption at 0.5 moles of CO_2 per mole of ML.

The theoretical chemisorption for all amines investigated was 0.5 moles of CO_2 per mole of ML, shown by the dashed line in Figure 3.15. For comparison, the CO_2 capacity of a 30 wt% aqueous solution of MEA has been found to be 0.22 moles of CO_2 per mole of MEA.[6] For TEtSA, TPSA, and THSA, increasing the length of the alkyl group on the silicon increases the CO_2 capacity. The one notable exception to this relationship between R group length and CO_2 capacity is FSA. This fluorinated silylated amine was selected for synthesis due to the known CO_2-philicity of perfluorinated hydrocarbons;[26] it was proposed that this feature could increase CO_2 capacity through physisorption. However, Figure 3.15 shows that the

CO_2 physisorption of the fluorinated silane is comparable to the other 3 first-generation RevILs. Further evidence of physisorption can be seen in Figure 3.16, where the attenuated total reflectance Fourier transfer infrared (ATR FTIR) spectra of the molecular liquid form of TPSA and the ionic liquid form thereof are compared.

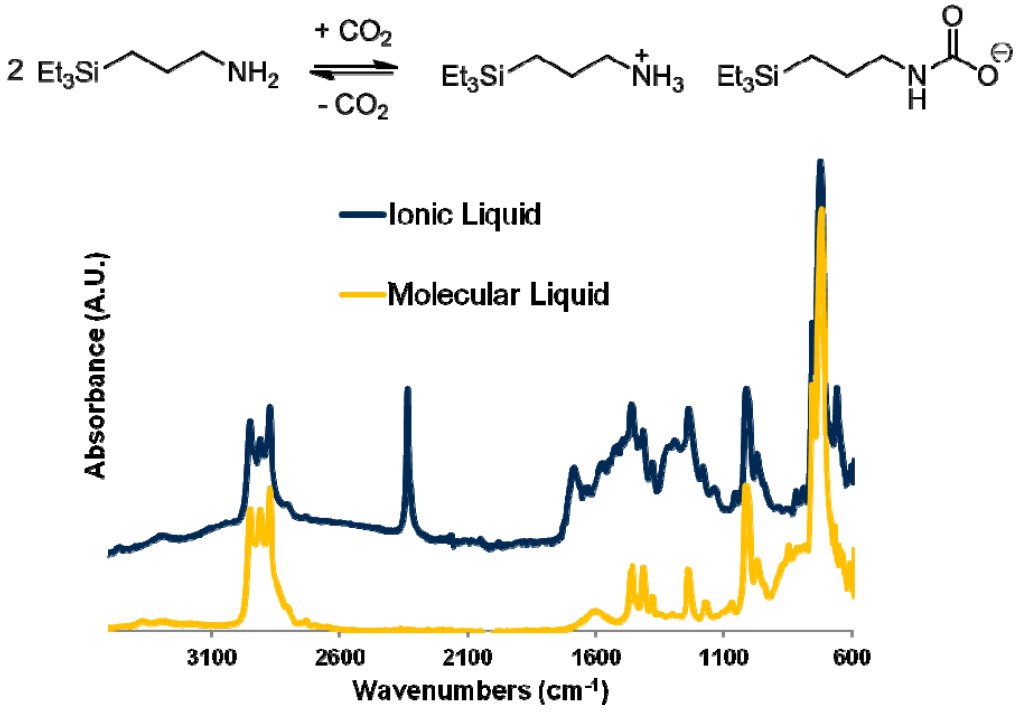

Figure 3.16. Offset FTIR spectra of TPSA molecular liquid (*bottom*) and ionic liquid (*top*). Note sharp peak at 2400 cm^{-1}, indicating presence of free (physisorbed, unreacted) CO_2.

There are three main regions in which significant differences between the two spectra can be observed. The broadening of the peak just below 3000 cm^{-1} is due to the absorption of the ammonium group, and the formation of the sharp peak at 1700 cm^{-1} is due to the stretching frequency of the carbonyl group in the carbamate moiety of the RevIL anion. The strong

sharp absorption at 2400 cm^{-1} is due to the asymmetric stretch of free unreacted CO_2 present as physisorbed CO_2 in the RevIL.

Physisorption of a gas into a liquid can be calculated using Henry's Law, which states that the solubility of a gas in a liquid is directly proportional to the partial pressure of the gas in contact with the liquid.[22] Calculating the Henry's Law constants could permit us to calculate the maximum amount of CO_2 that could be physisorbed into our RevIL, providing us with a theoretical limit for physisorption. Determination of the Henry's Law constants for our silylated amines was performed by my colleague Amy Rohan. The absorbance of the asymmetric stretch of free CO_2 was determined at a series of pressures (0-60 bar) for each RevIL, and from these values, the mole fraction of CO_2 dissolved in the RevIL at the pressure in question was calculated. The Henry's Law constants for the first-generation RevILs were then determined by plotting the mole fraction of CO_2 as a function of CO_2 pressure and fitting a straight line to the data points; the slope of the line is the Henry's constant. Using the calculated Henry's constants, the theoretical physisorption of each RevIL at 25°C and 1 bar CO_2 pressure was calculated. For TPSA, the theoretical chemisorption is 2.32 moles of CO_2 per mole of ML (Figure 3.14); the theoretical physisorption was calculated to be 0.05 moles of CO_2 per mole of ML, for a total CO_2 capacity of 2.37 moles of CO_2 per mole of ML. However, the observed capacity is 2.99 moles of CO_2 per mole of ML—still higher than the combined theoretical chemi- and physisorption. Several explanations for this enhanced capacity were investigated. The presence of water has been shown to increase the CO_2 capacity of hindered amines; however, our amines were found to have almost no water present via Karl Fischer titration. Another possibility was the presence of small bubbles of CO_2 entrained within the viscous RevIL; the small radius of curvature of these bubbles would cause high local partial

pressures of CO_2, which would increase the physisorption. No evidence of these bubbles was found via dynamic light scattering (DLS), which is a technique commonly used to size micelles or particulates in solution. The final possibility we considered was the formation of carbamic acid in our RevILs.

My co-worker Jackson Switzer has shown, through the use of quantitative ^{13}C NMR, that carbamic acid is formed upon reaction of TPSA with CO_2. If the silylated amines are indeed reacting with CO_2 in a 2:1 stoichiometric ratio, we would expect peaks *a* and *a'* from Figure 3.13 (as well as *b* and *b'*) to have equal integrations in a quantitative ^{13}C NMR spectrum. However, it was found that the ratio of the integrations of the downfield "carbamate" peaks and the upfield ammonium peaks was 1.4:1. Although this would seem to indicate that more carbamate ions are present than ammonium ions, this is not possible—there must be another species present that has the same chemical shifts for the carbons α and β to the amine. Carbamic acid is such a compound. The proposed mechanism of carbamic acid formation is shown below in Figure 3.17.

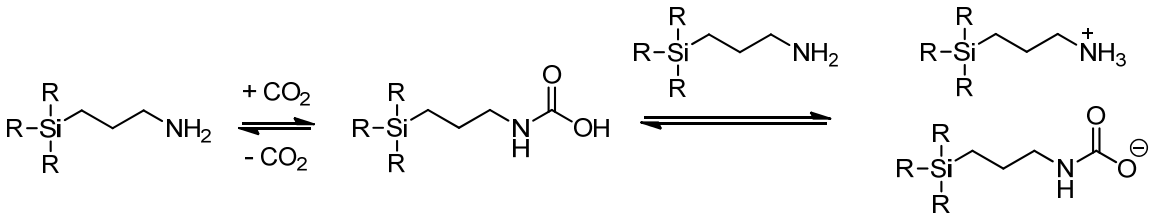

Figure 3.17. Formation of carbamic acid as intermediate to fully converted RevIL form.

The silylated amine reacts with CO_2 to form a carbamic acid intermediate. This is then deprotonated by another molecule of silylated amine to yield the anticipated ammonium-carbamate ion pair. However, if not all of the carbamic acid is deprotonated, the CO_2

capacity of the RevIL will seem to be closer to a 1:1 ratio of amine to CO_2, rather than the expected 2:1 stoichiometric ratio of amine to CO_2. The evidence therefore supports the presence of carbamic acid in our system, which results in an increase in capacity over the theoretical chemisorptive and physisorptive capacities combined.

3.4.1.2 First-Generation RevILs: Reversal Temperature

As mentioned before, the ionic forms of these molecules will convert back to the molecular amines upon heating. The temperature at which this occurs is designated the reversal temperature, or T_{rev}, and is determined using differential scanning calorimetry (DSC). In a DSC analysis, the temperature of the sample in question is increased, and the amount of heat supplied to the system to achieve that temperature increase is recorded. Phase transitions such as melting and evaporation can be observed using this technique. Approximately 2 mg of the pre-formed RevIL under consideration was sealed in an aluminum pan, which was then heated from -40 to 400°C at a ramp rate of $5°C \cdot min^{-1}$. The temperature at which the reversal event occurred was determined by finding the intersect of the baseline of the event and the line tangent to the peak of the event. A sample DSC thermogram for TPSA is shown in Figure 3.18.

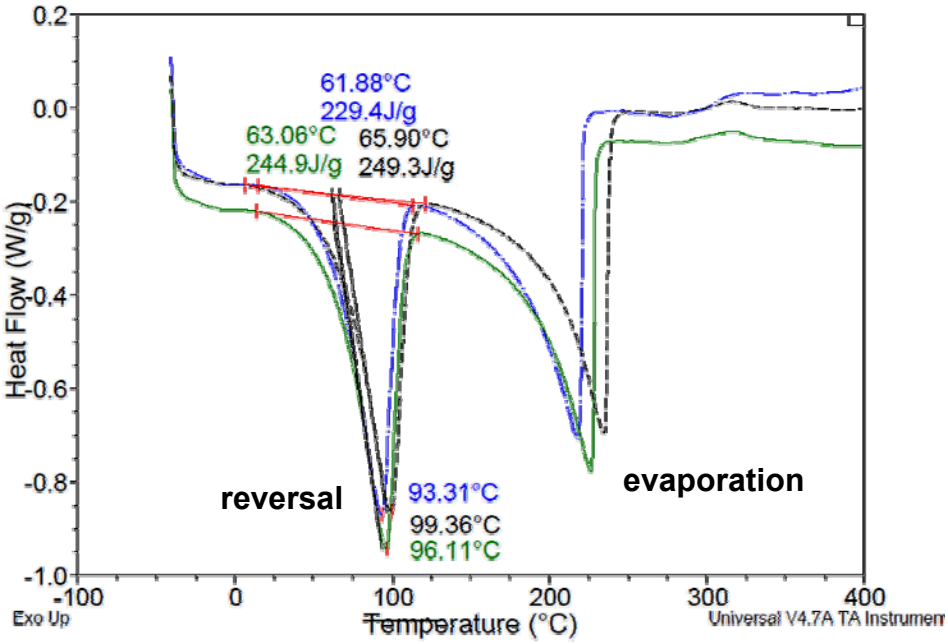

Figure 3.18. DSC thermogram of TPSA (in triplicate).

The two events present in the DSC thermogram correspond to the release of CO_2 (i.e. the transition from RevIL to ML) and the evaporation of the ML. The evaporation temperature, or T_{evap}, is reported rather than the boiling point, as the small amount of sample analyzed via DSC has a high surface area-to-volume ratio and does not accurately reflect the boiling point. For a more accurate determination of boiling point, extrapolation from the distillation temperature under vacuum is recommended. The T_{rev} and T_{evap} of the first-generation RevILs can be seen in Figure 3.19.

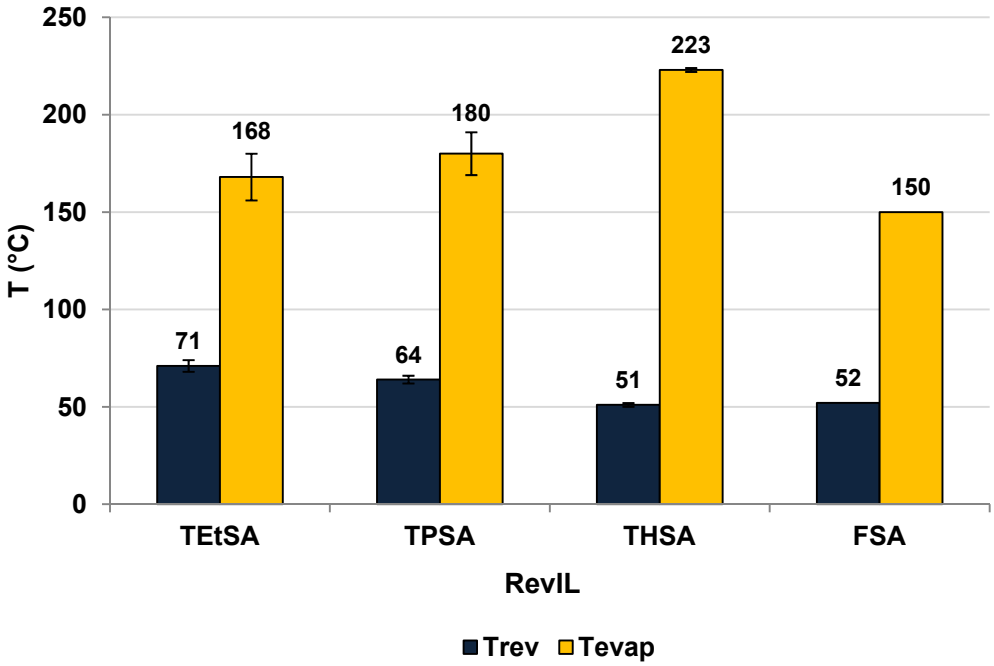

Figure 3.19. T_{rev} and T_{evap} of first-generation RevILs.

Although the reversal temperature decreases with increasing length of the alkyl chains on the silicon, the evaporation temperature increases. This large difference between T_{rev} and T_{evap} is desirable for an actual CO_2 capture process, as it minimizes the amount of solvent lost to evaporation during regeneration. For a 30 wt% solution of MEA, the scrubbing solution must be heated to 110-120°C in order to release the captured CO_2.[27] All of the first-generation silylated amines exhibit T_{rev} lower than this benchmark when run neat.

3.4.1.3 First Generation RevILs: Viscosity

One of the other properties investigated was the viscosity of the RevIL formed upon reaction with CO_2. The viscosities of the first-generation RevILs were measured at two temperatures: 25 and 40°C, which represents the operating temperature of a flue gas stack. The pre-formed RevILs were allowed to thermally equilibrate prior to measurement using a Rheosys Merlin II viscometer with a 2° cone and plate system.

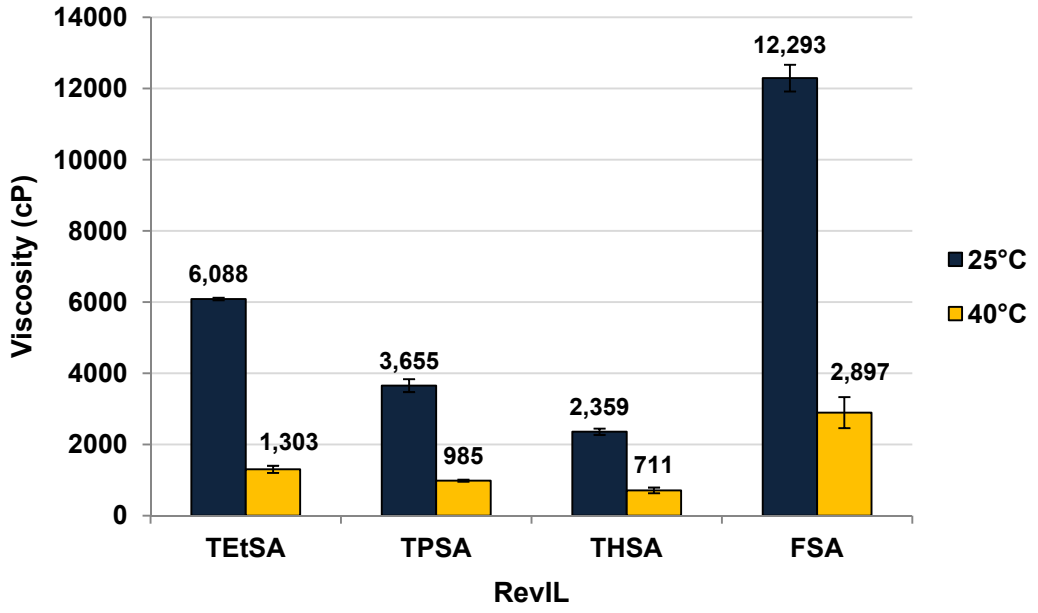

Figure 3.20. Viscosities of first-generation RevILs at 25 and 40°C.

All molecular liquids investigated have viscosities lower than 100 cP. Two trends can be observed in Figure 3.20. The viscosity decreases as the length of the alkyl chain increases; additionally, the viscosities of all RevILs shown are significantly lower at 40°C than at 25°C. As an actual flue gas stack temperature is close to 40°C, this shows that, with some modifications, our RevILs could be industrially viable. However, all RevILs depicted still have viscosities higher than the 100 cP industrial viability limit. While one could theoretically continue to increase the length of the alkyl chains on the silane, this would result in a decrease in capacity, which, as mentioned above, is typically expressed in moles of CO_2 per kilogram of sorbent. Increasing the molar weight of the sorbent, while retaining the same 2:1 stoichiometric ratio of moles of sorbent to moles of CO_2, would result in a decrease in capacity. It was also hypothesized that the non-symmetric substitutents on the silicon of

FSA would disrupt the packing of the RevIL formed and thus decrease the viscosity. However, the opposite effect was observed. This is most likely due to the presence of highly polarized fluorine-carbon bonds; these can interact with the ammonium cations via hydrogen bonding and therefore increase the viscosity when compared to the non-perfluorinated RevILs.

Viscosity of the RevILs can be controlled not only through modification of structure, but also through conversion. As mentioned before, the viscosities of the molecular liquids are all low—in fact, they are below the detection limit of the viscometer in our lab. The viscosities of the RevILs are several orders of magnitude higher. However, the increase in viscosity is not linear with respect to conversion, as seen in Figure 3.21. To obtain these viscosity measurements, the TPSA ML was reacted with CO_2 for brief periods of time. Refractive index (RI) was used to determine the extent of conversion—the RI of the partially-converted TPSA was measured and compared to values that had previously been determined over a range of conversions. As the difference in RI between the molecular and ionic forms of TPSA is 0.02, and the refractometer is accurate to ± 0.0001, this was a faster and more accurate method of determining conversion than ^{1}H NMR.[25]

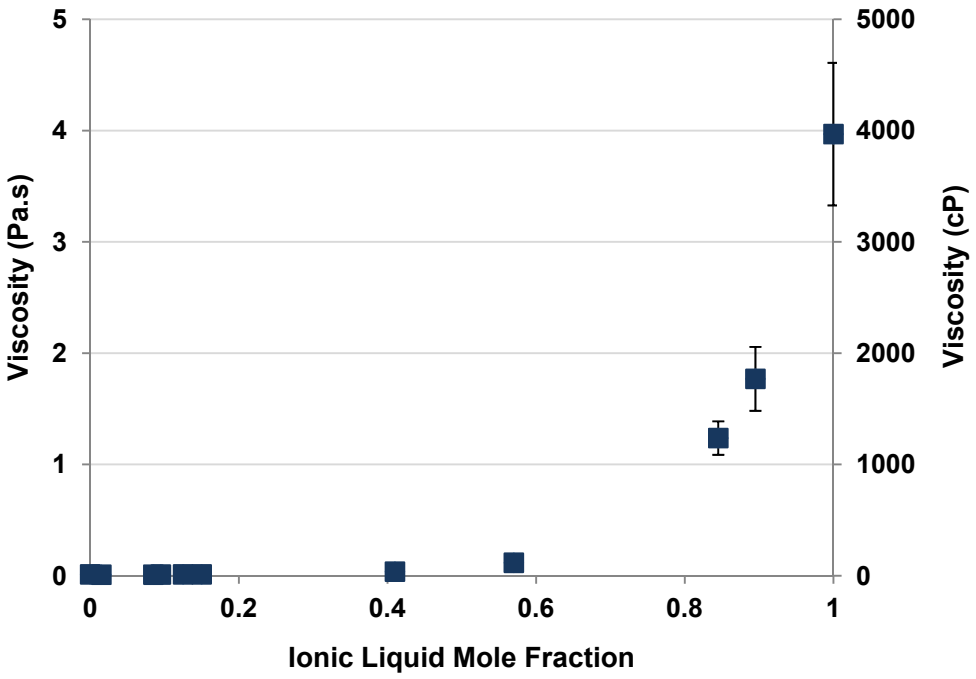

Figure 3.21. Viscosity of TPSA RevIL as a function of conversion. Note relatively composition-independent region below 60% conversion.

Although the fully converted RevILs are very viscous—the example shown in Figure 3.21, TPSA, has a viscosity of approximately 4000 cP at full conversion—at conversions less than 60%, the viscosities are quite low—in fact, the viscosity of the system stays below the 100 cP mark until approximately 50% conversion. This is likely due to the unreacted molecular liquid solvating the ammonium and carbamate ions, limiting ionic pairing. Importantly, this behavior suggests that, in an actual CO_2 capture system, the viscosity could be controlled by limiting the extent of reaction. This non-linear increase in viscosity gives our system an advantage over traditional ILs or amine-functionalized ILs as CO_2 sorbents—the viscosities of those solvents will remain extremely high regardless of the extent of CO_2 capture.[4]

Desiring more flexibility in our system, we sought to synthesize new amines that would exhibit a lower viscosity without relying on extent of reaction. At full conversion, the

viscosities and capacities of the first-generation RevILs are inextricably linked—by increasing the length of the alkyl groups on the silicon, not only does the viscosity decrease, but the capacity decreases as well. We investigated other structural modifications that would decrease the viscosity with minimal impact on capacity. There are three main sections of the silylated amines that can be modified to affect their performance as liquid sorbents for CO_2: the alkyl groups on the silicon; the linker between the silicon and the amine group; and the environment around the amine group itself. We therefore began to focus on the other two possibilities, namely modification of the propyl linker and introduction of branching around the amine group.

3.4.2 Second-Generation RevILs

It was postulated that if a silylated amine with an unsaturated linker were synthesized, a mixture of the *cis* and *trans* stereoisomers, as in Figure 3.22, would disrupt the packing of the RevIL and decrease the viscosity.

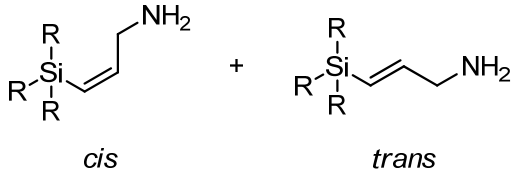

Figure 3.22. *Cis* and *trans* stereoisomers of an unsaturated silylated amine.

The unsaturation would also slightly decrease the molecular weight of the sorbent, giving a small boost in capacity when expressed in moles of CO_2 per kilogram of molecular liquid. Terminal alkynes can act as hydrosilylation substrates, similar to the analogous allylamine. Although Karstedt's catalyst is not stereoselective when used in hydrosilylations of terminal alkynes,[28] bulky azaphosphatranes have been shown to facilitate regio- and stereoselective

hydrosilylation of these compounds.[28-29] Aneetha *et al.* have shown that the use of the aminophosphine ligand shown below in Figure 3.23, yields only the *trans* isomer of the adduct obtained from the reaction between propargylamine and triethylsilane.[29]

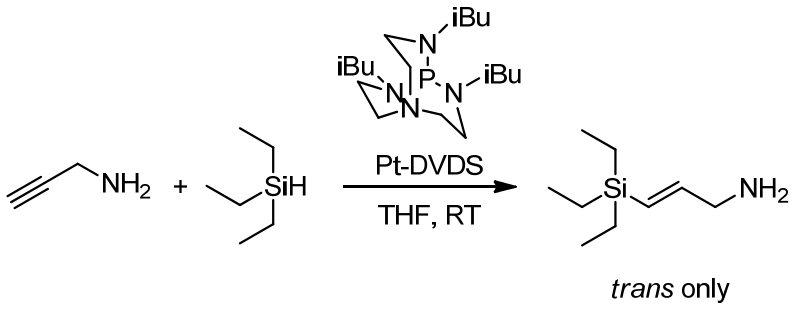

Figure 3.23. Synthesis of *trans*-3-(triethylsilyl)-2-propen-1-amine using Karstedt's catalyst and an azaphosphatrane ligand.

The desired catalyst was synthesized *in situ* prior to hydrosilylation by combining Pt-DVDS in xylenes with the commercially available azaphosphatrane ligand and heating at 60°C for 10 minutes. THF was then added to the catalyst mixture, followed by triethylsilane; this was then allowed to stir for 10 minutes. The propargylamine was added to the reaction mixture and allowed to stir at room temperature overnight. Using this protocol, the *trans*-3-(triethylsilyl)-2-propen-1-amine was synthesized in multi-gram quantities (45.57% isolated yield).

Investigation of the properties of *trans*-3-(triethylsilyl)-2-propen-1-amine is underway; preliminary viscosity measurements indicate that the viscosity is lower than that of the saturated analog at full conversion at room temperature (i.e. lower than 6000 cP). Synthesis of the *cis* stereoisomer of this compound will be discussed in the Path Forward section.

Hydrosilylation is generally thought to proceed via the Chalk-Harrod mechanism, proposed in 1965 and depicted in Figure 3.24.[28]

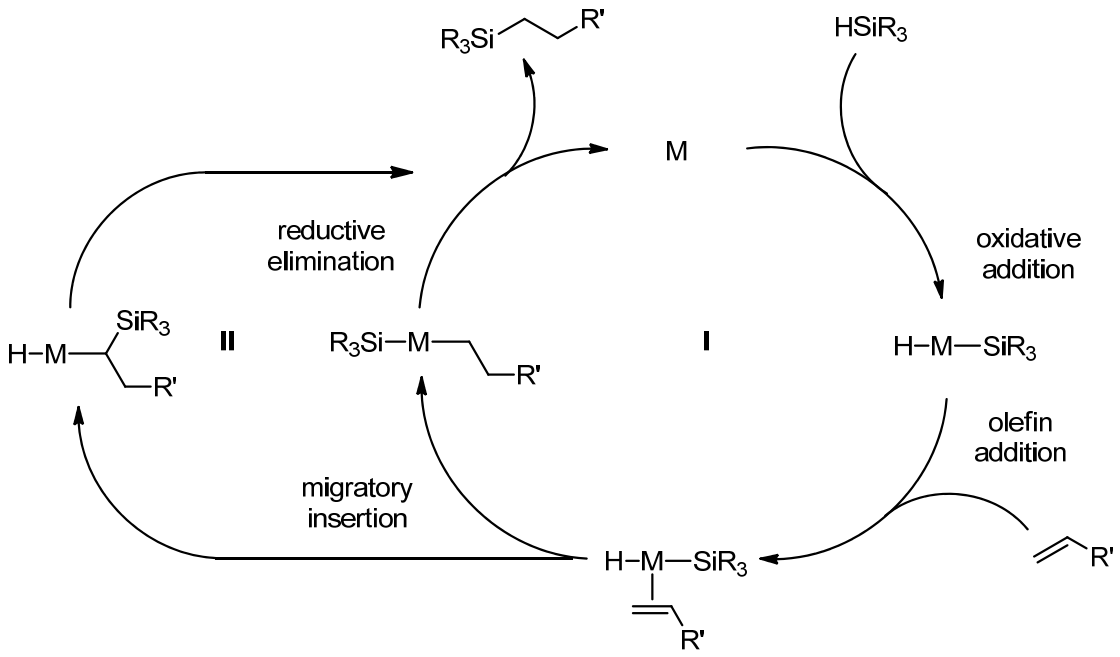

Figure 3.24. Chalk-Harrod mechanism for hydrosilylation (*right*, I) and modified Chalk-Harrod mechanism (*left*, II) for late transition metals (e.g. Pt, Rh, Ir).[28]

Oxidative addition of the trialkylsilane to the active catalyst yields a silyl metal hydride, which coordinates with an olefin. In the traditional Chalk-Harrod mechanism, migratory insertion of the alkene into the metal-hydride bond yields an alkyl-silyl metal complex (cycle I in Figure 3.24), whereas in the modified Chalk-Harrod mechanism (cycle II, Figure 3.24), the alkene inserts into the metal-silyl bond. Both substrates undergo reductive elimination to yield the silylated anti-Markownikoff product. When a terminal alkyne is the hydrosilylation substrate, the stereochemistry of the resulting alkene is thought to be dictated by the stereochemistry of the intermediate following the migratory insertion step. The presence of a bulky ligand at this point in the catalytic cycle—in the case of this synthesis, the

azophosphatrane ligand—will further increase the proportion of thermodynamically favored *trans*-alkene in the product.[28]

3.4.3 Third-Generation RevILs

The third section of silylated amines that can be varied is, as mentioned previously, the environment of the amino group. Hindered amines are defined as compounds containing primary amines adjacent to a tertiary carbon, or secondary amines adjacent to secondary or tertiary carbons.[30] These amines with steric hindrance near the reactive site have been shown to form weaker carbamate bonds in aqueous solution;[31] it was postulated that this phenomenon could decrease the T_{rev} of the ionic liquids formed from branched amines. A weaker carbamate bond is also more susceptible to hydrolysis;[31b] in the case of flue gas, where water is present, hydrolysis of the carbamate will result in the formation of bicarbonates and the *in situ* regeneration of free amines, which are then free to react further with CO_2.[30b] This would result in an increase in overall sorbent capacity.

Additionally, the presence of branching could potentially decrease the viscosity of the RevILs formed by disrupting the packing efficiency of the ion pairs. A retrosynthetic analysis of a prototypical trialkylsilylpropylamine with branching at the positions α and β to the amine group shows that these compounds can be obtained via a hydrosilylation reaction between an allylamine and a trialkylsilane, as in the case of our typical (i.e. unbranched) RevILs (Figure 3.25).

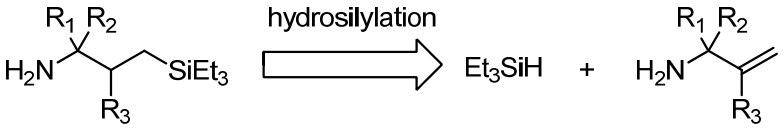

Figure 3.25. Retrosynthetic analysis of a (3-aminopropyl)triethylsilane with branching at positions α and β to the amine.

Few branched allylic amines are commercially available; however, they are obtainable via the Overman synthesis, in which a branched allyl alcohol is reacted with trichloroacetonitrile to yield a trichloroacetimidate, shown in Figure 3.26. Upon heating in refluxing *p*-xylene, this trichloroacetimidate then undergoes a [3,3] sigmatropic rearrangement to yield a trichloroacetamide. Residual groups R_1 and R_2 begin at a position *γ* to the allylic heteroatom (in the starting material, oxygen); following the rearrangement, they are *α* to the allylic heteroatom nitrogen. The trichloroacetamine can then be deprotected under basic conditions to yield the allylic amine.[32]

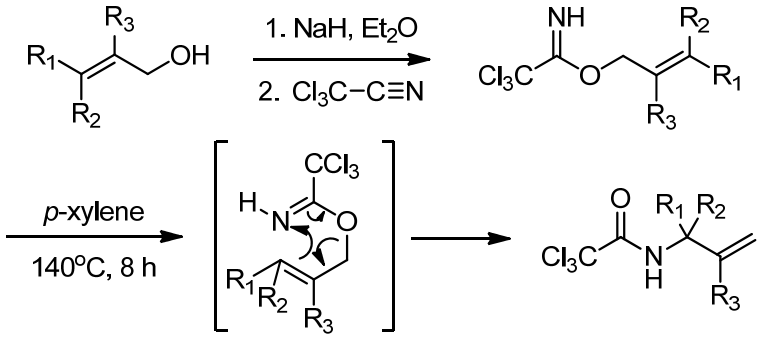

Figure 3.26. Overman rearrangement.

Alternatively, the trichloroacetamide could be used directly as a hydrosilylation substrate, with deprotection carried out following the hydrosilylation, as shown Figure 3.27.

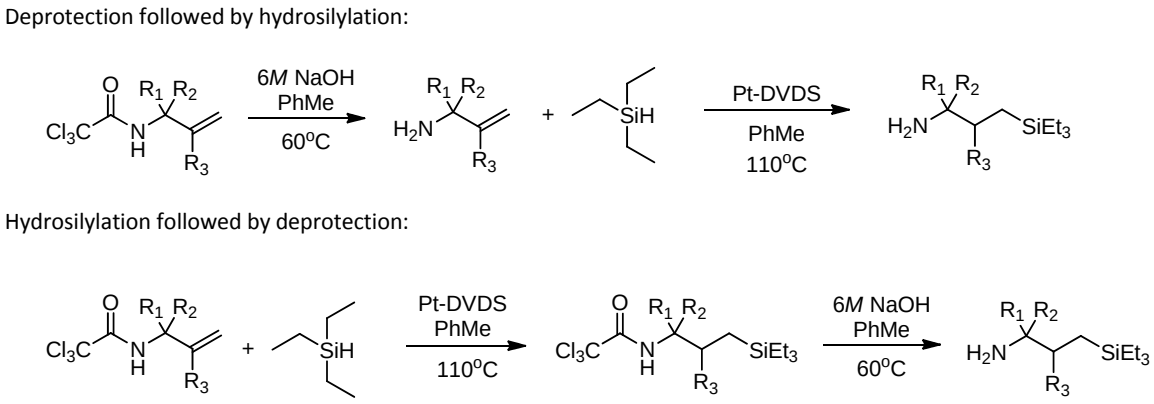

Figure 3.27. *Top*, deprotection of the trichloroacetamide followed by hydrosilylation to yield silylated amine; *bottom*, hydrosilylation using the trichloroacetamide as substrate, followed by removal of protecting group to yield silylated amine.

As an initial panel of branched amines, we selected three, shown in Figure 3.28. The amines chosen had methyl groups present at either the α carbon, adjacent to the amino group, or the β carbon, in the middle of the propyl linker.

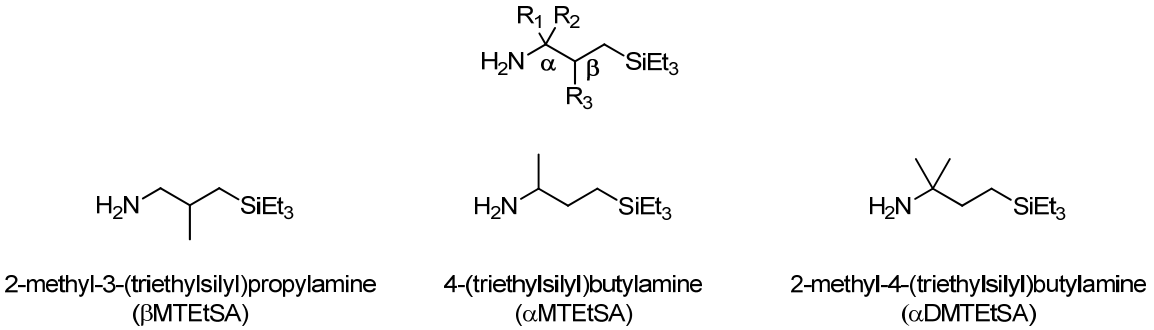

Figure 3.28. Initial third-generation silyated amines chosen as synthetic targets. *Left*, 2-methyl-3-(triethylsilyl)propylamine (βMTEtSA). *Middle*, 4-(triethylsilyl)-butyl-2-amine (αMTEtSA). *Right*, 2-methyl-4-(triethylsilyl)-butyl-2-amine (αDMTEtSA).

The three amines were: 2-methyl-3-(triethylsilyl)propylamine (βMTEtSA); 4-(triethylsilyl)-butyl-2-amine (αMTEtSA); and 2-methyl-4-(triethylsilyl)-butyl-2-amine (αDMTEtSA).

Methyl groups were selected as our initial "branches," as these groups would contribute steric bulk without greatly increasing the weight of the ML and decreasing the capacity. We anticipated that all 3 branched amines could be synthesized via the Overman rearrangement.

3.4.3.1 Synthesis of βMTEtSA

We first attempted to synthesize the β-methyl silyated amine (i.e. methylated at the R_3 position depicted in Figure 3.28) via an Overman rearrangement, as seen in Figure 3.29.[33]

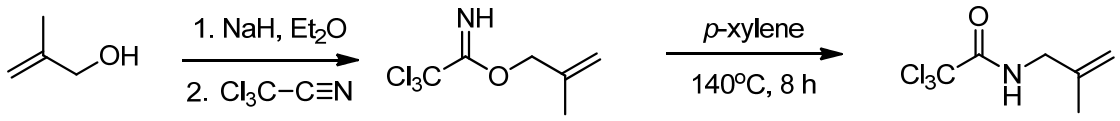

Figure 3.29. Overman rearrangement of 2-methyl-2-propenol to form β-methyl trichloroacetamide precursor to βMTEtSA.

The starting allyl alcohol was 2-methyl-2-propenol, which was deprotonated with sodium hydride and then acted as a nucleophile towards trichloroacetonitrile. Synthesis of the trichloracetimidate was successful; the product was not isolated, but subjected to rearrangement conditions without further purification. Although the trichloroacetamide was shown to have been formed via ^{13}C NMR, purification of the trichloroacetamide via column chromatography was not successful, as the product degraded on the column. We then found a commercial source for the 2-methylallylamine, which could be used in the more straightforward hydrosilylation. Ultimately βMTEtSA was synthesized via hydrosilylation as shown in Figure 3.30, analogous to the preparation of the unbranched RevIL precursors.

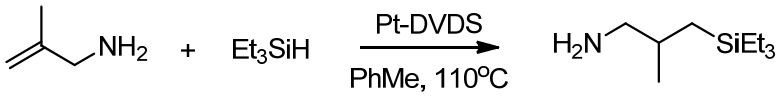

Figure 3.30. Hydrosilylation of 2-methylallylamine to yield 2-methyl-3-(triethylsilyl)propylamine (βMTEtSA).

This hydrosilylation reaction differed from that of the first-generation RevILs only in that the amine was the limiting reagent, rather than the silane as before. βMTEtSA was isolated in 76.4% yield and stored under inert atmosphere.

3.4.3.2 Synthesis of αMTEtSA

We initially attempted to synthesize αMTEtSA via an Overman rearrangement with crotyl alcohol as shown in Figure 3.31.

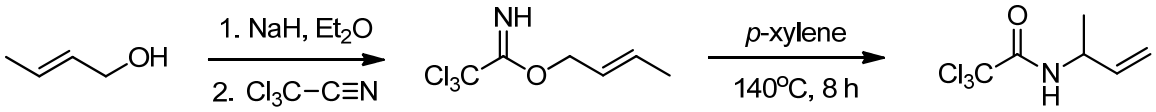

Figure 3.31. Overman rearrangement of crotyl alcohol to form α-methyl trichloroacetamide precursor to αMTEtSA.

Crotyl alcohol was combined with sodium hydride and trichloroacetonitrile in ether to yield the desired trichloroacetimidate. The Overman rearrangement itself proceeded smoothly; the low isolated yield (17%) of the α-methyltrichloroacetamide is due to losses resulting from column chromatography purification. Hydrosilylation was carried out with triethylsilane in accordance with the usual protocol using Karstedt's catalyst. However, the trichloroacetamide protecting group proved intractable. Several methods of deprotection were attempted, including: prolonged heating with concentrated NaOH;[34] treatment with sodium borohydride;[35] and heating with cesium chloride in *N*,*N*-dimethylformamide

(DMF).[36] Ultimately, we decided to abandon use of the Overman rearrangement and took another synthetic route.

The Gabriel synthesis is a common method to synthesize primary amines from alkyl halides. The nucleophilic attack of potassium phthalimide on an alkyl halide yields a protected primary amine. The Ing-Manske deprotection protocol uses hydrazine to remove the phthalimide protecting group, yielding the desired primary amine and the side product phthalyl hydrazide.[37] As a starting material, we used the allylic alkyl halide 3-chloro-1-butene. The synthetic scheme used for synthesis of the protected amine 3-phthalimido-1-butene was set forth by Semenow *et al.* and is shown in Figure 3.32.[38]

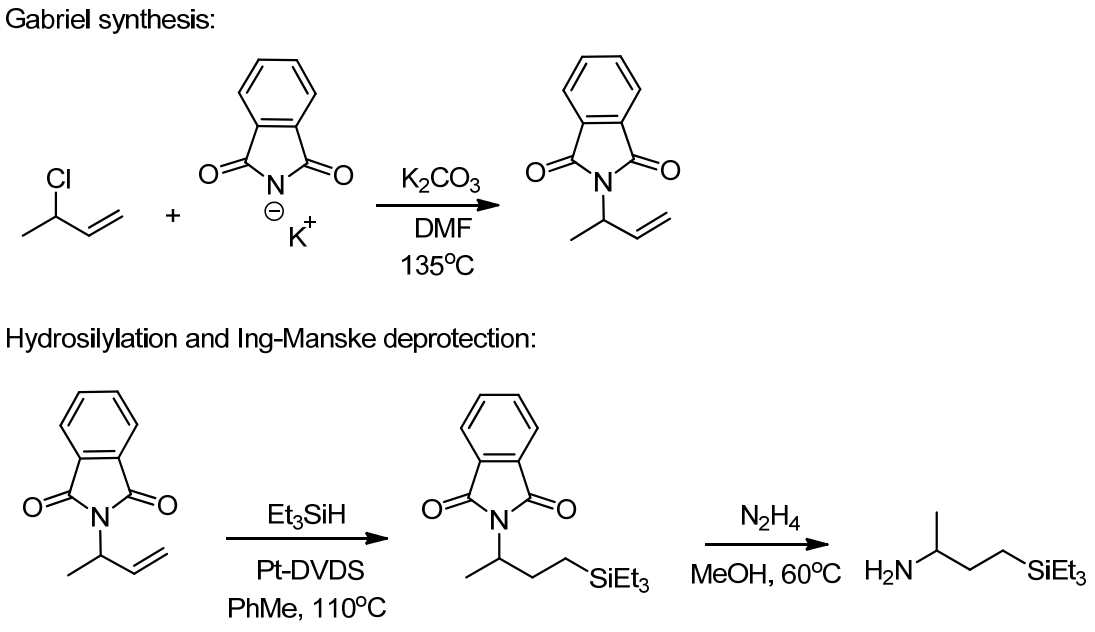

Figure 3.32. *Top*, Gabriel synthesis using 3-chloro-1-butene to yield protected primary amine; *bottom*, hydrosilylation and Ing-Manske deprotection to yield 4-(triethylsilyl)-butyl-2-amine (αMTEtSA).

Potassium phthalimide reacted with the allylic halide 3-chloro-1-butene in DMF to yield the protected primary amine 3-phthalimido-1-butene in good yield from the Gabriel synthesis,

and hydrosilylation using this substrate proceeded well. The hydrosilylated product was isolated via distillation prior to deprotection with anhydrous hydrazine, yielding the desired product 4-(triethylsilyl)-butyl-2-amine. Distillation of the hydrosilylation product 3-(phthalimidobutyl)triethylsilane prior to deprotection required very high temperatures (approximately 160°C at the distillation head under vacuum), and we found that distillation was not necessary for deprotection to occur with high yields. The combination of the Gabriel synthesis, hydrosilylation, and Ing-Manske deprotection proved a reliable method to synthesize αMTEtSA, and large quantities of the amine were prepared in this way for characterization and property analysis.

3.4.3.3 Synthesis of αDMTEtSA

The Overman rearrangement was also attempted in the synthesis of αDMTEtSA, shown in Figure 3.33; following the work of Nagashima *et al.*, the starting allylic alcohol was prenyl alcohol.[39]

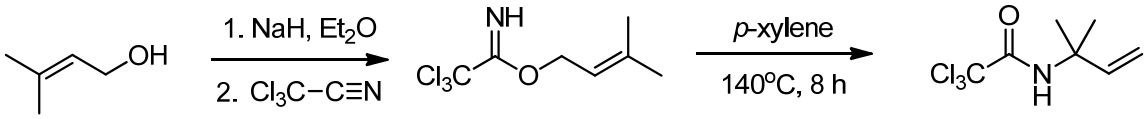

Figure 3.33. Overman rearrangement of prenyl alcohol to form α-dimethyl trichloroacetamide precursor to αDMTEtSA.

Again, the Overman rearrangement proceeded smoothly and the product α-dimethyl trichloroacetamide was obtained in high yields. However, all attempts at hydrosilylation using the trichloroacetamide were unsuccessful, possibly due to the steric bulk of the protected amine. Silanes can also act as *N*-alkylating agents or reducing agents in the presence of amides and transition metal catalysts.[40] Attempts to remove the

trichloroacetamide protecting group via literature methods[34] and isolate the volatile allylic amine were also unsuccessful. We fortuitously found that the alkyne analogue 2-methyl-3-butyn-2-amine was commercially available. The procedure for the synthesis of the *trans*-3-(triethylsilyl)prop-2-ene-1-amine (described in the second-generation RevILs section above, page 112) was adapted for the branched alkyne; a subsequent hydrogenation of the double bond formed in the hydrosilylation, following a modification of the procedure outlined by Schilling, would yield the desired branched product as shown in Figure 3.34.[41]

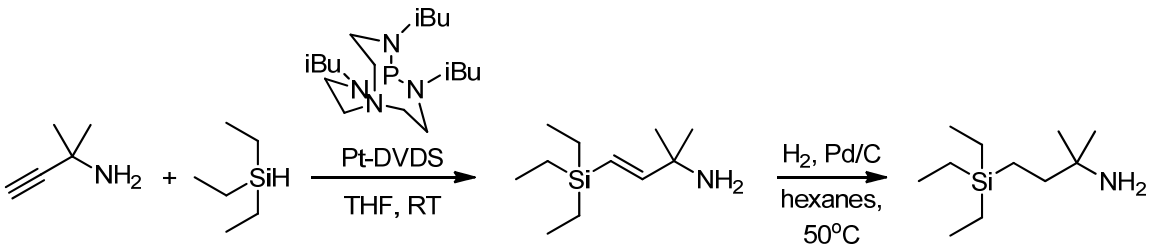

Figure 3.34. Hydrosilylation of 2-methyl-3-butyn-2-amine with triethylsilane, followed by palladium-catalyzed hydrogenation.

Again, the catalyst was synthesized *in situ* by combining equimolar amounts of Pt-DVDS and azaphosphatrane, then heating the system at 60°C for 10 minutes. THF was then added to the system, which was cooled in a brine and ice bath prior to addition of triethylsilane. A large exotherm occurs upon addition of 2-methyl-3-butyn-2-amine; the reaction temperature was monitored for several hours until the system no longer heated up upon removal from the ice bath. The reaction mixture was then allowed to stir at room temperature overnight. Although use of the stereoselective catalyst system was not strictly necessary for the synthesis of the ultimate saturated product, αDMTEtSA, this synthetic route allowed us access to the unsaturated intermediate—as the unsaturated version of TEtSA exhibits a

decrease in viscosity, it was hypothesized that this unsaturated branched analog would show improvements as well. To date, the CO_2 capacity of this unsaturated branched silylated amine has not been determined.

3.4.3.4 Characterization of Third-Generation RevILs: CO_2 Capacity

The RevIL forms of all third-generations were synthesized as described above, and capacities and viscosities have been determined for all three branched amines. The results for CO_2 capacity are shown below in Figure 3.35. The capacities of the first-generation RevILs and the theoretical capacities are included for easy comparison.

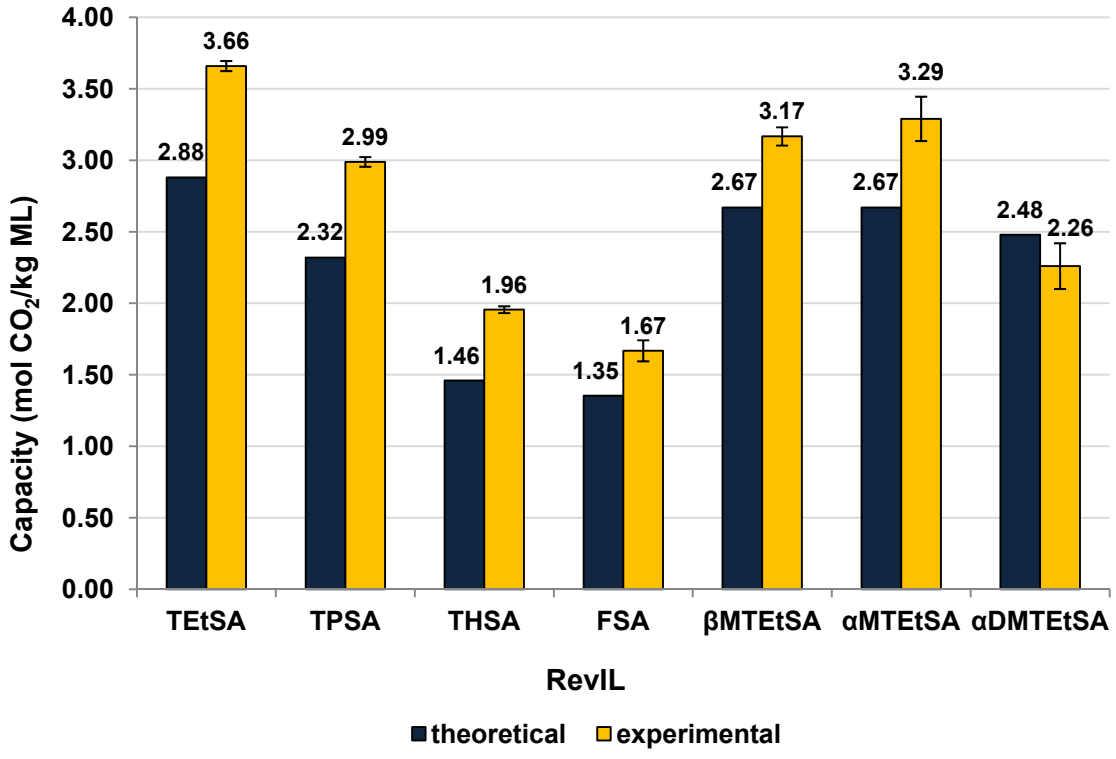

Figure 3.35. Comparison of theoretical and experimental CO_2 capacities expressed in moles of CO_2 per kilogram of sorbent.

Capacities of our RevILs were measured gravimetrically in triplicate. Although the commonly used unit for CO_2 capture in industry is moles of CO_2 per kilogram of sorbent, for the purposes of direct comparison of sorbents, the unit of moles of CO_2 per mole of sorbent is often useful. These figures are compared in Figure 3.36

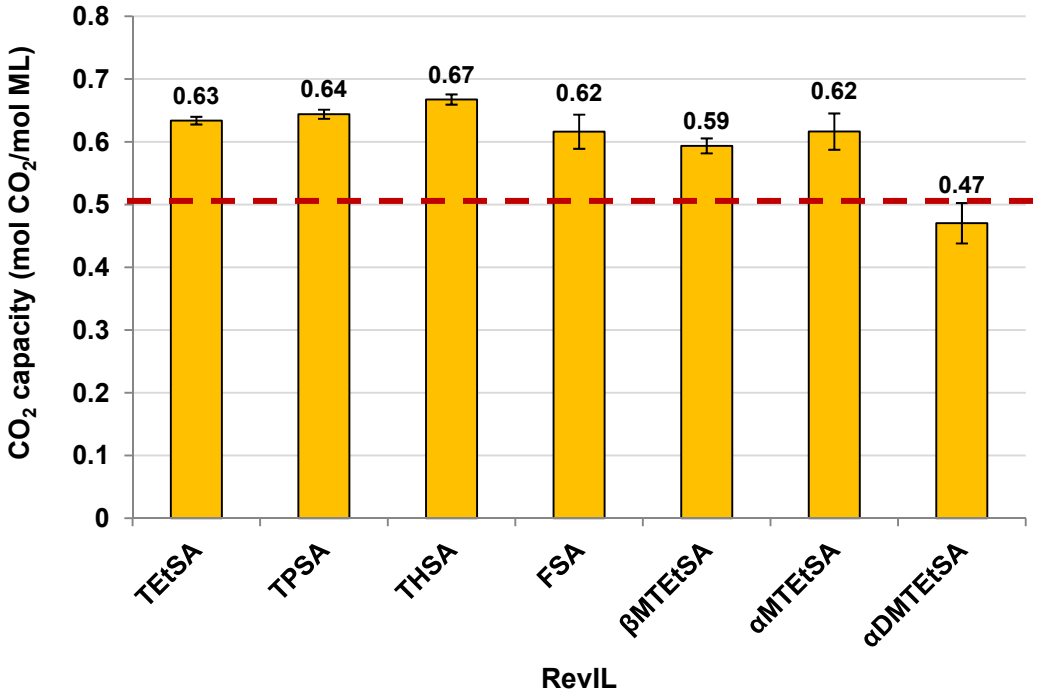

Figure 3.36. Experimental CO_2 capacities expressed in moles of CO_2 per mole of ML. Red dashed line indicates theoretical capacity (0.5 mol CO_2/mol ML).

As before, capacities were obtained gravimetrically at full conversion. Amines with steric hindrance proximal to the reactive site have been shown to form weaker carbamate bonds when reacted with CO_2 in aqueous solution;[31] this could lead to an increase in CO_2 capacity by altering the equilibrium of ammonium-carbamate ion pair formation. However, destabilization of the carbamate appears to prevent αDMTEtSA from achieving full

conversion to the RevIL form, as the capacity is lower than the anticipated 0.5 moles of CO_2 per mole of ML. It has been demonstrated that steric hinderance around the amino group causes a slower rate of reaction with CO_2;[31a] it remains to be seen whether full conversion of αDMTEtSA can be obtained after a longer reaction time. Single branching near the amine (αMTEtSA and βMTEtSA) does not significantly affect CO_2 capacity deleteriously—both of these singly-branched amines have capacities (0.62 and 0.59 moles of CO_2 per mole of ML, respectively) close to that of TEtSA (0.63 moles of CO_2 per mole of ML). Although βMTEtSA and αMTEtSA have the same molecular weight, and therefore the same theoretical capacity, αMTEtSA appears to have a slightly higher CO_2 capacity than βMTEtSA.

3.4.3.5 Characterization of Third-Generation RevILs: Viscosity

Another important parameter for industrial viability is viscosity, and here we can see the marked difference that the addition of a methyl group makes. The viscosities of the pre-formed RevILs (at equilibrium capacity) were measured in triplicate using a Rheosys Merlin II viscometer with a 2° cone and plate system. Viscosities were measured at 25 and 40°C; samples were allowed to reach thermal equilibrium prior to measurement. The measured viscosities can be seen in Figure 3.37.

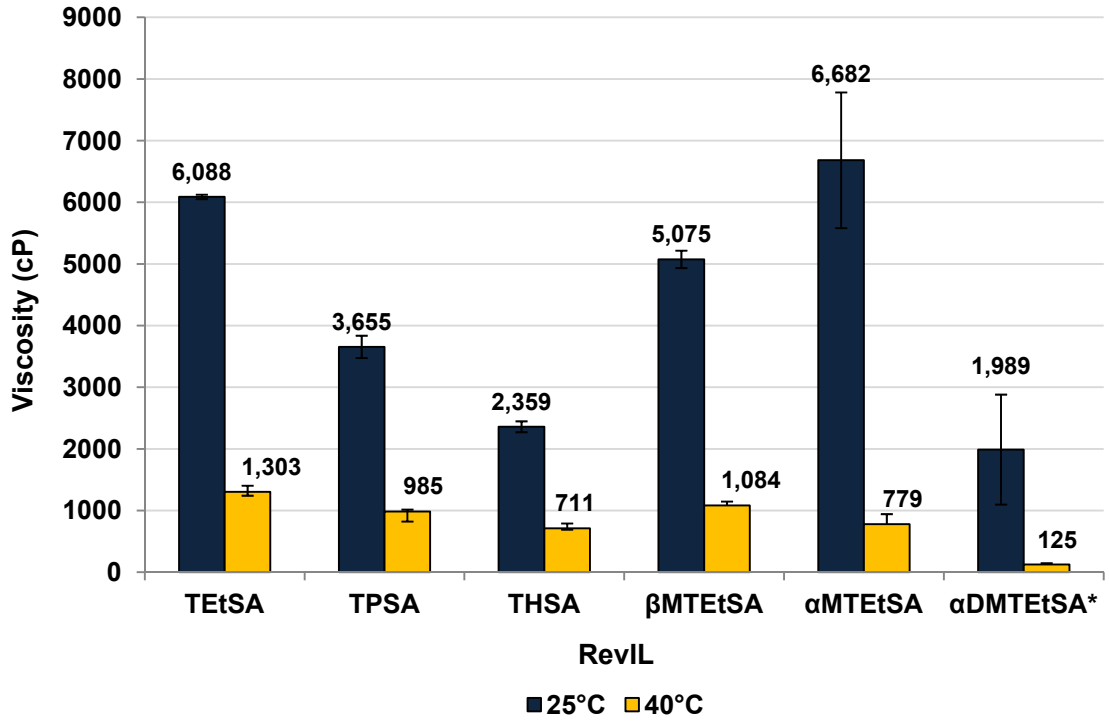

Figure 3.37. Viscosities of first- and third-generation RevILs at equilibrium conversion at 25 and 40°C.
***most likely not at full conversion of ML to RevIL**

For ease of comparison, the viscosities of FSA have been omitted—the measured values are so large that they dwarf those of the five other compounds. At 25°C, the viscosity of FSA was found to be 12,293 cP (±375 cP), and at 40°C, the viscosity was found to be 2,897 cP (±436 cP), as shown in Figure 3.20. All viscosities—other than for αDMTEtSA—are measured at full conversion. It is important to note that, although we have reacted αDMTEtSA molecular liquid with CO_2 for at least the standard 75 minutes and up to 200 minutes, we do not believe we have reached full conversion of the molecular liquid to the RevIL form. Therefore, the low viscosities exhibited by αDMTEtSA at 25 and 40°C may not be representative of the viscosity at full conversion.

Again, for all RevILs investigated, viscosity decreases as temperature increases. We had predicted that the presence of branching could potentially decrease the viscosity of the RevILs formed by disrupting the packing efficiency of the ion pairs. However, using TEtSA as a reference, the viscosities of αMTEtSA and βMTEtSA do not vary greatly 25°C—the viscosity of the RevILs is relatively insensitive to the addition of a single methyl group to the basic silylamine framework. However, at 40°C, the viscosity of αMTEtSA is 779 cP—similar to that of THSA (711 cP). Referring back to Figure 3.35, the CO_2 capacity of THSA is 1.96 moles of CO_2 per mole of THSA ML, while the CO_2 capacity of αMTEtSA is 3.29 moles of CO_2 per mole of αMTEtSA ML. By adding methyl branches near the reactive amine site, we can therefore control viscosity without decreasing capacity. Future work in this area includes determining the viscosity of αMTEtSA and αDMTEtSA over a range of conversions, as seen in Figure 3.21 for TPSA.

3.4.3.6 Characterization of Third-Generation RevILs: Reversal and Evaporation Temperatures

T_{rev} of the third-generation RevILs were determined using a Q20 TA Instruments DSC, as before. Hermetically sealed aluminum pans were used, into which approximately 2 mg of the pre-formed RevIL under consideration was measured. The temperature was ramped from -40 to 400°C at a ramp rate of $5°C \cdot min^{-1}$. The temperature at which the reversal event occurred was determined by finding the intersection of the baseline of the event and the line tangent to the peak of the event. Samples were run in triplicate.

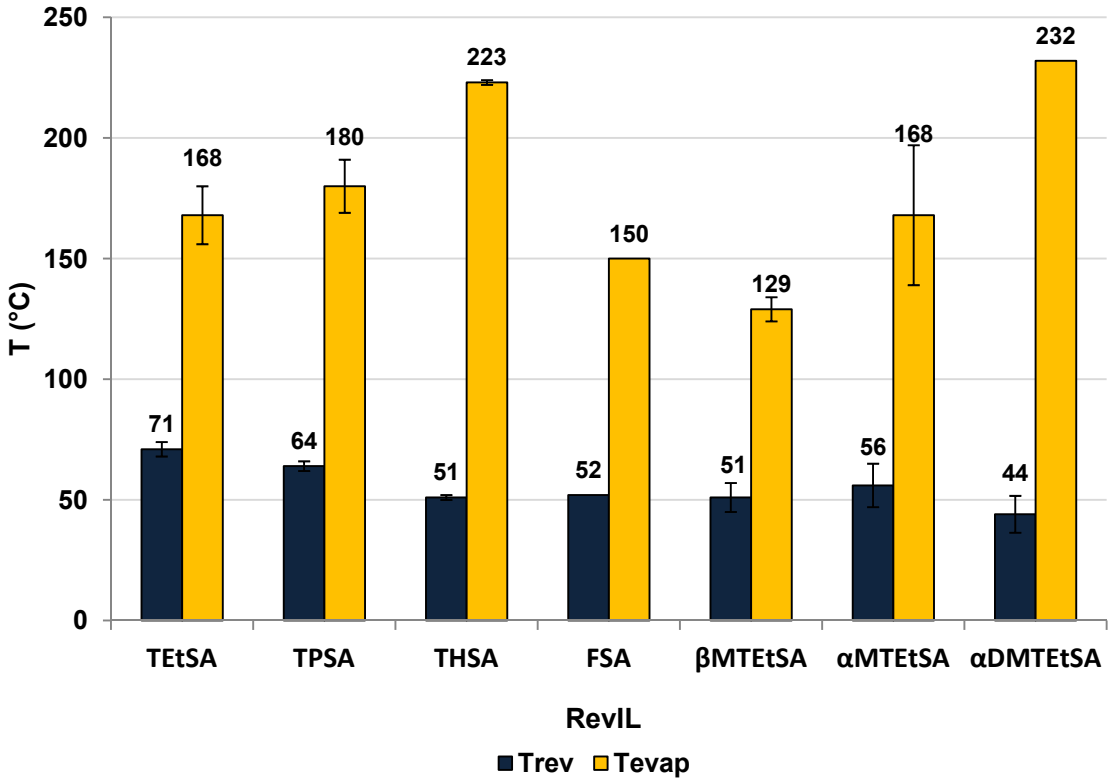

Figure 3.38. T_{rev} and T_{evap} of third-generation RevILs; first-generation RevILs included for comparison.

Again, all amines have a T_{rev} below that of a 30 wt% solution of MEA (110-120°C).[27] Although we previously observed only small changes in CO_2 capacity and viscosity of the branched amines when compared to TEtSA (T_{rev} = 71°C), the presence of branching on the silylamine backbone causes a decrease in T_{rev} of at least 15 degrees. Simply by adding one methylene group to TEtSA we can decrease the reversal temperature to 56°C (as in the case of αMTEtSA) or even 51°C (for βMTEtSA). In contrast, the reversal temperature of TPSA is 64°C—seven degrees lower than that of TEtSA—but the CO_2 capacity of TPSA is lower than that of either αMTEtSA or βMTEtSA. The T_{rev} for αDMTEtSA, 44°C, could be too low for CO_2 capture from flue gas, which is at 40°C. If significant reversal did occur at 40°C, the capacity of αDMTEtSA would decrease. Additionally, as with the CO_2 capacities

described above, we can see that two RevILs that have the same molar mass and differ only in the placement of a methyl group— αMTEtSA and βMTEtSA—exhibit different reversal temperatures.

3.4.3.7 Characterization of Third-Generation RevILs: Enthalpy of Regeneration

Here I introduce a property of our RevILs that I have not previously discussed—the enthalpy of regeneration (ΔH_{regen}). This quantity represents the amount of heat required to strip the RevIL of CO_2 and reform the ML for recycle of the sorbent. A higher ΔH_{regen} indicates that ultimately, more energy is required to recycle the solvent. As with the T_{rev}, the ΔH_{regen} were calculated from DSC thermograms. Heat supplied to the system was calculated taking degree of conversion into account.

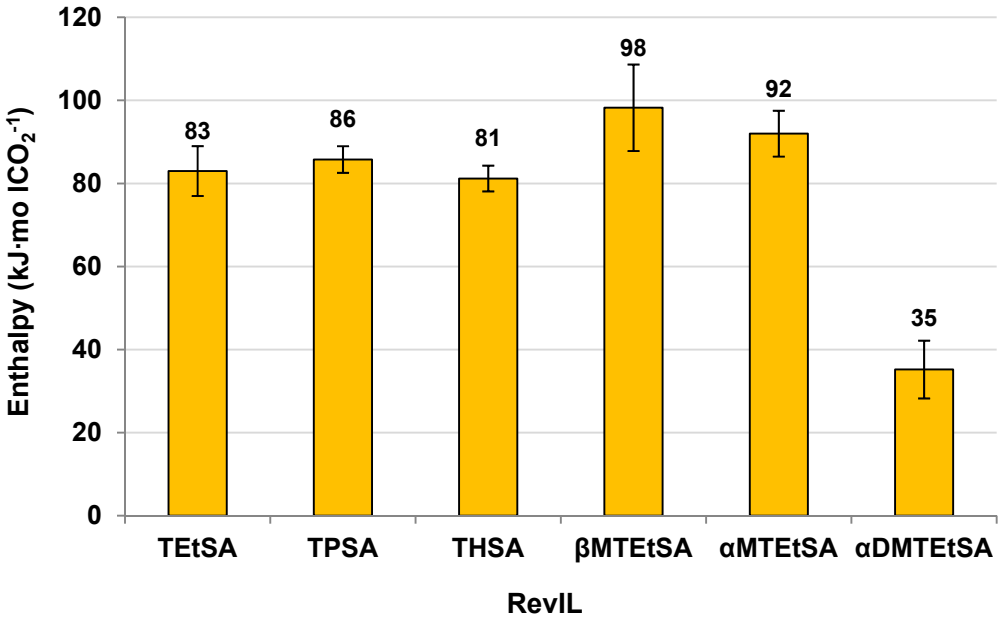

Figure 3.39. ΔH_{regen} for first- and third-generation RevILs.

Previous work has demonstrated that unbranched silylated 1° amines exhibit very similar ΔH_{regen} (approximately 80 kJ per mole of CO_2 captured), irrespective of the identity of the residual groups on the silicon.[42] However, the addition of a single methyl branch near the 1° amine moiety alters the enthalpy of regeneration. For αMTEtSA and βMTEtSA, the addition of a methyl group at the *a* or *β* position, respectively, actually increases the enthalpy of regeneration from that of their reference TEtSA. In contrast, the ΔH_{regen} found for αDMTEtSA is almost one-third that of TEtSA and exhibits the lowest ΔH_{regen} of all silylated amines included in this study. We posit that this low heat of regeneration is due to destabilization of the carbamate formed from the branched amine.

3.5 Conclusions

Novel silylated amines have been synthesized; upon reaction with CO_2, these amines form a RevIL consisting of an ammonium-carbamate ion pair. These RevILs capture CO_2 via chemi- and physisorption, although the former dominates at 1 atm of CO_2 (i.e. near flue gas conditions). The CO_2 capacities, viscosities, reversal temperatures, and evaporation temperatures of these molecular and ionic liquids have been determined, and, in many cases, found to compare favorably to the current mature technology, monoethanolamine. Flexible synthetic approaches allow us to vary different aspects of the silylated amines, including but not limited to: the residual groups on the silicon; the degree of unsaturation and stereochemistry of the alkyl linker between the silicon and the amine; and the steric hinderance of the primary amine group.

We have shown not only that a strong structure-property relationship exists for our RevILs, but also that minor modifications of a basic RevIL structure can lead to drastic changes in bulk properties. Our original goal was to increase CO_2 capacity, as this would

decrease the amount of solvent ultimately needed for post-combustion carbon capture (PCC).[23] We have demonstrated that increasing the length of the alkyl groups on the silicon (R in Figure 3.8) decreased the viscosity and T_{rev} of the RevILs formed upon reaction with CO_2; however, this increase in molecular weight also led to a decrease in overall CO_2 capacity. We have now shown that a modest degree of branching at the position α to the amine in our RevILs results in a significant beneficial impact on industrially relevant RevIL properties (viscosity, T_{rev}, ΔH_{regen}) without a decrease in CO_2 capacity. The ideal candidate of this form would exhibit high capacity, low viscosity, a moderate reversal temperature, and a low enthalpy of regeneration. Currently, the RevIL that appears to be the best candidates for pilot plant-scale carbon capture would be TPSA—it has been studied the most extensively and has a relatively simple synthesis and purification procedure. However, αDMTEtSA has a low viscosity in the RevIL form and a low enthalpy of regeneration; if the low CO_2 capacity can be overcome, this silylated amine could be a promising candidate for PCC as well.

3.6 References

1. United States Department of State. U.S. Climate Action Report 2010. Global Publishing Services: Washington, D.C., June 2010.

2. Olajire, A. A. CO_2 capture and separation technologies for end-of-pipe applications - A review. *Energy* **2010,** *35* (6), 2610-2628.

3. D'Alessandro, D. M.; Smit, B.; Long, J. R. Carbon Dioxide Capture: Prospects for New Materials. *Angew. Chem. Int. Ed.* **2010,** *49* (35), 6058-6082.

4. Brennecke, J. E.; Gurkan, B. E. Ionic Liquids for CO_2 Capture and Emission Reduction. *J. Phys. Chem. Lett.* **2010,** *1* (24), 3459-3464.

5. Ciferno, J. P.; Fout, T. E.; Jones, A. P.; Murphy, J. T. Capturing carbon from existing coal-fired power plants. *Chem. Eng. Prog.* **2009,** *105* (4), 33-41.

6. Rao, A. B.; Rubin, E. S. A technical, economic, and environmental assessment of amine-based CO_2 capture technology for power plant greenhouse gas control. *Environ. Sci. Technol.* **2002,** *36* (20), 4467-4475.

7. Aaron, D.; Tsouris, C. Separation of CO_2 from flue gas: A review. *Sep. Sci. Technol.* **2005,** *40* (1-3), 321-348.

8. Shannon, M. S.; Bara, J. E. Reactive and Reversible Ionic Liquids for CO_2 Capture and Acid Gas Removal. *Sep. Sci. Technol.* **2012,** *47* (2), 178-188.

9. Danckwerts, P. V. The reaction of CO_2 with ethanolamines. *Chem. Eng. Sci.* **1979,** *34* (4), 443-446.

10. Bello, A.; Idem, R. O. Pathways for the formation of products of the oxidative degradation of CO_2-loaded concentrated aqueous monoethanolamine solutions during CO_2 absorption from flue gases. *Ind. Eng. Chem. Res.* **2005,** *44* (4), 945-969.

11. Abanades, J. C.; Rubin, E. S.; Anthony, E. J. Sorbent cost and performance in CO_2 capture systems. *Ind. Eng. Chem. Res.* **2004,** *43* (13), 3462-3466.

12. Puxty, G.; Rowland, R.; Allport, A.; Yang, Q.; Bown, M.; Burns, R.; Maeder, M.; Attalla, M. Carbon Dioxide Postcombustion Capture: A Novel Screening Study of the Carbon Dioxide Absorption Performance of 76 Amines. *Environ. Sci. Technol.* **2009,** *43* (16), 6427-6433.

13. (a) Strazisar, B. R.; Anderson, R. R.; White, C. M. Degradation pathways for monoethanolamine in a CO_2 capture facility. *Energy Fuels* **2003,** *17* (4), 1034-1039; (b) Veawab, A.; Tontiwachwuthikul, P.; Bhole, S. D. Studies of corrosion and corrosion control in a CO_2-2-amino-2-methyl-1-propanol (AMP) environment. *Ind. Eng. Chem. Res.* **1997,** *36* (1), 264-269.

14. Veawab, A.; Aroonwilas, A.; Chakma, A.; Tontiwachwuthikul, P. Solvent formulation for CO_2 separation from flue gas streams. In *First National Conference on Carbon Sequestration*, Washington, D.C., 2001.

15. Gutowski, K. E.; Maginn, E. J. Amine-Functionalized Task-Specific Ionic Liquids: A Mechanistic Explanation for the Dramatic Increase in Viscosity upon Complexation with CO_2 from Molecular Simulation. *J. Am. Chem. Soc.* **2008,** *130* (44), 14690-14704.

16. Bates, E. D.; Mayton, R. D.; Ntai, I.; Davis, J. H. CO_2 capture by a task-specific ionic liquid. *J. Am. Chem. Soc.* **2002,** *124* (6), 926-927.

17. Gurkan, B. E.; de la Fuente, J. C.; Mindrup, E. M.; Ficke, L. E.; Goodrich, B. F.; Price, E. A.; Schneider, W. F.; Brennecke, J. F. Equimolar CO_2 Absorption by Anion-Functionalized Ionic Liquids. *J. Am. Chem. Soc.* **2010,** *132* (7), 2116-2117.

18. Goodrich, B. F.; de la Fuente, J. C.; Gurkan, B. E.; Zadigian, D. J.; Price, E. A.; Huang, Y.; Brennecke, J. F. Experimental Measurements of Amine-Functionalized Anion-Tethered Ionic Liquids with Carbon Dioxide. *Ind. Eng. Chem. Res.* **2011,** *50* (1), 111-118.

19. Camper, D.; Bara, J. E.; Gin, D. L.; Noble, R. D. Room-Temperature Ionic Liquid−Amine Solutions: Tunable Solvents for Efficient and Reversible Capture of CO_2. *Ind. Eng. Chem. Res.* **2008,** *47* (21), 8496-8498.

20. (a) Jessop, P. G.; Heldebrant, D. J.; Li, X. W.; Eckert, C. A.; Liotta, C. L. Green chemistry - Reversible nonpolar-to-polar solvent. *Nature* **2005,** *436* (7054), 1102-1102; (b) Phan, L.; Chiu, D.; Heldebrant, D. J.; Huttenhower, H.; John, E.; Li, X. W.; Pollet, P.; Wang, R. Y.; Eckert, C. A.; Liotta, C. L.; Jessop, P. G. Switchable solvents consisting of amidine/alcohol or guanidine/alcohol mixtures. *Ind. Eng. Chem. Res.* **2008,** *47* (3), 539-545; (c) Hart, R.; Pollet, P.; Hahne, D. J.; John, E.; Llopis-Mestre, V.; Blasucci, V.; Huttenhower, H.; Leitner, W.; Eckert, C. A.; Liotta, C. L. Benign coupling of reactions and separations with reversible ionic liquids. *Tetrahedron* **2010,** *66* (5), 1082-1090; (d) Blasucci, V.; Dilek, C.; Huttenhower, H.; John, E.; Llopis-Mestre, V.; Pollet, P.; Eckert, C. A.; Liotta, C. L. One-component, switchable ionic liquids derived from siloxylated amines. *Chem. Commun.* **2009,** (1), 116-118; (e) Blasucci, V.; Hart, R.; Mestre, V. L.; Hahne, D. J.; Burlager, M.; Huttenhower, H.; Thio, B. J. R.; Pollet, P.; Liotta, C. L.; Eckert, C. A. Single component, reversible ionic liquids for energy applications. *Fuel* **2010,** *89* (6), 1315-1319.

21. (a) Perry, R. J.; O'Brien, M. J. Amino disiloxanes for CO_2 capture. *Energy & Fuels* **2011,** *25* (4), 1906-1918; (b) Perry, R. J.; Grocela-Rocha, T. A.; O'Brien, M. J.; Genovese, S.; Wood, B. R.; Lewis, L. N.; Lam, H.; Soloveichik, G.; Rubinsztajn, M.; Kniajanski, S.; Draper, S.; Enick, R. M.; Johnson, J. K.; Xie, H. B.; Tapriyal, D. Aminosilicone solvents for CO_2 capture. *Chemsuschem* **2010,** *3* (8), 919-930.

22. Atkins, P.; Jones, L. *Chemistry: Molecules, Matter, and Change.* 3rd ed.; W. H. Freeman and Company: New York, 1997.

23. Rubin, E. S.; Mantripragada, H.; Marks, A.; Versteeg, P.; Kitchin, J. The outlook for improved carbon capture technology. *Prog. Energy Combust. Sci.* **2012**, in press.

24. Marzinke, M.; MacMillan, J. H.; August, T. F.; Telepchak, M. J. Method for the preparation of aminopropyl of aminoalkyl functional polyalkyl or aryl siloxanes. US 6,177,583 BI, 2001.

25. Hart, R. J. Designing switchable solvents for sustainable process development. PhD thesis, Georgia Institute of Technology, Atlanta, 2011.

26. DeSimone, J. M.; Maury, E. E.; Menceloglu, Y. Z.; McClain, J. B.; Romack, T. J.; Combes, J. R. Dispersion polymerizations in supercritical carbon dioxide. *Science* **1994,** *265* (5170), 356-359.

27. Rochelle, G. T. Amine scrubbing for CO_2 capture. *Science* **2009,** *325* (5948), 1652-1654.

28. Marciniec, B. *Hydrosilylation: A comprehensive review on recent advances*. Springer: Dordrect, the Netherlands, 2009; Vol. 1.

29. Aneetha, H.; Wu, W.; Verkade, J. G. Stereo- and regioselective Pt(DVDS)/P(iBuNCH$_2$CH$_2$)$_3$N-catalyzed hydrosilylation of terminal alkynes. *Organometallics* **2005,** *24* (11), 2590-2596.

30. (a) Chakraborty, A. K.; Astarita, G.; Bischoff, K. B. CO_2 absorption in aqueous solutions of hindered amines. *Chem. Eng. Sci.* **1986,** *41* (4), 997-1003; (b) Vaidya, P. D.; Kenig, E. Y. CO_2-alkanolamine reaction kinetics: A review of recent studies. *Chem. Eng. Technol.* **2007,** *30* (11), 1467-1474.

31. (a) Sartori, G.; Savage, D. W. Sterically hindered amines for CO_2 removal from gases. *Ind. Eng. Chem. Fundam.* **1983,** *22* (2), 239-249; (b) Hook, R. J. An investigation of some sterically hindered amines as potential carbon dioxide scrubbing compounds. *Ind. Eng. Chem. Res.* **1997,** *36* (5), 1779-1790.

32. (a) Overman, L. E. General method for synthesis of amines by rearrangement of allylic trichloroacetamides. 1,3 transposition of alcohol and amine functions. *J. Am. Chem. Soc.* **1976,** *98* (10), 2901-2910; (b) Overman, L. E.; Carpenter, N. E. *The allylic trihaloacetamide rearrangement*. John Wiley & Sons, Inc.: Hoboken, 2005.

33. Bujard, M.; Briot, A.; Gouverneur, V.; Mioskowski, C. Ring closing metathesis of phenyl-substituted dienes. *Tetrahedron Lett.* **1999,** *40* (50), 8785-8788.

34. Fletcher, A. J.; Bax, M. N.; Willis, M. C. Palladium-catalysed *N*-annulation routes to indoles: the synthesis of indoles with sterically demanding *N*-substituents, including demethylasterriquinone A1. *Chem. Commun.* **2007,** (45), 4764-4766.

35. Weygand, F.; Frauendorfer, E. Reduktive Entfernung des *N*-Trifluoracetyl- und *N*-Trichloracetylrestes durch Natriumborhydrid mit Anwendungen in der Peptidchemie. *Chem. Ber. Recl.* **1970,** *103* (8), 2437-2449.

36. Urabe, D.; Sugino, K.; Nishikawa, T.; Isobe, M. A novel deprotection of trichloroacetamide. *Tetrahedron Lett.* **2004,** *45* (51), 9405-9407.

37. Gibson, M. S.; Bradshaw, R. W. The Gabriel synthesis of primary amines. *Angew. Chem. Int. Ed.* **1968,** *7* (12), 919-930.

38. (a) Semenow, D.; Shih, C.-H.; Young, W. G. Allylic rearrangements. XL. The reaction of allylic diazonium ions in acetic acid. *J. Am. Chem. Soc.* **1958,** *80* (20), 5472-5475; (b) Roberts, J. D.; Mazur, R. H. Small ring compounds. IV. Interconversion reactions of cyclobutyl, cyclopropylcarbinyl, and allylcarbinyl derivatives. *J. Am. Chem. Soc.* **1951,** *73* (6), 2509-2520.

39. Nagashima, H.; Wakamatsu, H.; Ozaki, N.; Ishii, T.; Watanabe, M.; Tajima, T.; Itoh, K. Transition metal catalyzed radical cyclization: new preparative route to g-lactams from allylic alcohols via the [3.3]-sigmatropic rearrangement of allylic trichloroacetimidates and the subsequent ruthenium-catalyzed cyclization of *N*-allyltrichloroacetamides. *J. Org. Chem.* **1992,** *57* (6), 1682-1689.

40. Addis, D.; Das, S.; Junge, K.; Beller, M. Selective reduction of carboxylic acid derivatives by catalytic hydrosilylation. *Angew. Chem. Int. Ed.* **2011,** *50* (27), 6004-6011.

41. Schilling Jr., C. L. Sterically hindered aminohydrocarbylsilanes and process of preparation. 5030746, 1991.

42. Rohan, A. L.; Switzer, J. R.; Flack, K. M.; Hart, R. J.; Sivaswamy, S.; Biddinger, E. J.; Talreja, M.; Verma, M.; Faltermeier, S.; Nielsen, P. T.; Pollet, P.; Schuette, G. F.; Eckert, C. A.; Liotta, C. L. The synthesis and the chemical and physical properties of non-aqueous silylamine solvents for CO_2 capture. *Unpublished manuscript.*

CHAPTER 4. REVERSIBLE IONIC LIQUIDS AS SWITCHABLE SURFACTANTS FOR THE SYNTHESIS OF GOLD NANOPARTICLES

4.1 Introduction

Gold nanoparticles have found uses in such varied fields as catalysis,[1] microelectronics,[2] and nanomedicine;[3] as the properties of these nanoparticles are highly dependent on size and shape, control of these factors during synthesis is of high concern.[4] For example, supported gold nanoparticles with a diameter smaller than 10 nm are highly active oxidation catalysts, while bulk gold is catalytically inactive.[5] When nanoparticles are prepared in solution, this control is commonly achieved through the use of capping agents—ligands that have a high affinity for the metal in question. These capping agents not only control the morphology of a nanoparticle, but they also prevent agglomeration of the highly active particles.[5] One of the most well-known capping agents is dodecanethiol, which forms a covalent bond with the surface of gold nanoparticles (AuNP).[6] AuNP protected with this capping agent can be isolated and treated as any other shelf-stable chemical reagent; they can also be redispersed later without suffering any change in activity or properties.[7] In what has become known as the Brust-Schiffrin method of gold nanoparticle synthesis, the gold salt chloroauric acid ($HAuCl_4$) is dissolved in water, while the phase transfer catalyst tetraoctylammonium bromide (TOAB) is dissolved in toluene. Vigorous mixing of the two solutions results in transfer of the anion $AuCl_4^-$ into the organic phase; the orange color of the gold salt makes this transfer easy to observe. Addition of dodecanethiol to the organic phase, followed by reduction with sodium borohydride ($NaBH_4$), yields capped nanoparticles.[7] Here, the capping agent is dodecanethiol. Another common capping agent for gold nanoparticles is the more labile sodium citrate; this was introduced by Turkevich *et*

al., who treated a boiling solution of $HAuCl_4$ with sodium citrate.[8] The sodium citrate functions as both a capping agent and a reducing agent.

However, before use of any capped nanoparticles, the capping agents must be removed to free up surface sites, or replaced with more tolerant surface groups, as in the case of nanoparticles intended for biological applications.[9] This removal or ligand exchange produces high amounts of waste, including phase transfer agents and solvent washes.[10] For the Brust method of gold nanoparticle synthesis and purification, Anastas has calculated the E-factor (mass of byproducts per unit mass of product) of the process to be as high as 3,320;[11] this is astronomical even when compared to the E-factors of multi-step pharmaceutical syntheses, where the typical range is from 25 to 100. Methods that rely on post-synthetic separation of polydisperse nanoparticles to achieve monodisperse fractions are also time- and waste intensive, and can result in additional processing-related loss of product.[10]

An attractive alternative to capping agents is the use of reverse micelles as microreactors for nanoparticle synthesis. A reverse micelle (also known as a water-in-oil micelle) is an aggregation of surfactants in a nonpolar, hydrophobic phase: the alkyl tails of the surfactants point outwards, towards the hydrophobic continuous phase, while the polar heads of the surfactants are oriented inwards, as shown in Figure 4.1. Reverse micelles can contain a polar phase as the core of the micelle, known as a disperse phase; this can be water or a non-aqueous polar solvent. A solution containing reverse micelles is a microemulsion.

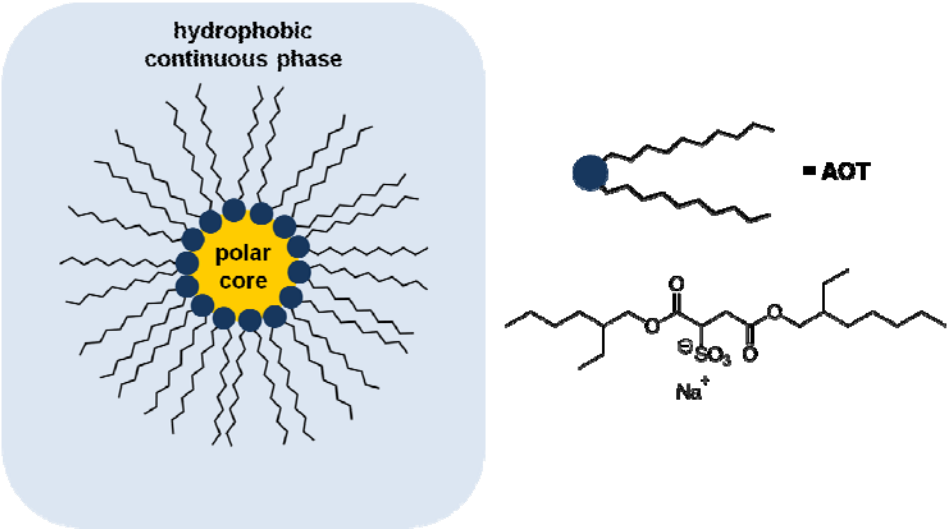

Figure 4.1. Schematic of typical microemulsion with hydrophobic continuous phase polar (aqueous or non-aqueous) core, and AOT as surfactant.

Figure 4.1 shows a reverse micelle formed with the surfactant dioctyl sulfosuccinate sodium salt, also known as Aerosol OT (AOT). Due to its ability to stabilize a large amount of water in the reverse micelle core, it is one of the most widely studied surfactants for reverse micelles.[12] A metal salt will only be soluble in the polar core of the reverse micelle; theoretically, if one can control the size of the reverse micelle, one can control the size of the nanoparticles formed upon reduction.[13] Reverse micelles continuously collide, coalesce, and reform;[14] this property can be used in synthesis. A solution of a metal salt in reverse micelles is combined with a similar solution of the reducing agent in reverse micelles; the intermicellar exchange mixes the reactants and leads to controlled reduction of the metal salt.[12-13] When reverse micelles are used as templates to synthesize nanoparticles, the surfactant prevents aggregation.[14] Surfactants that have proved useful in this field include AOT, cetyltrimethylammonium bromide (CTAB), Triton X100, as well as a number of compounds from the Tween and Brij series of surfactants.[14] The identities of the surfactant, continuous phase, and disperse phase, as well as their ratios relative to one another, all

influence the size of reverse micelles. Additionally, the metal salt and the reducing agent will influence the size and shape of nanoparticles synthesized in reverse micelles. We believe that we can use the built-in "switch" in our reversible ionic liquids (RevILs), previously described in Chapter 3, to not only form reverse micelles, but turn off the micellar structure when desired, essentially releasing the nanoparticles on command. In the following section, I will describe how these RevILs can be applied to the synthesis of nanoparticles.

4.2 Background

A recent paper from the Han group detailed the use of reverse micelles in supercritical carbon dioxide ($scCO_2$) as templates for the synthesis of gold nanoparticles.[15] The core of the micelle was the series of guanidinium-based ionic liquids (ILs) in Figure 4.2, and the metal salt was $HAuCl_4$.

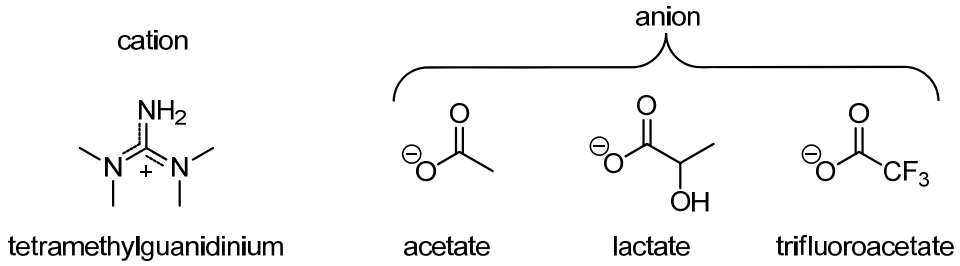

Figure 4.2. Traditional ILs used by the Han group: tetramethylguanidinium acetate, lactate, and trifluroacetate.[15]

The surfactant was *N*-ethyl perfluorooctylsulfonamide; reduction was achieved via rapid expansion of the supercritical system into an aqueous solution of $NaBH_4$. Although spherical gold nanoparticles were successfully synthesized when the weight ratio of gold salt to ionic liquid (W_{HAuCl4}/W_{IL}) was 0.01, the products showed a high polydispersity. Moreover, the

system was not recyclable. The authors proposed that the protonated guanidinium cation of the ionic liquid was able to participate in hydrogen bonding with the polar head of the sulfonamide surfactant, thus stabilizing the micellar structure.[15] We noticed a resemblance to a class of switchable solvents that we have developed, known as 2-component reversible ionic liquids.[16]

Although I have previously discussed 1-component RevILs in the context of CO_2 capture (see Chapter 3), our group's initial research concerning switchable solvents involved 2-component RevILs. When CO_2 is bubbled through an equimolar mixture of a straight-chain alcohol and an amidine or guanidine, a reversible ionic liquid is formed, as shown in Figure 4.3.[17]

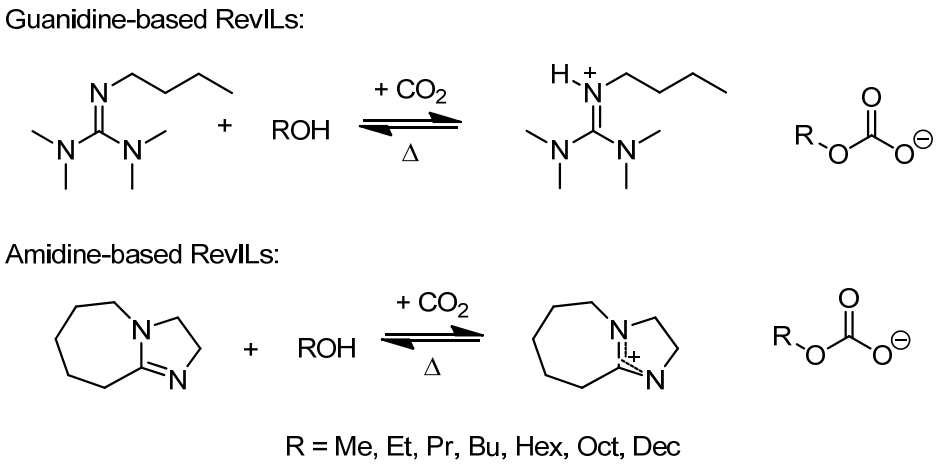

Figure 4.3. RevILs formed from straight chain alcohols reacting with CO_2 in the presence of guanidine 2-butyl-1,1,3,3-tetramethylguanidine (TMBG, *top*); and cyclic amidine 1,8-diazobicyclo[5.4.0]undec-7-ene (DBU, *bottom*).

These 2-component RevILs behave in the same way as the 1-component RevILs described in Chapter 3 of this work—the only difference is that the 2-component RevILs are made up of a guanidinium or amidinium cation, and an alkylcarbonate anion. The RevIL formed has

properties differing greatly from those of the molecular liquids, including conductivity, viscosity, and polarity. Heating or sparging the ionic liquid with an inert gas drives off the CO_2 and regenerates the molecular precursors—this process can be repeated numerous times. These switchable solvent systems have been used to couple reaction and separation: examples include the Claisen-Schmidt condensation of butanone and benzaldehyde, as well as the Heck coupling of bromobenzene and styrene.[18] However, they have never before been used in the synthesis of nanoparticles. We hypothesized that we could make use of our RevILs' built-in "switch" to improve the deposition method described in the work by Han *et al.*[15] and create a recyclable system.

The initial conceptualization of our system involved using a guanidinium-based RevIL as the core of a reverse micelle; a hydrocarbon continuous phase; and a surfactant capable of forming a hydrogen bond with the cation of the RevIL. The gold salt would be soluble only in the core of the reverse micelle. The ML precursors would not be able to hydrogen bond, and no reverse micelle would form. A conceptual schematic of the 2-component reverse micelle system can be seen in Figure 4.4.

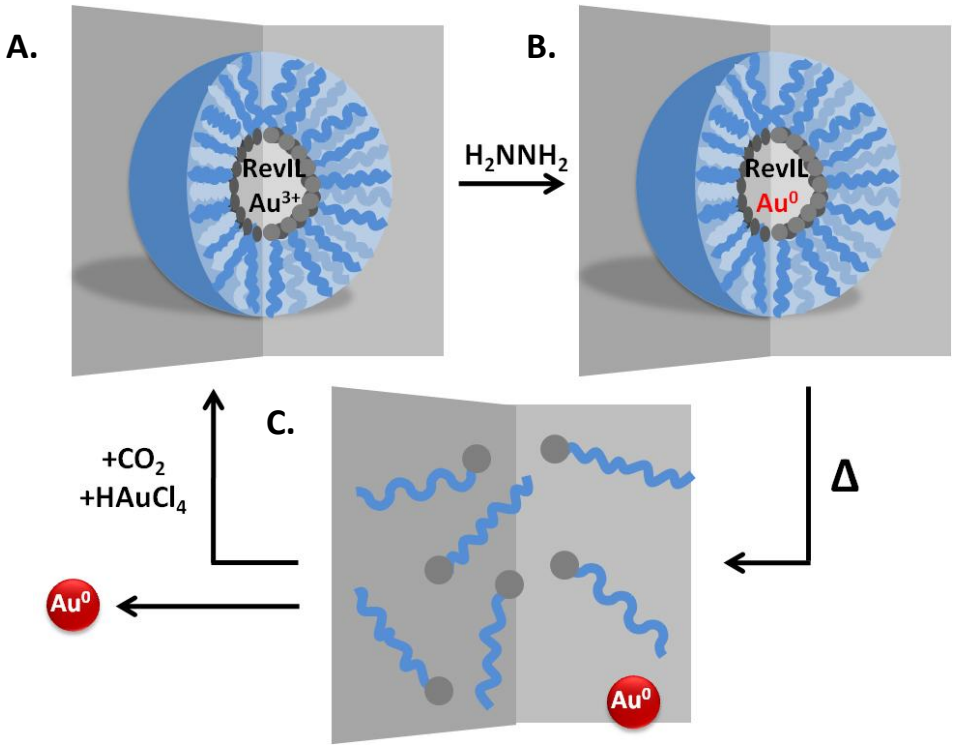

Figure 4.4. Illustration *A*, reverse micelle containing gold salt and RevIL; *B*, reduction of gold salt to form AuNP; *C*, release of nanoparticles; recycle.

The RevIL and the gold salt comprise the interior of the reverse micelle, which is supported in the hydrocarbon phase by a surfactant (illustration *A* in Figure 4.4). Reduction of the gold salt by hydrazine (H_2NNH_2) yields gold nanoparticles, still suspended within the reverse micelles (*B* in Figure 4.4); heating causes the RevIL to revert back to the molecular precursors and CO_2, destroying the micellar structure and releasing the gold nanoparticles (*C* in Figure 4.4). We envisioned a fully recyclable system, requiring only the addition of more gold salt and CO_2 to reform the micelles and prepare the system for another round of nanoparticle synthesis.

As our system would utilize a hydrocarbon continuous phase instead of $scCO_2$, a perfluorinated surfactant was not required. The analogous hydrocarbon surfactant, *N*-

propyl-octylsulfonamide, is not known in the literature and was synthesized via analogy with published reactions[19] according to the method shown in Figure 4.5.

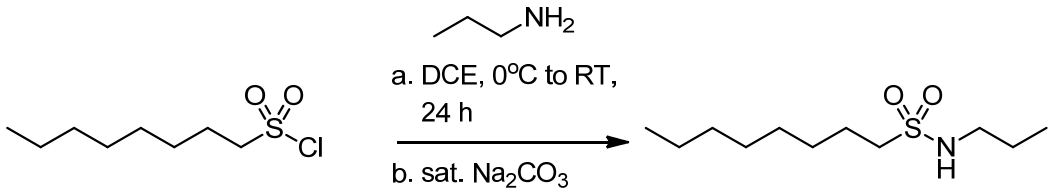

Figure 4.5. Synthesis of surfactant *N*-propyl octylsulfonamide.

Performed in 1,2-dichloroethane (DCE), nucleophilic attack of the propylamine on the sulfur of the sulfonyl chloride resulted in the formation of *N*-propyl-octylsulfonamide, which was isolated in high yield following trituration. This surfactant was chosen because the polar sulfonamide head group can form a hydrogen bond with the guanidinium cation, stabilizing the reverse micellar structure. In the molecular form, the guanidine is not protonated, and this stabilizing hydrogen bond does not exist.

The synthesis of TMBG was adapted from the literature[20] and optimized by a former group member, Dr. Hillary Huttenhower.[21]

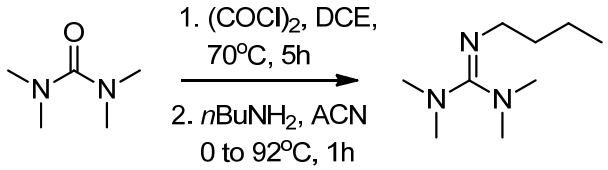

Figure 4.6. Synthesis of TMBG.

Oxalyl chloride [$(COCl)_2$] was slowly added to a solution of tetramethylurea in DCE, forming the chloride salt. This was then reacted with *n*-butylamine (nBuH$_2$) in acetonitrile

(ACN) to yield TMBG, which was isolated via distillation in yields of approximately 70%. TMBG can then be reacted with methanol and CO_2 to form the RevIL [TMBGH][MeOCOO], shown in Figure 4.7.

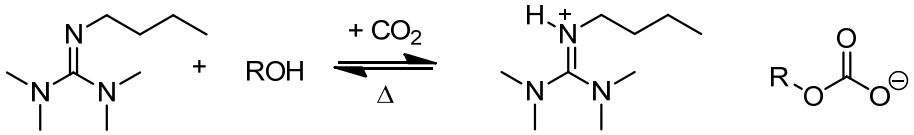

Figure 4.7. Formation of RevIL [TMBGH][MeOCOO] from TMBG, MeOH, and CO_2.

Preliminary investigations of the reverse micelle formation were carried out using the UV-active sodium salt methyl orange (MO; Figure 4.8) as a gold salt analog—MO is sparingly soluble in the hydrocarbon continuous phase, and, as such, should only exhibit a wavelength of maximum absorption (λ_{max}) when present in the core of the reverse micelles. The reverse micelles, in turn, should only be present when the guanidinium ion is present—i.e., when the RevIL is formed.

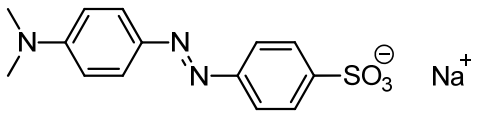

Figure 4.8. Structure of sodium salt methyl orange.

The RevIL was formed by combining equimolar amounts of TMBG and methanol and sparging with CO_2. Methyl orange was then added to the RevIL; after the addition of surfactant, the hydrocarbon continuous phase was added, and the solution was stirred for one hour. The UV-Vis spectrum of the system was then taken. The λ_{max} of MO is sensitive

to solvent polarity, but is generally centered near 400 nm in hydrocarbons.[22] The system was then heated at 150°C for two hours to reverse the ionic liquid, after which time the UV-Vis spectrum of the system was taken again. One equivalent of methanol was added to the system, as the boiling point of methanol (65°C) is well below the temperature at which the system was heated. Carbon dioxide was then bubbled through the system for one hour to re-form both the RevIL and the micellar structure, after which a final UV-Vis spectrum was taken. These results are summarized below in Figure 4.9.

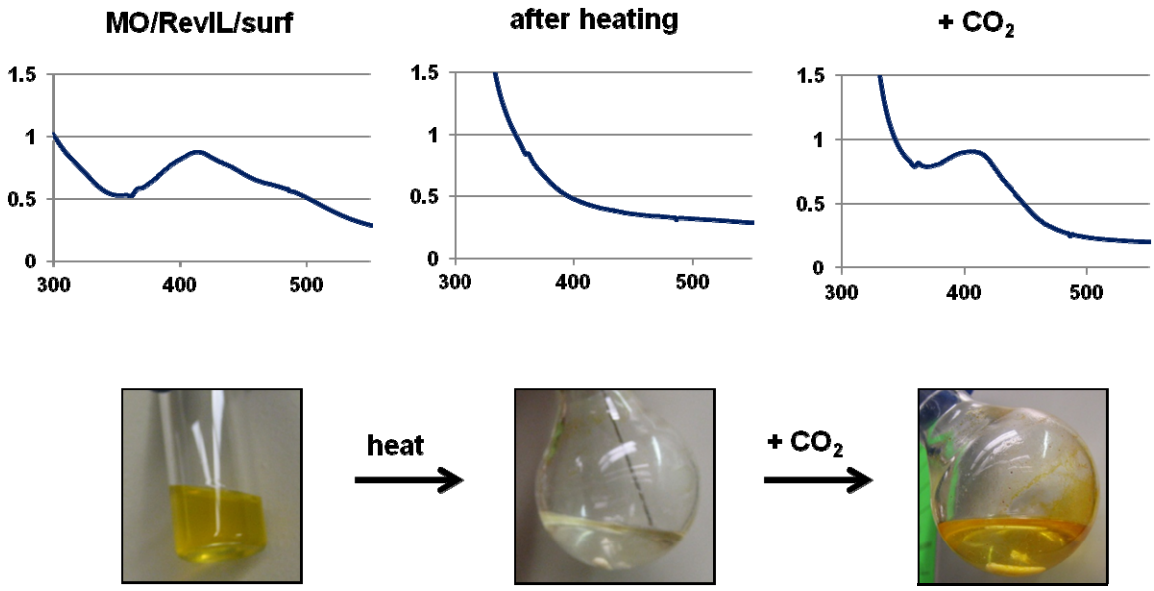

Figure 4.9. *Top*, UV-Vis spectra of micelle formation, dissolution, and reformation in dodecane; *bottom*, photographs of corresponding reaction mixtures.

As predicted, the MO absorption peak, seen at approximately 420 nm, was only observed when the RevIL was present (left and right graphs and images in Figure 4.9). Additionally, an MO absorption was not seen when the RevIL had been reversed. (middle graph and image in Figure 4.9). Finally, when either the surfactant or the RevIL was omitted from the

solution, no MO absorption was observed (spectra not pictured). All three components—RevIL, MO, and surfactant—had to be present in the hydrocarbon continuous phase in order for the reverse micelles to form and solubilize the MO. These preliminary results supported the formation of reverse micelles.

Using the RevILs as the disperse phase in a reverse micellar system will not only enable us to control the size of the nanoparticles formed, but also allow us to deposit the nanoparticles on a solid support on command. This should eliminate not only the use of capping agents, but also the use of additional solvents in post-synthetic size specific separation. This would result in a dramatic decrease in the overall E-factor of the process. This facile separation of nanoparticles from the reaction mixture will reduce the need for capping agents and solvent washes, and therefore reduce the waste stream associated with the production of nanoparticles.[23] We have used the results described above as a basis for the structure of our initial experiments using gold tetrachloroaurate to form gold nanoparticles. I will describe the initial syntheses of nanoparticles performed with 2-component RevILs, and discuss how the results of those experiments led to the progression towards 1-component RevILs. I will then show how we have successfully synthesized AuNP using 1-component RevILs and discuss the nature of our system.

4.3 Experimental Section

4.3.1 Materials

All chemicals were purchased from Sigma-Aldrich and used as received unless otherwise noted. Chemicals used were: oxalyl chloride (98%); tetramethylurea (99%); butylamine (*n*$BuNH_2$; 99.5%); propylamine (98%); methanol (anhydrous; 99.8%); dodecanethiol (≥98%); methyl orange (MO; ACS reagent, dye content 96%); chloroauric

acid or gold (III) chloride trihydrate ($HAuCl_4$; 99.9+% metals basis); bromothymol blue sodium salt; Chromotrope FB (dye content 50%); new methylene blue N (zinc free); toluidine blue O (certified; dye content 88%); methylene violet (Bernthsen; dye content 65%); hexanes (anhydrous, mixture of isomers, ≥99%); heptane (anhydrous, 99%); THF (anhydrous, inhibitor-free); diethyl ether (Et_2O; anhydrous, ≥99.0%, containing 1% BHT as inhibitor); titania (TiO_2; technical grade); magnesia (MgO_2; puriss); alumina (Al_2O_3); dioctyl sulfosuccinate sodium salt (AOT; 98%). Hydrazine (anhydrous, 98%) was used as received and stored under inert atmosphere at 5°C.

1-Octanesulfonyl chloride (95%) was obtained from TCI America. Spherical mesoporous silica (pore size 150Å; diameter 75-200 μm) was obtained from Sorbant Technologies. Molecular liquid precursors were synthesized in house and stored under dry nitrogen. 1,2-Dichloroethane (DCE) was obtained from Sigma-Aldrich, dried over 4 Å molecular sieves, and stored under inert atmosphere. Acetonitrile (ACN) was obtained from Sigma-Aldrich, distilled from calcium hydride onto 4 Å molecular sieves at atmospheric pressure, and stored under inert atmosphere. Grids used for TEM were obtained from Ted Pella. Carbon dioxide used was SFE grade from Airgas (99.999%).

4.3.2 Experimental

4.3.2.1 2-Butyl-1,1,3,3-tetramethylguanidine (TMBG)

A typical synthesis was carried out as follows. 14 mL oxalyl chloride (0.165 mol) was added dropwise to a solution of 9.6 mL tetramethylurea (0.08 mol) in 80 mL dry DCE (1.016 mol) at room temperature under inert atmosphere. The reaction mixture turned yellow and was heated at 70°C for 5 hours, after which point it was allowed to cool to room temperature. The solvent was then removed via rotavap, yielding yellow crystals. These crystals were then dissolved in 80 mL dry ACN (1.532 mol) under inert atmosphere. The

solution was placed in an ice bath and 15 mL *n*$BuNH_2$ (0.152 mol) was added dropwise via an addition funnel. The reaction mixture was removed from the ice bath and heated at 92°C for 1 hour. Removal of the ACN via rotavap yielded a thick yellow oil; this was treated with 30 mL 30 wt% aqueous NaOH and extracted with Et_2O to yield the crude product. Vacuum distillation yielded the desired product 2-butyl-1,1,3,3-tetramethylguanidine (bp 75°C at 1 mmHg; 80%).

^{1}H NMR (400.13 MHz, $CDCl_3$, 25°C) 3.05 (t, *J* = 6.9 Hz, 2H), 2.68 (s, 6H), 2.59 (s, 6H), 1.45 (p, *J* = 7.2 Hz, 2H), 1.30 (sextet, *J* = 7.4 Hz, 2H), 0.84 (t, *J* = 7.3 Hz, 3H)

^{13}C NMR (100.57 MHz, $CDCl_3$, 25°C) 160.02, 49.48, 39.81, 38.98, 35.23, 20.75, 14.21

4.3.2.2 *N*-Propyl octyl sulfonamide

A typical synthesis was carried out as follows. A 1.7 *M* solution consisting of 2.8 mL propylamine (0.0341 mol) in 20 mL DCE (0.254 mol) was added dropwise to an 8.4 *M* solution of 6.62 mL 1-octanesulfonylchloride (0.0840 mol) in 10 mL DCE (0.127 mol) at 0°C under argon. The solution was allowed to warm to room temperature and stirred for 24 hours. The solution was then washed with an aqueous solution of saturated sodium carbonate (Na_2CO_3) and dried with magnesium sulfate ($MgSO_4$); removal of the solvent under reduced pressure yielded the product *N*-propyl octyl sulfonamide (isolated yield: 79%).

^{1}H NMR (400.13 MHz, $CDCl_3$, 25°C) 4.16 (s, 1H), 3.05 (t, *J* = 6.9 Hz, 2H), 2.96 (m, 2H), 1.75 (m, 2H), 1.54 (sextet, *J* = 7.3 Hz, 2H), 1.39 (m, 2H), 1.26 (m, 8H), 0.93 (t, *J* = 7.3 Hz, 3H), 0.86 (t, *J* = 6.9 Hz, 3H)

^{13}C NMR (100.57 MHz, $CDCl_3$, 25°C) 52.91, 45.23, 31.92, 29.28, 29.17, 28.52, 23.90, 22.81, 14.29, 11.34

4.3.2.3 RevIL Synthesis: 1-Component RevILs

For all 1-component RevILs discussed in this chapter, synthesis was carried out as follows unless otherwise noted. A 2 dram vial was fitted with a rubber septum and purged with inert gas for 5 minutes. The capped vial was then weighed; approximately one gram of the molecular liquid in question was added and the capped vial was weighed again. Dry carbon dioxide was sparged through the molecular liquid for 75 minutes at a flow rate of 200 $mL \cdot min^{-1}$ at 25°C and 1 atm, using a diffuser tube (glass tube with frit on the end). The resulting ionic liquid in the capped vial was then weighed in order to determine that complete conversion had been achieved.

4.3.2.4 Gold Nanoparticle Synthesis: 2-Component RevILs

A typical synthesis was carried out as follows. The 2-component RevIL was synthesized by combining equimolar amounts of TMBG (0.6975 g; 4.072 mmol) and methanol (0.1325 g; 4.135 mmol) and sparging with CO_2. $HAuCl_4$ (0.01 g; 2.539×10^{-5} mol) was added to the RevIL, and *N*-propyl octyl sulfonamide (0.1284 g; 0.546 mmol) and the dodecane continuous phase (15 mL; 66.05 mmol) were added to form a visually homogeneous orange solution. A stoichiometric amount of hydrazine (or a solution of hydrazine in anhydrous inhibitor-free THF) was added to the system to reduce the gold salt. The RevIL was reversed by heating the solution at 100°C for 1 hour.

4.3.2.5 Gold Nanoparticle Synthesis: 1-Component RevILs

A typical synthesis was carried out as follows. The RevIL (TPSA or THSA) was synthesized by sparging the molecular liquid precursor with dry CO_2 for 75 min at 200 $mL \cdot min^{-1}$. $HAuCl_4$ (0.0034 g; 8.633×10^{-6} mol) was dissolved in the RevIL (0.5519 g TPSA; 1.162 mmol); 0.227 g of this mixture was mixed with 2 mL of hexane (15.20 mmol). 0.1 mL of 3.18×10^{-2} *M* of hydrazine in anhydrous inhibitor-free THF was added to the system.

Nanoparticles formed were allowed to ripen until no change in λ_{max} was seen via UV-Vis. For supported nanoparticles, solid support was added after reduction but prior to reversal. Unsupported nanoparticles were diluted in absolute ethanol for deposition on TEM grids; supported nanoparticles were instead heated at approximately 70°C to reverse the RevIL and deposit the nanoparticles onto the solid support.

4.3.2.6 Surface Tension Measurements: Capillary Rise

A typical surface tension measurement was carried out as follows. Precision bore capillaries with an inner diameter of 0.254 mm were procured from Wilmad Labglass. Prior to each experiment, these capillaries were soaked in a 2 *M* HNO_3 solution overnight; rinsed with DI H_2O (18 MΩ·cm), acetone, and hexane; and stored in a drying oven at 120°C. The RevIL was formed as above, by sparging dry CO_2 through an ML for 75 minutes at 200 $mL \cdot min^{-1}$ at 25°C. The desired amounts of the RevIL were then weighed out directly into 25 mL volumetric flasks and then diluted to volume with hexane. Concentrations investigated ranged from 0.1 to 0.0001 *M*. As the RevILs used are quite viscous, stirbars were added to the volumetric flasks and the capped solutions were stirred until uniform. Densities of all solutions were measured in triplicate. Clean dry glass beads (d = 0.5 mm) were added to a 4 dram glass vial to a depth of approximately 5 mm in order to support the capillary tube; a small amount of the solution was then added to the vial, and the vial was closed using a lid with a hole bored in the center of it. The capillary was then placed into the vial through the hole in the lid and the liquid therein was allowed to equilibrate. The height of the capillary rise was then measured using a cathetometer. Measurements were carried out in triplicate, using a fresh aliquot of solution for each measurement in order to minimize errors due to solvent loss by evaporation. A clean capillary tube was used for each measurement.

4.3.3 Instrumentation

^{1}H and ^{13}C NMR spectra were collected on a Varian Mercury Vx 400, using $CDCl_3$ as the lock solvent. UV-Vis spectra were collected under ambient conditions using an Agilent 8453 UV-Visible Spectrophotometer. Transmission electron microscope (TEM) images were obtained either at Emory University, on the JEOL JEM-1210 TEM (2-component RevILs), or at Georgia Tech, using the Hitachi HF-2000 FEG instrument (1-component RevILs). All TEM images were analyzed using ImageJ. Dynamic light scattering (DLS) measurements were performed using either a Dynapro DLS in the laboratory of Dr. Andrew Lyon at Georgia Tech, or a Malvern Instruments Zetasizer Nano ZS in the laboratory of Dr. Sven Behrens (also at Georgia Tech). For instruments performed using the Zetasizer Nano ZS, samples were delivered to a glass cuvette via a luer-lock syringe fitted with a 0.1 μm PTFE Millipore filter.[24] Water contents of AOT and solvents were determined using a Metroohn 852 Titrando Karl Fischer titration system. Densities were measured in triplicate using an Anton Paar DMA 38 Laboratory Density Meter.

4.4 Results and Discussion

4.4.1 Two-Component RevILs: AuNP Synthesis

After successfully showing the formation, dissolution, and reformation of the reverse micelle system with MO, we next applied our system to the formation of gold nanoparticles. We began with a target of 0.01 as our W_{HAuCl4}/W_{RevIL} ratio. Table 4.1 shows the parameters investigated in our preliminary experiments with 2-component RevILs.

Table 4.1. Testing parameters of RevIL/$HAuCl_4$/*N*-propyl octyl sulfonamide system in 15 mL dodecane as continuous phase.

Vial	Surfactant (g)	RevIL (g)	$HAuCl_4$ (g)	W_{HAuCl4}/W_{RevIL}
1	0.133	0.040	0.0019	0.048
2	0.066	0.022	0.0027	0.123
3	0.030	0.041	0.0024	0.058
4	0.131	0.051	0.0020	0.039

In order to compare our system with that of the Han group,[15] the W_{HAuCl4}/W_{RevIL} ratio was calculated for each experiment. The [TMBGH][MeOCOO] RevIL was pre-formed by combining equimolar amounts of TMBG and methanol and sparging with CO_2. Neat hydrazine was used as the reducing agent; following reduction, the solutions were heated at 100°C for one hour. We found that a ratio of approximately 0.1 yielded a stable system in which the nanoparticles remained suspended in solution and did not appear to aggregate. Moreover, we were able to recycle the system with this weight ratio several times. The system in vial 2 was recycled twice; after the solution was heated to reverse the RevIL back to the molecular form, the nanoparticles were allowed to settle, the supernate was decanted, and additional $HAuCl_4$ and methanol were added to the system. The assumption was made that all methanol was lost during the heating of the reaction mixture. CO_2 was then sparged through the system. Nanoparticles were deposited on copper mesh grids with carbon films and imaged using the JEOL JEM-1210 transmission electron microscope (TEM) at Emory University. Although the TEM images did reveal the presence of nanoparticles (Figure 4.10), upon analysis with ImageJ, they were found to be polydisperse, with a size range from 7 to 14 nm (Figure 4.11).

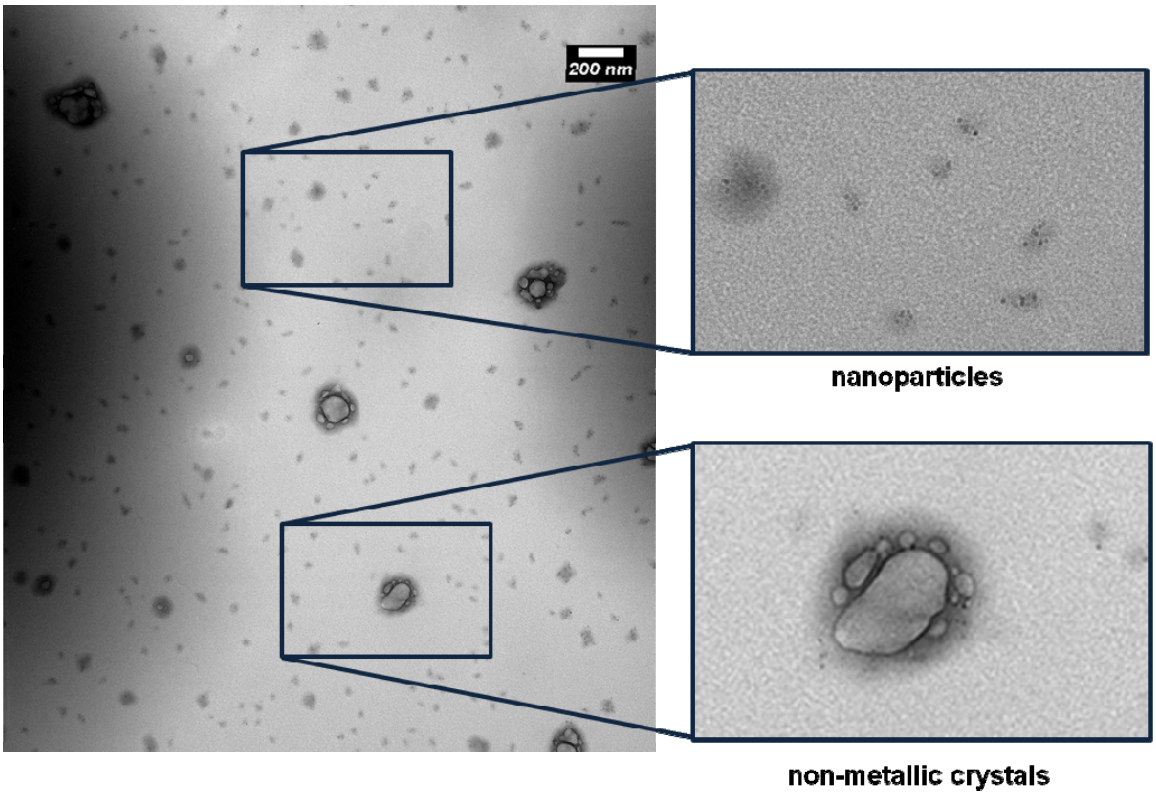

Figure 4.10. TEM image of AuNP synthesized using $HAuCl_4$, [TMBGH][MeOCOO], and dodecane. Enlargement, *top*, shows nanoparticles; *bottom*, large non-metallic crystals on grids.

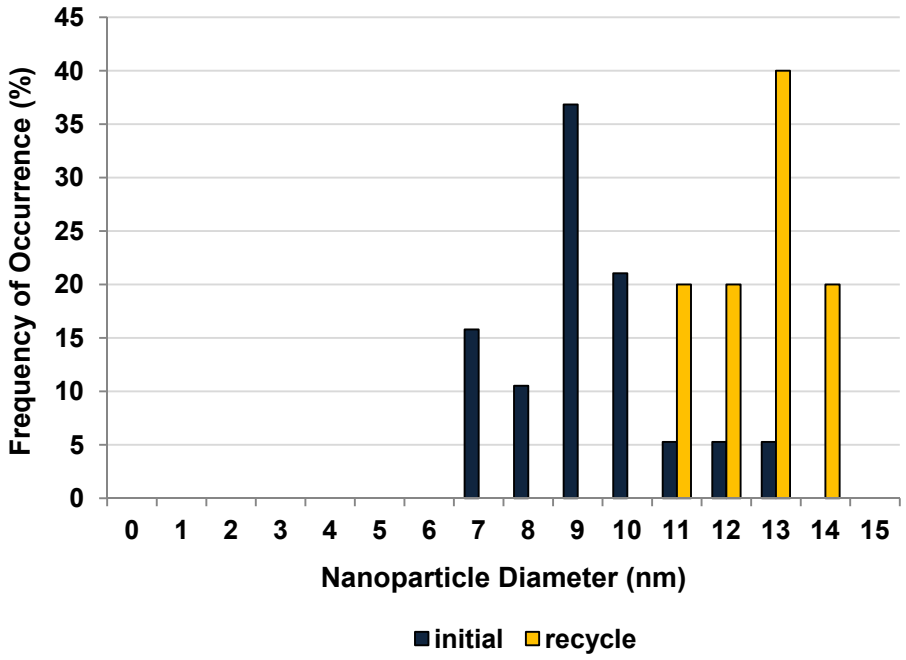

Figure 4.11. Range of nanoparticle sizes observed via TEM for initial experiments in dodecane.

Further complicating imaging was the presence of large crystals on the grids, seen in Figure 4.10. We surmise these to be deposits of surfactant and RevIL precursors.

It is important to note that our sample sets were very small—i.e., the nanoparticles were highly dilute and the number of AuNP observed on the TEM grids was low. The initial results were promising—we could indeed form gold nanoparticles with our system. There were, however, some challenges. The gold salt is hygroscopic, making it difficult to weigh out the small amounts required to reform the system for the recycles. Similarly, we frequently overshot the amount of hydrazine needed for reduction of the gold salt—the unreacted hydrazine in the system immediately reduced the gold salt added for the recycle. In the second iteration of our system, we addressed these issues by making several stock solutions—$HAuCl_4$ in methanol, which was used to replenish the gold salt and the alcohol for the recycle; and hydrazine in THF, which was used as the reducing agent. The dodecane

continuous phase was also changed to hexane after finding that the surfactant was more soluble in hexane, allowing us to reach higher concentrations of nanoparticles in solution. The system was again recycled twice. We altered our deposition technique slightly: in addition to depositing multiple drops of the reaction mixture onto the grids in order to effectively concentrate the nanoparticles, we also washed the grids with a few drops of hexane to remove the organic components. Grids were then stored under vacuum prior to imaging. An example image can be seen in Figure 4.12.

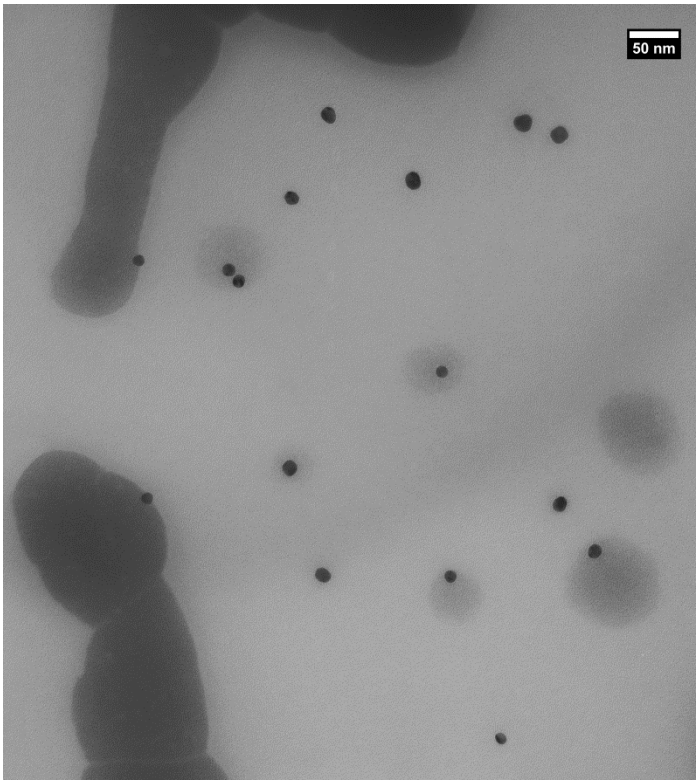

Figure 4.12. TEM image of AuNP synthesized in second round of experiments. Note dark areas, presumed to be high-boiling organic compounds (e.g. TMBG).

TEM imaging revealed that there was still organic material on the grids and relatively few nanoparticles. However, the number of nanoparticles we were able to see via TEM

increased. The average diameter of the AuNP formed in the initial reaction was found to be 7 ±3 nm. ImageJ analysis again showed a high degree of polydispersity for the initial reaction as well as the recycles (Figure 4.13).

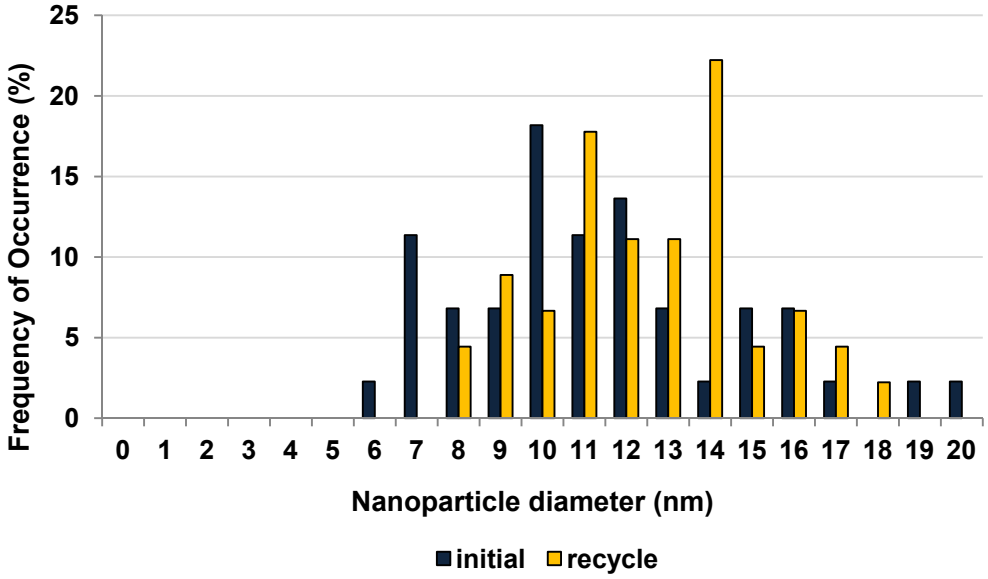

Figure 4.13. Range of nanoparticle sizes observed via TEM for experiments in hexane.

Realizing that our deposition technique was not optimal, we tried several methods of removing the organics from our imaging grids. Storage under vacuum overnight prior to imaging did not remove all of the organics; washing the grids with hexane following deposition removed not only the organics, but also the nanoparticles. Capping the nanoparticles with dodecanethiol prior to reversal of the RevILs allowed for better imaging (as in Figure 4.14) upon slow evaporation of the organic continuous phase.

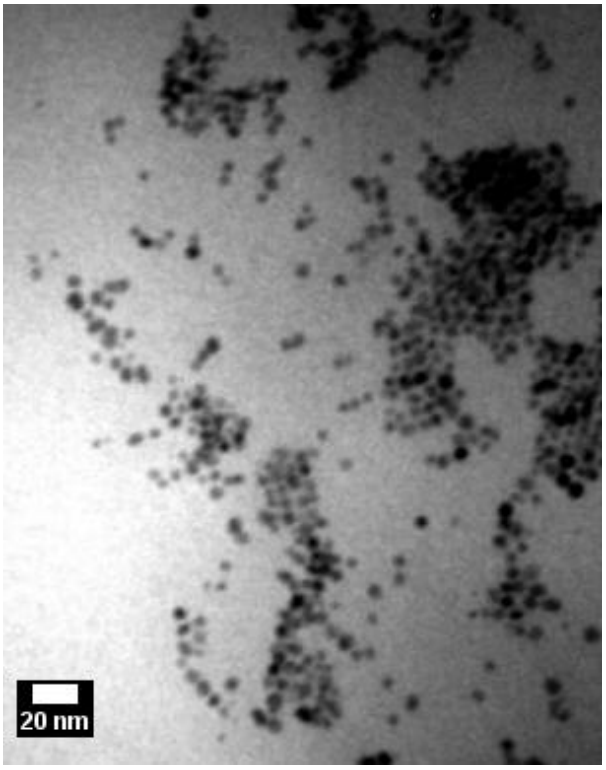

Figure 4.14. Dodecanethiol-capped gold nanoparticles. Stabilization allows for better deposition and imaging.

It became apparent that our initial goal of creating a fully recyclable system was not practical for several reasons. Formation of the 2-component RevILs requires a stoichiometric mixture of TMBG and methanol; deviation from a 1:1 molar ratio will affect the solvent properties of the resulting RevIL. Additionally, the methanol lost during heating and reversal must be quantified and added in order to recycle the system. The hydrazine added to the system must also be precisely controlled, as overshooting the stoichiometric amount required to reduce the gold salt will result the presence of excess hydrazine in the reaction mixture, and near-instantaneous reduction of the gold salt as soon as it is added to prime the system for recycle (i.e. before the micelles can be re-formed). Finally, although hydrazine breaks down into nitrogen and hydrogen upon heating, it forms the byproduct hydrochloric acid (HCl) upon reacting with $HAuCl_4$, as shown below in Equation 4.1.

$$2HAuCl_4 + 2N_2H_4 \rightarrow 8HCl + 2Au^0 + 2N_2 + H_2 \qquad \text{Equation 4.1}$$

If any HCl were to remain in solution, it would protonate our molecular liquid upon reduction and reversal. With these problems in mind, we decided to simplify our system by switching to our 1-component RevILs, which would eliminate the need for precise equimolar amounts of TMBG and alcohol.

4.4.2 One-component RevILs: Preliminary Experiments

Amines—both aromatic and aliphatic—have also been used as capping agents for gold nanoparticles.[25] Aromatic amines in particular, such as anilines or tryptophan, can stabilize gold nanoparticles not only by passivating the surface of the metal, but also via a concurrent polymerization reaction of the amine.[26] Some amines can even act as reducing and capping agents, eliminating the need for two separate reagents in the synthesis of AuNP.[27] Amines can also be introduced to the surface of gold nanoparticles via ligand exchange, as in the work from Hutchison *et al.*[28] The bond between the amino group and the gold surface does not appear to be as strong as the covalent bond that is formed between sulfur and gold, although there is some debate in the literature about this.[29]

However, our 1-component RevILs contain not uncharged amines, but ammonium cations and carbamate anions, as shown in Figure 4.15.

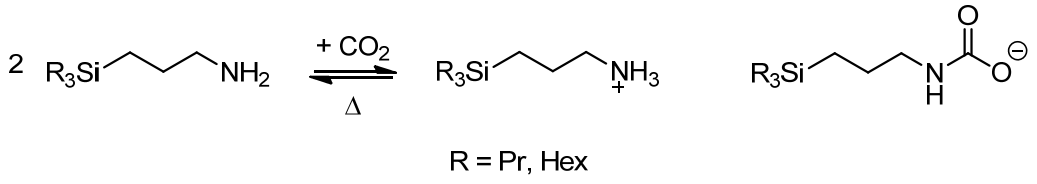

Figure 4.15. 1-component RevILs discussed in this chapter.

Quaternary ammonium salts have been used as capping agents for AuNP synthesis in a modification of the Brust method that omits dodecanethiol; these AuNP are also reported to be stable in solution for extended periods of time.[30] Based on the literature precedent, it seemed likely that the ionic form of the RevIL could therefore interact with the gold salt[31]—perhaps even via ion exchange, which has been shown to stabilize reverse micelles formed with ionic surfactants.[14] Traditional ionic liquids have also been shown to form stabilizing monolayers around metal nanoparticles during their synthesis, with no additional surfactant required due to their high charge.[32] Our 1-component RevILs also bear a resemblance to "catanionic" surfactants, which are formed from the reaction of a long-chain carboxylic acid and amine (shown in Figure 4.16).[33]

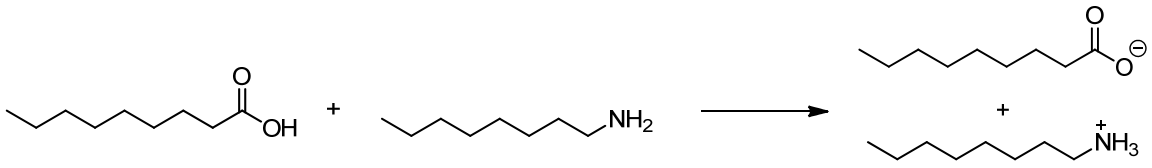

Figure 4.16. "Catanionic" surfactant synthesized by Abécassis *et al.*[33]

These catanionic surfactants have been shown to form unusual topologies such as icosahedra and flat discs, both in regular (i.e. oil-in-water) and reverse micelles.[34]

Preliminary experiments using one-component RevILs and MO showed that no additional surfactant was needed to solubilize the UV-active salt, as shown in Figure 4.17. A solution of (3-aminopropyl)tripropylsilylamine (TPSA; R = Pr in Figure 4.15) molecular liquid (ML) in heptane was prepared, and an excess of MO was added to this solution.

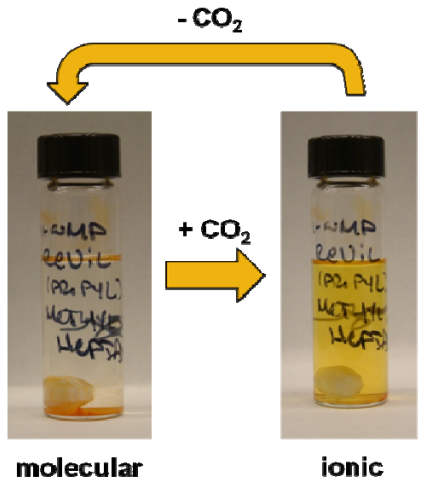

Figure 4.17. *Left*, solution of TPSA molecular liquid in heptane with MO. *Right*, solution of TPSA RevIL in heptane with MO.

As shown in Figure 4.17, when the molecular form of TPSA is combined with heptane and MO, the MO is not solubilized and remains on the bottom of the reaction vessel. Upon reaction with CO_2, the RevIL is formed; reverse micelles are created; and the MO is solubilized, giving the solution on the right its orange color. Heating the solution to reverse the RevIL resulted in the precipitation of MO out of solution.

We surmised that the alkyl chains on the RevIL acted as surfactant tails and could theoretically stabilize a reverse micellar structure, as shown in Figure 4.18.

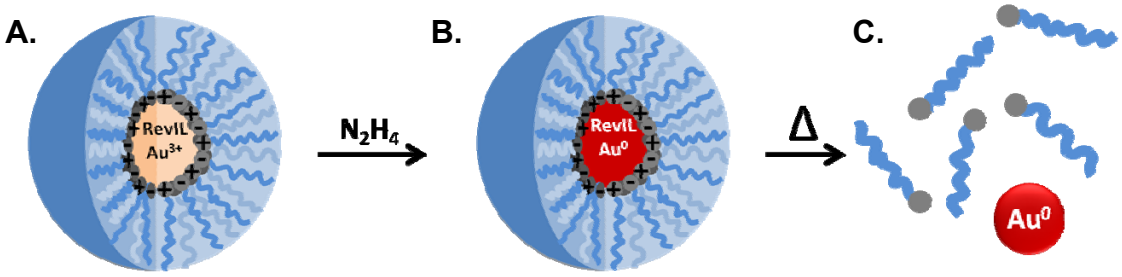

Figure 4.18. *Left*, reverse micelle containing gold salt and RevIL; *middle*, reduction of gold salt to form gold nanoparticles; *right*, destabilization of micelles and release of nanoparticles.

In illustration *A* in Figure 4.18, the pre-formed RevIL has been combined with a gold (III) salt in a hydrocarbon continuous phase. The 1-component RevIL could either act as a surfactant, or act as both a solvent (i.e. the disperse phase within the reverse micelle) and surfactant. Reduction of the gold salt with hydrazine could form nanoparticles (*B* in Figure 4.18), which would remain encapsulated within the reverse micelles. Heating would reverse the RevIL and release the AuNP (*C* in Figure 4.18). There are two major differences between the hypothetical system illustrated here and the 2-componenent RevIL analog shown in Figure 4.4. The first difference is that the 2-component RevIL system requires the use of a separate surfactant molecule, while the 1-component RevIL system does not. The second difference is that the 1-component RevIL system is not specifically designed to be recycled. While the 2-component RevILs were intended to be switchable solvents for AuNP synthesis, the 1-component RevILs are intended to be switchable surfactants. As such, we decided to characterize the surfactant-like behavior of the 1-component RevILs.

4.4.3 One-Component RevILs: Structure of Reverse Micelles

One of the most important parameters for any surfactant is the critical micelle concentration, or CMC. For surfactants in aqueous media, the CMC is the concentration below which surfactants are present as monomers, with minimal (if any) aggregation occurring.[35] This can be seen on the left of Figure 4.19. As the concentration of surfactant continues to increase, surfactant molecules will also orient themselves at the air-water interface, with the polar heads oriented downwards into the water. Above the CMC, the air-water interface is saturated with surfactant molecules; micelles form; and any monomers present are in equilibrium with said micelles, as shown on the right in Figure 4.19.[36]

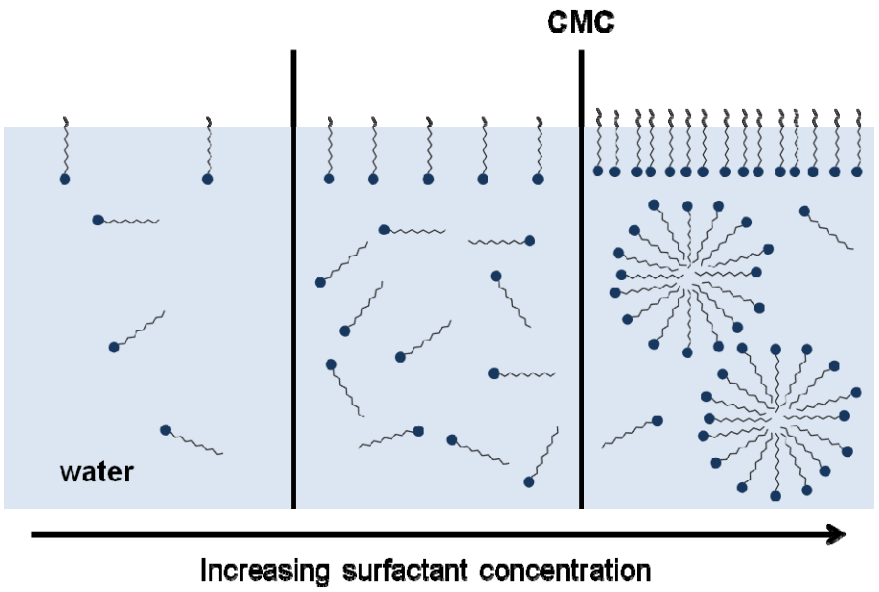

Figure 4.19. Reaching critical micelle concentration in aqueous solution.

Addition of more surfactant to a solution already above the CMC will cause the formation of new micelles or the growth of micelles that are already present. As a result, the properties of the solution—for example, conductivity and surface tension—will change abruptly once the CMC is reached.[35a]

Surface tension and dye solubilization are the most common properties used to determine CMC for aqueous solutions.[35b] In the dye solubilization technique, a dye that is soluble in the discrete lipophilic phase but largely insoluble in the aqueous continuous phase is introduced to a solution of aqueous surfactant.[37] Unless micelles are present, the dye will not be soluble and there will be no absorption peak present in the UV-Vis spectrum of the solution.[35a] A plot of the absorption at the λ_{max} of the dye as a function of surfactant concentration should then be at zero before the CMC, and begin to sharply increase after the CMC is reached.[37a] This is akin to our preliminary experiments with MO (page 160).

The most studied method for determining CMC, however, is the capillary rise technique.[35a] Introduction of a capillary to the surface of a solution will result in the liquid rising up the capillary. If the capillary is small enough (i.e. with a diameter less than 1 mm),[38] the meniscus can be assumed to be hemispherical, and the surface tension can be calculated using the equation:

$$\gamma = \frac{\rho g h r}{2} \qquad \text{Equation 4.2}$$

where γ is surface tension, ρ is the density of the solution, *h* is the height of the liquid in the capillary (measured from the surface of the bulk solution), and *r* is the inner radius of the capillary.[35a] The capillary rise height is measured at a range of different concentrations; if the densities of the different solutions are known, the surface tension can be calculated from this data. The CMC can then be determined by plotting surface tension as a function of concentration, fitting straight lines to the various regions of the graph, and locating their intersection.[35b] Water has a high surface tension; for oil-in-water micelles, the surface tension should remain stable below the CMC. The surfactant molecules will orient themselves such that the alkyl tail points upwards at the water-air interface; the polar head will point downwards into the water. Once this interface is saturated, the surface tension will drop, and this concentration is the CMC (Figure 4.19). After this point, any further addition of surfactant will lead to the formation of aggregates in the water.

4.4.3.1 Dye Solublization

The dye solubilization technique described by Schott uses water-insoluble dyes to determine the CMC of oil-in-water micelles;[37] we sought dyes that would perform in the opposite manner, i.e. dyes that were insoluble in a hydrocarbon continuous phase and soluble in an orthogonal polar phase. Although our initial experiments with methyl orange, described previously (page 158), showed that the sodium salt was soluble only in the presence of the RevIL form of TPSA, they did not conclusively prove that reverse micelles were formed. TPSA RevIL could be acting as a cosolvent, changing the polarity of the solution just enough to make MO soluble in hexane. Methyl orange proved to be a poor dye for CMC experiments due to its tendency to smear on the walls of the cuvette and deliver an absorption peak in the UV-Vis spectrum, even when not in solution. Through trial and error, we identified four dyes that were insoluble in hexane but soluble in acetonitrile (ACN), which we used as a polar stand-in for the more expensive TPSA RevIL: bromothymol blue sodium salt, Chromotrope FB, new methylene blue N, and toluidine blue O. The structures of these dyes are shown in Figure 4.20.

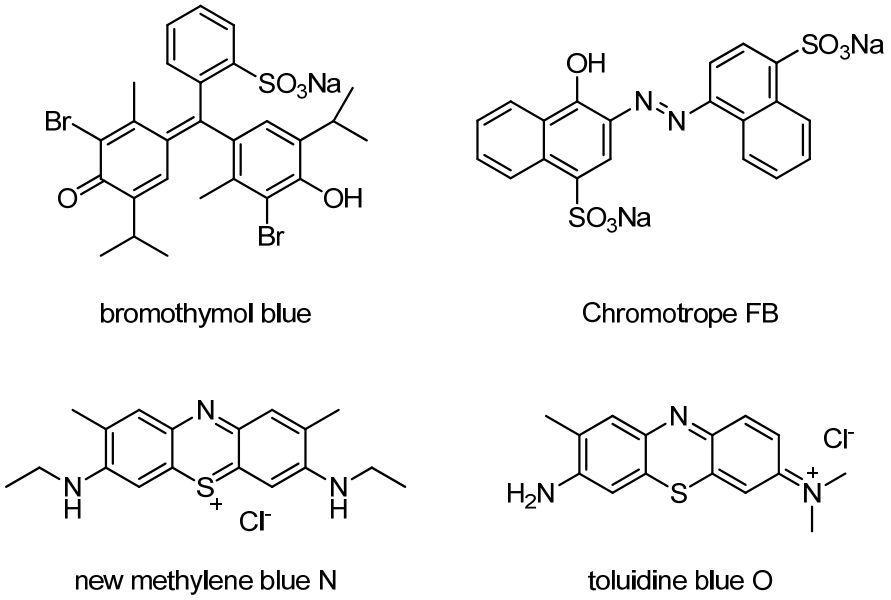

Figure 4.20. Dyes used for CMC determination with dye solubility.

The absence of a peak in the UV-Vis spectrum of the hexane and dye mixture indicated that, for our purposes, the dye was insoluble in hexane. We then tested the solubility of these four dyes in TPSA RevIL. However, when these dyes were introduced to the TPSA RevIL, the color of the solution changed over time; this seemed to indicate that the dyes were reacting with our ammonium-carbamate ion pair. As the four dyes investigated contained either phenolic groups (bromothymol blue, Chromotrope FB) or amines (toluidine blue O, 1° amine; new methylene blue N, 2°), we looked for a dye candidate that did not contain either of these reactive functional groups. The final dye we attempted to use was methylene violet, which contains a relatively unreactive tertiary amine.[39]

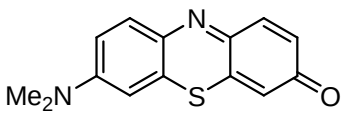

Figure 4.21. Methylene violet.

However, this dye was too soluble in hexane to be useful. We decided to discontinue dye solubilization experiments and attempt to determine the CMC of TPSA RevIL via the surface tension of solutions of TPSA RevIL in hydrocarbons.

4.4.3.2 Surface Tension Measurements Via Capillary Rise

Capillary rise was then used to determine the change in surface tension over a range of concentrations of TPSA RevIL in hexane. To verify the accuracy of our experimental setup, we first measured the surface tension of *n*-hexane, which is well established in the literature over a range of temperatures.[40] Our experimental value of 17.7326 ±0.1229 $mN \cdot m^{-1}$ at 20°C was in good agreement with the literature value of 17.90 $mN \cdot m^{-1}$ at 293.15K.[40] We then prepared a wide range of solutions of TPSA RevIL in hexane, spanning a range in concentrations from 0.1 to 0.0001 *M*. The density of each solution was also measured, and these values were used in Equation 3.1 to determine the surface tension of each solution (γ). The compiled data is shown in Figure 4.22. The expected trend in surface tension is the opposite of that seen in oil-in-water micelles; that is, one would expect the surface tension of the solution to increase as the concentration of surfactant increases.[41]

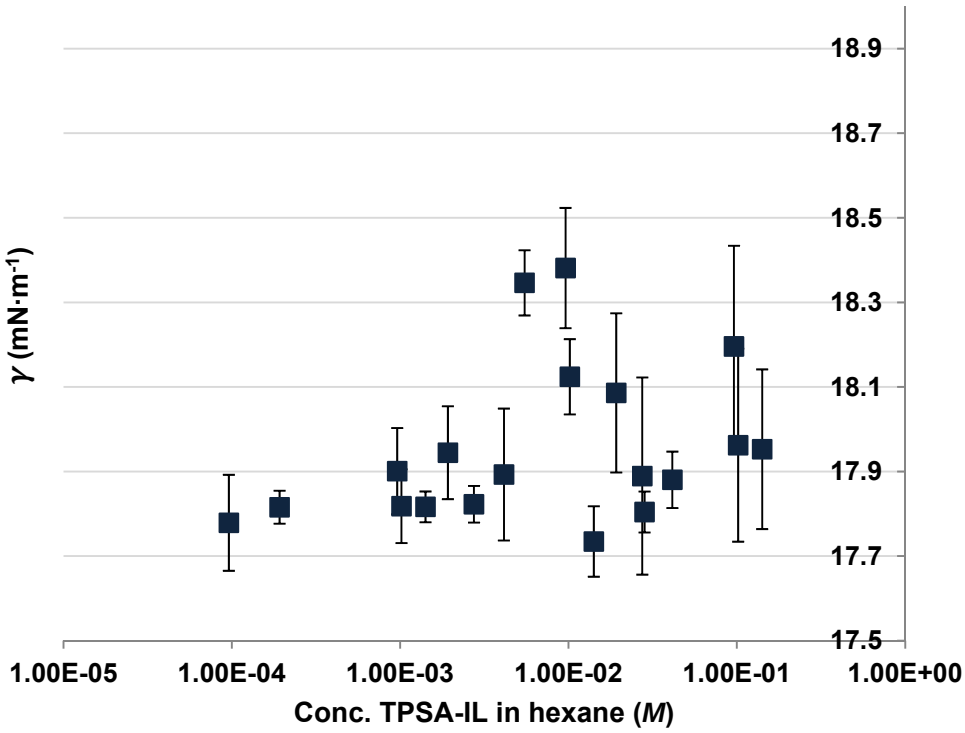

Figure 4.22. Surface tension of TPSA RevIL in hexane as a function of concentration, determined via capillary rise method.

Despite being able to accurately measure the surface tension of *n*-hexane, we did not observe any discernable trend in the data. Additionally, as can be seen in Figure 4.22, there were large sources of error in our measurements.

The two experimental techniques I have just described are frequently used for CMC determination in oil-in-water micelles. For water-in-oil micelles, which are the most similar to our system, the existence of a CMC is a topic of much debate in the literature.[42] The earliest attempts to determine a CMC in an organic continuous phase were performed in 1952 by Singleterry *et al.*, using the dye solubilization technique to find the CMC of the soap calcium xenylsterate in benzene.[43] However, more recent literature seems to disprove the existence of a CMC. To be more specific, the idea that reverse micelles exist is not disputed;

rather, the presence of a sharp, well-defined change in solution properties over a narrow range of surfactant concentrations is.[44] The factors driving self-assembly of reverse micelles are not as strong as the hydrophobic effect, which leads to self-assembly of micelles in water. Surfactants in water will tend to self-assemble to minimize the unfavorable interactions between the polar phase and the nonpolar phase; combination of the individual surfactant molecules will decrease the total hydrophobic surface area of the greasy tails.[41] The release of the ordered water around these tails back into the disordered bulk water is an entropic reason for the ordering of surfactant molecules as well.[45] In contrast, the only intramolecular forces in play between surfactant molecules in reverse micelles are weak van der Waals forces.[46] Additionally, the clustering together of polar surfactant heads in the core of the reverse micelle—particularly for ionic surfactants—seems as if it would tend to lead to dissociation of the reverse micelles.[41] The current prevailing theory is that the aggregation process of surfactants in non-polar solvents is a continuous process, rather than a stepwise change. Surfactants will begin to aggregate as dimers, trimers, etc., until small clusters of surfactant molecules are present.[44]

Compounding this debate is the fact that very small amounts of impurities or contaminants—for example, the small amounts of water usually found in AOT[47]—can alter the composition and the structure of the reverse micelles.[48] Langevin asserts that, in the total absence of water, no CMC is observed, and the reverse micelles observed contain small numbers of surfactants.[49] Ruckenstein and Nagarajan state that the use of the dye solubilization technique to determine the CMC for reverse micelles could lead to false readings, as the presence of the dye changes the interaction between surfactant molecules.[42] In fact, the work performed by Singleterry *et al.* used "moist" benzene,[43] and, if the presence of water can effectively "glue" reverse micelles together, this may indeed be an inaccurate

determination of the CMC for that particular system. Given the many differing opinions on this topic, and the experimental difficulties associated with the two CMC determination methods described above, it may be more efficient to attempt to size the reverse micelles instead, as discussed below.

4.4.3.3 Dynamic Light Scattering

We also have attempted to use dynamic light scattering (DLS) to determine the size of the reverse micelles, and thus link the size of the reverse micelles to the size of the nanoparticles formed therein. Initially, a range of concentrations of TPSA RevIL in hexane were prepared and measured using a Dynapro DLS instrument; however, these experiments were inconclusive, as no aggregates could be detected. Given the small size (5-10 nm) of the nanoparticles formed using our system, we hypothesized that the diameters of the reverse micelles were below the detection limit of the instrument used. Use of an orthogonal disperse phase in the micelle core has been shown to enable finer control of the size of reverse micelles, regardless of whether this disperse phase is water or a non-aqueous polar solvent.[50] In fact, some researchers claim that the presence of a disperse phase is necessary for any significant aggregation of surfactants to occur in a water-in-oil system.[51] Regardless, larger micelles would be more readily observed using DLS. For most reverse micelles, the micelle core is made up of water. However, our RevILs will react with water to form bicarbonates, thus altering their ability to act as a surfactant. A non-aqueous polar solvent such as acetonitrile that is largely immiscible with hexane could potentially serve as a micelle core.[50]

To this end, we decided to form reverse micelles using TPSA RevIL as the "switchable surfactant," heptane as the continuous phase, and acetonitrile (ACN) as the orthogonal core phase. As it is sometimes difficult to accurately measure the size of reverse

micelles (namely, the hydrodynamic radius; r_h) due to their small size (relative to normal micelles[46]), we initially prepared solutions of AOT, water, and isooctane to ascertain the sensitivity of the instrument we were using. The concentration of AOT in isooctane and the w_0 ratio (mol water/mol AOT) from the work by Zulauf *et al.*[52] were used, so that we could compare known sizes of reverse micelles with our experimental values. We would then switch out one element at a time—first switching water for ACN, then the continuous phase to heptane, and finally the surfactant to TPSA RevIL, so that we would ultimately be working with the desired system for gold nanoparticle synthesis. The r_h for certain concentrations and w_0 of AOT-water-heptane and AOT-ACN-heptane mixtures are available in the literature for comparison.[50, 53] The results of our experiments using an AOT-water-isooctane system are shown in Table 4.2. Viscosities and refractive indices of the various components were taken from the literature.[53b, 54]

Table 4.2. Experimental parameters for determination of r_h for AOT-water-isooctane system. ‡no water was added; H_2O from AOT only.

mol AOT	Mol H_2O	w_0 = [water]/[AOT]	Experimental r_h (nm)	Literature r_h (nm)
2.510×10^{-4}	0.124×10^{-3}‡	0.49	--	1.5
	4.901×10^{-3}	20.02	5.6	4.8
	9.997×10^{-3}	40.32	10.0	10.3
	12.167×10^{-3}	48.96	11.4	12.0

These DLS measurements were obtained using a different instrument, a Malvern Instruments Zetasizer Nano ZS. Our samples were prepared from a stock solution of AOT in isooctane. As commercially available AOT almost always contains some small amount of water,[47, 55] the weight fraction of water in our AOT was determined via Karl Fischer titration

and found to be 2 wt%. This small additional amount of water has been accounted for in the calculations used to produce Table 4.2, and totaled with the amount of water added to the stock solution of AOT in isooctane for each measurement to determine the actual amount of water present in each sample. The experimentally determined r_h values are in good accordance with the literature values at the higher w_0; when no additional water was added to the system, no aggregation was observed via DLS, supporting our reasoning that a simple solution of TPSA RevIL in hydrocarbon was unlikely to produce aggregates of a size able to be observed via DLS due to the lack of a disperse phase. We therefore proceeded with the switch to TPSA RevIL as a surfactant, rather than AOT.

While exploring the solubility of TPSA RevIL in hydrocarbons, we found that it was highly soluble in isooctane—much more than in heptane. Although the solubility limit of TPSA RevIL in isooctane or heptane has not been determined, we decided to switch to using isooctane as our continuous phase. Solutions of TPSA RevIL-ACN-isooctane were prepared at two different concentrations of TPSA RevIL in isooctane and visually checked for homogeneity. Microemulsions appear clear because the diameter of the reverse micelle is much smaller than the wavelength of visible light, allowing the light waves to pass through unhindered. A solution that cannot support a microemulsion will appear cloudy or even biphasic.[56] The results of these preliminary experiments can be seen in Table 4.3.

Table 4.3. Solubility of ACN in isooctane in the presence of TPSA RevIL.

mol TPSA RevIL	Mol ACN	w_0 = [ACN]/[TPSA RevIL]	Homogeneous?
6.340×10^{-4}	2.982×10^{-3}	4.70	Yes
	6.040×10^{-3}	9.53	Yes
	12.205×10^{-3}	19.25	No
	24.472×10^{-3}	38.60	No
5.152×10^{-4}	2.396×10^{-3}	4.65	Yes
	4.881×10^{-3}	9.48	No
	9.665×10^{-3}	18.78	No
	19.588×10^{-3}	38.02	No

The results of these titration experiments were initially very exciting—the TPSA RevIL appeared able to function as a surfactant and support a microemulsion at certain concentrations and w_0. However, we found that the homogeneous samples had w_0 values close to the solubility limit of ACN in isooctane, which is 0.08 (mole fraction).[50] This implies that the TPSA RevIL is not contributing to the solubilization of ACN in isooctane, neither via a reverse micellar structure nor by acting as a co-solvent. This may be due to a lack of strong interactions between the polar head of TPSA RevIL and the ACN disperse phase core. Polar solvents that are almost completely immiscible (as opposed to only slightly miscible, as with ACN and isooctane) allow better control of microemulsion size with the variation of w_0.[46] There are relatively few polar organic solvents that are almost completely immiscible with hydrocarbons such as hexane: two other candidates for the polar core phase are *N*,*N*-dimethylformamide (DMF) and dimethylsulfoxide (DMSO). DMSO has been shown to act as a capping agent for nanoparticles,[57] but it could be used as the disperse phase in a proof-of-concept experiment to demonstrate how the 1-component RevILs function as switchable surfactants. Although DMF can act as a reducing agent for AuNP

synthesis if seed AuNP or Au^0 are present, it is thought to be unreactive with respect to Au^{3+} and could be used as the polar disperse phase.[58]

4.4.4 One-Component RevILs: AuNP Synthesis

Despite being unable to conclusively show that reverse micelles were present in a solution of TPSA RevIL and hexane, we decided to continue with the synthesis of AuNP using this system. Our initial experiments focused on the RevIL THSA (R = Hex in Figure 4.15), as it had the most "surfactant-like" structure. The THSA RevIL was pre-formed by sparging the THSA ML with dry CO_2 at a rate of 200 mL·min^{-1} for 75 minutes. 0.6933 g of this RevIL was then combined with 0.0054 g of the gold salt $HAuCl_4$ and 1.8 mL of the continuous phase hexane. Reduction of the system was carried out using a stoichiometric amount of hydrazine (3.18×10^{-2} *M* in ACN). We were able to reproducibly form nanoparticles using a system with an approximate W_{HAuCl4}/W_{RevIL} of 7.789×10^{-3}; however, the nanoparticles formed using this system were found to be polydisperse (diameters ranging between 15 and 20 nm) and non-spherical, as shown in Figure 4.23.

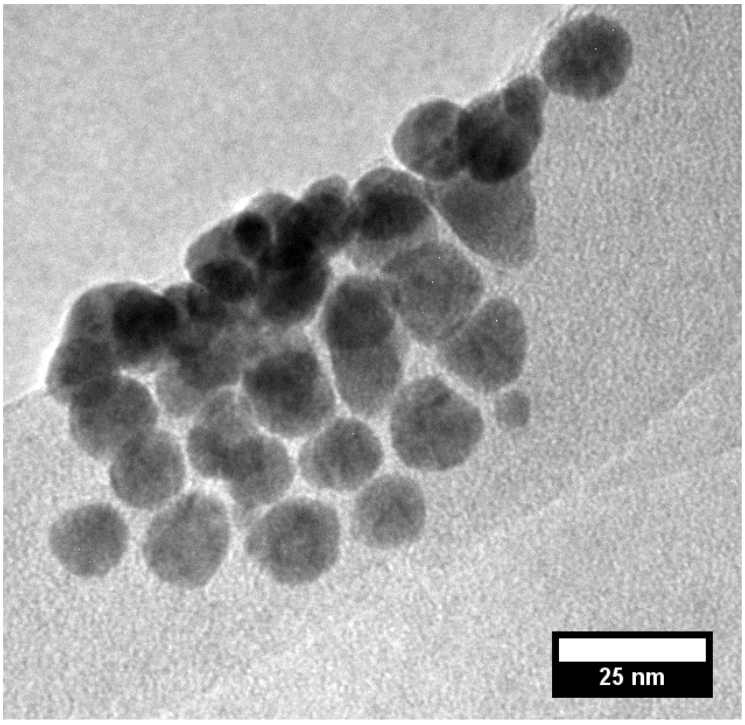

Figure 4.23. TEM of gold nanoparticles formed using $HAuCl_4$, THSA RevIL, and hexane.

Due to the irregular shape of the AuNP formed via this method, we did not attempt to size them using ImageJ. We were encouraged by our ability to form nanoparticles. However, due to the delay between nanoparticle synthesis and imaging, we sought another method of analysis to supplement TEM.

We decided to use UV-visible light spectroscopy (UV-Vis) as a complementary analytical method that would allow for more rapid characterization of our system. This technique permits us to quickly determine the effects of the changes on nanoparticle formation and size by checking for the presence of a surface plasmon resonance (SPR) band using UV-Vis, before confirming size and shape via TEM. The SPR of gold nanoparticles is dependent on the size and agglomeration of the AuNP, but is generally located in the vicinity of 520 nm.[59] The presence of this band is due to the delocalization of the free *d* electrons in the nanoparticle; when irradiated, these electrons will oscillate in resonance with

the light wave, and the resulting SPR can be observed via UV-Vis spectrocopy.[60] No SPR band should be observed for large particles with a diameter greater than 50 nm or bulk metal.[60] Combining this analytical technique with the use of the carousel reactor allowed us to run up to 12 reactions conditions simultaneously, allowing us to determine the factors that controlled nanoparticle formation and quickly analyze the results. A sample compilation of these UV-Vis spectra can be seen below, in Figure 4.24, wherein the effect of the hydrazine solvent and concentration on nanoparticle formation was investigated. A stock solution comprising 0.0187 g $HAuCl_4$, 2.3136 g TPSA RevIL, and 190 mL anhydrous hexane was prepared and divided up amongst the carousel tubes.

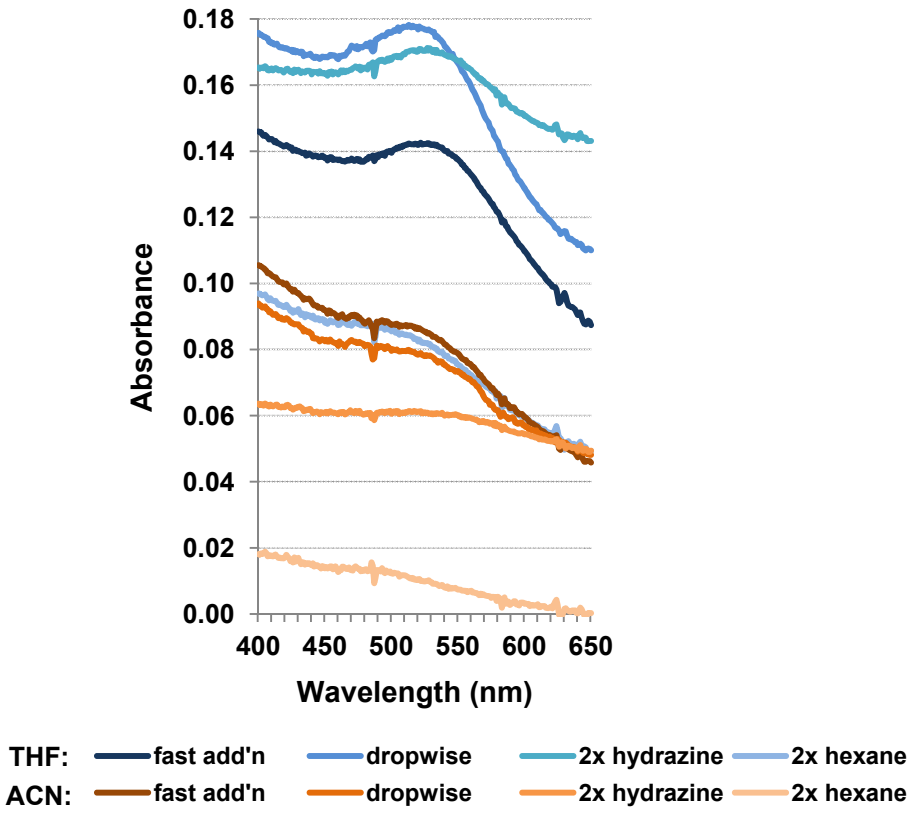

Figure 4.24. UV-Vis spectra of AuNP synthesized in carousel reactor using $HAuCl_4$, TPSA RevIL, hexane, and solutions of hydrazine in THF or ACN.

Two different solvents for hydrazine were investigated: THF and ACN. The concentration of both hydrazine solutions was 3.18 x 10^{-2} *M*. Several variables were also investigated: fast addition of the reducing solution; slow addition (i.e. dropwise); twice the stoichiometric amount of hydrazine; and twice the amount of continuous phase hexane. Although this was not a qualitative study, we can still glean a number of trends from Figure 4.24. The SPR band is not as pronounced for the samples which used ACN as the hydrazine solvent. As ACN is only minimally soluble in hexane, the reaction mixture was biphasic; the nanoparticles seemed to preferentially partition into the ACN phase, which quickly turned blue, indicating agglomeration.[61] The hexane phase remained colorless. As THF and hexane are fully miscible, this problem did not occur in those samples prepared using a solution of hydrazine in THF as the reducing agent. When we compare the samples prepared using hydrazine in THF, we can see that slow addition of the reducing agent results in a broader absorption peak, indicating a more disperse sample.

The information collected from these UV-Vis spectra allowed us to refine the parameters for our next experiments, which used $HAuCl_4$, TPSA as the RevIL (W_{HAuCl4}/W_{RevIL} = 7.997 x 10^{-3}), and a solution of hydrazine in THF (3.18 x 10^{-2} *M*) as the reducing agent. Representative nanoparticles formed using this system can be seen in Figure 4.25, and a size distribution of this sample can be seen in Figure 4.26. The nanoparticles were deposited by diluting several drops of the reaction mixture in absolute ethanol, then depositing three drops of this solution on the grids.

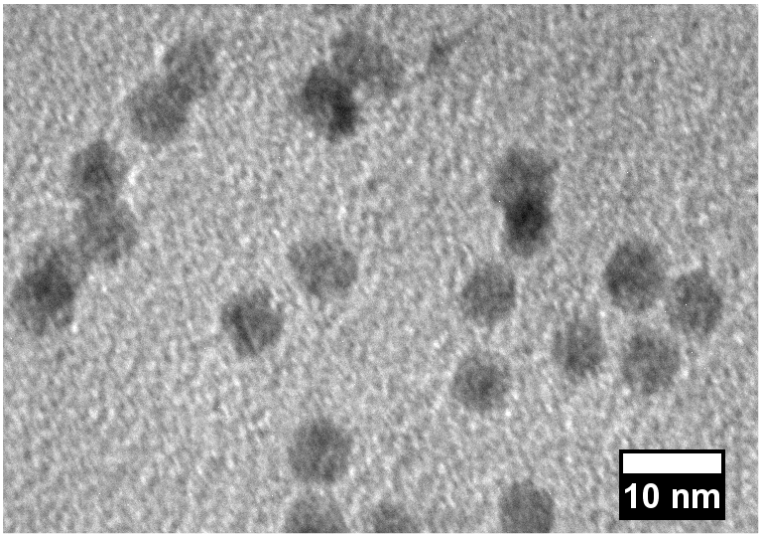

Figure 4.25. TEM image of gold nanoparticles synthesized using $HAuCl_4$, TPSA RevIL, and hexane.

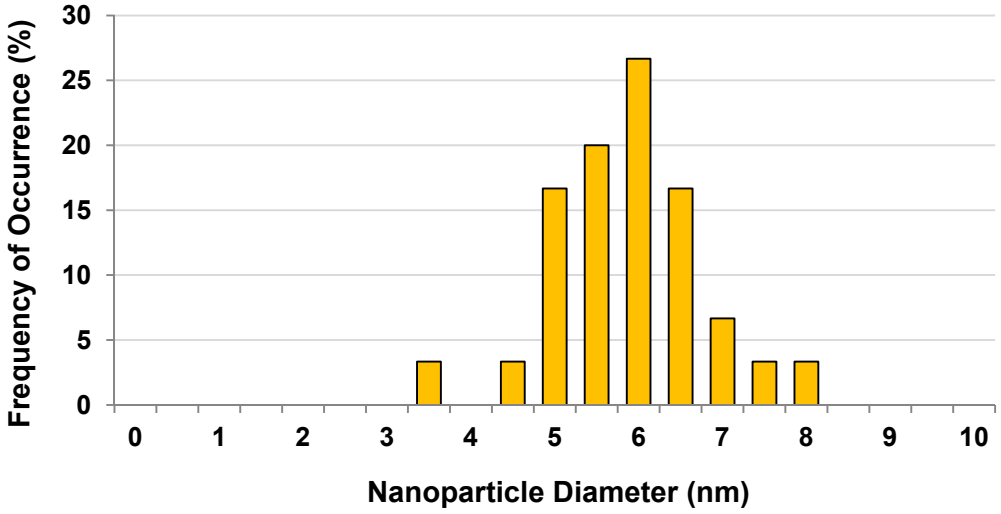

Figure 4.26. Size distribution of nanoparticles from sample shown in Figure 4.25.

As can be seen in Figure 4.25 and Figure 4.26, it is clear that the nanoparticles formed are more uniform and more spherical than those synthesized in our previous experiments. When analyzed using ImageJ, the average diameter of the nanoparticles formed was found to be 6.1

±0.9 nm. This diameter gold nanoparticle has been found to be active in oxidation reactions.[62]

It is important to note that the RevIL was not reversed prior to deposition; that is to say, the reverse micelles, if present, were still intact. We attempted to reverse the RevIL and release the nanoparticles from the reverse micelles by heating the reaction mixture in an oil bath at 65°C for 1 hour—a temperature and time that should result in full reversal of the TPSA RevIL to the ML. The solution became a lighter purple in color, but did not fully decolorize as would be expected if all AuNP were dropping out of solution. We then deposited a sample from this reaction mixture on a TEM grid for analysis. One of the images resulting from this experiment can be seen in Figure 4.27; the size distribution taken from this sample can be seen in Figure 4.28.

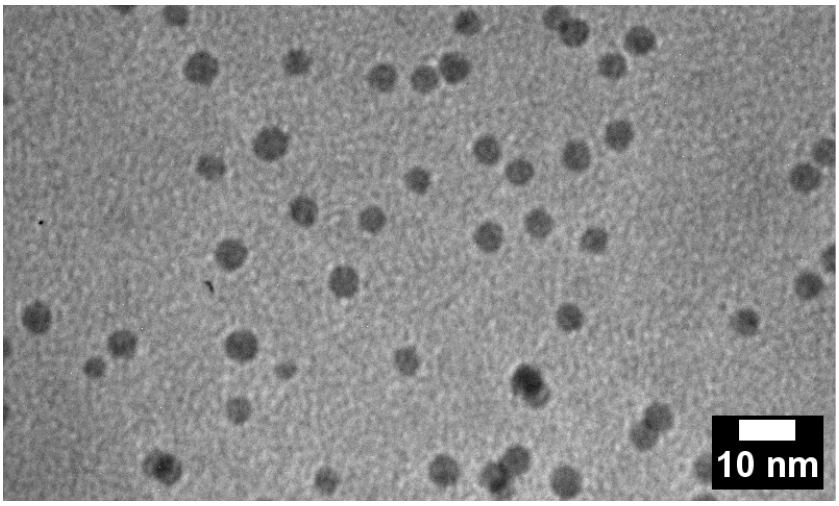

Figure 4.27. TEM image of gold nanoparticles formed using $HAuCl_4$, TPSA RevIL, and hexane after thermal reversal of RevIL; from same experiment as Figure 4.25.

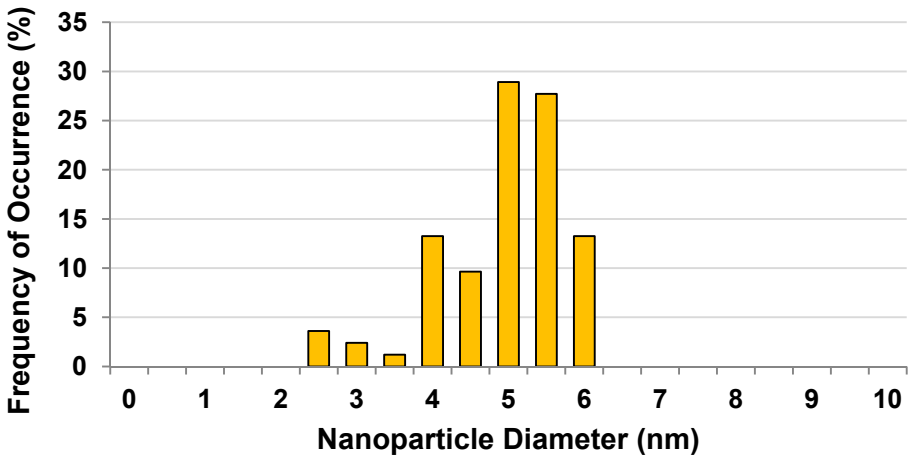

Figure 4.28. Size distribution of nanoparticles from sample shown in Figure 4.27.

ImageJ analysis of this sample showed the average nanoparticle diameter to be 5.2 ±0.8 nm; moreover, the formerly Gaussian distribution seen in Figure 4.26 was now skewed to the lower diameters. It seems likely that our reversal procedure is ultimately affecting the size of the nanoparticles present in solution. The presence of smaller nanoparticles in the sample used for TEM imaging indicates that the larger nanoparticles are dropping out of solution over time, and possibly aggregating. It could be that some of the reverse micelles, if present, are destabilizing and releasing the larger nanoparticles; the newly-freed silylated amines could then add to other reverse micelles, further stabilizing smaller AuNP still in solution.

A similar reaction mixture was then heated for 24 hours at 65°C, after which time the solution still had not fully lost color, indicating that some nanoparticles still remained in solution. Although the RevIL is expected to fully reverse back to the molecular liquid at this point, the molecular liquid alone could also be acting as some sort of surfactant or capping agent to keep the nanoparticles suspended. As mentioned before, amines have been shown to function as capping agents for AuNP.[25, 63] However, preliminary experiments performed

using the ML precursors rather than the RevILs as a switchable surfactant showed results very different from those observed with the RevILs. Rather than turning a dark red, as with the RevILs, the reaction mixture immediately turned a dark blue. This blue color indicates agglomeration or the presence of very large nanoparticles.[61] A dark blue solid precipitated out of solution, and TEM imaging of the supernate showed virtually no nanoparticles. therefore, it seems unlikely that the molecular liquids alone are able to act as effective surfactants for our purposes.

Similar difficulties with reversal have been encountered when we have attempted to deposit the nanoparticles onto a solid substrate such as silica (SiO_2), titania (TiO_2), or alumina (Al_2O_3). Although the support does take on the red-purple color of the nanoparticle solution, the solution does not fully decolorize even after extensive heating. Elemental analysis of both the unsupported and supported nanoparticles should allow us to determine if any of the molecular liquid is still present following solvent washes and drying. The presence of nanoparticles in the supernate could simply indicate that all available pore space in the solid support has been saturated with nanoparticles at the concentrations used; however, TEM imaging of these solid-supported AuNP has shown that very few AuNP are actually present on the support.

4.5 Conclusions

We have successfully synthesized gold nanoparticles using both 2-component and 1-component RevILs. Using the RevIL [TMBGH][MeOCOO] as the core of reverse micelles, gold nanoparticles with a diameter range of 6-20 nm were synthesized; difficulties with the 2-component RevIL system led us to investigate our 1-component RevILs as switchable surfactants. Preliminary results using methyl orange as a substitute for $HAuCl_4$ indicated that

the ionic form of the silylated amines was required to solubilize the salt. Application of this system to gold nanoparticle synthesis resulted in the formation of relatively monodisperse gold nanoparticles with a diameter range of 3-8 nm. These experiments have been reproducible. Attempts to deposit the nanoparticles on a solid metal oxide support "on command" by making use of the ionic-to-molecular switch did not succeed in removing all of the AuNP from the supernate. To this date, we have not been able to fully characterize the behavior of the RevILs—1-component or 2-component—in a solution of hydrocarbons; namely, if they are forming reverse micelles or solubilizing the gold salt via a co-solvent effect. The 1-component RevILs are able to act as a novel capping agent for gold nanoparticles—it remains to be seen whether they can function as a switchable surfactant.

4.6 References

1. Haruta, M. Catalysis of gold nanoparticles deposited on metal oxides. *Cattech* **2002,** *6* (3), 102-115.

2. Schön, G.; Simon, U. A fascinating new field in colloid science: small ligand-stabilized metal clusters and possible application in microelectronics. Part I: State of the art. *Colloid. Polym. Sci.* **1995,** *273* (2), 101-117.

3. (a) El-Sayed, I. H.; Huang, X. H.; El-Sayed, M. A. Selective laser photo-thermal therapy of epithelial carcinoma using anti-EGFR antibody conjugated gold nanoparticles. *Cancer Letters* **2006,** *239* (1), 129-135; (b) Gibson, J. D.; Khanal, B. P.; Zubarev, E. R. Paclitaxel-functionalized gold nanoparticles. *J. Am. Chem. Soc.* **2007,** *129*, 11653-11661.

4. Daniel, M. C.; Astruc, D. Gold nanoparticles: Assembly, supramolecular chemistry, quantum-size-related properties, and applications toward biology, catalysis, and nanotechnology. *Chem. Rev.* **2004,** *104* (1), 293-346.

5. Campelo, J. M.; Luna, D.; Luque, R.; Marinas, J. M.; Romero, A. A. Sustainable preparation of supported metal nanoparticles and their applications in catalysis. *Chemsuschem* **2009,** *2* (1), 18-45.

6. Badia, A.; Cuccia, L.; Demers, L.; Morin, F.; Lennox, R. B. Structure and dynamics in alkanethiolate monolayers self-assembled on gold nanoparticles: A DSC, FT-IR, and deuterium NMR Study. *J. Am. Chem. Soc.* **1997,** *119* (11), 2682-2692.

7. Brust, M.; Walker, M.; Bethell, D.; Schiffrin, D. J.; Whyman, R. Synthesis of thiol-derivatized gold nanoparticles in a two-phase liquid-liquid system. *J. Chem. Soc., Chem. Commun.* **1994,** (7), 801-802.

8. Turkevich, J.; Stevenson, P. C.; Hillier, J. A study of the nucleation and growth processes in the synthesis of colloidal gold. *Discuss. Faraday Soc.* **1951,** (11), 55-75.

9. Murphy, C. J. Sustainability as an emerging design criterion in nanoparticle synthesis and applications. *J. Mater. Chem.* **2008,** *18* (19), 2173-2176.

10. Dahl, J. A.; Maddux, B. L. S.; Hutchison, J. E. Toward greener nanosynthesis. *Chem. Rev.* **2007,** *107* (6), 2228-2269.

11. Eckelman, M. J.; Zimmerman, J. B.; Anastas, P. T. Toward green nano: E-factor analysis of several nanomaterial syntheses. *J. Ind. Ecol.* **2008,** *12* (3), 316-328.

12. Uskoković, V.; Drofenik, M. Synthesis of materials within reverse micelles. *Surf. Rev. Lett.* **2005,** *12* (2), 239-277.

13. Pileni, M. P. Reverse micelles as microreactors. *J. Phys. Chem.* **1993,** *97* (27), 6961-6973.

14. Eastoe, J.; Hollamby, M. J.; Hudson, L. Recent advances in nanoparticle synthesis with reversed micelles. *Adv. Colloid Interface Sci.* **2006,** *128*, 5-15.

15. Liu, J. H.; Cheng, S. Q.; Zhang, J. L.; Feng, X. Y.; Fu, X. G.; Han, B. X. Reverse micelles in carbon dioxide with ionic-liquid domains. *Angew. Chem. Int. Ed.* **2007,** *46* (18), 3313-3315.

16. Jessop, P. G.; Heldebrant, D. J.; Li, X. W.; Eckert, C. A.; Liotta, C. L. Green chemistry - Reversible nonpolar-to-polar solvent. *Nature* **2005,** *436* (7054), 1102-1102.

17. Phan, L.; Chiu, D.; Heldebrant, D. J.; Huttenhower, H.; John, E.; Li, X. W.; Pollet, P.; Wang, R. Y.; Eckert, C. A.; Liotta, C. L.; Jessop, P. G. Switchable solvents consisting of amidine/alcohol or guanidine/alcohol mixtures. *Ind. Eng. Chem. Res.* **2008,** *47* (3), 539-545.

18. Hart, R.; Pollet, P.; Hahne, D. J.; John, E.; Llopis-Mestre, V.; Blasucci, V.; Huttenhower, H.; Leitner, W.; Eckert, C. A.; Liotta, C. L. Benign coupling of reactions and separations with reversible ionic liquids. *Tetrahedron* **2010,** *66* (5), 1082-1090.

19. (a) Burns, M. R.; Jenkins, S. A.; Vermeulen, N. M.; Balakrishna, R.; Nguyen, T. B.; Kimbrell, M. R.; David, S. A. Structural correlation between lipophilicity and lipopolysaccharidesequestering activity in spermine-sulfonamide analogs. *Bioorg. Med. Chem. Lett.* **2006,** *16* (24), 6209-6212; (b) Deck, P.; Pendzialek, D.; Biel, M.; Wagner, M.; Popkirova, B.; Ludolph, B.; Kragol, G.; Kuhlmann, J.; Giannis, A.; Waldmann, H. Development and biological evaluation of acyl protein thioesterase 1 (APT1) inhibitors. *Angew. Chem. Int. Ed.* **2005,** *44* (31), 4975-4980.

20. Schuchardt, U.; Vargas, R. M.; Gelbard, G. Alkylguanidines as catalysts for the transesterification of rapeseed oil. *J. Mol. Catal. A: Chem.* **1995,** *99* (2), 65-70.

21. Huttenhower, H. A. Development of new chemistry for a dual use hydrazine thruster, switchable room temperature ionic liquids, a study of silane grafting to polyethylene and its model compounds, synthesis of the novel hydrazine replacement fuel molecules 1,1-dimethyl-2-[2-azidoethyl]hydrazine and 1,1-dimethyl-2-[2-azidoethyl]hydrazone. PhD thesis, Georgia Institute of Technology, Atlanta, GA, 2010.

22. Karukstis, K. K.; D'Angel, N. D.; Loftus, C. T. Using the optical probe methyl orange to determine the role of surfactant and alcohol chain length in the association of 1-alkanols with alkyltrimethylammonium bromide micelles. *J. Phys. Chem. B* **1997,** *101* (11), 1968-1973.

23. Sheldon, R. A. The E factor: fifteen years on. *Green Chem.* **2007,** *9* (12), 1273-1283.

24. Laia, C. A. T.; Lopez-Cornejo, P.; Costa, S. M. B.; d'Oliveira, J.; Martinho, J. M. G. Dynamic light scattering study of AOT microemulsions with nonaqueous polar additives in an oil continuous phase. *Langmuir* **1998,** *14* (13), 3531-3537.

25. Leff, D. V.; Brandt, L.; Heath, J. R. Synthesis and characterization of hydrophobic, organically-soluble gold nanocrystals functionalized with primary amines. *Langmuir* **1996,** *12* (20), 4723-4730.

26. (a) Subramaniam, C.; Tom, R. T.; Pradeep, T. On the formation of protected gold nanoparticles from $AuCl_4^-$ by the reduction using aromatic amines. *J. Nanopart. Res.* **2005,** *7* (2-3), 209-217; (b) Selvakannan, P.; Mandal, S.; Phadtare, S.; Gole, A.; Pasricha, R.; Adyanthaya, S. D.; Sastry, M. Water-dispersible tryptophan-protected gold nanoparticles prepared by the spontaneous reduction of aqueous chloroaurate ions by the amino acid. *J. Colloid Interface Sci.* **2004,** *269* (1), 97-102.

27. (a) Newman, J. D. S.; Blanchard, G. J. Formation of gold nanoparticles using amine reducing agents. *Langmuir* **2006,** *22* (13), 5882-5887; (b) Aslam, M.; Fu, L.; Su, M.; Vijayamohanan, K.; Dravid, V. P. Novel one-step synthesis of amine-stabilized aqueous colloidal gold nanoparticles. *J. Mater. Chem.* **2004,** *14* (12), 1795-1797.

28. Brown, L. O.; Hutchison, J. E. Controlled growth of gold nanoparticles during ligand exchange. *J. Am. Chem. Soc.* **1999,** *121* (4), 882-883.

29. Kumar, A.; Mandal, S.; Selvakannan, P. R.; Pasricha, R.; Mandale, A. B.; Sastry, M. Investigation into the interaction between surface-bound alkylamines and gold nanoparticles. *Langmuir* **2003,** *19* (15), 6277-6282.

30. Fink, J.; Kiely, C. J.; Bethell, D.; Schiffrin, D. J. Self-organization of nanosized gold particles. *Chem. Mater.* **1998,** *10* (3), 922-926.

31. Porta, F.; Krpetic, Z.; Prati, L.; Gaiassi, A.; Scari, G. Gold-ligand interaction studies of water-soluble aminoalcohol capped gold nanoparticles by NMR. *Langmuir* **2008,** *24* (14), 7061-7064.

32. (a) Redel, E.; Walter, M.; Thomann, R.; Hussein, L.; Kruger, M.; Janiak, C. Stop-and-go, stepwise and "ligand-free" nucleation, nanocrystal growth and formation of Au-NPs in ionic liquids (ILs). *Chem. Commun.* **2010,** *46* (7), 1159-1161; (b) Fonseca, G. S.; Machado, G.; Teixeira, S. R.; Fecher, G. H.; Morais, J.; Alves, M. C. M.; Dupont, J. Synthesis and characterization of catalytic iridium nanoparticles in imidazolium ionic liquids. *J. Colloid Interface Sci.* **2006,** *301* (1), 193-204.

33. Abecassis, B.; Testard, F.; Arleth, L.; Hansen, S.; Grillo, I.; Zemb, T. Phase behavior, topology, and growth of neutral catanionic reverse micelles. *Langmuir* **2006,** *22* (19), 8017-8028.

34. (a) Dubois, M.; Deme, B.; Gulik-Krzywicki, T.; Dedieu, J. C.; Vautrin, C.; Desert, S.; Perez, E.; Zemb, T. Self-assembly of regular hollow icosahedra in salt-free catanionic solutions. *Nature* **2001,** *411* (6838), 672-675; (b) Zemb, T.; Dubois, M.; Deme, B.; Gulik-Krzywicki, T. Self-assembly of flat nanodiscs in salt-free catanionic surfactant solutions. *Science* **1999,** *283* (5403), 816-819.

35. (a) Adamson, A. W. *Physical Chemistry of Surfaces*. 5th ed.; Wiley: New York, 1990; (b) Domínguez, A.; Fernández, A.; González, N.; Iglesias, E.; Montenegro, L.

Determination of critical micelle concentration of some surfactants by three techniques. *J. Chem. Educ.* **1997,** *74* (10), 1227-1231.

36. Kertes, A. S. Aggregation of surfactants in hydrocarbons. Incompatibility of the critical micelle concentration concept with experimental data. In *Micellization, solubilization, and microemulsions*, Mittal, K. L., Ed. Plenum Press: New York, 1977; Vol. 1, pp 445-454.

37. (a) Schott, H. Solubilization of a water-insoluble dye. II. *J. Phys. Chem.* **1967,** *71* (11), 3611-&; (b) Schott, H. Solubilization of a water-insoluble dye as a method for determining micellar molecular weights. *J. Phys. Chem.* **1966,** *70* (9), 2966-&.

38. Thiessen, D. B.; Man, K. F. Surface tension measurement. In *The measurement, instrumentation, and sensors handbook*, Webster, J. G., Ed. CRC Press: Boca Raton, FL, 1999.

39. Sartori, G.; Savage, D. W. Sterically hindered amines for CO_2 removal from gases. *Ind. Eng. Chem. Fundam.* **1983,** *22* (2), 239-249.

40. Perez-Gregorio, V.; Montano, D.; Giner, B.; Lafuente, C.; Royo, F. M. Surface and bulk behaviour of some (*n*-hexane plus chloroalkane) mixtures. *J. Chem. Thermodyn.* **2009,** *41* (4), 553-559.

41. Myers, D. *Surfactant Science and Technology*. 3rd ed.; John Wiley & Sons, Inc.: Hoboken, New Jersey, 2006.

42. Ruckenstein, E.; Nagarajan, R. Aggregation of amphiphiles in non-aqueous media. *J. Phys. Chem.* **1980,** *84* (11), 1349-1358.

43. Kaufman, S.; Singleterry, C. R. The critical range for micelle formation by an oil-dispersible soap in a hydrocarbon solvent. *Journal of Colloid Science* **1952,** *7* (5), 453-464.

44. Ravey, J. C.; Buzier, M.; Picot, C. Micellar structures of nonionic surfactants in apolar media. *J. Colloid Interface Sci.* **1984,** *97* (1), 9-25.

45. Ganguli, A. K.; Ganguly, A.; Vaidya, S. Microemulsion-based synthesis of nanocrystalline materials. *Chem. Soc. Rev.* **2010,** *39* (2), 474-485.

46. Silber, J. J.; Biasutti, A.; Abuin, E.; Lissi, E. Interactions of small molecules with reverse micelles. *Adv. Colloid Interface Sci.* **1999,** *82* (1-3), 189-252.

47. Tanaka, R.; Shiromizu, T. Stepwise process forming AOT W/O microemulsion investigate by dielectric measurements. *Langmuir* **2001,** *17* (26), 7995-8000.

48. (a) Yu, Z. J.; Zhou, N. F.; Neuman, R. D. The role of water in the formation of reversed micelles: an antimicellization agent. *Langmuir* **1992,** *8* (8), 1885-1888; (b) Patist, A.; Bhagwat, S. S.; Penfield, K. W.; Aikens, P.; Shah, D. O. On the

measurement of critical micelle concentrations of pure and technical-grade nonionic surfactants. *J. Surfactants Deterg.* **2000,** *3* (1), 53-58.

49. Langevin, D. Structure of reverse micelles. In *Structure and Reactivity in Reverse Micelles*, Pileni, M. P., Ed. Elsevier: New York, 1989; pp 13-43.

50. Riter, R. E.; Kimmel, J. R.; Undiks, E. P.; Levinger, N. E. Novel reverse micelles partitioning nonaqueous polar solvents in a hydrocarbon continuous phase. *J. Phys. Chem. B* **1997,** *101* (41), 8292-8297.

51. Tanaka, R.; Yokoyama, T.; Sameshima, K.; Kawase, T. Growth of AOT reversed micelles and the solvent effect investigated by dielectric and light-scattering measurements. *Bull. Chem. Soc. Jpn.* **2005,** *78* (4), 599-603.

52. Zulauf, M.; Eicke, H. F. Inverted micelles and microemulsion in the ternary system H_2O/Aerosol-OT/isooctane as studied by photon correlation spectroscopy. *J. Phys. Chem.* **1979,** *83* (4), 480-486.

53. (a) Goffredi, M.; Liveri, V. T.; Vassallo, G. Refractive index of water-AOT-*n*-heptane microemulsions. *J. Solution Chem.* **1993,** *22* (10), 941-949; (b) Gomez-Diaz, D.; Navaza, J. M. Density, speed of sound, surface tension, and refractive index of AOT+2,2,4-trimethylpentane plus water mixtures from (5 to 60) degrees C. *J. Chem. Eng. Data* **2006,** *51* (5), 1702-1704.

54. Gomez-Diaz, D.; Mejuto, J. C.; Navaza, J. M. Density, viscosity, and speed of sound of solutions of AOT reverse micelles in 2,2,4-trimethylpentane. *J. Chem. Eng. Data* **2006,** *51* (2), 409-411.

55. Fletcher, P. D. I.; Howe, A. M.; Robinson, B. H. The kinetics of solubilisate exchange between water droplets of a water-in-oil microemulsion. *J. Chem. Soc., Faraday Trans. 1* **1987,** *83*, 985-1006.

56. Voortmans, G.; de Schryver, F. C. Polymerization in and of reverse micelles. In *Structure and Reactivity in Reverse Micelles*, Pileni, M. P., Ed. Elsevier: New York, 1989; pp 221-229.

57. Liu, J.; Ruffini, N.; Pollot, P.; Llopis-Mestre, V.; Dilek, C.; Eckert, C. A.; Liotta, C. L.; Roberts, C. B. More benign synthesis of palladium nanoparticles in dimethyl sulfoxide and their extraction into an organic phase. *Ind. Eng. Chem. Res.* **2010,** *49* (17), 8174-8179.

58. Pastoriza-Santos, I.; Liz-Marzan, L. M. *N*,*N*-Dimethylformamide as a Reaction Medium for Metal Nanoparticle Synthesis. *Adv. Funct. Mater.* **2009,** *19* (5), 679-688.

59. (a) Amendola, V.; Meneghetti, M. Size Evaluation of Gold Nanoparticles by UV-vis Spectroscopy. *J. Phys. Chem. C* **2009,** *113* (11), 4277-4285; (b) Jain, P. K.; Lee, K. S.; El-Sayed, I. H.; El-Sayed, M. A. Calculated absorption and scattering properties of gold nanoparticles of different size, shape, and composition: Applications in biological imaging and biomedicine. *J. Phys. Chem. B* **2006,** *110* (14), 7238-7248; (c)

Liu, X. O.; Atwater, M.; Wang, J. H.; Huo, Q. Extinction coefficient of gold nanoparticles with different sizes and different capping ligands. *Colloids Surf., B* **2007,** *58* (1), 3-7.

60. Eustis, S.; El-Sayed, M. A. Why gold nanoparticles are more precious than pretty gold: Noble metal surface plasmon resonance and its enhancement of the radiative and nonradiative properties of nanocrystals of different shapes. *Chem. Soc. Rev.* **2006,** *35* (3), 209-217.

61. Wilcoxon, J. P.; Williamson, R. L.; Baughman, R. Optical properties of gold colloids formed in inverse micelles. *J. Chem. Phys.* **1993,** *98* (12), 9933-9950.

62. Haruta, A. When gold is not noble: catalysis by nanoparticles. *Chem. Rec.* **2003,** *3* (2), 75-87.

63. Zhu, H. G.; Pan, Z. W.; Hagaman, E. W.; Liang, C. D.; Overbury, S. H.; Dai, S. Facile one-pot synthesis of gold nanoparticles stabilized with bifunctional amino/siloxy ligands. *J. Colloid Interface Sci.* **2005,** *287* (1), 360-365.

CHAPTER 5. CONCLUSIONS AND RECOMMENDATIONS

5.1 Chapter 2: A Fundamental Study of Silane Grafting onto Polyethylene Analogs

5.1.1 Conclusions: Chapter 2

To simulate the grafting of vinyltrialkoxysilanes onto polymers in the SIOPLAS process, we have used the model compounds dodecane and heptane in reaction with vinytrimethoxysilane (VTMS) and the radical initiator di-*tert*-butylperoxide (DTBP). In the course of our experiments, we found that a three-day reaction time was required for the capping reaction that replaces the water-sensitive methoxy groups with phenyl groups for analysis; this was not fully understood in the literature prior to our work. This discovery enabled us to more accurately determine how many grafts were present per hydrocarbon backbone. Analysis using matrix-assisted laser desorption ionization mass spectrometry (MALDI MS), although semi-quantitative, provided information regarding the maximum number of grafts that occurred per hydrocarbon backbone. Up to 6 grafts were found per heptane molecule, and up to 8 grafts were found per dodecane molecule. These values are much higher than would be expected if radical propagation occurred only via a 1,5-intramolecular hydrogen shift, which would yield a maximum of 3 grafts per heptane and 5 grafts per dodecane molecule (assuming the terminal methyl groups are not susceptible to free radical hydrogen abstraction, due to the high instability of the resulting 1° radical). The grafted and capped product mixture, heptane-*g*-VTPS, was separated via semi-preparative HPLC based on number of grafts, and the di- and penta-grafted fractions were collected, isolated, and examined using the 2D NMR techniques edited HSQC and HSQC-TOCSY. Here, further evidence that the 1,5-hydrogen shift was not the only form of intramolecular radical propagation occurring was found—the presence of di-grafted products with grafts on

carbons 2 and 3 (resulting from a 1,4-intramolecular hydrogen shift) as well as carbons 2 and 4 (resulting from a 1,5-shift) of the heptane backbone was ascertained. Finally, theoretical calculations performed by Dr. Liotta showed that the transition state energies of the 1,4- and 1,5-intramolecular hydrogen shifts were within 30 $kJ \cdot mol^{-1}$ of one another, implying that these two modes of intramolecular hydrogen shifts were likely to occur under grafting reaction conditions (heating at 200°C for 7 hours).

Our results show that multi-grafting occurs quite readily, despite the low concentration of VTMS in the model compound. In an actual polyethylene (PE) melt, this would most likely result in the uneven distribution of grafts along the polymer backbone, and cause ungrafted sections to perform differently from those that are grafted.[1] It was proposed that the prevalence of multi-grafted product was due to the presence of high local concentrations of VTMS in the hydrocarbon. The presence of these "clusters" of VTMS, however, was not supported via dynamic light scattering (DLS). We attempted to dilute the "clusters" with non-grafting silanes or increased CO_2 pressure during the grafting reaction, but were not able to verify a change in the grafting distribution to lower grafted fractions within experimental error. The comparable stabilities of the radical intermediates formed indicates that any change to the polymer formulation—e.g. concentration of silane or initiator—is unlikely to affect the grafting distribution.

5.1.2 Recommendations: Chapter 2

Although we have demonstrated conclusively that multi-grafting of the hydrocarbon model compound is favored, we have not yet determined why this phenomenon occurs. DLS measurements of VTMS in dodecane at room temperature over a range of concentrations were inconclusive and the results were not repeatable. No direct evidence of "clusters" of VTMS in hydrocarbon has been demonstrated in the literature; however, other

researchers have noted the uneven graft distribution of silanes along PE backbones.[2] A more sensitive DLS instrument may be able to detect the presence of high local concentrations of the silane in hydrocarbon. However, it must be cautioned that the preliminary DLS measurements performed were carried out at 25 and 40°C, and measurements at 200°C—i.e. at grafting reaction temperature—are well beyond the capabilities of DLS.

An alternative method that could be used is the measurement of vapor-liquid equilibria. Raoult's Law states that "the vapor pressure of a solvent in the presence of a non-volatile solute is proportional to the mole fraction of the solvent."[3] The vapor pressure of an ideal solution should therefore have a direct correlation to the concentration of the solute, and a plot of solution vapor pressure as a function of solute concentration should be a straight line. Any deviations from ideality would indicate that there are unexpected intramolecular interactions occurring,[4] and could provide evidence in our system of the aggregation of VTMS. If clustering of VTMS in the hydrocarbon solvent were occurring, we would expect to see a negative deviation from ideality.

5.2 Chapter 3: Synthesis of Silylated Amines for Post-Combustion CO_2 Capture

5.2.1 Conclusions: Chapter 3

Silylated amines have been shown to function as CO_2 capture agents, reacting with CO_2 at atmospheric pressure to form an ammonium-carbamate ion pair that is liquid at room temperature. This amines are part of a class of compounds is known as reversible ionic liquids (RevILs) A number of novel silylated amines were synthesized and characterized, and their performance as potential CO_2 capture agents was evaluated. These properties included CO_2 capacity, viscosity, temperature of reversal (T_{rev}), and enthalpy of regeneration (H_{regen}).Theoretically, these amines will react with CO_2 in a 2:1 molar ratio; however,

enhanced capacity was achieved via physisorption and the formation of carbamic acid, as demonstrated by my colleagues Amy Rohan and Jackson Switzer. Although the viscosities of the RevILs were found to be well above the industrial limit of 100 cP at room temperature, the viscosity decreased at 40°C. Additionally, viscosity can be controlled by controlling the extent of reaction; when the molecular liquid (ML) is less than 60% converted to the RevIL form, the viscosity is low enough to be industrially viable. Branching adjacent to the amine functional group was also found to decrease the viscosity of the RevILs. Such branching also lowered the T_{rev} and ΔH_{regen} of the RevILs. When compared to an aqueous solution of monoethanolamine (MEA), the current standard for CO_2 removal from flue gas, our RevILs showed marked improvements in not only CO_2 capacity, but also T_{rev} and ΔH_{regen}. Silylated amines with an unsaturation between the silicon and the nitrogen have been synthesized and characterized, but not yet evaluated in terms of performance.

5.2.2 Recommendations: Chapter 3

5.2.2.1 Synthesis of *cis*-TEtSA

I propose synthesizing *cis*-TEtSA as a complement to the *trans* isomer that has already been synthesized. The properties of *trans*-TEtSA, such as CO_2 capacity, viscosity, density, T_{rev}, T_{evap}, and ΔH_{regen}, are currently being determined. Prior to synthesizing the *trans*-isomer, I hypothesized that a RevIL comprising a mixture of the *cis* and *trans* isomers would have a lower viscosity than the RevIL formed from the saturated analog. It was a pleasant surprise to discover that the *trans*-isomer alone seems to have a lower viscosity at room temperature than TEtSA. However, further exploration of this topic would most likely find the *cis*-isomer to be an interesting target molecule as well.

Using an alkyne as the hydrosilylation substrate does pose some challenges. Three isomers of the product are possible, as shown in Figure 5.1: a β-*trans* isomer, in which the

silane and the alkyne substituent are *trans* to one another; a β-*cis* isomer, in which the silane and alkyne substituent are *cis* to one another; and an α Markownikoff product containing a vinyl group.

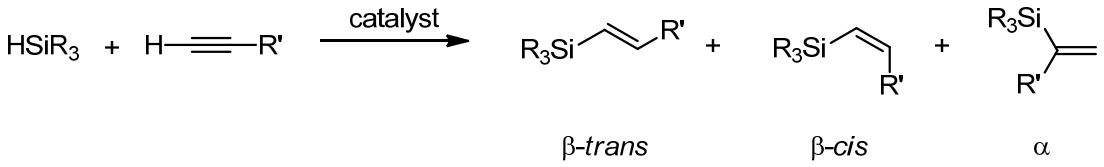

Figure 5.1. Possible stereoisomers resulting from hydrosilylation of terminal alkyne.

The *trans* product is formed via a *syn* addition, where the silicon and the hydrogen add to the same face of the triple bond; the *cis* product, in contrast, is formed via an *anti* addition where the silicon and hydrogen add to opposite faces of the triple bond.[5] Numerous stereoselective synthetic routes are available to the *trans* product, which is thermodynamically favored. The *cis* product, however, is more difficult to access via hydrosilylation. In the hydrosilylation of alkynes utilized previously in the synthesis of (*trans*)-3-(triethylsilyl)prop-2-en-1-amine, the *trans* product is thought to be favored due to the presence of the bulky azaphosphatrane ligand; this forces the intermediate resulting from migratory insertion (see Figure 3.24 in Chapter 3) to adopt the more sterically favorable *trans* position.

An alternative approach is therefore required to access the *cis* stereoisomer; the first part of the proposed synthesis is shown in Figure 5.2.

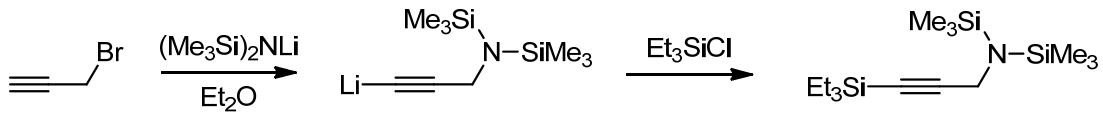

Figure 5.2. Proposed synthesis of protected silylated propargylamine.

A synthesis of a similar *cis* silylated amine has been performed by Corriu *et al*.[6] I propose a modification of their method, wherein propargyl bromide and lithium bis(trimethylsilyl)amide will serve as starting materials. Reaction of the amide and the alkyne in a 2:1 molar ratio in diethylether should yield 1-lithio-3-bis(trimethylsilyl)aminoprop-1-yne. This lithium acetylide will not be isolated, but reacted with chlorotriethylsilane *in situ* to yield the triethylsilyl propargylic amine. To the best of my knowledge, this synthesis has not been performed before.

The *cis* product is then attainable via a Grignard reaction as per Corriu *et al*; the synthetic route is detailed in Figure 5.3.[6]

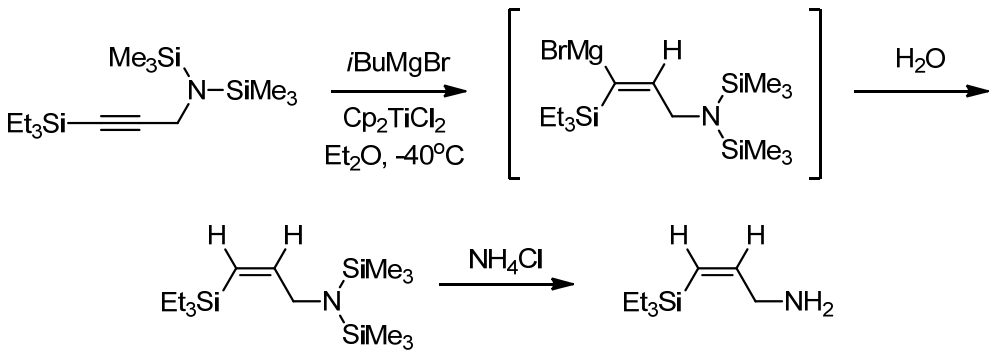

Figure 5.3. Proposed synthesis of *cis*-3-(triethylsilyl)-2-propen-1-amine, following Grignard protocol.

A solution of the silylpropargylamine in THF should react with bis(cyclopentadienyl)titanium (IV) dichloride and isobutyl magnesium bromide to yield a

Grignard reagent, which, when quenched with water, will yield the protected alkene. Deprotection with an aqueous solution of ammonium chloride should yield the desired *cis* product.

However, I believe a simpler approach may also work. Hydrogenation of the triethylsilyl propargylic amine over a Lindlar catalyst in a Parr autoclave should yield the *cis* product exclusively. Deprotection of the amino group can then be achieved with methanol, following a similar procedure laid out by Schilling.[7] This reaction scheme is depicted in Figure 5.4. Alternatively, the two steps could be reversed: deprotection followed by selective hydrogenation.

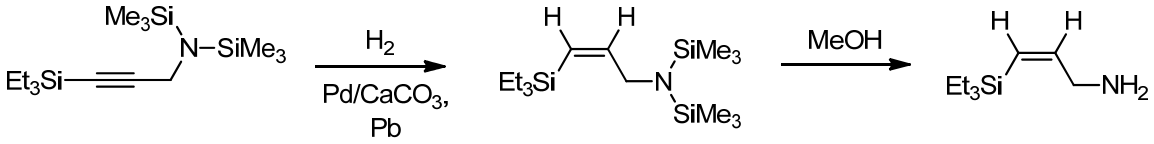

Figure 5.4. Proposed stereoselective reduction and deprotection to form *cis*-3-(triethylsilyl)-2-propen-1-amine.

The *cis* isomer can then be fully characterized as we have done for the other silylated amines we have synthesized, including CO_2 capacity, viscosity, density, T_{rev}, T_{evap}, and ΔH_{regen}. The capacities, viscosities, and densities of mixtures of the *cis* and *trans* isomers could also be characterized in the same manner. Although it seems unlikely that the *cis* isomer would be a practical CO_2 capture agent, given its multi-step synthesis, I feel that its synthesis could give us further insights into the behavior of silylated amines as RevILs—in particular, their viscosity.

5.2.2.2 Synthesis of Further Branched Amines

The effect of two methyl groups at the α position of TEtSA is quite surprising—the carbamate of the RevIL is apparently so destabilized that the ML does not fully convert to the RevIL form at room temperature. It would be interesting to see if other residual groups at the α position have a similar effect. Few of these highly hindered primary amines are commercially available. They can be synthesized with high yields following a protocol outlined by Kopka *et al.*,[8] shown in Figure 5.5.

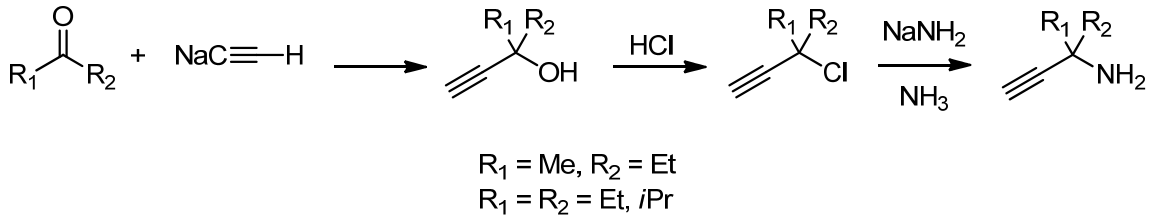

Figure 5.5. Synthesis of highly hindered propargylamines from ketones.

Reaction of a ketone with an acetylide anion yields a propargyl alcohol, which can be converted to a propargylic chloride via reaction with hydrochloric acid. When treated with sodamide in liquid ammonia, the product propargylic amine can then be used in a stereospecific hydrosilylation and hydrogenation as shown in Figure 3.24 in Chapter 3. As an initial target, I would recommend the branched amine synthesized from methyl ethyl ketone. An ethyl group is slightly more flexible than a methyl group, and, as such, may result in a happy medium between carbamate destabilization and reversal temperature when located at the α position of a silylated amine. The three compounds whose synthesis is outlined in Figure 5.5 are only those whose synthesis has previously been documented in the literature; other branched propargylic amines are, of course, possible. Additionally, combining

branching at the amine with various residual groups on the silicon provides a number of other possibilities for low molecular weight silylated amines that could exhibit the desired CO_2 capture properties.

5.3 Chapter 4: Reversible Ionic Liquids as Switchable Surfactants for the Synthesis of Gold Nanoparticles

5.3.1 Conclusions: Chapter 4

Gold nanoparticles (AuNP) were successfully synthesized using both 2-component and 1-component RevILs. A novel surfactant, *N*-propyl octylsulfonamide, was synthesized and used in conjunction with the RevIL [TMBGH][OCOOMe], the gold salt $HAuCl_4$, and the continuous phase dodecane to form nanoparticles with a diameter range of 6 to 20 nm. It was hypothesized that the hydrogen bonding between the protonated guanidinium and the polar head of the sulfonamide surfactant stabilized the structure of the reverse micelle. Heating destabilized the micellar structure by reversing the RevIL back to the molecular form, and the nanoparticles were released. We were able to recycle the system once, but did not evaluate how the recycle affected the particle size distribution. However, several challenges led us to change our system to use 1-component RevILs as switchable surfactants, rather than 2-component RevILs as switchable solvents.

Overall, the 1-component RevIL system was much simpler to use than the 2-component RevIL system, as it eliminated the need for an additional surfactant. It also simplified the preparation of the RevIL itself—to synthesize the 2-component RevIL [TMBGH][OCOOMe], equimolar amounts of tetramethylbutylguanidine and methanol must be reacted with CO_2. We were able to use TPSA RevIL and THSA RevIL to reproducibly synthesize AuNP. TPSA RevIL, in particular, yielded spherical nanoparticles with an average diameter of 6 nm. However, we were not able to conclusively demonstrate that reverse

micellar structures were responsible for the production of our relatively monodisperse, spherical AuNP.

Several methods were attempted to determine the CMC of TPSA RevIL in hexane—dye solubilization, surface tension determination via capillary rise, and DLS. However, none of these methods were successful. Our RevILs were too reactive to be used in conjunction with dyes; the capillary rise measurements showed no clear trend in surface tension as a function of concentration; and DLS was not able to determine the presence of any reverse micelles at the concentrations of TPSA RevIL in hexane that we were using to synthesize nanoparticles. Attempts to reverse the RevILs, destabilize the reverse micelles, and deposit the AuNP on solid supports were not wholly successful. I will address these concerns in the Recommendations section below.

5.3.2 Recommendations: Chapter 4

5.3.2.1 Characterization of Reverse Micelles: 1-Component RevILs

Evidence in the literature strongly supports the theory that a disperse phase is needed to control the size of reverse micelles with a low polydispersity.[9] To this end, I suggest that we consider disperse phases that satisfy the following conditions: 1.) are highly immiscible with the hydrocarbon continuous phase; 2.) will dissolve $HAuCl_4$; 3.) will not act as ligands for AuNP; and 4.) will not react with the RevIL. To date, no such disperse phases have been identified—the most promising candidate is DMF, but the amide moiety could react with the RevIL. Should DMF satisfy all four conditions listed above, the DLS experiments described previously should be repeated, using a RevIL-DMF-hydrocarbon system. As a hydrocarbon continuous phase, I would suggest using isooctane, as TPSA RevIL was observed to have a high solubility in this solvent. We are also currently attempting to locate and use a small angle x-ray scattering (SAXS) instrument that could

allow us to characterize smaller reverse micelles that do not contain a disperse phase in the core.

5.3.2.2 Reversal Temperature of 1-component RevILs in Solution

Despite heating the solutions of gold nanoparticles with RevILs at temperatures well above the T_{rev} of the RevILs used, some nanoparticles remained in solution. There are two explanations as to why this might occur. The first possibility is that the MLs are continuing to act as efficient capping agents and are able to keep the nanoparticles suspended in solution despite no longer possessing an ionic character. However, when an attempt was made to synthesize AuNP with TPSA ML present in place of TPSA RevIL, aggregation occurred.

The other possibility is that the T_{rev} of the RevILs is altered when the RevILs are in solution. One of the benefits presented by our silylated amines when used in CO_2 capture is that they can be used neat, and we have therefore never investigated the effect of solvent on the reversal temperature of our silylated amines. The separation of the RevIL components by solvent molecules could cause a change in reversal temperature. A qualitative method for investigating this possibility could be FTIR, which is used extensively by our group to determine physical absorption capacities and other characteristics of our CO_2-capturing amines. A solution of RevIL would be introduced to the sample cell, which would be heated at a steady temperature ramp. Disappearance of the distinctive carbonyl stretching vibration of the carbamate would indicate that the RevIL had reversed back to molecular form. Solvents with boiling points higher than the neat reversal temperatures of our RevILs would have to be used in order to prevent solvent loss during heating. We would like to investigate a series of solvents of changing polarity, and, given our use of hydrocarbon continuous

phases in nanoparticle synthesis, a series of hydrocarbons having different boiling points and degrees of branching.

5.3.2.3 Catalytic Activity of Gold Nanoparticles

Ultimately, we will compare the properties and activities of the AuNP with literature results to determine if our synthesis impacts features of the nanoparticles, and if the switchable surfactants can easily be removed. Supported gold nanoparticles have been used as oxidants in many reactions, including the oxidation of glucose to the feedstock chemical gluconic acid[10] and the oxidation of alcohols.[11] The proof of concept reaction that we use will depend on the size of the gold nanoparticles that we are able to synthesize. We can reproducibly synthesize relatively monodisperse nanoparticles with an average diameter of 5 nm—conveniently, a size commonly used in oxidations.[12]

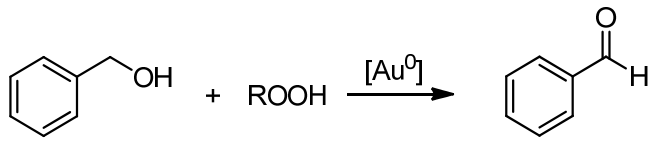

Figure 5.6. Proof-of-concept reaction for gold nanoparticles. Oxidation of benzyl alcohol to benzaldehyde with a peroxide oxidant and a gold nanoparticle catalyst.

A convenient proof-of-concept reaction would be the oxidation of benzyl alcohol to benzaldehyde, as shown in Figure 5.6. Supported gold has been shown to catalyze the oxidation of benzyl alcohol using several different peroxides under a variety of experimental conditions.[13]

Once we have used the preparation of gold nanoparticles to fine-tune our reaction conditions, we will move on to other catalytic metals. We plan to use our optimized reaction conditions from the gold nanoparticle synthesis to synthesize platinum and palladium

nanoparticles; we will then use these nanoparticles in proof of concept reactions to test their activity. For palladium, we plan to look at the catalytic hydrogenation of 4-methoxyacetophenone, as seen in Figure 5.7; for platinum, we plan to use the catalytic hydrogenation of nitrobenzene to aniline.

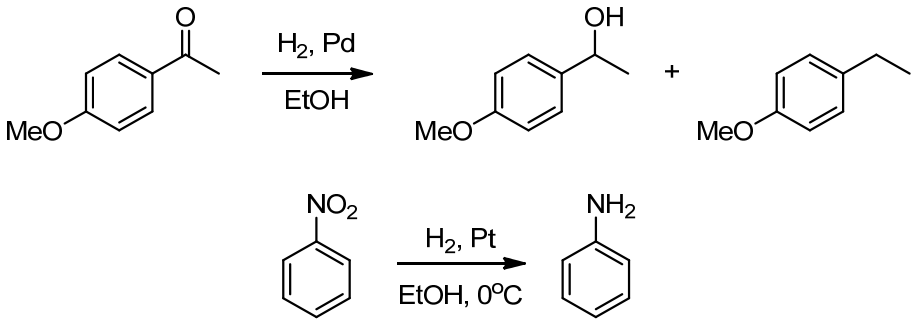

Figure 5.7. Proof-of-concept reactions for Pd (*top*) and Pt (*bottom*) nanoparticles synthesized using our switchable surfactant.

The products of these reactions will be analyzed via NMR and HPLC, and the yields, conversion, and activity of the nanoparticles compared with figures reported in the literature.[14]

5.4 References

1. Sirisinha, K.; Meksawat, D., Preparation and properties of metallocene ethylene copolymer crosslinked by vinyltrimethoxysilane. *Polym. Int.* **2005,** *54* (7), 1014-1020.

2. Rätzsch, M.; Bucka, H.; Ivanchev, S. S.; Mesh, A. M.; Khaikine, Some peculiar features of radiation grafting of monomers of various structures and reactivities onto polyolefins. *J. Appl. Polym. Sci.* **2000,** *77* (4), 711-718.

3. Atkins, P.; Jones, L., *Chemistry: Molecules, Matter, and Change*. 3rd ed.; W. H. Freeman and Company: New York, 1997.

4. Antosik, M.; Sandler, S. I., Vapor-liquid equilibria of hydrocarbons and *tert*-amyl methyl ether. *J. Chem. Eng. Data* **1994,** *39* (3), 584-587.

5. Marciniec, B., *Hydrosilylation: A comprehensive review on recent advances*. Springer: Dordrect, the Netherlands, 2009; Vol. 1.

6. Corriu, R. J. P.; Huynh, V.; Iqbal, J.; Moreau, J. J. E.; Vernhet, C., Silylamines in organic synthesis. Facile synthetic routes to unsaturated protected primary amines. *Tetrahedron* **1992,** *48* (30), 6231-6244.

7. Schilling Jr., C. L. Sterically hindered aminohydrocarbylsilanes and process of preparation. 5030746, 1991.

8. Kopka, I. E.; Fataftah, Z. A.; Rathke, M. W., Preparation of a series of highly hindered secondary amines, including bis(triethylcarbinyl)amine. *J. Org. Chem.* **1980,** *45* (23), 4616-4622.

9. (a) Langevin, D., Structure of reverse micelles. In *Structure and Reactivity in Reverse Micelles*, Pileni, M. P., Ed. Elsevier: New York, 1989; (b) Ravey, J. C.; Buzier, M.; Picot, C., Micellar structures of nonionic surfactants in apolar media. *J. Colloid Interface Sci.* **1984,** *97* (1), 9-25; (c) Tanaka, R.; Shiromizu, T., Stepwise process forming AOT W/O microemulsion investigate by dielectric measurements. *Langmuir* **2001,** *17* (26), 7995-8000; (d) Ruckenstein, E.; Nagarajan, R., Aggregation of amphiphiles in non-aqueous media. *J. Phys. Chem.* **1980,** *84* (11), 1349-1358.

10. Baatz, C.; Thielecke, N.; Prusse, U., Influence of the preparation conditions on the properties of gold catalysts for the oxidation of glucose. *Appl. Catal., B* **2007,** *70* (1-4), 653-660.

11. Abad, A.; Concepcion, P.; Corma, A.; Garcia, H., A collaborative effect between gold and a support induces the selective oxidation of alcohols. *Angew. Chem. Int. Ed.* **2005,** *44* (26), 4066-4069.

12. (a) Haruta, A., When gold is not noble: catalysis by nanoparticles. *Chem. Rec.* **2003,** *3* (2), 75-87; (b) Haruta, M., Catalysis of gold nanoparticles deposited on metal oxides. *Cattech* **2002,** *6* (3), 102-115.

13. (a) Choudhary, V. R.; Dumbre, D. K.; Bhargava, S. K., Oxidation of benzyl alcohol to benzaldehyde by *tert*-butyl hydroperoxide over nanogold supported on TiO_2 and other transition and rare-earth metal oxides. *Ind. Eng. Chem. Res.* **2009,** *48* (21), 9471-9478; (b) Oliveira, R. L.; Kiyohara, P. K.; Rossi, L. M., High performance magnetic separation of gold nanoparticles for catalytic oxidation of alcohols. *Green Chem.* **2010,** *12* (1), 144-149; (c) Liu, Y. M.; Tsunoyama, H.; Akita, T.; Tsukuda, T., Size effect of silica-supported gold clusters in the microwave-assisted oxidation of benzyl alcohol with H_2O_2. *Chem. Lett.* **2010,** *39* (3), 159-161.

14. (a) Ikeda, S.; Ishino, S.; Harada, T.; Okamoto, N.; Sakata, T.; Mori, H.; Kuwabata, S.; Torimoto, T.; Matsumura, M., Ligand-free platinum nanoparticles encapsulated in a hollow porous carbon shell as a highly active heterogeneous hydrogenation catalyst. *Angew. Chem. Int. Ed.* **2006,** *45*, 7063-7066; (b) Ley, S. V.; Stewart-Liddon, A. J. P.; Pears, D.; Perni, R. H.; Treacher, K., Hydrogenation of aromatic ketones, aldehydes, and epoxides with hydrogen and Pd(0)EnCat (TM) 30NP. *Beilstein J. Org. Chem.* **2006,** *2*.

15. Moss-Racusin, C. A.; Dovidio, J. F.; Brescoll, V. L.; Graham, M. J.; Handelsman, J. Science faculty's subtle gender biases favor male students. *Proc. Natl. Acad. Sci. USA* **2012**.

APPENDIX A. SWITCHABLE CROWN ETHERS

A.1 Introduction

Crown ethers are, in their simplest form, macrocyclic polyethers comprising repeats of the ethylenoxy structural unit; the lone pairs of the ring oxygens can interact with cations, effectively binding them inside the ring. As the IUPAC nomenclature of the crown ethers quickly becomes quite complex, they are commonly referred to in the form *X*-crown-*Y*, where *X* is the total number of atoms in the ring, and *Y* is the number of ring oxygens. The size of the crown ether largely dictates its selectivity for a particular cation. For example, 12-crown-4 selectively binds Li^+; the larger 15-crown-5 selectively binds Na^+; finally, 18-crown-6 selectively binds K^+.[1] Although there are numerous variations on the form, including aromatic rings, for the purposes of this discussion, I would like to define two specific subclasses of crown ethers: azacrowns and lariat ethers, examples of which are shown in Figure A.1.

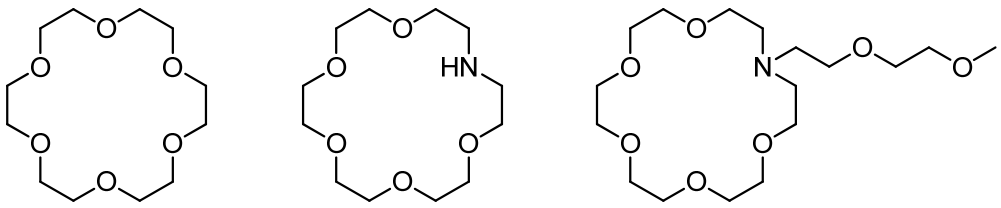

Figure A.1. Examples of crown ethers. *Left*, 18-crown-6, a typical crown ether; *middle*, 1-aza-18-crown-6, an azacrown ether, and *right*, a lariat ether.

Azacrowns are crown ethers in which one or more of the ring oxygens has been replaced with a nitrogen, resulting in a secondary amine. Lariat ethers are crown ethers bearing a sidearm that also contains a donor group; this group can bend back over the crown ring and

interact with the cation guest therein. This sidearm can be attached at a nitrogen or a ring carbon.[2] Crown ethers are most commonly used as phase transfer catalysts (PTCs); as the exterior of the crown ether is hydrophobic, and the interior is hydrophilic, they can "shuttle" ions from an aqueous phase to a polar phase.[3] Their resistance to radiolysis[4] has made them attractive candidates for nuclear waste remediation, which commonly involves the extraction of radioactive cations from an aqueous phase into an organic phase.

The fission products ^{90}Sr and ^{137}Cs command high interest due to their relatively brief half-lives (29 and 30 years, respectively)[5] and their generation of large amounts of thermal heat.[6] Additionally, radionuclides with half-lives shorter than 50 years generate more than 99% of the radioactivity in high level waste.[7] If these "short-lived" radionuclides such as ^{90}Sr and ^{137}Cs could be isolated from nuclear waste, they would require a shorter isolation period before their radiation levels decayed to acceptably safe ranges. As high activity waste (HAW) requires vitrification and geological sequestration—the goal for stability was projected as 1 million years for the now-abandoned Yucca Mountain project—minimizing the amount of long-lived HAW via separation will decrease costs associated with remediation. A discussion of the isolation of ^{137}Cs will follow in the Path Forward section (page 231); for now, I will discuss the isolation of ^{90}Sr.

Argonne National Lab has developed a process for the extraction of ^{90}Sr from acidified nuclear waste streams (a common condition, as spent nuclear fuel rods are generally dissolved in concentrated nitric acid).[8] The strontium extraction process, or SREX, contacts the acidified strontium solution with a solution of a crown ether in a hydrocarbon diluent. The original crown ether solution used was dicyclohexano-18-crown-6 in 1-octanol,[4] although this was later changed to di-*t*-butylcyclohexano-18-crown-6 with tri-*n*-butyl-phosphate (TBP) in kerosene. This change was made in order for the solvent system to be

more compatible with the actual form of nuclear waste encountered after the initial step in waste processing, recovery of plutonium (via the plutonium recovery by extraction process, or PUREX).[6, 8]

Other groups have continued to develop this extraction technology. Traditional ionic liquids (ILs) have been examined as replacements for the organic solvents, such as dodecane and kerosene, commonly used in nuclear waste separations. Visser *et al.* used the crown ether 4,4'-(5')-di-(*t*-butylcyclohexano)-18-crown-6 to extract actinide fission products from an aqueous phase into a series of 1-alkyl-3-methylimidazolium hexafluorophosphate ($[C_n mim][PF_6]$) IL phases.[9] However, the ILs used were found to be susceptible to acid-catalyzed hydrolysis; as nuclear waste treatment commonly uses acidic solutions to strip the cations and recycle the solvent system, this is problematic. Luo *et al.* modified this system by using a series of monoazacrown ethers to transport Group I and II cations from an aqueous phase to an IL phase of 1-alkyl-3-methylimidazolium bis(trifluoromethane)sulfonimide ($[C_n mim][NTf_2]$) ILs, which were not susceptible to acid-catalyzed hydrolysis. The bound cations were stripped from the azacrowns upon protonation with nitric acid; neutralization of the protonated crowns with lithium hydroxide allowed for recycle of the system.[10] Task-specific ILs (TSILs) modified with azacrown ethers have also been used to extract fission products.[11]

A.2 Background

Ionizable groups have been attached to crown ethers in order to promote extraction. Strzelbickl *et al.* controlled the extraction efficiency of a carboxylic acid-bearing benzocrown ether via the pH of the aqueous phase.[12] CO_2 has also been used as a stimulus to induce extraction of cations by ionizable crown ethers. Benzocrown ethers have been modified at

the aromatic ring with lysine residues and used to transfer salts from an aqueous layer to an organic layer; these lysine-modified benzocrowns are then exposed to CO_2 to form crosslinked reversible polymeric materials, which precipitate from the organic solution.[13] However, to the best of my knowledge, CO_2 has not been used to cause the release of cations from a crown ether complex.

Given our work with reversible ionic liquids (RevILs), a portion of which has been described in Chapters 3 and 4, we wondered if the same principles could be applied to crown ethers—specifically, azacrowns and lariat ethers. We hypothesized that, upon reaction with CO_2, as seen in Figure A.2, a nitrogen-containing or –bearing crown ether would form an ammonium-carbamate ion pair.

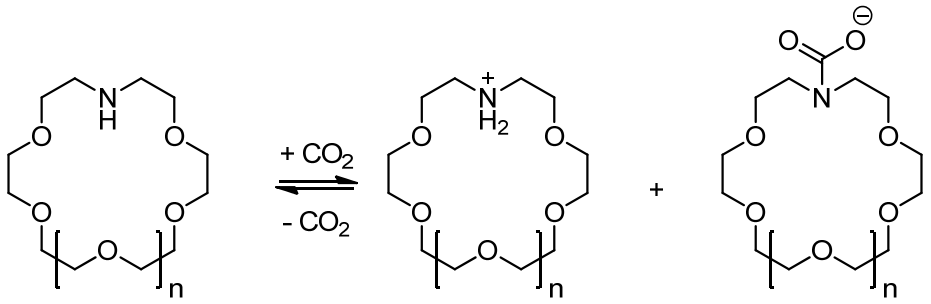

Figure A.2. Theoretical reaction of azacrown with CO_2 to form ammonium-carbamate ion pair.

The positive charge on the ammonium cation could then expel a bound metal cation, as shown in Figure A.3.

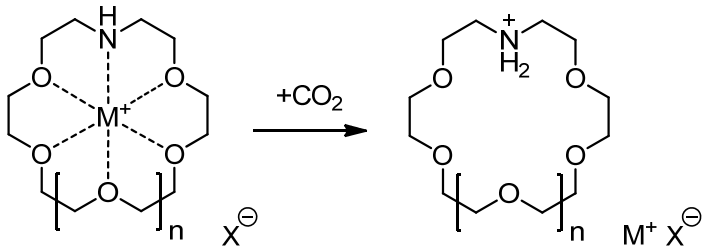

Figure A.3. Expulsion of metal cation due to electrostatic repulsion between metal cation and endocyclic ammonium cation. Carbamate anion not shown.

The same principle would apply if a lariat ether were used as the substrate—upon reaction with CO_2, the positively charged tethered ammonium ion could interact with the crown ether ring, resulting in ejection of a bound metal cation from the ring.

For our proof-of-principle experiments, we identified three azacrowns and one lariat ether with a 1° amine sidearm; these candidates are shown in Figure A.4.

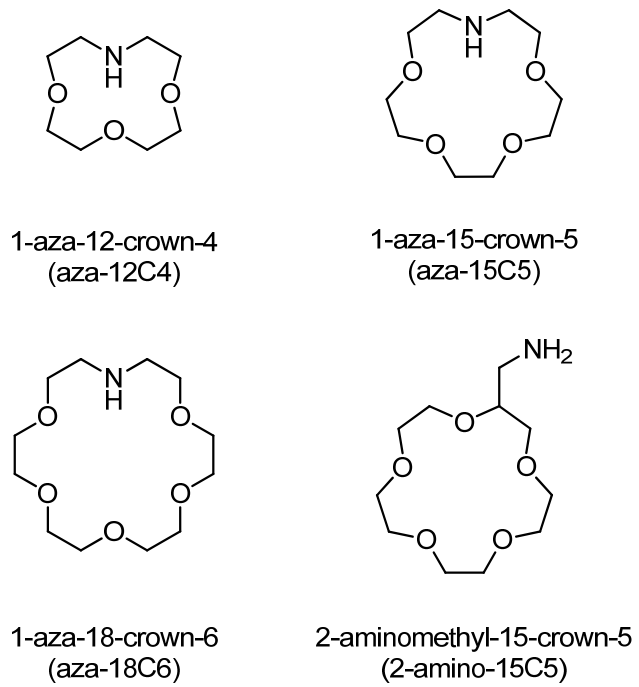

Figure A.4. Candidates for switchable crown ethers.

1-aza-12-crown-4, 1-aza-15-crown-5, and 1-aza-18-crown-6 are all azacrowns containing 2° amines; 2-aminomethyl-15-crown-5 is a lariat ether bearing a 1° amine. To date, we have performed preliminary experiments wherein we react simple, commercially available azacrowns with CO_2 to determine if ionic species do form. The appendix that follows will present the preliminary data from these experiments, and also detail suggestions for future work and possible applications.

A.3 Experimental Section

A.3.1 Materials

All chemicals were purchased from Sigma-Aldrich and used as received unless otherwise noted. Chemicals used were: 1-aza-12-crown-4 (≥97.0%); 1-aza-15-crown-5 (97%); 1-aza-18-crown-6 (≥98.0%); 2-aminomethyl-15-crown-5 (95%); diethanolamine (≥98.0%); bis(2-methoxyethyl)amine (98%); and 2,2'-oxybis(ethylamine). Carbon dioxide used was SFE grade from Airgas (99.999%). Isotopically enriched $^{13}CO_2$ (^{13}C 99%, ^{18}O <1.5%)was purchased from Cambridge Isotope Laboratories, Inc.

A.3.2 Experimental

Reaction with CO_2 was carried out as follows unless otherwise noted. Approximately 0.15 g of the crown ether under investigation was dissolved in 1.0 mL anhydrous $CDCl_3$ and transferred to an NMR tube fitted with a rubber septum. Dry CO_2 was sparged through the solution for an hour at 25°C and 1 atm. The resulting solution was then analyzed via ^1H and ^{13}C NMR. For some secondary amines, isotopically enriched $^{13}CO_2$ was used as the sparging gas.

A.3.3 Instrumentation

^{1}H and ^{13}C NMR spectra were collected on a Varian Mercury Vx 400, using $CDCl_3$ as the lock solvent. ATR FT-IR data was collected using a Shimadzu IRPrestige21 with a DLaTGS detector with 32 scans and a resolution of 1 cm^{-1}, used in combination with a Specac, Ltd. heated "Golden Gate" ATR accessory with a diamond crystal and zinc selenide lenses.[14]

A.4 Results and Discussion

A.4.1 2-Methylamino-15-crown 5

2-amino-methyl-15-crown-5 was determined to be the most likely candidate for reversible reaction with CO_2, as primary amines react with CO_2 faster than secondary amines.[15] The proton and carbon spectra of the molecular precursor can be seen in Figure A.5 and Figure A.7; the proton and carbon spectra of the resulting ionic species can be seen in Figure A.6 and Figure A.8.

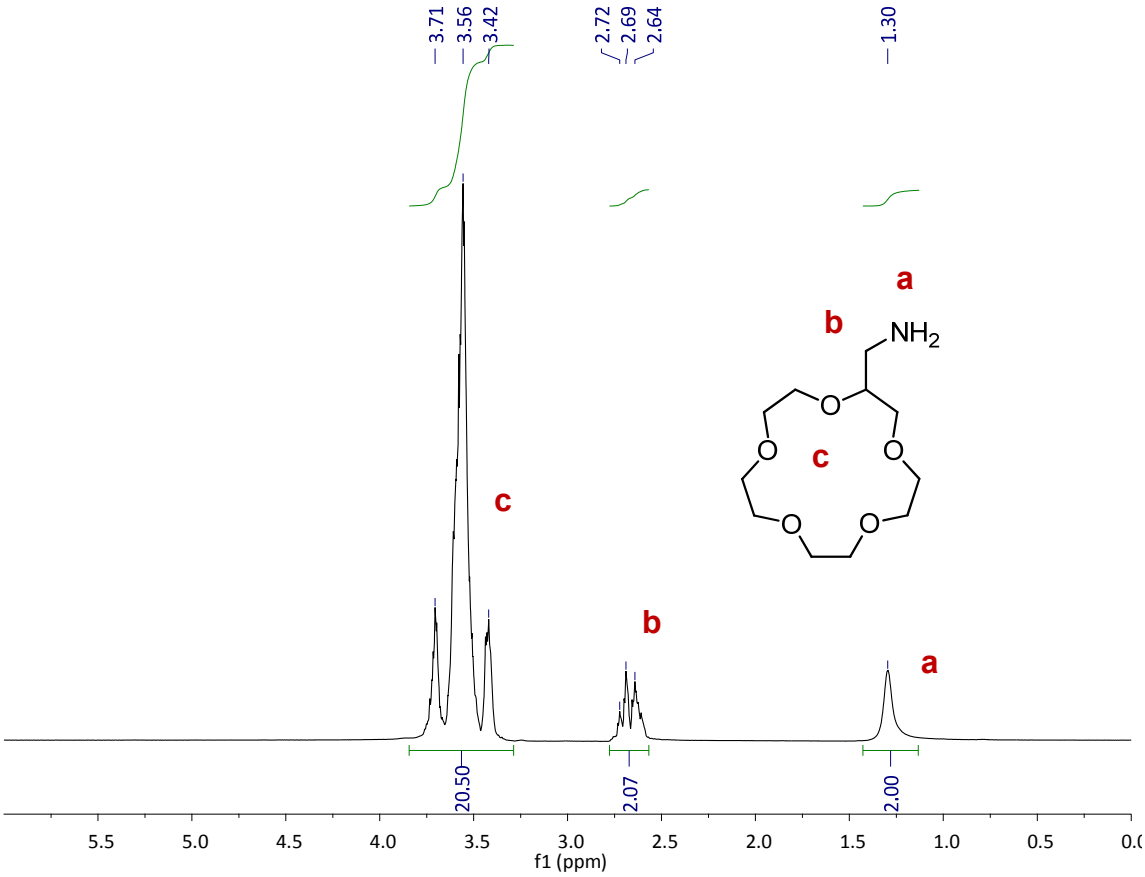

Figure A.5. ^{1}H NMR for 2-aminomethyl-15-crown-5. Peak a is from the amino protons; peak b from the methylene group bearing the amine; and peak c from the overlapping ring protons.

Despite the overlapping signals, the integrations in Figure A.5 can be divided into three regions: the amino group at δ1.30 (peak a); the amino-bearing methylene group around δ2.7 (peak b); and the remaining ring protons at δ3.4-3.8 (peak c).

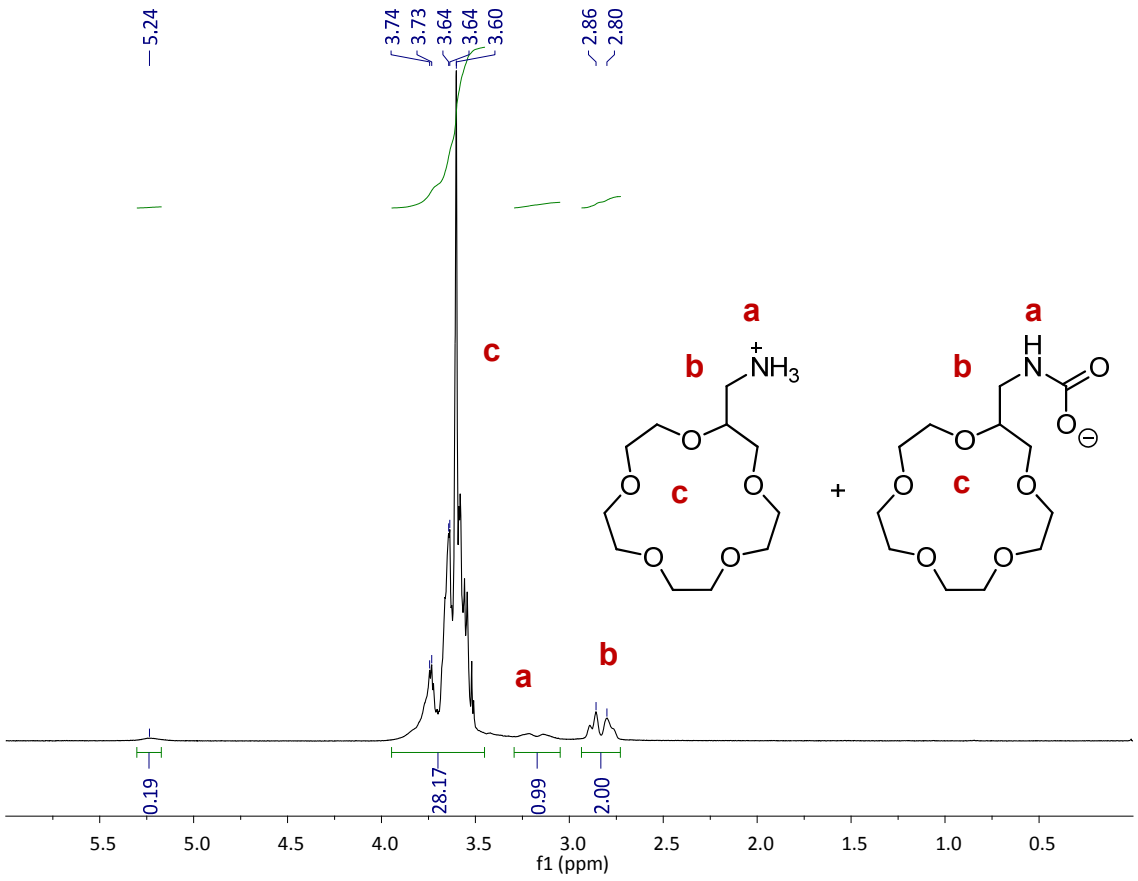

Figure A.6. ^{1}H NMR for 2-aminomethyl-15-crown-5 after reaction with CO_2.

The asymmetry present in 2-aminomethyl-15-crown-5 results in many overlapping signals for the ring atoms, both in the ^{1}H and ^{13}C NMR spectra. However, the pendant aminomethyl group is easy to distinguish. Prior to reaction in the ^{1}H NMR spectrum (Figure A.5), it appears as a multiplet at δ2.60; following reaction with CO_2 (Figure A.6), this multiplet is shifted downfield to δ2.8.

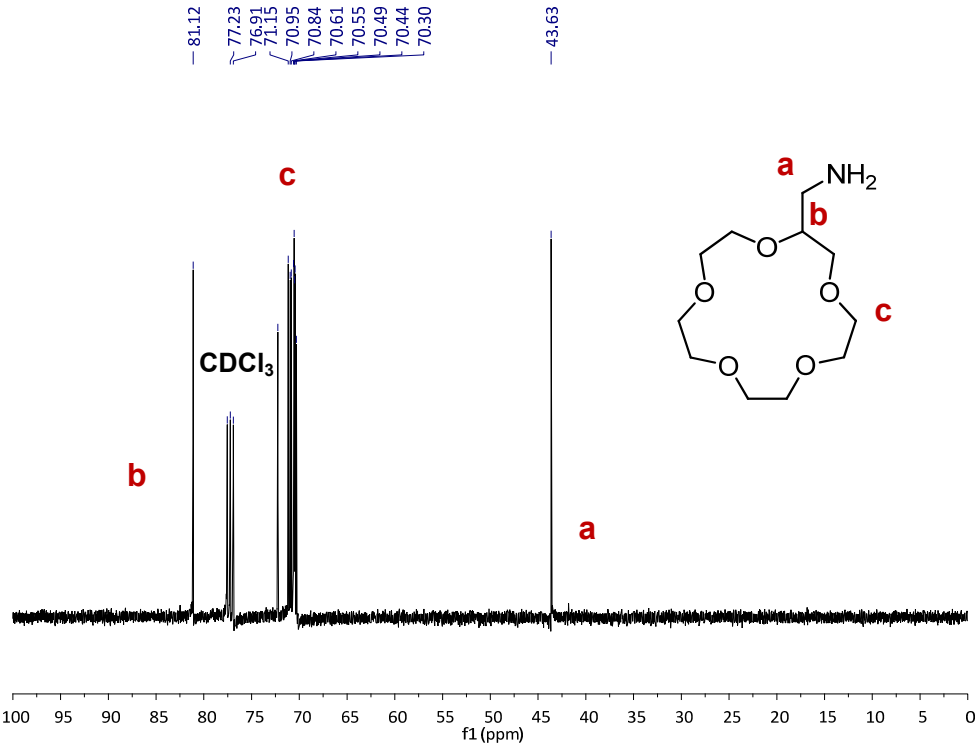

Figure A.7. ^{13}C NMR for 2-aminomethyl-15-crown-5. Peak a is from the amine-bearing methylene carbon; peak b from the methine carbon; and peak c from the remaining overlapping ring carbons.

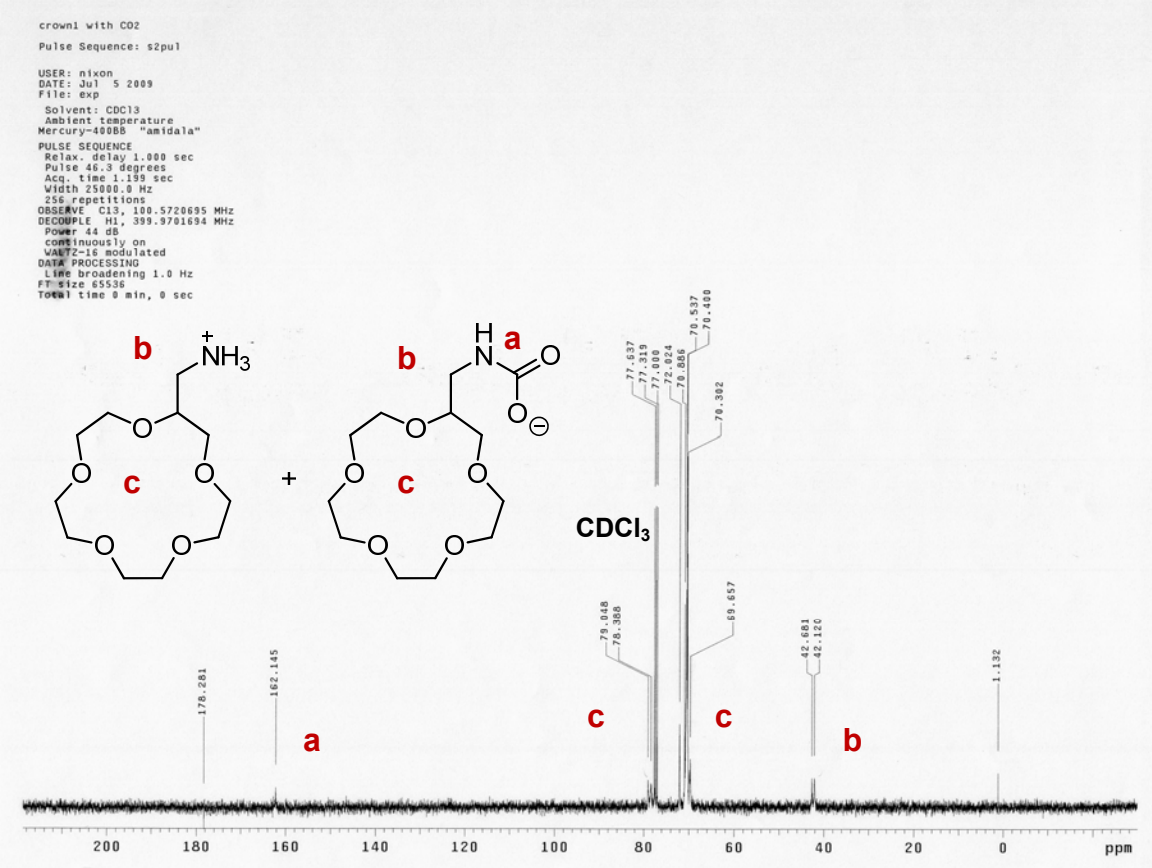

Figure A.8. ^{13}C NMR for 2-aminomethyl-15-crown-5 after reaction with CO_2. Note appearance of carbamate peak at δ162.145.

Following reaction with CO_2, the signal for the amine-bearing methylene carbon splits into two signals near δ42. Additionally, the signals of the overlapping ring carbons—previously closely grouped around δ70—split into two distinct groups at δ70 and δ78. Most importantly, the peak at δ162.1 indicates the formation of a carbamate anion.

A.4.2 1-Aza-12-crown-4

We then began proof-of-concept testing of the crown ethers containing an endocyclic nitrogen, i.e. the secondary amines. Initial reaction of 1-aza-12-crown-4 with CO_2 showed peak broadening in the post-reaction ^{1}H NMR spectrum, but no carbamate peak was observed in the ^{13}C NMR spectrum thereof—even when the relaxation delay was

increased from 1 to 4 seconds. We then decided to use isotopically enriched $^{13}CO_2$, which would increase the sensitivity of the ^{13}C NMR spectrum. The proton and carbon spectra of the molecular precursor can be seen in Figure A.9 and Figure A.11; the proton and carbon spectra of the resulting ionic species can be seen in Figure A.10 and Figure A.12.

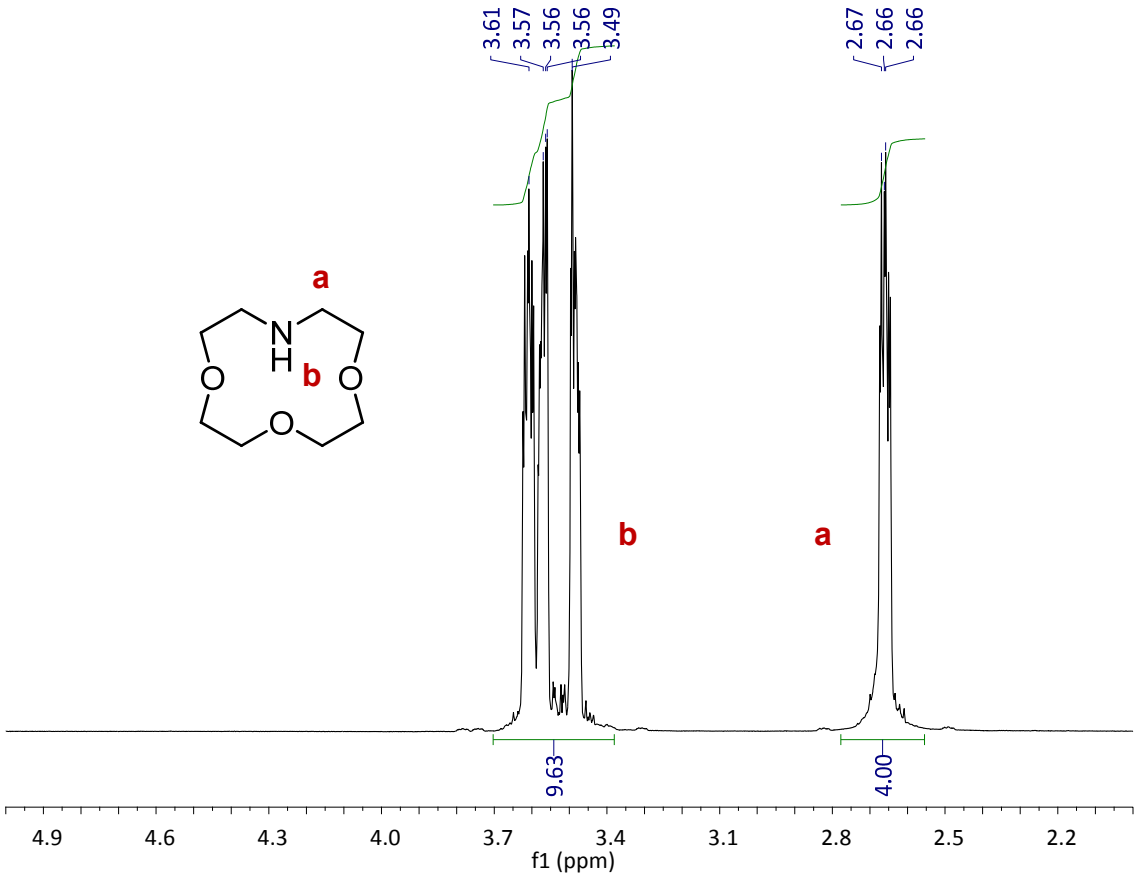

Figure A.9. ^{1}H NMR spectrum of 1-aza-12-crown-4.

The amine proton is not clearly visible in the ^{1}H NMR spectrum (Figure A.9), and, as such, is not labeled. The protons of the methylene group adjacent to the amine appear at δ2.66 (peak *a* in Figure A.9). The signals of the other ring protons overlap and appear from δ3.45-3.65 (peak *b* in Figure A.9).

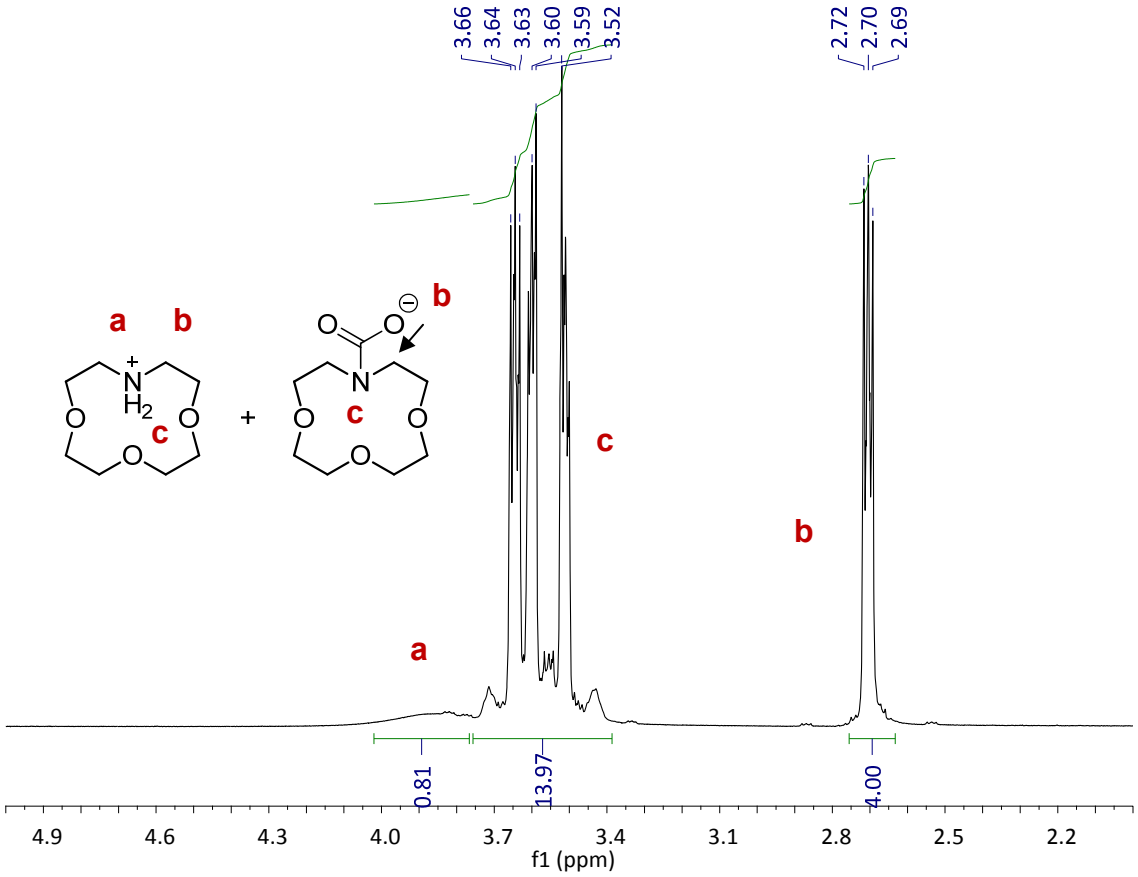

Figure A.10. ^{1}H NMR spectrum of 1-aza-12-crown-4 after reaction with isotopically enriched $^{13}CO_2$.

Upon reaction with CO_2, the signal for the nitrogen-adjacent protons moves slightly downfield to δ2.70, and resolves into a triplet (peak *b* in Figure A.10). Broadening of the other multiplet at δ3.5 (peak *c*) can also be observed, and the appearance of a broad peak at δ3.9 (peak *a*) could be due to the formation of an ammonium cation.

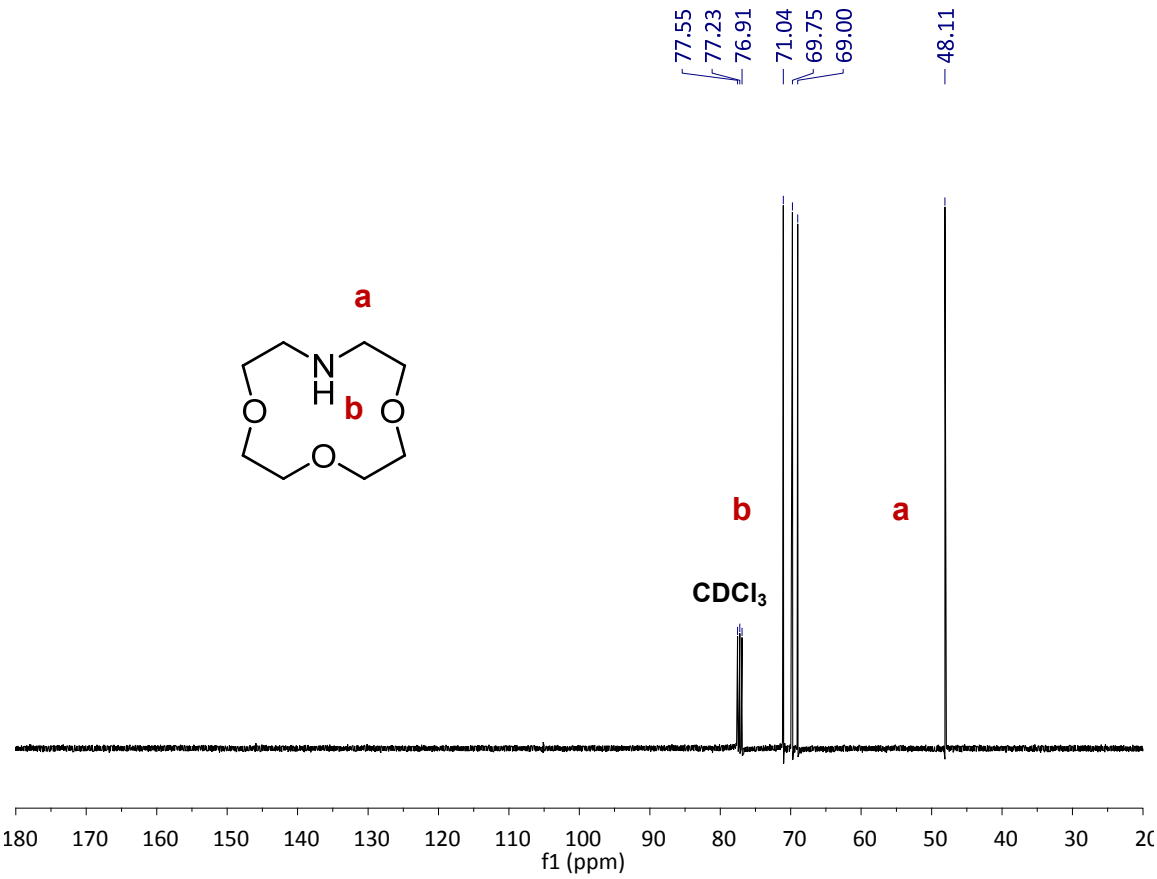

Figure A.11. ^{13}C NMR spectrum of 1-aza-12-crown-4.

Four distinct signals are present in the ^{13}C NMR prior to reaction with CO_2 (Figure A.11), as expected. The peak at δ48.11 (peak *a* in Figure A.11) is from the carbons adjacent to the nitrogen, while the other three peaks correspond to the other ring carbons (peaks *b*). As this azacrown is symmetrical, there is considerably less overlap of NMR peaks.

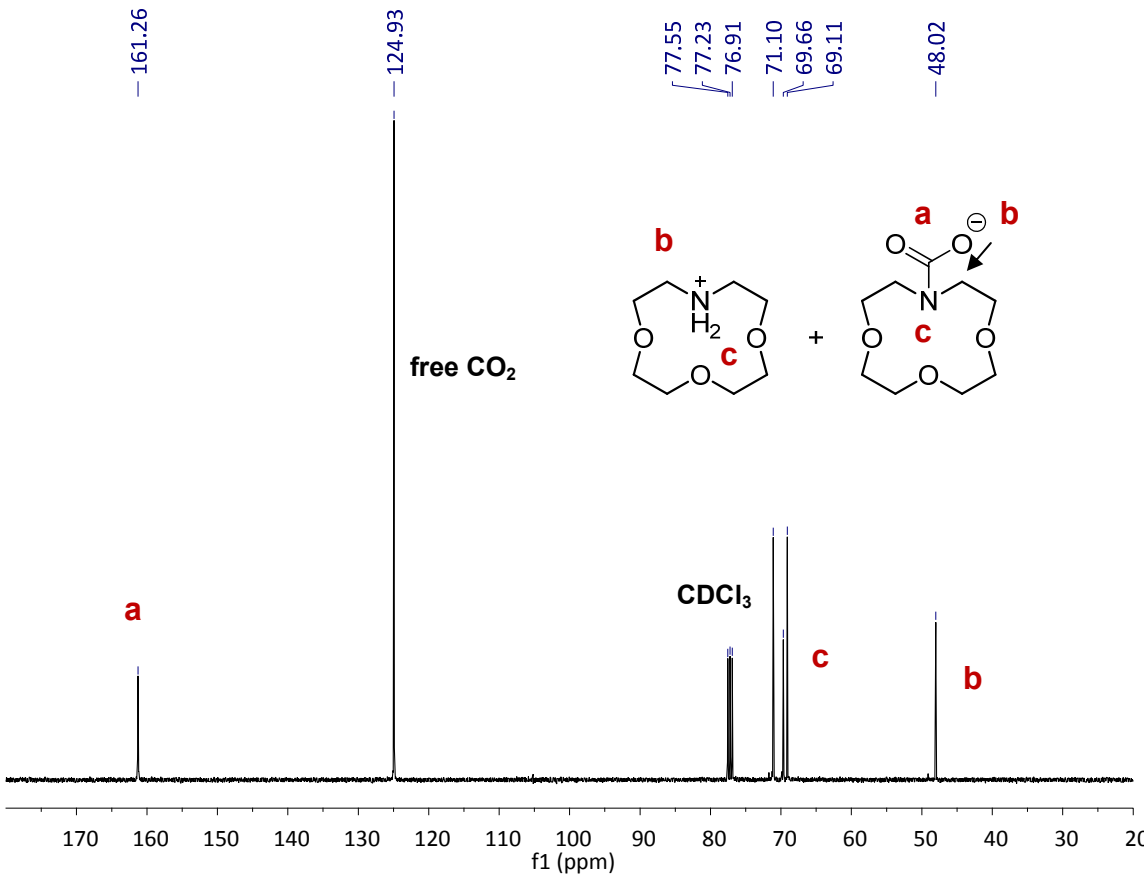

Figure A.12. ^{13}C NMR spectrum of 1-aza-12-crown-4 after reaction with isotopically enriched $^{13}CO_2$.Note appearance of carbamate peak at δ161.26. Large peak at δ124.93 is free (unreacted) $^{13}CO_2$.

The successful reaction of 1-aza-12-crown-4 with CO_2 can be seen by comparing both the ^{1}H and ^{13}C NMR spectra before and after sparging. In the proton spectrum in Figure A.9, protons adjacent to the nitrogen appear as a multiplet at δ2.66. The signals of the other oxygen-adjacent ring protons overlap, and appear as a multiplet in the range δ3.4-3.7. The amine proton does not appear prior to reaction with $^{13}CO_2$. After reaction with the $^{13}CO_2$, as shown in Figure A.10, the nitrogen-adjacent multiplet shifts slightly downfield to δ2.7 and resolves into a triplet; the oxygen-adjacent multiplet broadens. Additionally, a broad weak

ammonium signal at δ3.7-3.8 appears. Less significant changes to the ring carbons are seen when comparing the ^{13}C NMR spectra before (Figure A.11) and after (Figure A.12) reaction; however, the appearance of a peak at δ161.26 in Figure A.12 is due to the formation of a carbamate. The large peak at δ124.93 is due to free $^{13}CO_2$ present in the solution.

A.4.3 1-Aza-15-crown-5

The next secondary amine to be tested was 1-aza-15-crown-5. Again, initial reaction of this azacrown with CO_2 showed peak broadening in the post-reaction ^{1}H NMR spectrum, but no carbamate peak in the ^{13}C NMR spectrum. The proton and carbon spectra of the molecular precursor can be seen in Figure A.13 and Figure A.15; the proton and carbon spectra of the resulting ionic species can be seen in Figure A.14 and Figure A.16.

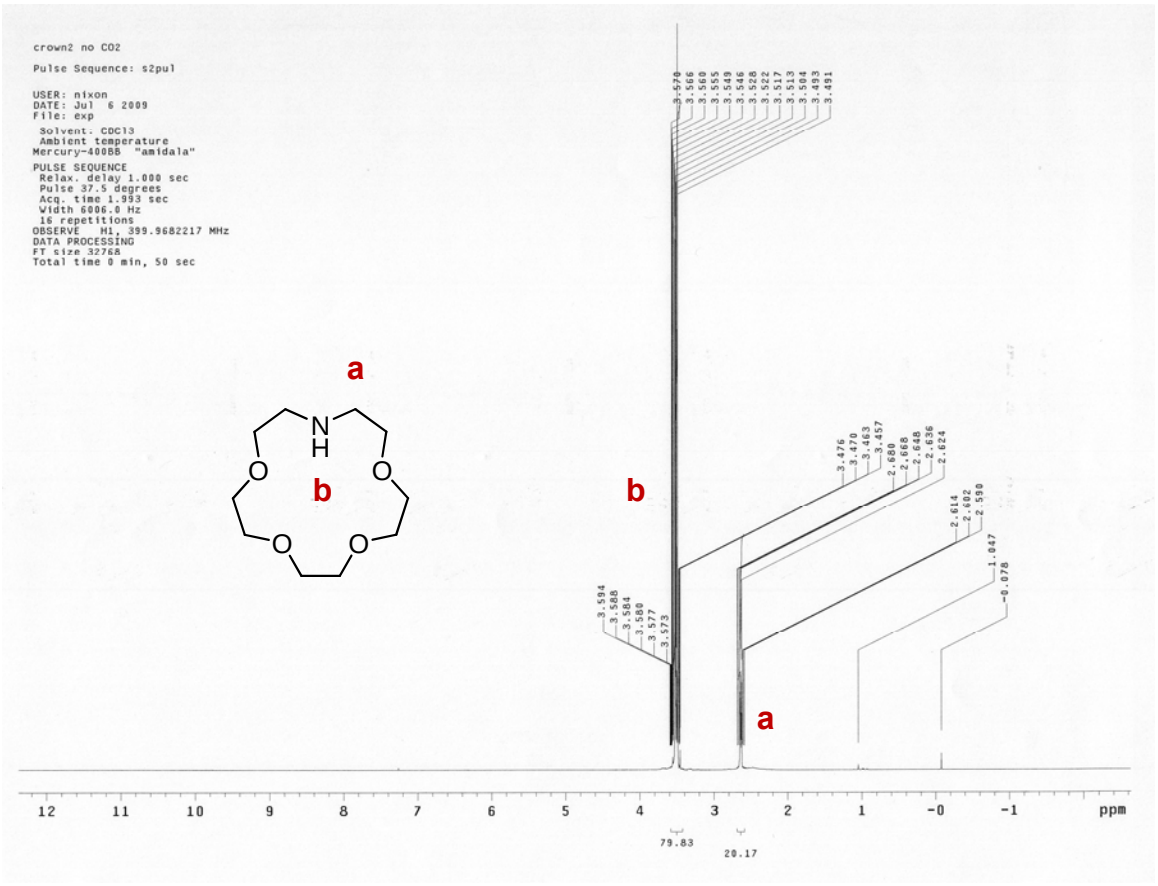

Figure A.13. ^{1}H NMR spectrum of 1-aza-15-crown-5.

In Figure A.13, the protons adjacent to the nitrogen appear at δ2.66 (peak *a*). The remaining protons in the ring appear as a multiplet at δ3.56 (peak *b*). The amine proton is not readily apparent but may be located just below peak *a*.

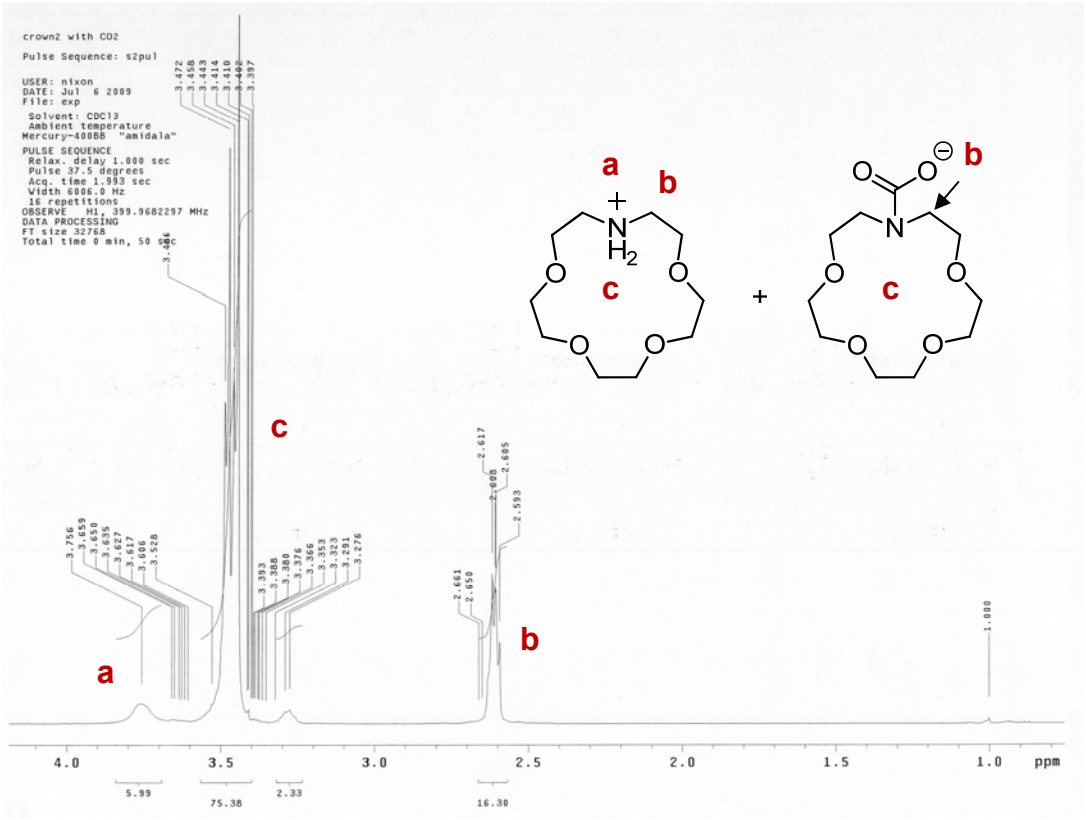

Figure A.14. ^{1}H NMR spectrum of 1-aza-15-crown-5 after reaction with CO_2.

Following reaction with CO_2, the protons adjacent to the nitrogen are shifted slightly upfield, to δ2.60-2.65 (peak *b* in Figure A.14). The multiplet from the other ring protons also shifts slightly upfield, from δ3.56 to δ3.41 (peak *c*). The broad peak at δ3.61 (peak *a*) may be due to the ammonium cation.

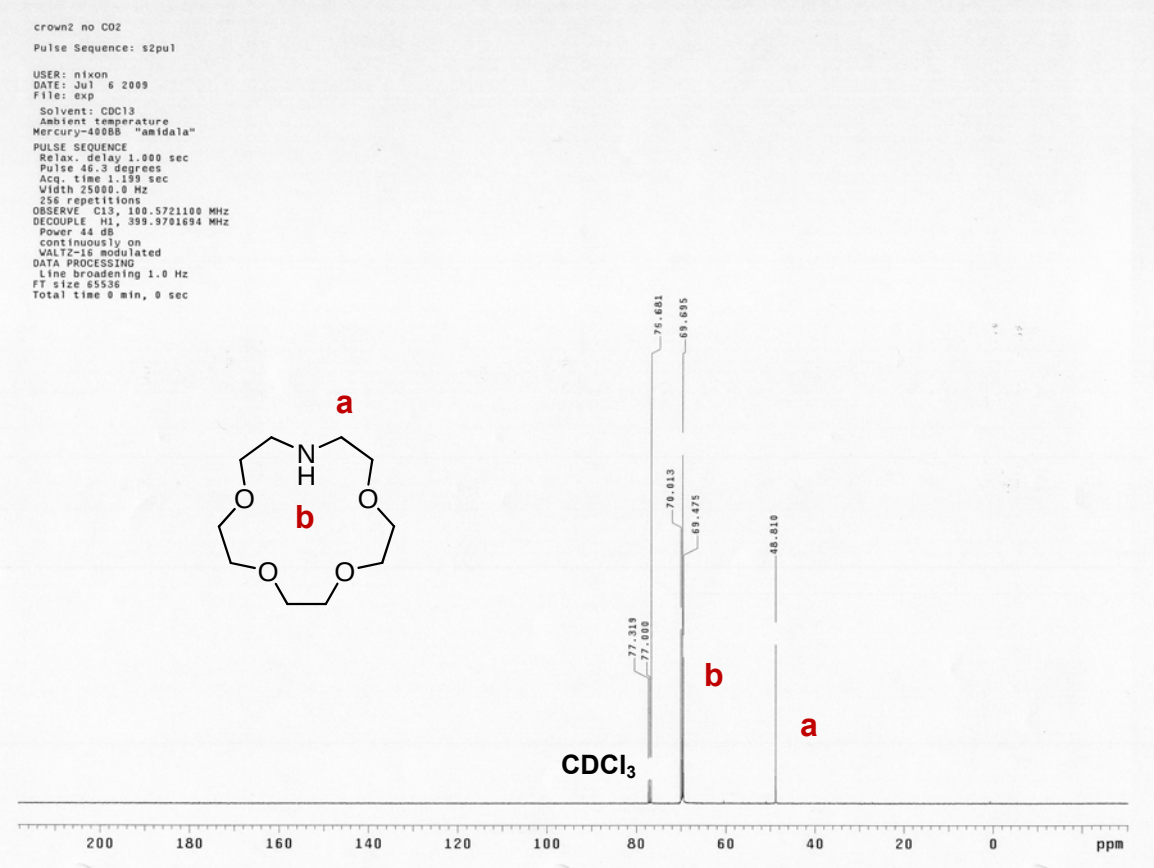

Figure A.15. ^{13}C NMR spectrum of 1-aza-15-crown-5.

In the ^{13}C NMR spectrum of 1-aza-15-crown-5 prior to reaction with CO_2 (Figure A.15), only 4 peaks are visible. The peak at δ48.8 (peak *a* in Figure A.15) is from the nitrogen-adjacent carbons, while the other overlapping peaks (peaks *b*) are from the oxygen-adjacent carbons.

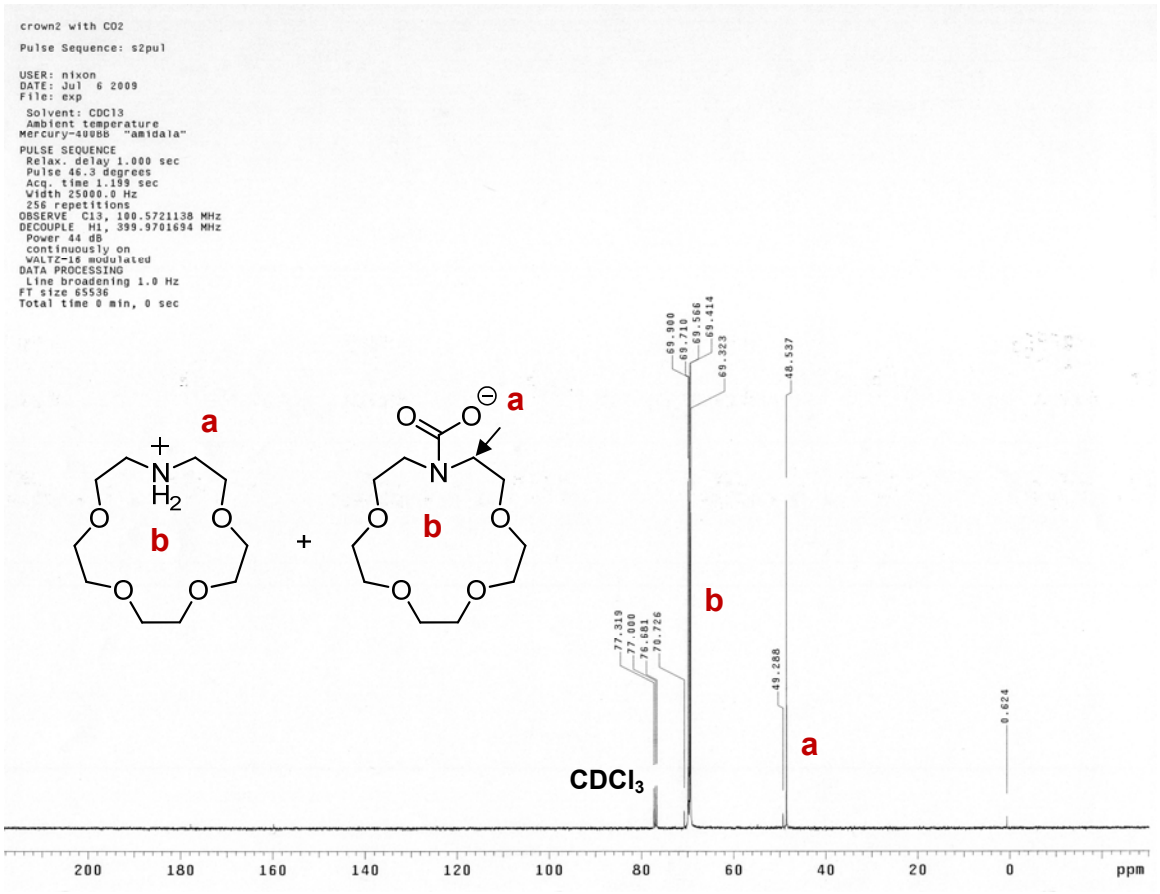

Figure A.16. ^{13}C spectrum of 1-aza-15-crown-5 after reaction with CO_2.

Although no carbamate peak can be seen in Figure A.16 after reaction with CO_2, there is an increase in the number of carbon signals. Only 4 signals are seen in the ^{13}C spectrum prior to reaction, with the nonequivalent carbons adjacent to the ring carbons presenting as 3 overlapping signals between δ69-70. After reaction with CO_2, the number of these overlapping signals increases to 6, while the signal of the nitrogen-adjacent carbon splits into 2 peaks at δ49.3 and δ48.5. This could indicate the presence of an ammonium-carbamate ion pair, as this "splitting" is commonly observed with our RevILs (see Chapter 3).

Rather than reacting 1-aza-15-crown-5 with isotopically enriched $^{13}CO_2$, we decided to use the more sensitive method of attenuated total reflectance Fourier transform infrared

spectroscopy (ATR-FTIR) to see if the carbamate peak was detectable. A solution of 1-aza-15-crown-5 in chloroform was prepared, introducted to the FTIR, and reacted with CO_2 at atmospheric pressure. The compared spectra of 1-aza-15-crown-5 before and after reaction with CO_2 can be seen in Figure A.17.

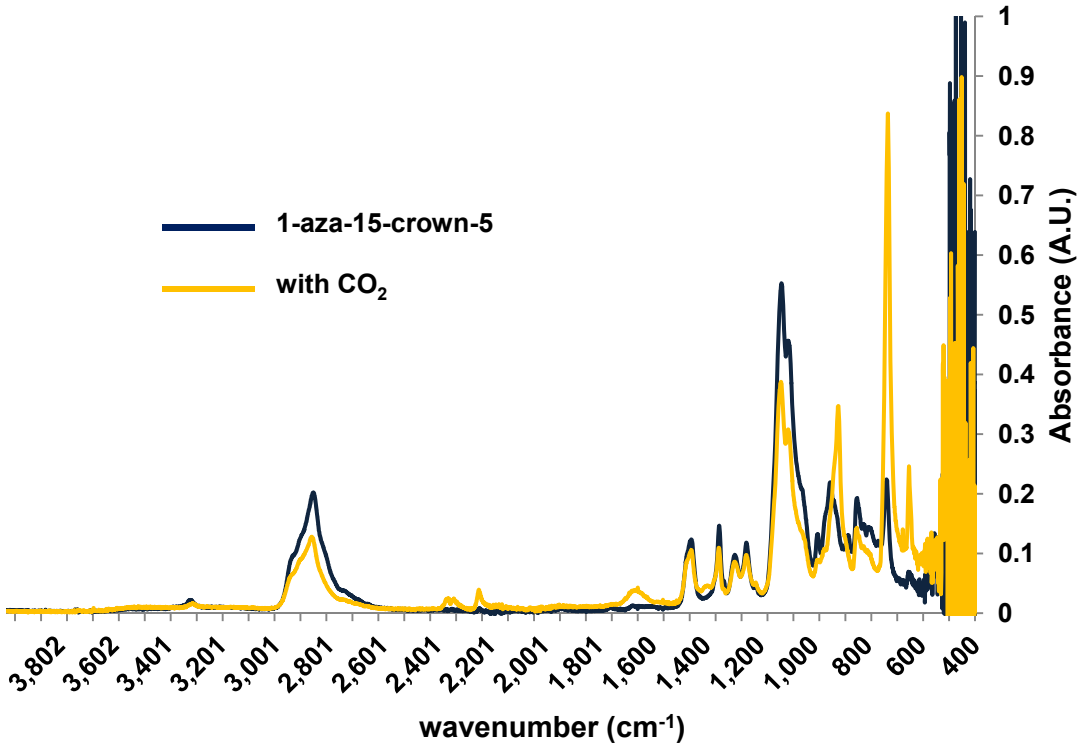

Figure A.17. FTIR spectra of 1-aza-15-crown-5 before and after reaction with CO_2. Note peak at approximately 1650 cm^{-1}, indicating formation of carbamate.

The primary region of difference between the two spectra occurs at approximately 1650 cm^{-1}, where a peak appears after reaction with CO_2, indicating the presence of a C==O stretch and the formation of a carbamate. In conjunction with the peak broadening observed in the ^1H NMR after reaction with CO_2, we have evidence that 1-aza-15-crown-5 does indeed react with CO_2 to form a carbamate. Additionally, we have shown that FTIR can be

used as an analytical technique to ascertain conversion of the molecular crown to the ionic form, without requiring expensive reagents such as $^{13}CO_2$.

A.4.4 1-Aza-18-crown-6

The final secondary amine to be tested was 1-aza-18-crown-6. Again, initial reaction of this azacrown with CO_2 resulted in peak broadening in the post-reaction ^{1}H NMR spectrum, but no carbamate peak in the ^{13}C NMR spectrum. The proton and carbon spectra of the molecular precursor can be seen in Figure A.18 and Figure A.20; the proton and carbon spectra of the resulting ionic species can be seen in Figure A.19 and Figure A.21.

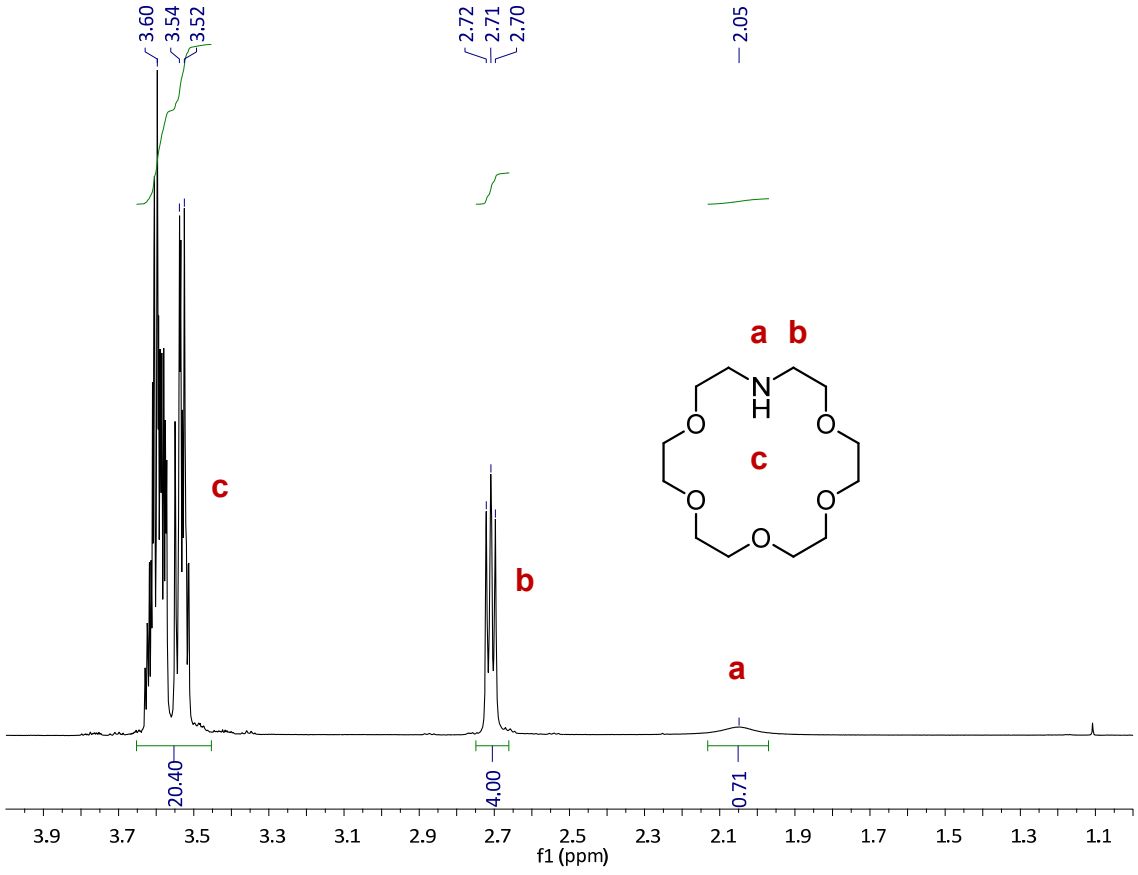

Figure A.18. ^{1}H NMR for 1-aza-18-crown-6.

The triplet at δ2.71 (peak *b* in Figure A.18) is from the protons adjacent to the ring nitrogen; the multiplet from δ3.5-3.6 (peak *c*) is from the other ring protons. The amine proton appears at δ2.05 (peak *a*).

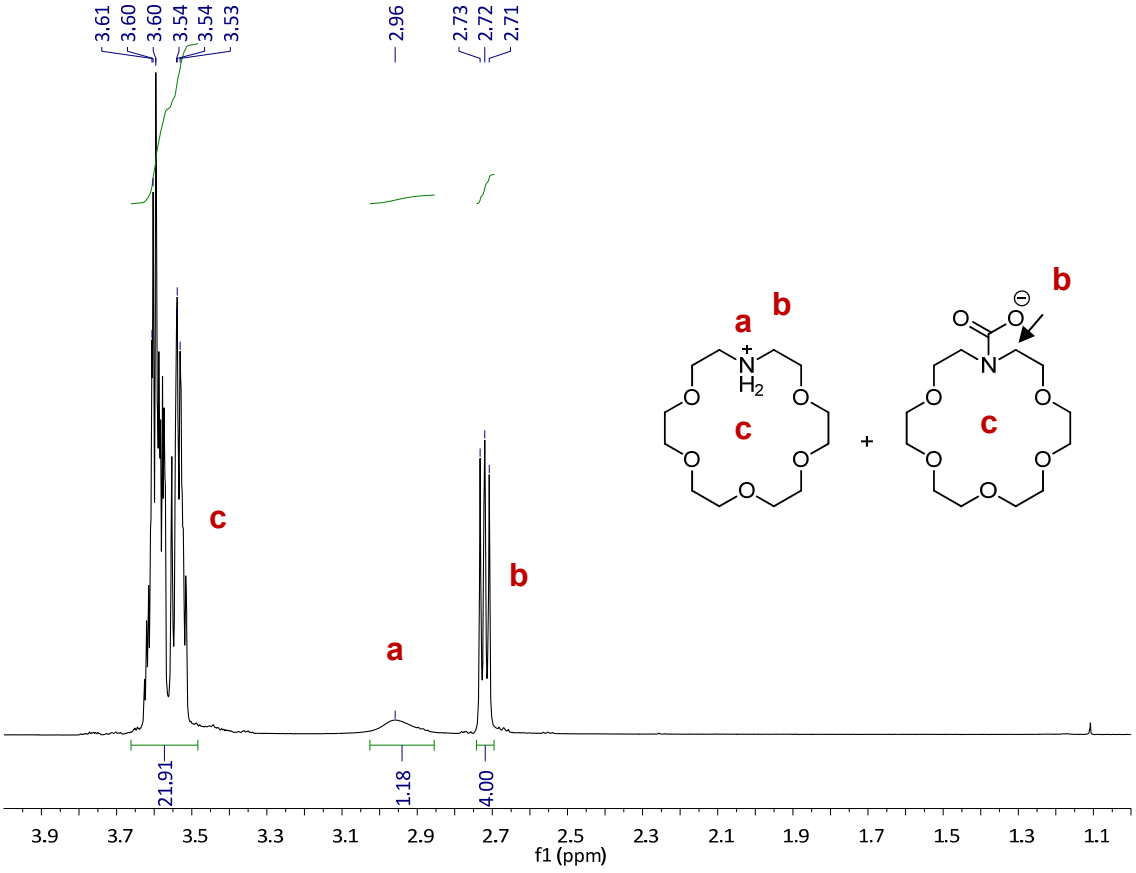

Figure A.19. ^{1}H NMR for 1-aza-18-crown-6 after reaction with isotopically enriched $^{13}CO_2$.

Upon reaction with CO_2, (Figure A.19) neither the triplet (peak *b*) or the multiplet (peak *c*) exhibit much change. However, the appearance of a broad singlet at δ2.96 (peak *a*) is most likely due to the formation of an ammonium cation.

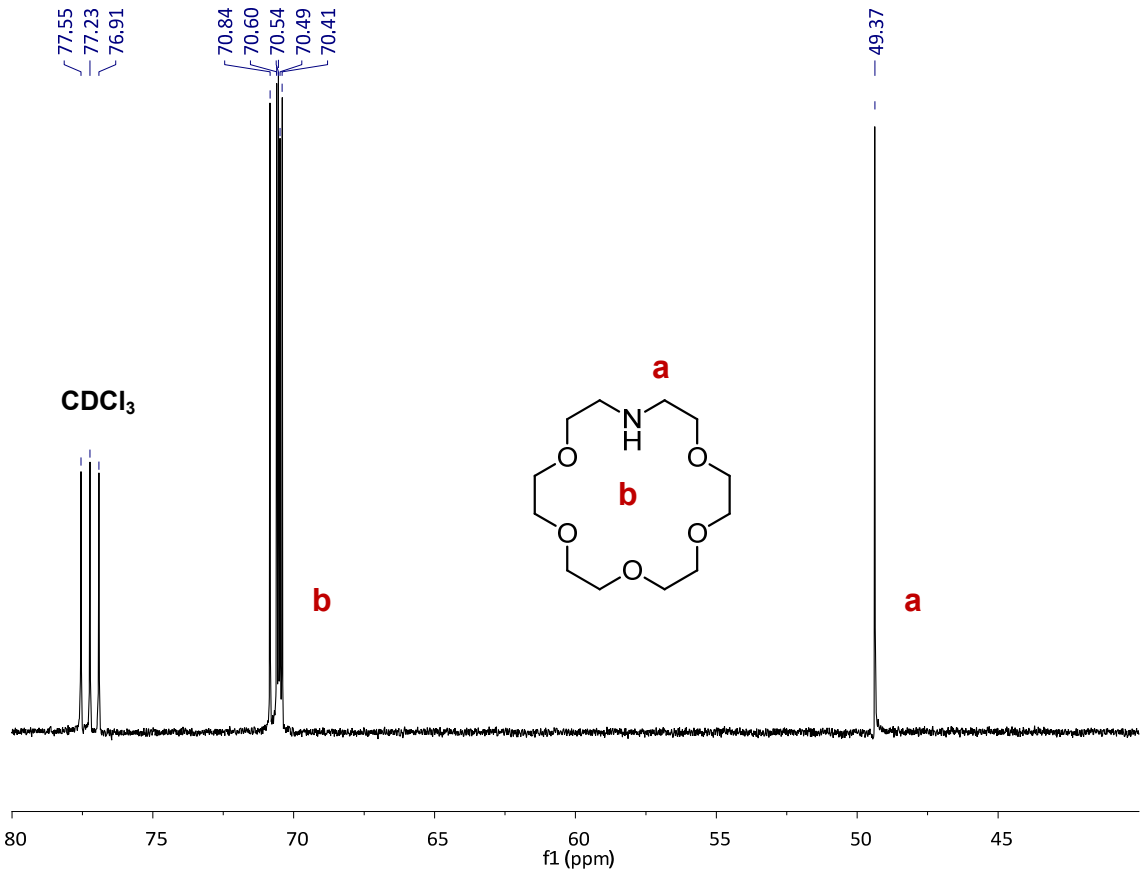

Figure A.20. ^{13}C NMR spectrum of 1-aza-18-crown-6.

Prior to reaction with CO_2 (Figure A.20), the nitrogen-adjacent carbons appear at δ49.37 (peak *a*), while the oxygen-adjacent carbons appear from δ70.4-70.9 (peaks *b*).

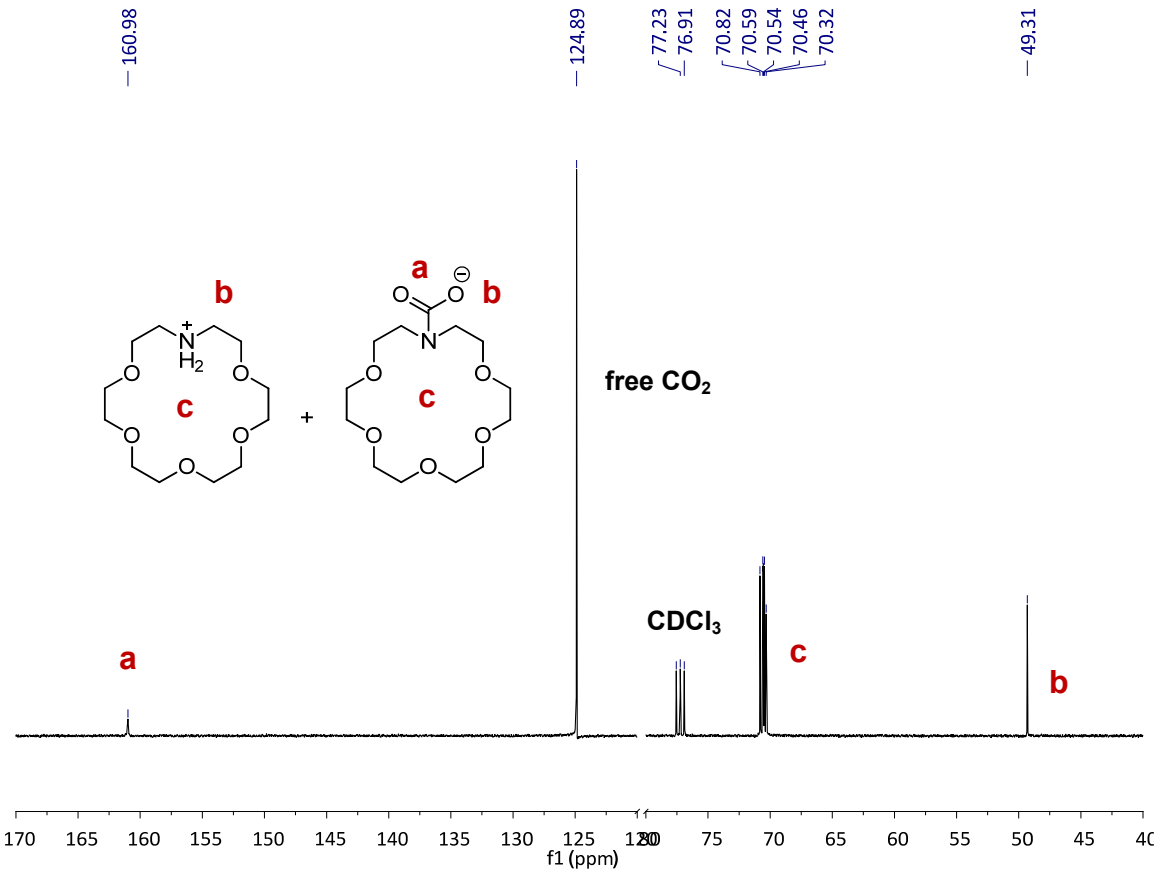

Figure A.21. ^{13}C NMR spectrum of 1-aza-18-crown-6 after reaction with isotopically enriched $^{13}CO_2$. Note appearance of carbamate peak at δ160.98. Large peak at δ124.89 is free (unreacted) $^{13}CO_2$.

After reaction with $^{13}CO_2$, there is very little change in the chemical shifts of the ring carbons, whether they are adjacent to the nitrogen or the ring oxygens. However, the appearance of a peak at δ160.98 (peak *a* in Figure A.21) is indicative of carbamate formation. The large peak present at 124.89 is due to the presence of free, unreacted $^{13}CO_2$. We have therefore shown that all four of our switchable crown ether candidates do react with CO_2 to form ionic species; however, we have not yet determined what the extent of reaction is, or what reaction time would be required to achieve full conversion of the molecular crown ether to the ionic form.

A.4.5 Conversion of Bis(2-methoxyethyl)amine as Function of CO_2 Pressure

At this point, we decided to switch to using what we termed "crown fragments" in order to gain a more fundamental understanding of the secondary amine behavior without using the expensive (approximately $100/g) azacrowns. We define crown fragments as secondary amines bearing ethylene oxide groups; these can also be methyl-capped. Examples are shown in Figure A.22.

Figure A.22. Crown fragments diethanolamine, *left*, and bis(2-methoxyethyl)amine, *right*.

The two simplest crown fragments commercially available are diethanolamine and bis(2-methoxyethyl)amine. These two fragments have the added benefit of being liquid at room temperature, permitting us to use them neat—all azacrowns mentioned previously are solid at room temperature and had to be reacted with CO_2 while in solution. As bis(2-methoxyethyl)amine most closely approximates the environment of the endocyclic amine found in an azacrown, we decided to use this fragment in our investigation of the effect of pressure on conversion.

CO_2 reacts with bis(2-methoxyethyl)amine in much the same way as our RevILs, forming an ammonium-carbamate ion pair. However, as the amine in question is a secondary amine, it should react at a slower rate than the primary ones found in our silylated amines.

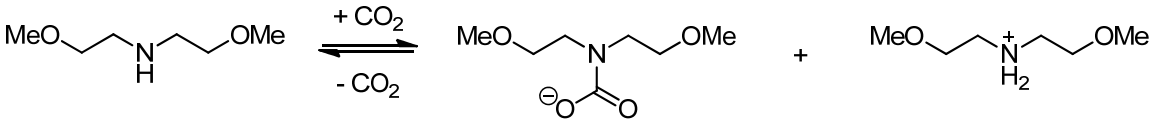

Figure A.23. Reaction of crown fragment bis(2-methoxyethyl)amine with CO_2 to form ammonium-carbamate ion pair.

We used FTIR to assess conversion to the ionic species by introducing bis(2-methoxyethyl)amine to the FTIR pressure cell and increasing the pressure of CO_2. Spectra were taken at a broad range of CO_2 pressures (2 psi to 881 psi) and can be seen in Figure A.24.

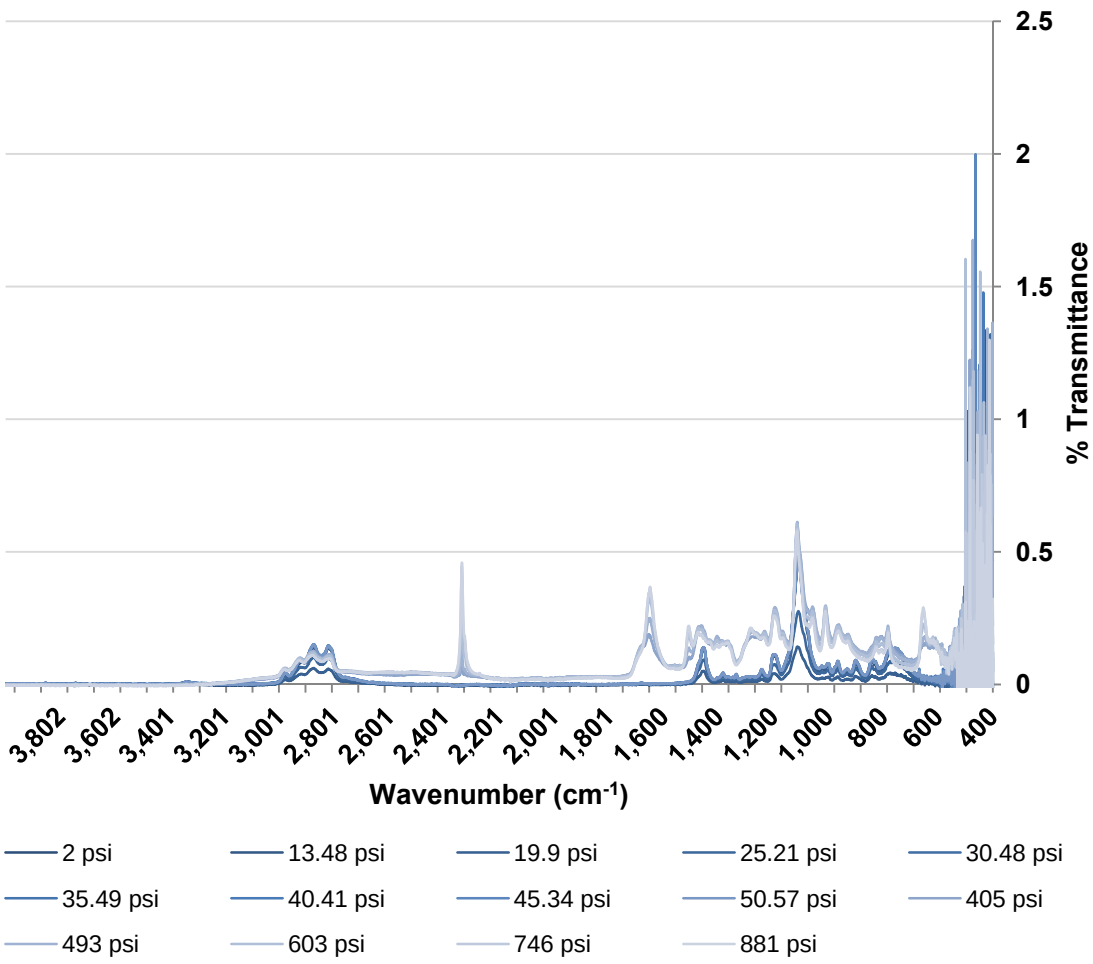

Figure A.24. Conversion of bis(2-methoxyethyl)amine as a function of CO_2 pressure. Carbamate peak (at ~1675 cm^{-1}) does not appear until approximately 400 psi.

The peak corresponding to the C==O stretch of the carbamate appears at 1675 cm^{-1} at approximately 400 psi, indicating that the secondary carbamate may not form at low pressures of CO_2. The peak seen at approximately 2300 cm^{-1} is due to the presence of free, unreacted CO_2.

A.5 Path Forward

A.5.1 Path Forward: Background

Our preliminary work with azacrowns shows that they do form ionic species when reacted with CO_2. Although certain crown ethers have been found to be selective for ^{90}Sr removal in nuclear waste streams, the other radionuclide of interest, ^{137}Cs, cannot be isolated as easily. Cs^+ has a low charge density and does not associate favorably with typical organic extractants; it is therefore difficult to completely remove the water from the hydration shell around the cation and for the Cs^+ to partition into the organic phase. Even the use of crown ethers, which present multiple coordination sites for the Cs^+, does not fully overcome this obstacle.[16] There is, however, another type of macrocyles that has shown selectivity for Cs^+—the calixarenes.

Calixarenes are a class of macrocycles formed from the condensation of aromatic alcohols and aldehydes. In particular, the class of compounds formed from phenols and formaldehyde are termed calixarenes. These host compunds were discovered by Zinke as early as the 1940s, but not fully explored, characterized, and named until Gutsche's investigations approximately 30 years later.[17] The structure of the most widely studied calixarene, *p-tert*-butyl-calix[4]arene, can be seen in Figure A.25. A calixarene with the common name calix[*n*]arene has *n* repeating units.

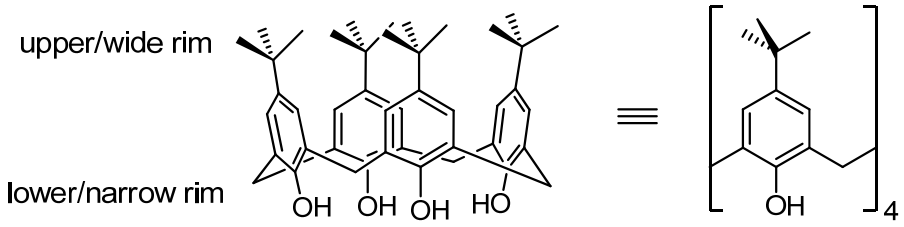

Figure A.25. Calixarene terminology and structure shorthand.

The hydroxyl groups are at the lower, or narrow rim, and the *t*-butyl groups are at the upper, or wider rim. Calixarenes can be modified at the upper or lower rim with myriad functional groups; additionally, use of different aldehydes or phenols during the initial synthesis of the calixarene can provide a foothold for further synthetic modification of the basic calixarene skeleton.

As with crown ethers, calixarenes are size-selective for cations. However, calixarenes are conformationally labile. The possible conformers of *p-tert*-butylcalix[4]arene (R = H) are shown in Figure A.26.

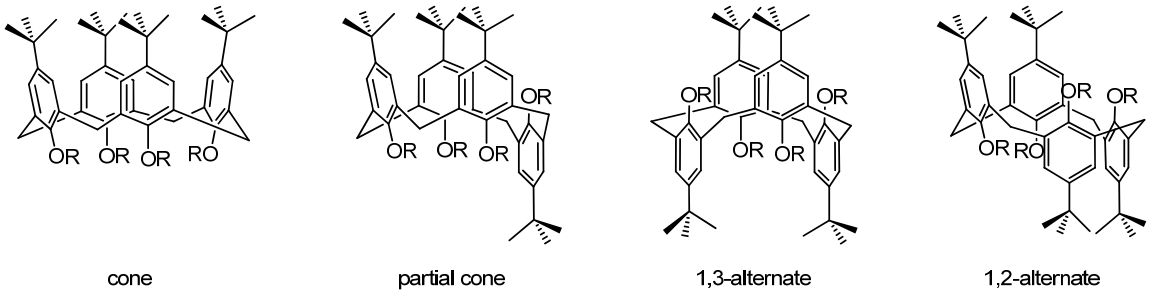

Figure A.26. Possible conformers of *p-tert*-butyl-calix[4]arene. *Far left*, cone conformation; *left*, partial cone, with one phenyl group opposed to the other 3; *right*, 1,3-alternate, where phenyl groups alternate orientation; and *far right*, 1,2-alternate, where 2 proximal phenyl groups have same orientation.

The conformation of a calixarene depends not only on the identity of the R groups, but also the attachment of other groups to the calixarene ring; additionally, some groups permit conformational lability while others hold the ring phenols in place. Calixarenes that are "locked" into one conformation show higher selectivity and extraction efficiency. The presence of certain functional groups can also enhance selectivity, as I will describe below.

A calixcrown is a calixarene that has been modified with a crown ether moiety or moieties. These were first synthesized by Alfieri *et al.* and shown to be more efficient

transporters of K^+ across a DCM membrane than the parent *p-tert*-butylcalix[4]arene alone, due to the amphiphilic character of the molecule.[1a] Ghidini *et al.* used this synthesis to create a calixbiscrown, in which each pair of distal phenoxy groups was linked by a crown ether; this linker caused the calixarene ring to adopt a 1,3-alternate conformation. The resulting calixbiscrown was found to have the highest selectivity for K^+ over Na^+ known at that time.[18] Ungaro *et al.* found that the presence of even one crown moiety on the calixarene caused the molecule to have a higher selectivity for Cs^+ over Na^+ due to the constrained interconversion between 1,3-alternate and cone formations.[19] It has been suggested that the pi clouds of the aromatic rings in the calixarene ring interact with the soft Cs^+ cation, resulting in the high cesium selectivity.[20]

This high selectivity of calixcrowns for Cs^+ has since been put to use in nuclear waste remediation. The composition of nuclear waste is largely site-dependent; however, as much nuclear waste contains high amounts of salt, Cs/Na selectivity is crucial, as is exclusion of K^+.[21] At the Savannah River nuclear waste site, the caustic-side solvent extraction process (CSSX) uses the calixarene calyx[4]arene-bis(*tert*-octylbenzo-crown-6) (BOBCalixC6) to extract ^{137}Cs from alkaline waste.[22] The structure of this calixbiscrown is shown in Figure A.27.

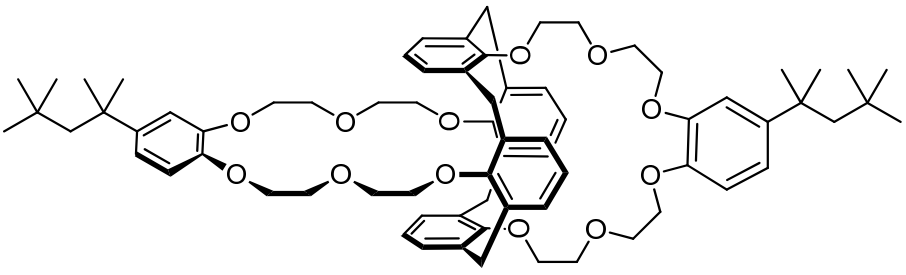

Figure A.27. Structure of BOBCalixC6.

BOBCalixC6 is used in conjunction with two modifiers that greatly increase the extraction capabilities of the calixbiscrown: trioctylamine (TOA) and 1-(2,2,3,3-tetrafluoropropoxy)-3-(4-*sec*-butylphenoxy)-2-propanol (Cs-7SBT), both shown in Figure A.28.

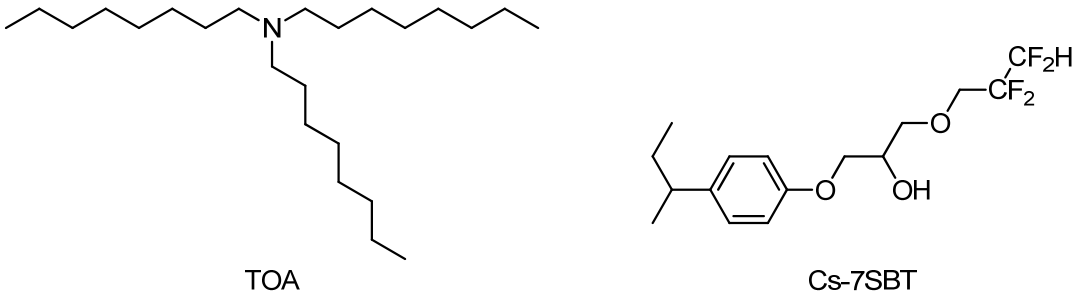

Figure A.28. Modifiers used in Savannah River Site CSSX solvent. *Left*, trioctylamine (TOA); *right*, 1-(2,2,3,3-tetrafluoropropoxy)-3-(4-*sec*-butylphenoxy)-2-propanol (Cs-7SBT).

These modifiers act as co-solvents, not only increasing the activity of BOBCalixC6, but also preventing its precipitation when complexed with Cs.[22] All three components are dissolved in the isoparaffinic solvent Isopar® L (concentration of BOBCalixC6: 7 m*M*),[23] and the solution is contacted with the aqueous alkaline tank waste. In addition to ^{137}Cs, the tank waste contains high amounts of potassium, sodium, and nitrate; as mentioned before, BOBCalix is highly selective for cesium and extracts this cation into the organic phase. Treatment with a solution of nitric acid (1 m*M*) strips the cesium from the organic phase. Bonnesen *et al.* have tested this solvent system with simulated waste (i.e., not actual nuclear waste) and found it to be very efficient at cesium removal; however, they have also identified several drawbacks. The aromatic rings of BOBCalixC6 were susceptible to nitration by nitric acid, albeit at a much higher concentration (1 *M*) than in the simulated or actual wastes (1 m*M*). Additionally, BOBCalixC6 exhibited a low solubility in Isopar® L, requiring a high

loading of Cs-7SBT; in turn, this increased the viscosity of the BOBCalixC6 solution, hindering mixing and pumping.

We propose to increase the stripping efficiency of BOBCalixC6 by modifying it with an amino group that can be reacted with CO_2 to form an ammonium-carbamate ion pair, which will result in ejection of Cs^+ from the calixcrown cavity. My recommendation for this project is that a calixarene or calixcrown structurally similar to BOBCalixC6, but bearing a 1° or 2° amine be synthesized following a known literature procedure. This macrocycle can then be reacted with CO_2; the formation of an ionic species can be determined; and the interaction of the ionic species with a candidate metal salt can be quantified. If these experiments are successful, further modification of the calixcrown skeleton to create novel macrocycles can be undertaken. In the following sections I will summarize the known calixarenes that I feel are the best candidates for our application.

A.5.2 Potential Candidates: Calixcrowns Bearing 1° Amines

Bazelaire *et al.* have synthesized a series of calixcrowns bearing 1° amines, which they have used as pH-switchable ligands. As the stripping of a bound metal ion is carried out at low pH (using a solution of nitric acid), the protonation of a primary amine causes an electrostatic repulsion and the metal ion is ejected from the cavity.[24] Although a number of these crowns have been synthesized and tested, the two most relevant to our work are shown in Figure A.29.

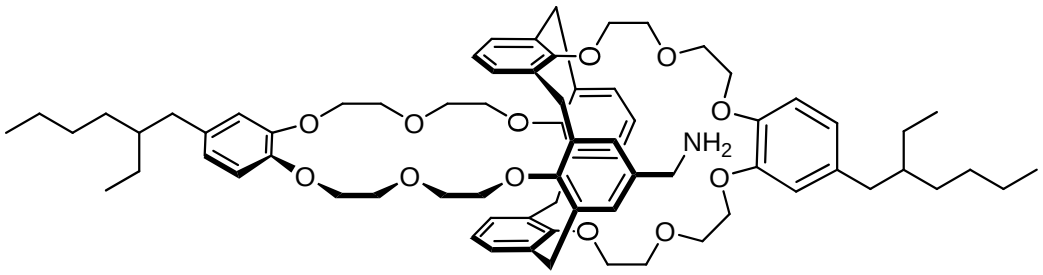

AMBEHB

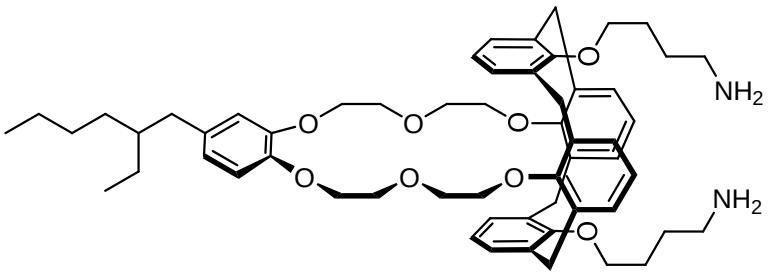

MEHB

Figure A.29. Calixcrowns containing 1° amine(s). *Top*, aminomethyl-calix[4]arene bis(4-(2-ethylhexyl)benzocrown-6) (AMBEHB); *bottom*, 25,27-bis(3-aminopropoxy)-calix[4]arene-4-(2-ethylhexyl) benzo-crown-6 (MEHB).

Aminomethyl-calix[4]arene bis(4-(2-ethylhexyl)benzocrown-6), or AMBEHB, contains a primary amine on the calixarene ring. In contrast, 25,27-bis(3-aminopropoxy)-calix[4]arene-4-(2-ethylhexyl) benzo-crown-6, or MEHB, has two pendant aminopropyl groups in place of one of the crown ether moieties; both have the same basic structure as BOBCalixC6. The ability of the calixarenes to extract Cs^+ was tested using simulated CSSX conditions, and the presence of the amine groups—either on the aromatic core of the calixarene in AMBEHB or as pendant crown fragments in MEHB—decreased the amount of Cs^+ that was extracted into the organic phase. This was thought to be due to the perturbation of the cavity by the presence of the amino groups, hindering the ability of the pi electron system to interact with Cs^+.

Wolf *et al.* synthesized a series of calixarenes modified at the lower rim with amines and amides. The two most relevant to our work are shown in Figure A.30.

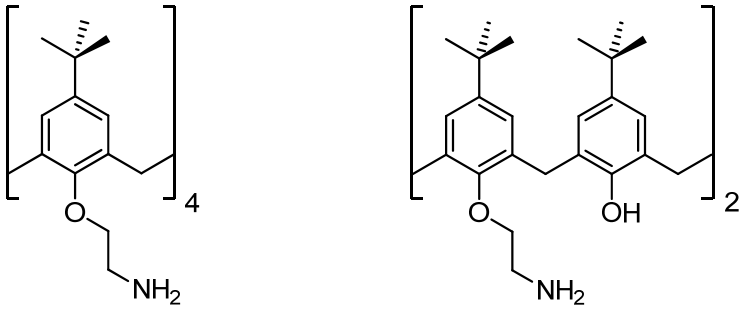

Figure A.30. Calixarenes containing 1° amines. *Left*, 5,11,17,23-*tert*-butyl-25,26,27,28-(2-aminoethoxy) calix[4]arene; *right*, 5,11,17,23-*tert*-butyl-25,27-(2-aminoethoxy) calix[4]arene.

5,11,17,23-*tert*-butyl-25,26,27,28-(2-aminoethoxy) calix[4]arene has an amino group on each aromatic ring of the calixarene core; 5,11,17,23-*tert*-butyl-25,27-(2-aminoethoxy) calix[4]arene has only two hydroxyl groups substituted with pendant amino groups. These calixarenes were evaluated for their ability to act as phase transfer agents for chromate and dichromate anions; the Cr(VI) ions were extracted from an aqueous phase into chloroform. To the best of my knowledge, these particular calixarenes have not been reacted with CO_2. However, these calixarenes do not contain the crown ether moiety, which imparts high cesium selectivity.

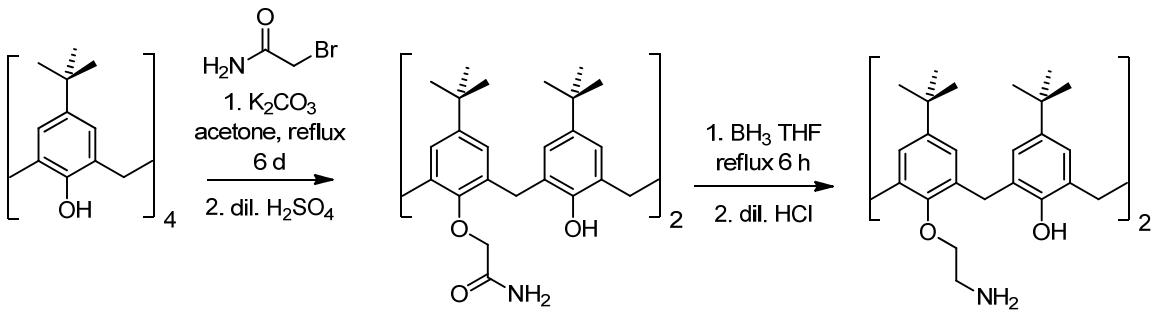

Figure A.31. Synthesis of 5,11,17,23-*tert*-butyl-25,27-(2-aminoethoxy) calix[4]arene.

The synthesis of these calixarenes, however, is straightforward (Figure A.31), which increases their appeal as proof-of-concept substrates for our project. The starting material is p-tert-butylcalix[4]arene, which, when deprotonated, reacts with bromoacetamide to yield pendant amide groups. These are then reduced with borane to yield pendant 1° amines on alternating phenol groups.

A.5.3 Potential Candidates: Calixarenes Bearing 2° Amines

Although our preliminary work with azacrowns has shown that 2° amines react more slowly than 1° amines, the ammonium cation located directly on the crown ether ring could have more of an effect on dissociation of a bound cation than a pendant amino group would. Seangprasertkij *et al.* have synthesized a series of calix(aza)crowns—calixcrowns where some of the oxygens in the crown ether subunit have been replaced with nitrogens, yielding 2° amines. Two examples are shown in Figure A.32.

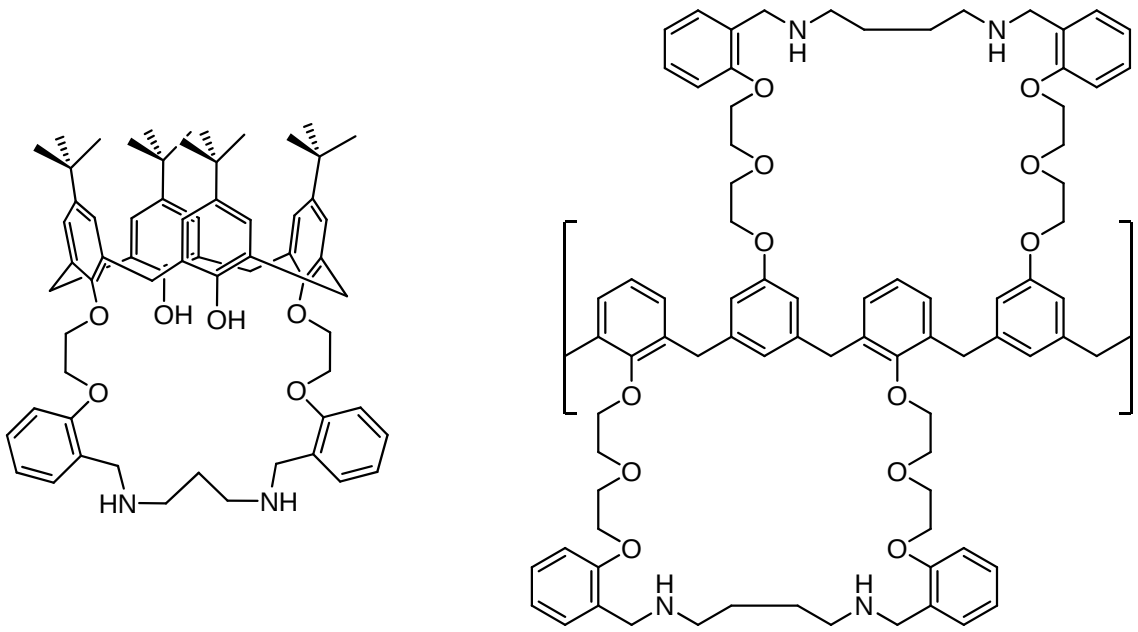

Figure A.32. Calix(aza)crowns containing 2° amines. *Left*, di-aza-benzo-crown ether *p-tert*-butyl calix[4]arene; *right*, 1,3-bis(di-aza-benzo-crown ether) *p-tert*-butyl calix[4]arene.

These calix(aza)crowns have been found, via ^{1}H NMR, elemental analysis (EA) and UV-Vis, to complex Zn^{2+}; the calix(aza)monocrown shown on the left in Figure A.32 complexes Zn^{2+} in a 1:1 ratio, while the calix(aza)biscrown shown on the right complexes Zn^{2+} in a 2:1 ratio. To the best of my knowledge, these calix(aza)crowns have not been reacted with CO_2. Azacrowns' effect on the binding selectivity for Cs^+ has also not been investigated.

A.5.4 Other Potential Candidates

Other candidates include thiacrowncalixarenes. As these sulfur-containing macrocyles are softer ligands than traditional oxygen-containing calixcrowns,[25] they could potentially bind softer anions such as Pb^{2+}. They could then be used for heavy metal remediation, rather than nuclear waste processing. We could also investigate the co-solvent used in nuclear waste remediation. Savannah River uses trioctylamine as a cosolvent to improve stripping; another amine (1° or 2°) could potentially be investigated.

A.5.5 Evaluating Candidate Efficiency

For extraction studies, analytical methods that avoid sampling are preferable, as they do not disturb the system's equilibrium. Two such analytical techniques that have been used to characterize the ion-binding abilities of crown ethers and calixarenes are ^{1}H NMR and UV-Vis. Methylene protons in the crown ether ring have exhibited a change in chemical shift upon binding of a guest;[26] this change in chemical shift could be used to quantify the amount of guest complexed by the ion. The use of UV-Vis requires the presence of chromophores in the host molecule in question, making this method most suitable for characterization of calixarenes and benzocrowns. The wavelength of maximum absorption (λ_{max}) of calixarenes, which is a function of the conjugation of the molecule, has been shown to change upon binding of a guest such as Cs^{+}.[27] If we desire a UV-active guest rather than a host, picrate salts have been used extensively to determine host-guest complexation.[28]

A.6 References

1. (a) Alfieri, C.; Dradi, E.; Pochini, A.; Ungaro, R.; Andreetti, G. D. Synthesis, and X-ray crystal and molecular structure of a novel macrobicyclic ligand: crowned *p-t*-butyl-calix[4]arene. *J. Chem. Soc., Chem. Commun.* **1983,** (19), 1075-1077; (b) Pedersen, C. J. The discovery of crown ethers. *Science* **1988,** *241* (4865), 536-540.

2. Gokel, G. W.; Leevy, W. M.; Weber, M. E. Crown ethers: Sensors for ions and molecular scaffolds for materials and biological models. *Chem. Rev.* **2004,** *104* (5), 2723-2750.

3. Starks, C. M.; Liotta, C. L.; Halpern, M. *Phase-Transfer Catalysis: Fundamentals, Applications, and Industrial Perspectives*. Chapman & Hall: New York, 1994.

4. Horwitz, E. P.; Dietz, M. L.; Fisher, D. E. SREX: A new process for the extraction and recovery of strontium from acidic nuclear waste streams. *Solvent Extr. Ion Exch.* **1991,** *9* (1), 1-25.

5. Law, J. D.; Brewer, K. N.; Herbst, R. S.; Todd, T. A.; Wood, D. J. Development and demonstration of solvent extraction processes for the separation of radionuclides from acidic radioactive waste. *Waste Manage. (Oxford)* **1999,** *19* (1), 27-37.

6. Dietz, M. L.; Horwitz, E. P.; Rogers, R. D. Extraction of strontium from acidic nitrate media using a modified PUREX solvent. *Solvent Extr. Ion Exch.* **1995,** *13* (1), 1-17.

7. U.S. Department of Energy. Linking legacies: connecting the Cold War nuclear weapons production processes to their environmental consequences. Office of Environmental Management: Washington, D.C., 1997; p 230.

8. Settle, F. A. Uranium to electricity: the chemistry of the nuclear fuel cycle. *J. Chem. Educ.* **2009,** *86* (3), 316-323.

9. (a) Visser, A. E.; Rogers, R. D. Room-temperature ionic liquids: new solvents for f-element separations and associated solution chemistry. *J. Solid State Chem.* **2003,** *171* (1-2), 109-113; (b) Visser, A. E.; Swatloski, R. P.; Reichert, W. M.; Griffin, S. T.; Rogers, R. D. Traditional extractants in nontraditional solvents: Groups 1 and 2 extraction by crown ethers in room-temperature ionic liquids. *Ind. Eng. Chem. Res.* **2000,** *39* (10), 3596-3604.

10. Luo, H. M.; Dai, S.; Bonnesen, P. V. Solvent extraction of Sr^{2+} and Cs^{+} based on room-temperature ionic liquids containing monoaza-substituted crown ethers. *Anal. Chem.* **2004,** *76* (10), 2773-2779.

11. Luo, H. M.; Dai, S.; Bonnesen, P. V.; Buchanan, A. C. Separation of fission products based on ionic liquids: Task-specific ionic liquids containing an aza-crown ether fragment. *J. Alloys Compd.* **2006,** *418* (1-2), 195-199.

12. Strzelbicki, J.; Bartsch, R. A. Extraction of alkali metal cations from aqueous solutions by a crown ether carboxylic acid. *Anal. Chem.* **1981,** *53* (12), 1894-1899.

13. Stastny, V.; Rudkevich, D. M. Separations using carbon dioxide. *J. Am. Chem. Soc.* **2007,** *129* (5), 1018-1019.

14. (a) Blasucci, V.; Hart, R.; Mestre, V. L.; Hahne, D. J.; Burlager, M.; Huttenhower, H.; Thio, B. J. R.; Pollet, P.; Liotta, C. L.; Eckert, C. A. Single component, reversible ionic liquids for energy applications. *Fuel* **2010,** *89* (6), 1315-1319; (b) Hart, R. J. Designing switchable solvents for sustainable process development. PhD thesis, Georgia Institute of Technology, Atlanta, 2011.

15. Hook, R. J. An investigation of some sterically hindered amines as potential carbon dioxide scrubbing compounds. *Ind. Eng. Chem. Res.* **1997,** *36* (5), 1779-1790.

16. Dietz, M. L.; Horwitz, E. P.; Rhoads, S.; Bartsch, R. A.; Krzykawski, J. Extraction of cesium from acidic nitrate media using macrocyclic polyethers: The role of organic phase water. *Solvent Extr. Ion Exch.* **1996,** *14* (1), 1-12.

17. Gutsche, C. D. *Calixarenes Revisited.* Royal Society of Chemistry: Cambridge, 1998.

18. Ghidini, E.; Ugozzoli, F.; Ungaro, R.; Harkema, S.; Abuelfadl, A.; Reinhoudt, D. N. Complexation of alkali metal cations by conformationally rigid, stereoisomeric calix[4]arene crown ethers: a quantitative evaulation of preorganization. *J. Am. Chem. Soc.* **1990,** *112* (19), 6979-6985.

19. Ungaro, R.; Casnati, A.; Ugozzoli, F.; Pochini, A.; Dozol, J.-F.; Hill, C.; Rouquette, H. 1,3-Dialkoxycalix[4]arenecrowns-6 in 1,3-Alternate Conformation: Cesium-Selective Ligands that Exploit Cation-Arene Interactions. *Angew. Chem. Int. Ed.* **1994,** *33* (14), 1506-1509.

20. Salorinne, K.; Nissinen, M. Calixcrowns: synthesis and properties. *J. Inclusion Phenom. Macrocyclic Chem.* **2008,** *61* (1-2), 11-27.

21. Haverlock, T. J.; Bonnesen, P. V.; Sachleben, R. A.; Moyer, B. A. Applicability of a calixarene-crown compound for the removal of cesium from alkaline tank waste. *Radiochim. Acta* **1997,** *76* (1-2), 103-108.

22. Bonnesen, P. V.; Delmau, L. H.; Moyer, B. A.; Leonard, R. A. A robust alkaline-side CSEX solvent suitable for removing cesium from Savannah River high level waste. *Solvent Extr. Ion Exch.* **2000,** *18* (6), 1079-1107.

23. Moyer, B. A.; Birdwell, J. F.; Delmau, L. H.; Schuch, D. L.; Stoner, E. L.; Williams, N. J.; Fink, S. D.; Peters, T. B.; Pierce, R. A.; Leonard, R. A.; Geeting, M. W. Next generation cesium solvent. 2010.

24. Bazelaire, E.; Gorbunova, M. G.; Bonnesen, P. V.; Moyer, B. A.; Delmau, L. H. pH-Switchable cesium nitrate extraction with calix 4 arene mono and bis(benzo-crown-6) ethers bearing amino functionalities. *Solvent Extr. Ion Exch.* **2004,** *22* (4), 637-661.

25. Duta, M.; Asfari, Z.; Kruchinina, N.; Thuery, P.; Hagege, A.; Leroy, M. Thiacrowncalix[4]arene derivatives: Synthesis and complexing properties. *Supramol. Chem.* **2005,** *17* (3), 221-226.

26. Seangprasertkij, R.; Asfari, Z.; Vicens, J. A di-aza-benzo crown ether derived from *p-tert*-butyl calix[4]arene. Synthesis and complexation of zinc cation. *J. Inclusion Phenom. Mol. Recognit. Chem.* **1994,** *17* (2), 111-118.

27. (a) Arnaud-Neu, F.; Schwingweill, M. J.; Ziat, K.; Cremin, S.; Harris, S. J.; McKervey, M. A. Selective alkali and alkaline earth cation complexation by calixarene amides. *New J. Chem.* **1991,** *15* (1), 33-37; (b) Arduini, A.; Pochini, A.; Reverberi, S.; Ungaro, R.; Andreetti, G. D.; Ugozzoli, F. The preparation and properties of a new lipophilic sodium selective ether ester ligand derived from *p-t*-butylcalix[4]arene. *Tetrahedron* **1986,** *42* (7), 2089-2100.

28. Kolthoff, I. M.; Chantooni, M. K. Crown ether complexed alkali metal picrate ion pairs in water-saturated dichloromethane as studied by electrolytic conductance and by partitioning into water. Effect of lithium chloride on partitioning. *J. Chem. Eng. Data* **1997,** *42* (1), 49-53.

APPENDIX B. BIMETALLIC CATALYST SYNTHESIS FOR DUAL MODE HYDRAZINE DECOMPOSITION

B.1 Introduction

Hydrazine is used as a propellant for rockets and satellites. There are two metal-catalyzed decomposition pathways for hydrazine: one yields hydrogen and nitrogen, while the other yields ammonia and nitrogen, as shown in Equations B.1 and B.2.

$$N_2H_4 \rightarrow N_2 + 2H_2 \qquad \text{Equation B.1}$$

$$3N_2H_4 \rightarrow 4NH_3 + N_2 \qquad \text{Equation B.2}$$

Hydrogen and nitrogen are used for chemical propulsion—the sudden release of high-volume gases at high temperatures propels the spacecraft forward. Ammonia, however, can be ionized and used for electrical propulsion, which provides more fine control and is commonly used for minute adjustments once in orbit. Low temperatures (below 300°C) are required for the production of ammonia from hydrazine, as further decomposition of ammonia (to hydrogen and nitrogen) occurs at higher temperatures.[1] As hydrogen and nitrogen are not of use as electrical propellants, this is an undesirable side reaction. Currently, the electrical propellant of choice is ionized xenon.

The most commonly used catalyst for hydrazine decomposition is a multi-layered iridium/ruthenium catalyst on a metal oxide support, synthesized by repeated deposition of the metal salt via a process known as the Shell Method.[2] However, several other metals have been found to be efficient catalysts for the decomposition of hydrazine. These include cobalt, copper, nickel, and rhodium, as well as the aforementioned iridium and ruthenium.[1] The goal of this project was to develop a metal catalyst that would maximize ammonia

output while minimizing the exotherm associated with decomposition—this would permit use of one fuel for both chemical and electrical propulsion, minimizing the payload of the rocket or satellite.

B.2 Background

In conjunction with the research group of Dr. Mitchell Walker (School of Aerospace Engineering, Georgia Institute of Technology), our research group has developed supported metal catalysts that selectively decompose hydrazine into ammonia at relatively low temperatures (75°C) for use in dual-propellant rocket thrusters.[3] Dr. Hillary Huttenhower demonstrated that Ni^0 nanoparticles supported on silica showed high selectivity for ammonia formation, with yields of 94% detected via GC-TCD. Additionally, it was demonstrated that ruthenium, rhodium, and iridium all performed well in our system.[3a] Here I will detail the synthesis of similar catalysts that were intended for the same purpose. This appendix is not intended to be an exhaustive chronicle of the discovery of the technology and its prior art; rather, its purpose is to gather the experimental details together in one locus.

B.3 Experimental Section

B.3.1 Materials

All chemicals were purchased from Sigma-Aldrich and used as received unless otherwise noted. Chemicals used were: iridium (III) chloride ($IrCl_3$); cobalt (II) chloride ($CoCl_2$); nickel (II) chloride ($NiCl_2$); dodecanethiol (98+%); sodium hydroxide (NaOH); ethanol (EtOH); ammonium hydroxide (NH_4OH; 28% aqueous solution); titania (TiO_2; technical grade); alumina (Al_2O_3; puriss); Hydrazine (N_2H_4; anhydrous, 98%) was used as received and stored at 5°C.

Spherical mesoporous silica (pore size 150Å; diameter 75-200 μm) was obtained from Sorbent Technologies. A custom mix of 40:60 H_2:N_2 was obtained from Airgas.

B.3.2 Experimental

B.3.2.1 Supported Nickel Catalysts: Dilute Method

A typical synthesis of supported nickel via the dilute method was carried out as follows. 0.2232 g $NiCl_2$ (1.722 mmol) was dissolved in 50 mL of DI H_2O (2.78 mol) in a 600 mL beaker with a magnetic stirbar, forming a green solution. 0.67 mL 28% NH_4OH (9.914 mmol) was then added, and the solution turned dark blue. 2.0113 g SiO_2 (33.48 mmol) was added to the reaction mixture, which was heated to 90°C and stirred at 140 rpm for 60 min. The reaction mixture was cooled and filtered via aspiration to yield a light green powder, which was air-dried overnight. Calcination was carried out at 550°C using a tube furnace and a gas stream of 40:60 H_2:N_2 for 16 hours. The yield of calcined Ni^0 on SiO_2 was 1.5428 g.

B.3.2.2 Supported Iridium Catalysts: Dilute Method

A typical synthesis of supported iridium via the dilute method was carried out as follows. 0.1510 g $IrCl_3$ (5.057×10^{-4} mol) was dissolved in 10 mL of DI H_2O (0.556 mol) in a 600 mL beaker with a magnetic stirbar, forming a dark purple solution. 0.21 mL 28% NH_4OH (3.107 mmol) was then added, and the solution turned yellowish green. The solid support (2.0070 g TiO_2, 25.13 mmol or 2.0010 g Al_2O_3, 19.62 mmol) was added to the reaction mixture, which was heated to 105°C and stirred at 140 rpm for 60 min. The reaction mixture was cooled and filtered via aspiration to yield a powder, which was air-dried overnight. Calcination was carried out at 550°C using a tube furnace and a gas stream of 40:60 H_2:N_2 for 16 hours. The yield of calcined Ir^0 on TiO_2 was 1.8676 g; the yield of calcined Ir^0 on Al_2O_3 was 1.9601 g.

B.3.2.3 Multilayer Supported Nickel Catalysts: Shell Method

A typical Shell Method synthesis of multilayer single-metal supported nickel was carried out as follows. The target loading for each layer was an additional 5 wt% Ni^0. For each iteration, approximately 2 grams of supported nickel catalyst was reserved for analysis; the remainder was used in the next coating step. The initial impregnation of nickel onto mesoporous SiO_2 and the calcination thereof was performed by Dr. Rani Jha.

To a 600 beaker with a magnetic stirbar was added 1.5482 g $NiCl_2$ (11.95 mmol) and 10 mL DI H_2O (0.556 mol). The solution turned from orange to green. Upon addition of 4.6 mL 28% NH_4OH (68.06 mmol), the solution turned a dark blue. 15.0142 g 5 wt% calcined Ni^0 on SiO_2 was added to the beaker, followed by 20 mL DI H_2O (1.11 mol). The reaction mixture was then stirred at 100°C until all liquid had evaporated; the uncalcined catalyst was a blue-green. This was stored in the oven at 120°C prior to calcination, which was carried out at 550°C using a tube furnace and a gas stream of 40:60 H_2:N_2 for 16 hours. The amount of recovered calcined catalyst was 14.7077 g. This process was repeated until 7 layers of nickel had been deposited and calcined.

B.3.2.4 Bimetallic Catalysts

A typical bimetallic supported catalyst was synthesized as follows. The target loading for each metal was 5 wt%. Combinations synthesized were iridium first, followed by cobalt (Ir@Co), Co@Ir, Ir@Ni, and Ni@Ir; the description that follows is for Ir@Co. To a 600 beaker with a magnetic stirbar was added 0.0711 g $IrCl_3$ (2.381×10^{-4} mol) and 12.4 mL DI H_2O (0.689 mol). The solution turned from black to dark purple. Upon addition of 0.12 mL 28% NH_4OH (1.776 mmol), the solution turned yellowish green. 1.9989 g SiO_2 (33.27 mmol) was added to the beaker. The reaction mixture was then stirred at 105°C until all liquid had evaporated. The remaining powder was stored in the oven at 120°C prior to

calcination, which was carried out at 550°C using a tube furnace and a gas stream of 40:60 H_2:N_2 for 16 hours. The amount of recovered calcined catalyst was 1.9659 g; this was then carried on to the next step.

To a 600 beaker with a magnetic stirbar was added 0.1093 g $CoCl_2$ (8.418×10^{-4} mol) and 10 mL DI H_2O (0.556 mol). The solution turned from dark blue to pink. Upon addition of 0.33 mL 28% NH_4OH (4.883 mmol), the solution turned turquoise. 1.9659 g SiO_2@Ir was added to the beaker. The reaction mixture was then stirred at 105°C until all liquid had evaporated. The remaining blue-black powder was stored in the oven at 120°C prior to calcination, which was carried out at 550°C using a tube furnace and a gas stream of 40:60 H_2:N_2 for 16 hours. The amount of recovered calcined catalyst was 1.9117 g.

B.3.2.5 Dodecanethiol-Capped Nickel Nanoparticle Synthesis

A typical synthesis of dodecanethiol-capped nickel nanoparticles was adapted from the work by Chen *et al.*[4] and carried out as follows. In a 250 mL 2-neck round-bottomed flask fitted with a condenser and magnetic stirbar, 1.0129 g nickel (II) chloride (7.816 mmol) was dissolved in 60 mL anhydrous ethanol (1.028 mol) under inert atmosphere. To this orange solution was added 1.3208 g NaOH (33.02 mmol). 1.95 mL dodecanethiol (8.141 mmol) was added, at which point the solution turned dark brown. This was heated at 60°C for 24 h, at which time 3 mL anhydrous hydrazine (95.57 mmol) was added. The reaction mixture was then heated for an additional 48 h. The cooled reaction mixture was then aspirated, and the resulting solid washed with ethanol, water, and acetone. Drying of the brown solid yielded 1.8277 g (%) dodecanethiol-capped nickel nanoparticles.

B.4 Results and Discussion

Multi-layered nickel catalyst supported on silica was synthesized following the Shell Method in the hope that it would combine the high efficiency of the Shell Method Ir and Ru catalysts[2] with the high ammonia selectivity of the Ni nanoparticle catalysts we have synthesized. These catalysts did not undergo any characterization, as the project was discontinued shortly after their synthesis. Should future researchers desire to re-synthesize and test these compounds, I suggest that they consult the thesis of Dr. Huttenhower for a more thorough treatment of the characterization and testing of these catalysts.

B.5 References

1. Maurel, R.; Menezo, J. C., Catalytic decomposition of ^{15}N-labeled hydrazine on alumina-supported metals. *J. Catal.* **1978,** *51* (2), 293-295.

2. Armstrong, W. E.; Ryland, L. B.; Voge, H. H. Catalyst comprising Ir or Ir and Ru for hydrazine decomposition. US 4,124,538, 1978.

3. (a) Huttenhower, H. A. Development of new chemistry for a dual use hydrazine thruster, switchable room temperature ionic liquids, a study of silane grafting to polyethylene and its model compounds, synthesis of the novel hydrazine replacement fuel molecules 1,1-dimethyl-2-[2-azidoethyl]hydrazine and 1,1-dimethyl-2-[2-azidoethyl]hydrazone. PhD thesis, Georgia Institute of Technology, Atlanta, 2010; (b) Fadhel, A. Z. Designing for sustainability: applications of tunable solvents, switchable solvents, and catalysis to industrial processes. PhD thesis, Georgia Institute of Technology, Atlanta, GA, 2011.

4. Chen, Y. Z.; Peng, D. L.; Lin, D. P.; Luo, X. H., Preparation and magnetic properties of nickel nanoparticles via the thermal decomposition of nickel organometallic precursor in alkylamines. *Nanotechnology* **2007,** *18* (50).

VITA

Emily C. Nixon was born in Marietta, Georgia. Her interest in chemistry started in 10th grade at the Walker School, where she was instructed by Don Parkhurst, who inspired her to pursue a career in chemistry. She attended Duke University, where she earned a B.S. in chemistry and a second degree in Geman. Following graduation from Duke, she was awarded two scholarships from the Deutscher Akademischer Austauschdienst (DAAD)—the Research Internship in Chemistry (RICh) scholarship in 2004, and the Research Internship in Science and Engineering (RISE) scholarship in 2006. These internships were the beginning of her interest in green chemistry. She began studying at the Georgia Institute of Technology in 2008 and joined the Eckert-Liotta research group there. She successfully defended her thesis in August of 2012. Her interests include knitting, traveling, and cheering for the Atlanta Braves. She is also very proud to be a feminist.